UNIVERSITY OF
BIRMINGHAM

Switchable Surfaces for Biomedical Applications

by

Eleonora Cantini

A thesis submitted to
The University of Birmingham
for the degree of
DOCTOR OF PHILOSOPHY

School of Chemical Engineering

College of Physical Sciences and Engineering

The University of Birmingham

May 2017

Abstract

Switchable oligopeptides, able to expose or conceal biomolecules on a surface, upon the application of an electrical potential, represent a versatile tool for the development of novel devices, presenting potential biomedical applications.

Recently, several studies have demonstrated the applicability of smart devices for the control of protein binding and cellular response. In this work, a detailed analysis of the steric requirements necessary to develop a mixed oligopeptide Self-Assembled Monolayer (SAM) presenting an optimum switching ability will be described. The influence of both the SAM components surface ratio and the switching unit length on the mixed SAMs switching performance will be investigated.

The findings of this investigation will be used to develop for the first time a device, based on electrically switchable oligopeptides, able to control the interaction between an antigen and its relative antibody. The influence of the biological medium on the oligopeptide switching ability will also be investigated.

Finally, an orthogonal functionalisation strategy will be investigated in detail, together with a new platform able to promote human sperm cells adhesion. The possible obstacles present in the process will be described and examined thoroughly.

The results of this research thesis will also represent the first building blocks towards the development of glass-gold micropatterned surfaces able to control the calcium signalling in human sperm cells. Hence, the work presented in this dissertation will have important applications in the development of both new devices to control antibodies response and new efficient methods to select human sperm cells for *in-vitro* fertilisation (IVF) treatments.

Dedicated to the memory of dear friend and colleague

Simone Basile (1988-2016)

Acknowledgments

My biggest thank you goes to my supervisor Professor Paula M. Mendes, for her fundamental support and advice throughout my PhD, but also for being patient and helpful during my writing-up. I would also thank my co-supervisor Professor Jon A. Preece, for his supervision, help and support. This research work would have not been completed without the guidance from you both.

Special thanks to Dr Jackson Kirkman-Brown, Dr Lorraine Frew and Dr Joao Correia for their precious help during the second part of this research work.

I would also like to say "thank you" to the members of both the Preece and Mendes group past and present: Dr James Bowen, especially for this help and support with the ellipsometer, Dr Paul Yeung, for his help and support with surface chemistry and SPR instrumentation, Dr Alice Pranzetti, Dr Parvez Iqbal Dr Alex Stevenson- Brown, Dr Minhaj Lashkor, Dr Nga Yip, Dr Aaron Acton, Dr Lewis Hart, Dr Stefano Tommasone, Simone Basile, Monika Köpf, Philippa Mitchell, Bárbara Santos-Gomes, Fatima Zia, Francia Allabush, Zarrar Hussain and both Greg O'Callaghan and Dennis Zhao for their support during my PhD.

Special thanks go to my friend Dr Steve Della Mora, for his friendship, his patience and his support during the whole duration of my thesis and for deterring me from giving up.

A big thank you also to Dr Peter Jervis, Dr Lucia Cardo, Dr Giacomo Volpe, Dr Claudio Zito, Javier Jimenez, Chiara Busà, Simone Damiani and all the people I met during my three years at University of Birmingham. You helped me to remain mentally healthy.

I cannot forget to say thank you to Dr Avril Day-Jones, Katharine Partington and all the people I met since September, while I was trying to write a PhD thesis and training as a Science teacher at the same time. Your support has been fundamental.

Finally, I would like to thank my parents for their support from Italy during my studies and to my boyfriend Darren, for supporting, encouraging me, reminding me “never give up” and especially teaching me what being patient mean. Thank you to Darren’s family too, for your encouragements.

Without the people name above, this work would have not been completed. I will always be grateful to you.

Table of Contents

List of Illustrations and Tables

Chapter 1

Figure 1.9 – Schematic representation of an antigen-antibody system. Several antigens are available for binding, but only one is specific for the antigen binding site on the antibody chains

Figure 1.10 – Schematic of the possible switches that can be obtained upon the application of a stimulus. a) Chemical switch: the chemical composition of the monolayer varies when an external stimulus is applied (e.g. a change in pH). b) Conformational switch: the chemical composition of the monolayer remains the same, while its conformation varies when an external stimulus is applied (e.g. application of an electrical potential).

Figure 1.11 – Illustration of the formation and switching of a LD-SAM by employing a precursor molecule presenting a bulky head-group. Upon the application of an electrical potential the monolayer can reverse its wettability by switching between hydrophilic and hydrophobic states.

Figure 1.12 – Schematic representation of the DNA lever; a) lying on the surface when a positive potential is applied and repelled when a negative potential is applied, fully exposing the fluorescent dye. b) When a protein is linked to the DNA's top end, the upward motion is slowed and lags behind the bare lever. The dark yellow circle represents the Cy3 dye when the fluorescence is quenched by the gold surface. The bright yellow circle corresponds to a high fluorescence emission, due to the DNA molecule carrying the fluorophore being fully extended on the surface.

Figure 1.13 – Schematic representation of the switching of Biotin-4KC:TEGT mixed SAM upon the application of an electrical potential.

Figure 1.14 – Cartoon representation of the control of bacteria cells adhesion by switching a MUA:MET mixed SAM.

dielectric interface, d is the thickness of the metal surface (usually 50 nm) and ε_m and ε_d are the dielectric constants of the metal and the dielectric, respectively.

Figure 2.9 – Illustration of the SPR sensing principle, using the Kretschmann optical configuration. a) The SPR detects the angle of reflection of the light when no analyte is bound to the SAM on the surface; b) when the analyte is present in solution, this comes into contact with the target molecules on the surface. The binding causes a variation in the mass present on the surface, therefore a shift in the angle of reflection (c) occurs, and a change in the intensity of the reflected is recorded by the photodiode array detector. d) A sensorgram is obtained by plotting the resonance angle signal against time, and it is used to monitor the changes occurring on the surface.

Figure 2.10 – Illustration of a) chronoamperometry potential stepping and b) current variation with time

Figure 2.11 – Series of linear sweep voltammograms recorded at different scan rate

Figure 2.12 – Changes in current response for voltammograms recorded at different scan rates.

Figure 2.13 – Schematic representation of the forward and back scans in cyclic voltammetry.

Figure 2.14 – Schematic representation of a cyclic voltammogram for a reversible single electrode transfer reaction, in the case of a solution containing only a single electrochemical reactant. E_{pc} and i_{pc} are the peak potential and peak current relative to the cathode, respectively, whereas E_{pa} and i_{pa} are the peak potential and peak current relative to the anode, respectively

Chapter 3

Chapter 4

Figure 4.3 – XPS spectra of N 1s (left) and S 2p (right) for biotin-4KC:TEGT 1:0 solution ratio

Figure 4.4 – XPS spectra of N 1s (left) and S 2p (right) for biotin-4KC:TEGT 1:1 solution ratio

Figure 4.5 – XPS spectra of N 1s (left) and S 2p (right) for biotin-4KC:TEGT 1:10 solution ratio

Figure 4.6 – XPS spectra of N 1s (left) and S 2p (right) for biotin-4KC:TEGT 1:40 solution ratio

Figure 4.7 – XPS spectra of N 1s (left) and S 2p (right) for biotin-4KC:TEGT 1:100 solution ratio

Figure 4.8 – XPS spectra of N 1s (left) and S 2p (right) for biotin-4KC:TEGT 1:500 solution ratio

Table 4.2 – Biotin-4KC:TEGT solution ratios and respective surface ratios calculated after XPS analysis.

Figure 4.9 – SPR sensorgram traces showing the binding of neutravidin to the biotin-4KC:TEGT mixed SAMs at solution ratios of 1:0, 1:1,1:10, 1:40, 1:100 and 1:500 under OC (no applied potential), ON (+0.3 V) and OFF (−0.4 V) conditions.

Table 4.3 – Biotin-4KC:TEGT Binding Capacity (BC), expressed in Resonance Units (RU) and Switching Efficiency calculated from SPR experiments.

Figure 4.10 – Binding capacity and switching efficiency in ON (+0.3 V), OC (no potential applied) and OFF (-0.4 V) states of biotin-4KC:TEGT mixed SAMs at the different solution ratios tested in this study (1:0, 1:1, 1:10, 1:40, 1:100 and 1:500).

Figure 4.11 – XPS spectra of N 1s (left) and S 2p (right) for biotin-2KC:TEGT 1:40 solution ratio

Figure 4.12 – XPS spectra of N 1s (left) and S 2p (right) for biotin-2KC:TEGT 1:100 solution ratio

Figure 4.13 – XPS spectra of N 1s (left) and S 2p (right) for biotin-6KC:TEGT 1:40 solution ratio

Figure 4.14 – XPS spectra of N 1s (left) and S 2p (right) for biotin-6KC:TEGT 1:2000 solution ratio

Table 4.4 – Solution ratios of biotin-2KC:TEGT and biotin-6KC:TEGT mixed SAMs and relative surface ratios calculated by XPS.

Figure 4.15 – SPR sensorgram traces showing the binding of neutravidin to the biotin-2KC:TEGT mixed SAMs (solution ratios of 1:40 and 1:100) and biotin-6KC:TEGT mixed SAMs (solution ratios of 1:40 and 1:2000) under open circuit conditions, an applied positive (+0.3 V) and negative(−0.4 V) potential.

Figure 4.16 – The surface models used in the MD simulations. The different colours in the biotin-nKC chain represent the biotin moiety (purple), the four lysine (blue) and the cysteine residues (dark green), respectively. Water molecules are represented by the orange dots. The green and yellow balls denote the chloride ions and the gold atoms respectively, and the short grey chains represent TEGT molecules.

Figure 4.17 – Conformational changes of biotin-2KC:TEGT (surface ratio of 1:8) and biotin-4KC:TEGT (surface ratio of 1:16) mixed SAMs, under different electric field, along with the MD simulation snapshots. The direction of the applied electric field is indicated by the black arrows. Water molecules and hydrogen atoms are omitted for clarity. The gap distance variation between the biotin moiety and the TEGT matrix is indicated by d.

Figure 4.18 – Conformational changes of biotin-6KC:TEGT (surface ratio of 1:15) mixed SAMs, under different electric field, along with the MD simulation snapshots. The direction of the applied electric field is indicated by the black arrows. Water molecules and hydrogen atoms are omitted for clarity.

Figure 4.19 – Conformational changes of the pure biotin-4KC SAM under different electric fields (left) and MD simulation snapshots (right). L represents the variation of the gap distance between the biotin end group and the gold substrate.

Figure 4.1 - Molecular structures and related cartoons of the oligopeptide (progesterone-C7-4KC) and the hexaethylene glycol-terminated thiol (EG6OH) used in the mixed SAMs, and their calculated molecular lengths in fully extended conformations.

Chapter 5

Figure 5.2 - Cartoon representation of the ON-OFF switching system that controls the biomolecular interaction between progesterone (red) on the surface and antibody (green) in solution.

Figure 5.3 – XPS spectra of the a) S 2p, b) N 1s, c) C 1s and d) O 1s regions for the 1:10 progesterone-C7-4KC:EG6OH mixed SAM solution ratio.

Figure 5.4 – XPS spectra of the a) S 2p, b) N 1s, c) C 1s and d) O 1s regions for the 1:40 progesterone-C7-4KC:EG6OH mixed SAM solution ratio.

Figure 5.5 – XPS spectra of the a) S 2p, b) N 1s, c) C 1s and d) O 1s regions for the 1:100 progesterone-C7-4KC:EG6OH mixed SAM solution ratio.

Table 5.1 - Advancing and receding water contact angle and ellipsometric thickness for the different monolayers formed for 24h. The calculated molecular lengths were determined using ChemBio3D Ultra 12.0 in which the molecules were in fully extended conformation. The averages and standard errors were calculated from at least three different measurements.

Figure 5.6 - SPR sensorgram, recorded in OC (no potential applied) conditions, for the injection of anti-mouse progesterone antibody on both biotin-4KC:EG6OH and EG6OH SAMs.

Figure 5.7 - SPR sensorgrams for the binding of anti-mouse progesterone antibody to the progesterone-C7-4KC:EG6OH at a) 1:10, b) 1:40 and c) 1:100 solution ratio, in PBS, under OC (no applied potential), ON (+0.3 V) and OFF (−0.4 V) conditions.

Table 5.2 – Progesterone-C7-4KC:EG6OH Binding Capacity (BC), expressed in Resonance Units (RU) and Switching Efficiency calculated from SPR experiments.

Figure 5.8 – Bar Chart representing the switching efficiency obtained for 1:10, 1:40 and 1:100 progesterone-C7-4KC:EG6OH mixed SAMs solution ratios

Figure 5.9 - SPR sensorgrams for the binding of anti-mouse progesterone antibody to the progesterone-C7-4KC:EG6OH at 1:40 solution ratio, in sEBSS + 0.3% BSA, under OC (no applied potential), ON (+0.3 V) and OFF (−0.4 V) conditions.

Figure 5.10 - SPR sensorgrams for the binding of anti-mouse progesterone antibody to the progesterone-C7-4KC:EG6OH at 1:40 solution ratio, in sEBSS + 0.1% BSA, under OC (no applied potential), ON (+0.3 V) and OFF (−0.4 V) conditions.

Figure 5.11 - SPR sensorgrams for the binding of anti-mouse progesterone antibody to the progesterone-C7-4KC:EG6OH at 1:40 solution ratio, in sEBSS + 0% BSA, under OC (no applied potential), ON (+0.3 V) and OFF (−0.4 V) conditions.

Table 5.3 – SPR data and switching efficiency of the progesterone-C7-4KC:EG6OH mixed SAMs in PBS, sEBSS + 0% BSA, sEBSS + 0.1% BSA and sEBSS + 0.3% BSA respectively

Figure 6.7 – Fluorescence images of cell adhered on PDL coated-surfaces (left), silane-PDL layers formed using a PDL concentration of 0.1 mg/ml (centre) and silane-PDL layers formed using a PDL concentration of 0.5 mg/ml (right).

Figure 6.8 – Fluorescence images of cell adhered on PDL coated-surfaces rinsed with ethanol (left), and silane-PDL layers formed using a PDL concentration of 0.5 mg/ml rinsed with ethanol (right).

Figure 6.9 - XPS spectra of the a) C 1s, b) N 1s, c) O, d) S 2s and e) Si 2p regions recorded on clean glass substrates.

Figure 6.10 - XPS spectra of the a) C 1s, b) N 1s, c) O and d) S 2p regions recorded on clean gold substrates.

Figure 6.11 – XPS spectra of the a) S 2p, b) C 1s, c) O 1s and d) N 1s regions of 11-mercapto-1-undecanol SAMs on gold.

Figure 6.12 – Molecular structure of 11-mercapto-1-undecanol

Figure 6.13 – XPS spectra of the a) C 1s, b) Si 2p, c) N 1s, d) S 2s and e) O 1s regions of 11-mercapto-1-undecanol SAMs on glass.

Figure 6.14 – XPS spectra of the a) C 1s, b) N 1s, c) O 1s, d) S 2p and e) Si 2s regions of silane-PDL SAMs on gold after the first step.

Figure 6.15 – XPS spectra of the a) C 1s, b) N 1s, c) O 1s and d) Si 2p regions of silane-PDL SAMs on glass after the first step.

Figure 6.16 - Cyclic voltammetry of bare gold after piranha cleaning (orange line), after MUD incubation (black line) and after 5, 10 and 20 minutes of -1.5 V chronoamperometry (green, light blue and purple lines)

Figure 6.17 – XPS spectra of the a) C 1s, b) N 1s, c) O 1s, d) Si 2s and e) S 2p regions after thiol removal on gold substrates.

Figure 6.18 – XPS spectra of the a) C 1s, b) N 1s, c) O 1s and d) Si 2p regions incubation of glass substrates in KOH for ten minutes, demonstrating that removal step will not affect the integrity of the silane-PDL layer on the glass substrate.

Figure 6.19 – XPS spectra of the a) C 1s, b) N 1s, c) O 1s, d) Si 2p and e) S 2s regions after the formation of Progesterone-C7-4KC:EG6OH mixed SAMs on gold substrates.

Figure 6.20 – XPS spectra of the a) C 1s, b) N 1s, c) O 1s and d) Si 2p regions after the formation of Progesterone-C7-4KC:EG6OH mixed SAMs on glass substrates.

Figure 6.21 – XPS spectrum of Si 2s. A small peak is visible in the region of S 2p

A deeper insight into the molecular coverage of the glass substrates can be obtained by calculating the ratios between the elements analysed by XPS.

Figure 6.22 – Fluorescence images of cell adhered on glass slides after the completion of the Progesterone-C7-4KC:EG6OH mixed SAM deposition step.

Chapter 7

Figure 7.1 – Cartoon representation of double-armed switching molecule. The aspartic acid oligopeptide arms (green) are connected to the alkyl chain (black) carrying the progesterone moiety (red) through a core central molecule (blue) in a dendron-like structure.

List of Definitions and Abbreviations

Ab: antibody

Ag: antigen

BSA: bovine serum albumin

CV: cyclic voltammetry

CVD: chemical vapour deposition

EDC: 1-Ethyl-3-(3-dimethylaminopropyl)carbodiimide

EG6OH: 11-(Mercaptoundecyl)hexa(ethylene glycol)

ICSI: intracytoplasmic sperm injection

IVF: *in-vitro* fertilisation

MD: molecular dynamics

MUD: 11-mercaptoundecan-1-ol

NHS: *N*-Hydroxysuccinimide

OEG: oligo(ethylene) glycol

PBS: phosphate-buffered saline

PDL: poly-D-lysine

SAM: self-assembled monolayer

SCE: standard calomel electrode

Silane: carboxyethylsilanetriol

sEBSS: modified Earle's balanced salt solution

SPR: Surface Plasmon Resonance

SPW: surface plasma wave

TEA: triethylamine

TEGT: triethylene glycol thiol

XPS: X-ray photoelectron spectroscopy

Chapter 1 – An introduction to Bionanotechnology and Self-Assembled Monolayers

Part of this chapter is reproduced from the paper "Electrically Responsive Surfaces: Experimental and Theoretical Investigations", Cantini, E.; Wang, X.; Koelsch, P.; Preece, J. A.; Ma, J.; Mendes, P. M. Accounts of Chemical Research 2016, 49, 1223.

Abstract: *This chapter provides a background to bionanotechnology, top-down and bottom-up approaches, followed by a brief introduction to Self-Assembled Monolayers (SAMs), specific and non-specific protein binding on surfaces and the state of the art of stimuli-responsive surfaces for biomedical applications.*

1.1 Bionanotechnology

In recent years, researchers made big efforts to develop nanomaterials and nanostructured surfaces that can have an impact in biological and biomedical applications. These efforts resulted in a new branch of science, called bionanotechnology. One of the aims of bionanotechnology is to create systems and biomaterials able to mimic cellular environment at the nanoscale, to study and understand the biological processes at cellular level. The comprehension of cell behaviour, signalling and biological processes, can lead to the creation of new tools that are applicable in biosensors and diagnostic, tissue engineering, regenerative medicine and drug delivery.[1,2]

1.1.1 Surface Functionalisation for biosensors, cell sensing and diagnostic

Artificial biological surfaces are nowadays widely used in biotechnology and medicine as biosensors to detect various diseases and health conditions.[3,4] These surfaces are

functionalised with bioactive molecules that can mimic natural processes[5]. The ability to reproduce biological systems with nano-scale structures, has enabled researchers to develop fast, low-cost biosensors, able to identify several types of biomarkers in real-time to design efficient point-of-care (POC) clinical devices[6–10].

During the last few decades, a huge research effort has been dedicated to the study of different functionalisation strategies for the development of novel, simple, low-costs, portable sensing devices applicable to biomedical diagnostic[3,10], such as devices for diagnosis of infectious diseases[11], cancer biomarker detection[12–14] metabolite quantification in living cells[15], DNA biosensing[16,17] and identification of antigen-antibody interactions[18,19].

Biosensing platforms can be obtained by chemically modifying a vast range of surfaces[5,16] such as flat metal surfaces[20], nanoparticles[21–24] and nanotubes[25,26], in a tailored manner with the desired chemistry and surface morphology[21,27]. In particular, carbon nanotubes (CNTs) are widely used in current biomedical research, thanks to their mechanical, electrical, magnetic and optical properties that make them suitable tools to create devices with several biomedical applications, from drug delivery[28–30] to diagnostics[27,31].

Various surface functionalisation strategies are available, such as layer-by-layer (LbL) strategies[32–34] and Self-Assembled Monolayers (SAMs) formation[35–38].

Layer-by-layer functionalisation of surfaces comprises several steps of layers addition or modification, to obtain the desired layered structures. Specifically, Sung et al.[39] used LbL-coating to modify polydimethylsiloxane surfaces to decrease the amount of non-specific binding and improve the detection of low levels of proteins. On the other hand, the formation of SAMs consists of a single step, where one or more component molecules organise themselves in an ordered nanometric monolayer on the substrate. SAMs will be described in detail in section 1.3.

1.1.2 Other materials used in biosensing

In addition to metal surfaces, metal nanoparticles and nanotubes mentioned, other materials, such as nanoporous materials[40–42], nanozymes[43,44] and hydrogels[45] have gained increasing interest for biomedical research.

Nanoporous materials[40,41] possess a bigger surface-to-volume ratio than conventional nanomaterials, offering an enhanced signal when the analyte interacts with the surface. In addition, they can be functionalised to mimic the protein nanochannels found on cell membranes. Therefore, they can be of paramount importance in the study of nanochannels single-molecule sensitivity and selectivity[42] . By tailoring the size of the nanopores, it is possible to obtain a selective control over the molecular transport through the nanochannels. These powerful materials can be made by self-ordering synthesis based on electrochemical anodization, and both anodic aluminium oxide (AAO) and titania nanotubes (TNTs) have already been used in biosensors fabrication[46,47] . In addition to the increased surface areas, such nanoporous materials can be prepared at relatively low costs and show chemical resistance, thermal stability, hardness and biocompatibility. These characteristics make them very useful when developing ultra-sensitive biosensing devices[40–42].

Nanozymes[8,43] are artificial enzymes presenting enzyme-like activities and are widely used in biomimetic, which attempt to mimic the characteristics and functions of natural enzymes. Some of the materials that have shown unexpected enzyme-like characteristics[43] are fullerenes[48,49], metal nanowires[50,51], nanorods[52] and several types of metal nanoparticles[48,53]. Such materials possess both the characteristics of natural enzymes and the properties of the material used to fabricate them.

For example, Ali et al.[48] were able to create a *tris*-malonic acid derivative of fullerene C_{60} molecules, capable of transforming the dangerous superoxide radical (O_2^-) into oxygen

molecules (O_2), mimicking superoxide dismutase (SOD) enzymatic activity. Wang et al.[48] have demonstrated the use of nanoparticles, chemically modified with oligonucleotides molecules, able to induce RNA cleavage and applicable to the treatment of Hepatitis C.

Researchers have been capable of mimicking other natural enzymes, such as catalases[53], oxidases[54] and peroxidases[55,56] making nanozymes unique, and applicable in sensing, imaging and therapeutics.

Hydrogels are hydrophilic materials formed by a polymer network that can absorb water from 10% to thousands times their dry weight[57] . By changing their chemical and physical characteristics, their structure can be tailored, and they can be integrated into micro-systems. Their biocompatibility and their sensitiveness to external stimuli make them largely employable as switchable biosensors to detect changes, for instance, in pH[58], monitoring biological processes[57], DNA sensing[58], carbohydrate sensing[59] and toxin screening[59]. Switchable materials will be described in detail in section 1.5.

1.2 Functionalisation approaches

This section describes the two approaches used as surface functionalisation strategies, namely the top-down and the bottom-up approach[60] (**Figure 1.1**).

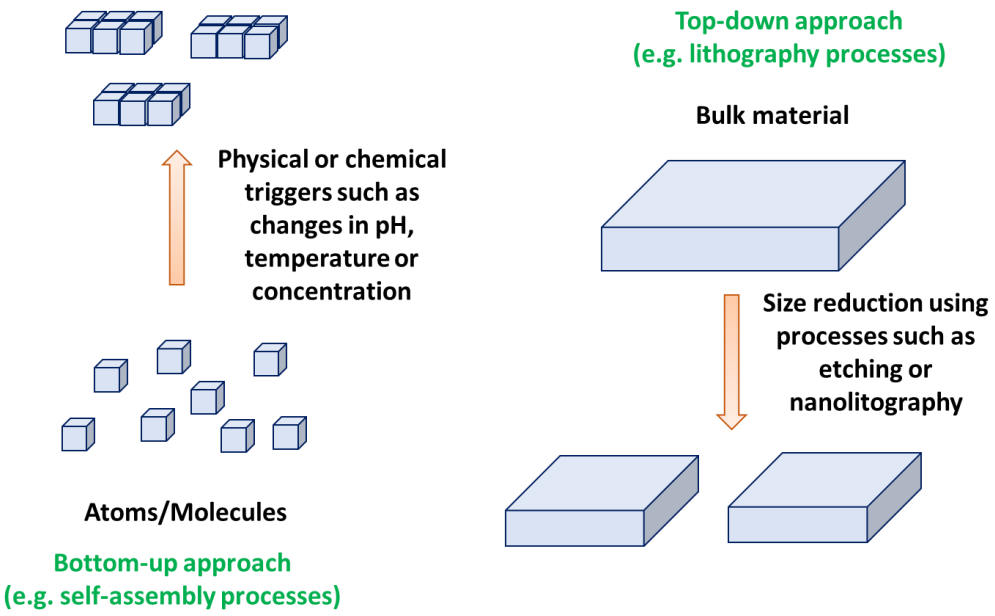

Figure 1.1 – *Cartoon representation of top-down and bottom-up approach*

1.2.1 Top-down approach

This approach consists in the removal of matter from a bulk material to achieve the desired smaller structure showing a specific order and shape[60,61]. The most used technique in this method is nanolithography that allows the construction of a pattern on the surface/material. There are many lithographic techniques that can be exploited, classical methods such as electron-beam lithography and photolithography or novel methods, such as dip-pen lithography[62], nanoimprint lithography[63,64], colloidal[65] and soft lithography[66,67]. In the classical methods, a substrate, covered in a polymer layer (e.g. resist) is irradiated with either UV light or an electron beam, to carve the resist layer and create a nanometric pattern (e.g. nanopattern). Then, using a technique called “etching”, the nanopattern is transferred to the substrate surface[68,69] (**Figure 1.2**).

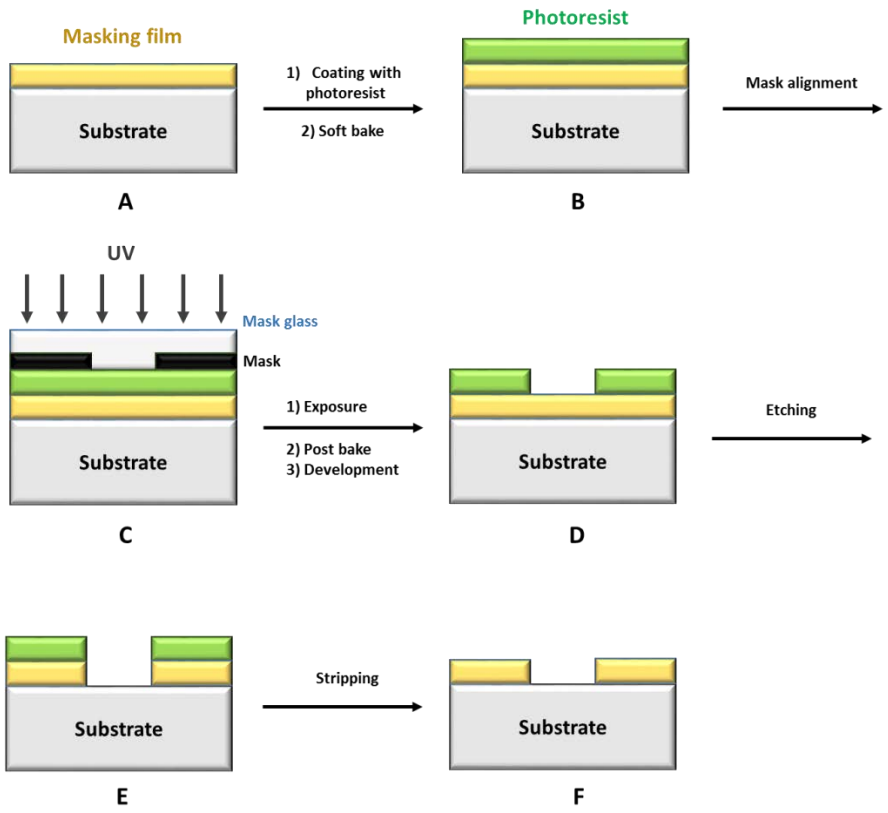

Figure 1.2 – *Schematic representation of the photolithographic process. The substrate covered with a masking film (A) is coated with a photoresist (B). A mask is then collocated on the photoresist film (C) to create the desired pattern after UV exposure (D) and etching (E). Finally, the photoresist is completely removed by stripping, to obtain the desired patterned substrate (F).*

The novel methods have been developed to overcome the constraints of common lithography. Soft lithography, for example, is a low-cost and flexible technique extensively used due to the possibility of creating large-scale nanostructured architectures, simply using a mold or a mask made using a nanopatterned elastomer[70,71]. The disadvantage of this technique is the need of being supported by standard lithography methods to create the molds and the masks. To solve this problem colloidal lithography has started to be extensively used[72]. This

technique uses nanodisperse colloidal particles which size goes from around 10 nm to around 10 μm that can self-assemble in 2D- and 3D-periodic arrays called colloidal crystals to create masks on the substrate surface[67,73]. The application of this kind of lithography is convenient when there is the necessity for nanostructures presenting periodic arrangements[65,73].

1.2.2 Bottom-up approach

The bottom-up methods, extensively used and studied as surface functionalisation methods[60], are based on the spontaneous self-assembly of small molecules into two-dimensional and three-dimensional composite structures showing defined physical and chemical properties, created atom-by-atom through covalent, non-covalent, ionic and metallic bonds and weak interactions, such as dipole-dipole and Van der Waals interactions[74,75].

The most broadly used nanofabrication method in this approach are Langmuir-Blodgett (LB)[76,77] and Self-Assembled Monolayers (SAMs)[78–81]. These methods allow the creation of well-ordered and packed monolayers by using a wide range of different molecules. However, the Langmuir-Blodgett approach presents the disadvantage of requiring long construction times, molecules with specific characteristic (i.e. amphiphilic) and expensive instrumentation. In addition, LB layers present limited mechanical stability and robustness because the fabrication does not involve chemisorption between the molecules and the substrates[82]. The lack of strong molecular interactions limits the applicability of LB layers in ambient and physiological conditions, limiting their suitability for biological and biomedical applications[82].

On the other hand, SAMs are commonly used in bionanotechnology due to their ease of fabrication and the possibility of tailoring their properties depending on desired purpose that overcome the drawbacks presented by some types of SAMs (e.g. thiol SAMs) such as

limited stability and robustness[78,83]. The next section describes in detail the characteristics and the possible uses of SAMs.

1.3 Self-Assembled Monolayers

SAMs have been intensively studied for the last decades. The first publication on the preparation of a molecular layer by adsorption is dated 1946[84], but the potential of SAMs was published only when Nuzzo and Dallara demonstrated that SAMs of alkanethiols can be prepared by adsorbing n-alkyl disulphides on gold substrates from diluted solutions[85]. SAMs were then thoroughly studied to tailor surfaces with various properties, on different substrates such as gold[86–88], indium tin oxide (ITO)[89], glass[90,91], silicon wafers (SiO_2)[92,93]and nanoparticles[94]. By carefully choosing both the head and the end groups of the molecules composing the SAMs, the characteristic of the surfaces, such as hydrophilicity/hydrophobicity charge and the type of biomolecules composing the end groups can be changed to obtain a monolayer that can be used in a wide range of applications, in both engineering (e.g. sensors[95], coating technologies[96,97], optics[95] and informatics[95]) and biomedical (e.g. biosensors[98], tissue engineering[99,100] and point of care diagnostics[101,102]) fields.

1.3.1 Surfactant

During the process of self-assembly, surfactant molecules adsorb on a solid surface (substrate) to form well-ordered molecular assemblies[78,87]. These molecules are formed by three parts: the head group, the backbone and the end group (**Figure 1.3**).

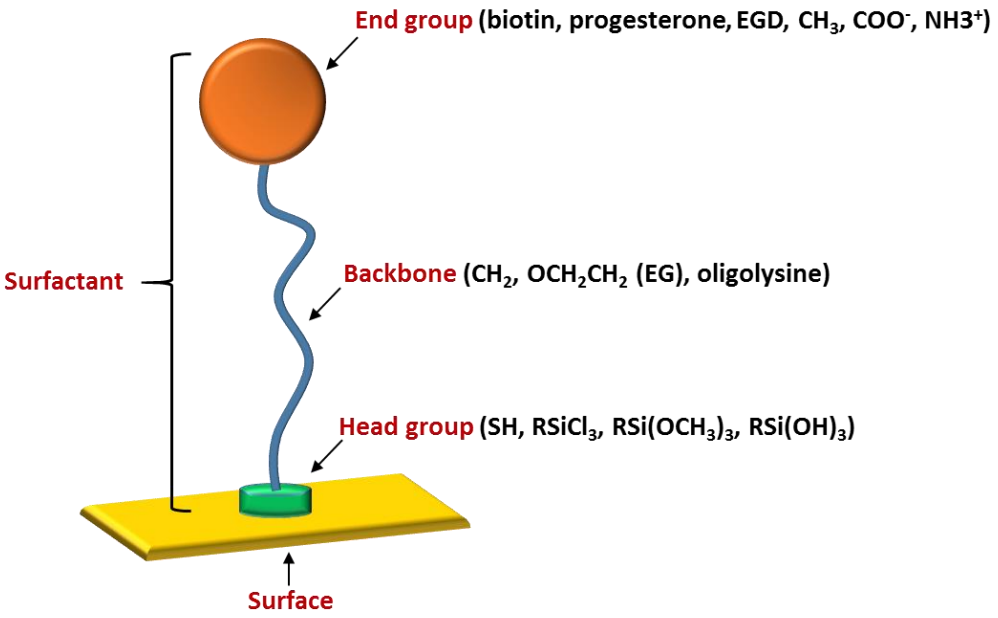

Figure 1.3 – *Schematic representation of a surfactant molecule*

The head group binds to the substrate surface, and therefore its choice depends on the substrate material used. The most commonly used SAMs are thiol molecules absorbed on gold or silver via the sulphur headgroup. Other head groups include silanes for SAMs on silicon oxide, silicone, mica and glass or carboxylic acid groups in the case of AgO/Ag substrates[86,87,103–107].

The backbone represents the central part of a surfactant molecule. It represents the connector between the head- and the end group, but it also plays an important role in the chemisorption process, depending on its characteristic[78,83,87,106–108]. By changing the length of the chain composing the backbone, it is possible to control density, orientation and ordering of SAMs molecules on the surface, e.g. long-chain alkanethiols ($HS(CH_2)_nX$, n>10) form densely-packed and well-ordered SAMs, at a 30˚ tilt angle on the surface[79,80,103].

Finally, by varying the end group, the SAM wettability, charge, together with the type of biomolecular interactions occurring on the surface can be tailored, allowing a wide range of applications in both engineering and biomedical fields[80,87].

1.3.2 Substrates and SAMs

Different substrates materials and surfactant molecules can be used in the preparation of SAMs. The following sections describe the SAMs used in this research work: silane SAMs and thiol-based SAMs.

1.3.2.1 Silane SAMs

Silane SAMs were first introduced by Sagiv in 1980, that studied the adsorption of n-octadecyltrichlorosilane (OTS) on glass substrates[109]. Many studies were conducted on silane monolayers in the past decades due to their potential many applications in a wide range of research areas, such as thin film technology, micro- and optoelectronics, chemical sensors and protective coatings. Silanes can also be used in biosensors, as bioactive surfaces or for cell adhesion and protein adsorption[98,110,111]. Silanes self-assemble via an hydrolisation reaction of the headgroup (trichloro-, trimethoxy- or triethoxysilane) that subsequently react with the hydroxyl groups (-OH) on the substrate surfaces (**Figure 1.4**), forming a cross-linked network of Si-O-Si bonds covalently linked to the substrate itself[93,112] .

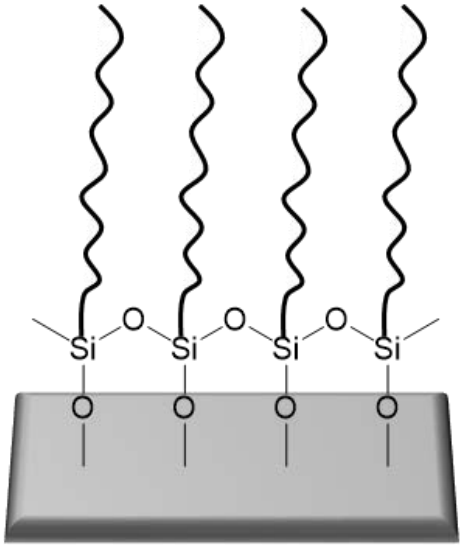

Figure 1.4 – *Cartoon representation of a silane SAM.*

Several research groups reported the possibility of the formation of islands of silanes on the surfaces, not creating a homogeneous layer[112,113]. This process strongly depends on several parameters, such as temperature, solvent used, pH, water content, and age of the solution. These parameters have to be carefully controlled, e.g. trichlorosilanes are sensitive to water and their headgroup present high reactivity, reducing the number of possible endgroups that can be incorporated into the surfactant molecule[104,111]. However, the water cannot be completely removed because its absence leads to an incomplete monolayers formation[111,112,114]. These problems can be circumvented by creating the desired silane layer in more than one step: 1) molecules able to give a specific surface organisation are used to create a precursor SAM and 2) the precursor SAM is modified via chemical surface reactions to obtain a well-organised silane layer[111,115]. Despite the challenges illustrated, silane monolayers are widely studied and used due to their greater thermal and mechanical stability compared to that of thiols on gold[104,105,116]. In addition, such monolayers prepared on smooth surfaces like silicon

wafers, present remarkable properties such ultra-low surface roughness, controlled wettability and chemical homogeneity that can be regulated by varying the silanes endgroup[104,117].

1.3.2.2 Thiol SAMs

SAM surfaces formed by adsorption of thiol molecules can be prepared on different metal substrates such as gold, silver, platinum, and copper.[83,94] However, thiol SAMs on gold are the most commonly used and studied due to their ease of preparation and characterisation. In addition, they play an important role in the building of a wide range of devices and systems that can have important applications in nanotechnology[100]. Alkanethiols SAMs with chain length between 10 and 22 carbon atoms have been extensively analysed[79,80] and it is known that alkyl chains self-assemble rapidly and spontaneously in a well-ordered and oriented manner, following a three step process (**Figure 1.5**)[83,94,100].

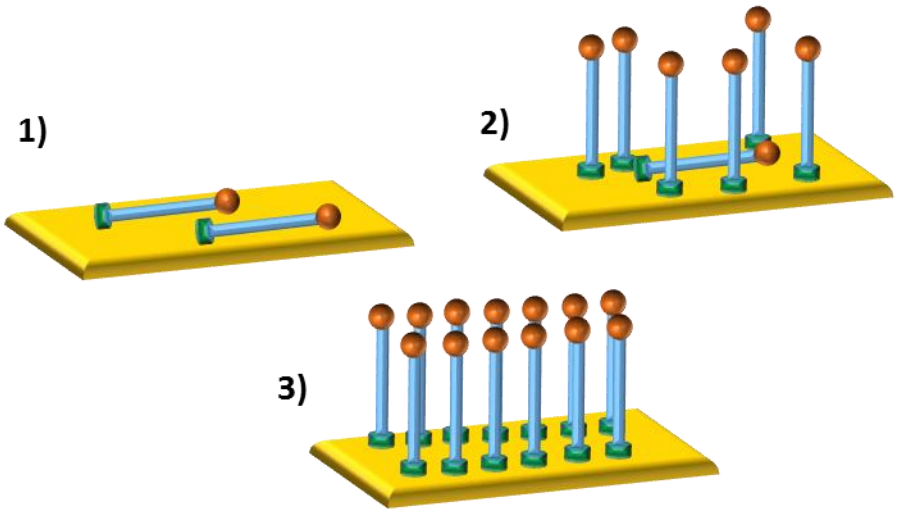

Figure 1.5 – *Schematic of the three-steps process for SAMs formation. 1) Physisorption, 2) chemisorption and 3) completion of SAM spatial orientation and packing.*

The first step is a physisorption process that depends on thiol concentration. The time necessary for this process increases as the thiol molecules concentration decreases. Thiol molecules lay parallel to the surface for all the duration of this step[118]. The second step is a chemisorption process during which the surfactant chains go from a disordered state to a more ordered one, organising themselves in a two-dimensional crystal[118]. The kinetics of this step is influenced by both the head group-substrate interactions and the chain-chain interactions in the molecules of the substrates (Van der Waals, dipole-dipole)[83,94,100]. This step takes hours and it is faster if the alkyl chains are longer[78]. The last step is the completion of the orientation and packing of surfactant molecules on the surface to obtain a well-ordered and stable SAM. This process is usually completed in 24 h. However, this has been demonstrated only for alkyl thiols with a backbone length >10 carbons[84,85]. If the backbone chain is shorter, the thiol molecules cannot reach a correct two-dimensional crystal structure during the second step and this leads to a disordered arrangement of molecules on the substrate surface that is not uniformly covered. Various electron diffraction studies, performed in the late 80s and early 90s showed that alkanethiolates adopt a (√3 x √3)R30˚ structure on Au (111) substrates[119]. In such structure, sulphur atoms are organised in an hexagonal arrangement, separated by a distance of 4.97Å[78,119]. Such studies suggested that each sulphur atom is bound to the 3-fold hollows present on the gold lattice, in a highly-ordered manner[120].

In addition, each alkanethiol molecule has an area of 2.14Å^2 and a cross-sectional area of 2.14Å^2. This difference forces the alkyl chains to tilt by an angle of around 30˚ to the gold surface normal (**Figure 1.6**)

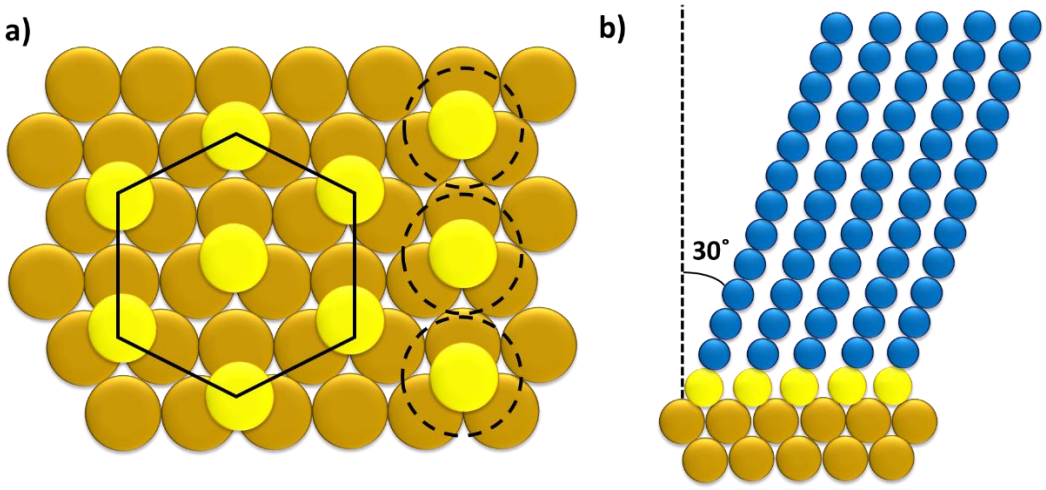

Figure 1.6 – *Schematic representation of the arrangement of dodecanethiol molecules on Au (111) substrates to achieve maximum surface coverage. (a) Structural model of the hexagonal arrangement of thiols (black hexagon) on gold and the area covered by each thiol molecule (dashed-lined circles). (b) Cross−section of the SAM formed showing the alkane chains 30˚ tilting in the direction of their next−nearest neighbours.*

This tilting angle allows the alkyl chains to maximise Van der Waals chain-chain interactions, leading to highly-packed monolayers[78,119].

1.3.3 Mixed SAMs

The preparation of mixed SAMs (multi-component SAMs) is more challenging than forming a single-component SAM. The routes that can be followed are usually two: 1) modifying the end groups of a single-component SAM in a selective manner, using different techniques such as photolithography[92], electron-beam lithography[68] and micro-contact printing[121,122] or 2) combination and co-adsorption of two or more different surfactants onto a surface[87,123] (**Figure 1.7**). The second method of preparation is the most widely used one.

However, the composition of the mixed SAM on the surface can differ from the one of the mixture of surfactants in solution.

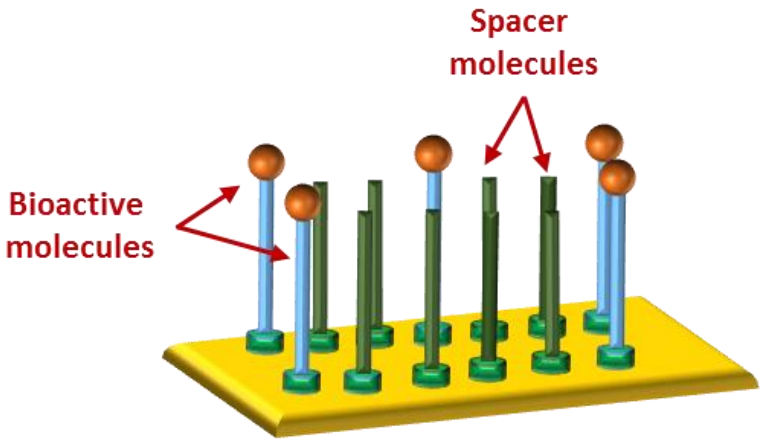

Figure 1.7 – *Cartoon representation of a mixed SAM*

This is due to backbone interactions between the molecules composing the mixed monolayer, but also to solvent-surfactant interactions that lead to the preferential adsorption of one of the components onto the surface[83,87,123,124]. In addition, the phase separation phenomenon can limit the formation of homogeneously-ordered mixed SAMs[119,125–128]. This event does not allow the mixed SAM components to bind to the surface showing a specific distribution[119,129]. The gold-thiolate interface can be considered motile, as demonstrated by several studies[130,131]. These studies showed that thiol molecules can diffuse on gold surfaces and exchange their position with another thiol. In particular, mixed alkanethiol SAMs can arrange into discrete domains at a diffusion rate independent from the alkanethiol chain length[132]. By carefully tailoring the composition of the mixed SAM, it is possible to overcome these limitations and control the exposure of active molecules on the surface, which can be used to control several biological and chemical interactions (e.g. separation of molecules[133],

specific biomolecular interaction[134]) and fabricate sensitive biosensors (e.g. immunosensors[135]).

1.3.3.1 Unspecific protein adsorption

As already stated in the previous sections, SAMs can be exploited to build sensitive molecular recognition systems. To obtain devices with optimum performances, the non-specific adsorption of unwanted molecules onto the substrate surface has to be reduced. These undesired molecules can hinder or block the binding sites on the active molecules composing the monolayer, reducing the efficiency of the biorecognition system. Non-specific binding can either increase the background noise, or give a "false positive" response[136]. Mixed SAMs are particularly appropriated for this purpose. By selecting the chemical functions on the surfactant molecules, it is possible to decrease the amount of unspecific binding. Several studies have been conducted on the use of oligo(ethylene glycol) (OEG)-terminated SAMs to suppress protein unspecific binding[136–138]. Prime and Whitesides, in 1993[137], studied the adsorption of four proteins on different SAMs on gold. Alkane-thiols, alkyl-alcohol thiols and oligo(ethylene glycol)-thiols were investigated. The latter monolayer was the only one able to resist the adsorption of all the four proteins tested. OEGs can therefore be used in numerous biological applications where unspecific protein adsorption has to be prevented[134,136]. The ability of OEGs SAMs to create a high surface coverage, make them able to resist non-specific protein adsorption.[137,139] These molecules are therefore often used as one of the surfactants composing multicomponent SAMs. By varying the ratio of OEGs molecules and bioactive molecules, it is possible to control the spatial distribution. This spatial control allows the best interaction between the bioactive surfactant and the target molecules of interest. In addition,

the length of OEGs chains and the number of ethylene glycol units affect the capability of OEGs SAM to block protein adsorption. OEG alkanethiols monolayers formed by $(CH_2)_{11}$-$(OCH_2CH_3)_n$-OH (EGn) chains, where n<3, are inefficient in suppressing protein adsorption[140,141]. The protein-repellent characteristics are due to the presence of strong repulsive forces between OEGs SAMs and proteins. Thanks to the presence of several oxygen atoms in the ethylene glycol units, these monolayers can form hydrogen bonds with water molecules. This interaction creates a hydrophilic layer that repels proteins as a result of the repulsive hydration forces action[141,142]. However, the presence of ethylene glycol thiol molecules does not have to block specific protein binding with bioactive molecules when needed.

1.3.3.2 Specific protein adsorption

In the case of protein affinity studies on surfaces, the receptor molecules composing the mixed SAM must interact in a specific manner with the protein of interest. Theoretically any protein-receptor system can be studied on such mixed architectures, but the most widely explored are the avidin-family proteins binding to biotin (receptor). This system has been used for several years in various application in biotechnology[143], such as immunoassays[143–147], biosensors[148], tissue engineering[149,150] and drug delivery[151,152]. All these systems exploit the high affinity and specificity between biotin and the avidin-family proteins. However, avidin also presents high non-specific binding[153], therefore streptavidin[154–156] and Neutravidin[157–159] are preferred. Avidin-family proteins are tetramers with a mass between 50 and 70 kDa, composed of four identical subunits, exhibiting extremely high binding affinity to biotin, with dissociation constants K_D on the order of $\approx 10^{-14}$-10^{-15} mol/L and forming a stable complex at different temperatures and pH values[153] (**Figure 1.8**).

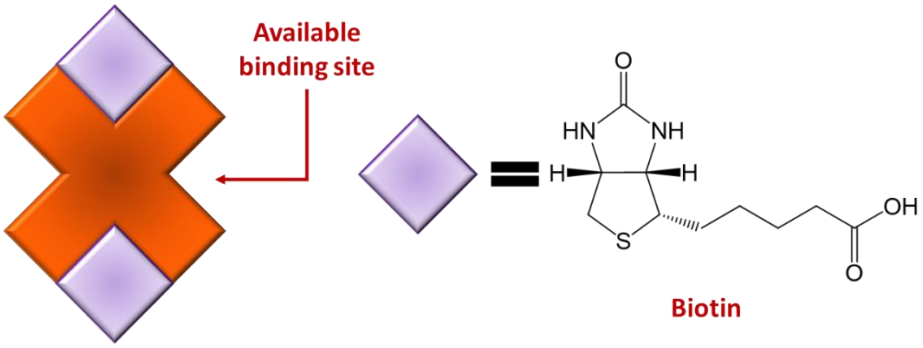

Figure 1.8 – *Cartoon representation of biotin binding to two of the four binding sites of the avidin family protein*

Avidin is a positively charged protein, that can interact with negatively charged substrates, such as silica based substrates[159] or cells membranes[153]. The isoelectric point of avidin is unusually high[153] (pI≈10) and the presence of carbohydrate moieties, formed by four mannose and three *N*-acetylglucosamine molecules per subunit, may explain why avidin is prone to high non-specific binding[160]. Neutravidin is a deglycosylated form of avidin, with a lower isoelectric point (pI≈6.3), whereas streptavidin is a non-glycosylated protein with a more acidic isoelectric point (pI≈5.6)[153].

Another type of specific binding widely studied in biotechnology is the antigen-antibody interaction[161,162]. Antibody-based biosensors[163] give the possibility of a rapid and sensitive detection of heavy metal ions[164], proteins blood levels[165–167], allergens[168] and pathogens[163,169]. Immunosensing exploit the immune system of a host (i.e. murine, leporine, ovine or avian), by injecting the molecules or cells of interest into the host's body, triggering an immune response. The immunoglobulins (IgG) produced by the host animal are collected after several immunisation processes. They present a structure composed by two heavy chains and two light chains[170] (**Figure 1.9**).

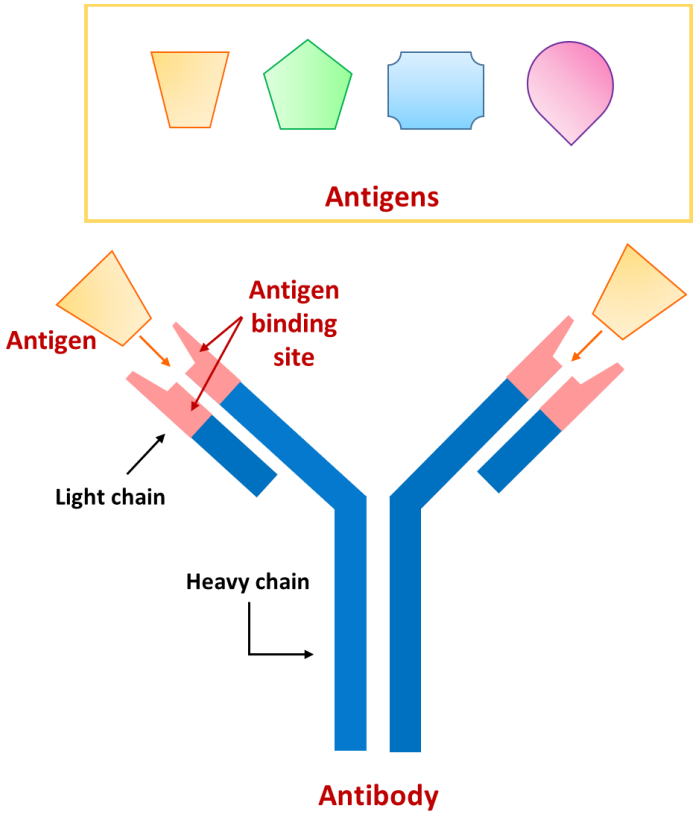

Figure 1.9 – *Schematic representation of an antigen-antibody system. Several antigens are available for binding, but only one is specific for the antigen binding site on the antibody chains*

Different types of antibodies can be produced: polyclonal, monoclonal and recombinant. Polyclonal antibodies (pAb) are usually produced using rabbits, goats or sheep as hosts[171] and frequently used in sensors for pathogens detections. Polyclonal antibodies recognise different epitopes on a single cell, therefore, when high specificity is required, the use of monoclonal or recombinant antibodies is preferable. Monoclonal antibodies (mAb) are produced using the hybridoma technology and mice are the most common used hosts. The spleen, together with the bone marrow and primary lymph nodes are employed as a source of B cells to obtain antibodies that are then fused to immortal myeloma cells[171]. The resulting

hybrid cells (hybridomas) secrete antibodies that recognise a single epitope on a single cell. Recombinant antibodies are prepared by using phage-display technology and antibodies libraries against the target of interest to achieve the detection of numerous antigens, including proteins, haptens and carbohydrate moieties[171].

Both biotin-neutravidin and antigen-antibody systems will be developed in this research work and will be described in detail in Chapter 3 and Chapter 4.

1.3.4 Dynamic SAMs

In recent years, researchers have focussed their studies on the development of stimuli-responsive surfaces. Such surfaces can be obtained by changing the end group and/or the backbone of the surfactant molecules composing SAMs, to create moieties presenting switchable/dynamic characteristics[1,172–175]. These tunable moieties can respond to a wide range of stimuli, such as temperature (thermo-responsive surfaces)[176–182] , light (photo-responsive surfaces)[183–185], pH and concentration (chemical/biological stimuli-responsive surfaces)[186–191], magnetic field (magneto-responsive surfaces)[192,193] and electrical potential (electrical-responsive surfaces)[10,194–199]. Smart surfaces have gained paramount importance due to the possibility to obtain a high spatial and temporal control, a rapid response and to be used in a wide range of biological and biomedical applications. To date, switchable surfaces have been employed in drug delivery[179,181], to control specific and unspecific protein binding[196,197] and mammalian and bacterial cell attachment and detachment[10,182,195,198–200], but also in tissue engineering[201,202] and regenerative medicine[200,203]. The application of an external stimulus results in a switch that can be either chemical or conformational (**Figure 1.10**).

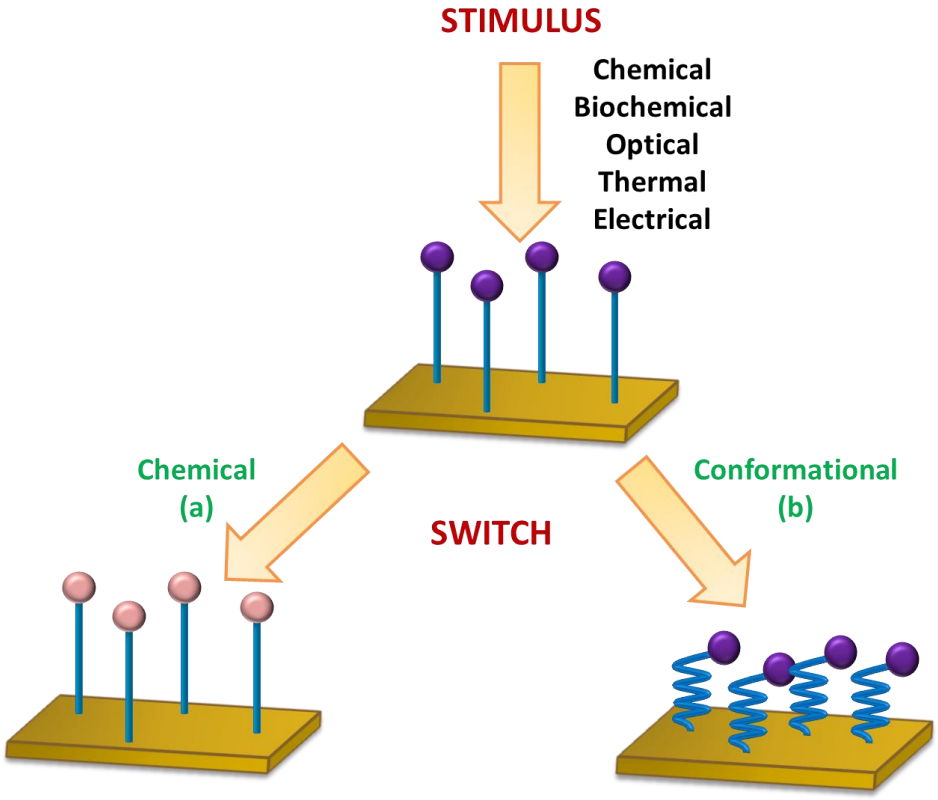

Figure 1.10 – *Schematic of the possible switches that can be obtained upon the application of a stimulus. a) Chemical switch: the chemical composition of the monolayer varies when an external stimulus is applied (e.g. a change in pH). b) Conformational switch: the chemical composition of the monolayer remains the same, while its conformation varies when an external stimulus is applied (e.g. application of an electrical potential).*

In the case of conformational switching, a high control of the monolayer spatial order must be achieved. Conventional SAMs (i.e. alkanethiols SAMs) are too high-density to allow conformational changes, therefore the switching is hampered[204]. Each molecule must possess enough spatial freedom, as shown by Lahann and co-workers in their study[205]. They designed a surface which wettability can be dynamically changed. Firstly, a low-density 16-Mercaptohexadecanoic acid (MHA) SAM was created on a gold surface. MHA molecules

create well-ordered and highly-packed SAM on gold, presenting both a hydrophobic alkyl chain and a hydrophilic carboxylate end group. Therefore, to give the monolayer enough space on the surface to undergo a conformational switch, a globular end group (spacer) was linked to the carboxylate moieties, prior of MHA SAM formation. The result is a monolayer with a low-density molecular distribution on the substrate. After the removal of the globular spacer by hydrolysis, a negatively-charged SAM is obtained that can then be exploited to induce a dynamic conformational change of MHA molecules. Upon the application of a positive electrical potential, the negative carboxylate groups are attracted towards the gold surface. This molecular change causes the exposure of hydrophobic alkyl chain, changing the wettability and making the surface hydrophobic overall. The process can be reversed by simply applying a negative electrical potential, causing the repulsion of the carboxylate end groups from the gold surface and creating a hydrophilic surface.

Another important research work was conducted by Liu and co-workers[206] starting from the findings of Lahann's group[205]. A low-density SAM (LD-SAM) was created on gold surfaces, by assembling MHA molecules pre-capped with cyclodextrins (CD) of different dimensions, covalently linked to the carboxylic end groups. The LD-SAMs created after removing the CD-caps, where used to selectively control the attachment of two proteins (avidin and streptavidin) in a reversible manner over the surface, by applying an electrical potential. When a negative potential is applied, the carboxylate groups are fully exposed on the surface and the positively charged avidin is adsorbed to the surface, whereas the negatively charged streptavidin, shows an opposite behaviour. Streptavidin was also used to demonstrate a similar adsorption and release process on an amino-terminated LD-SAM (**Figure 1.11**).

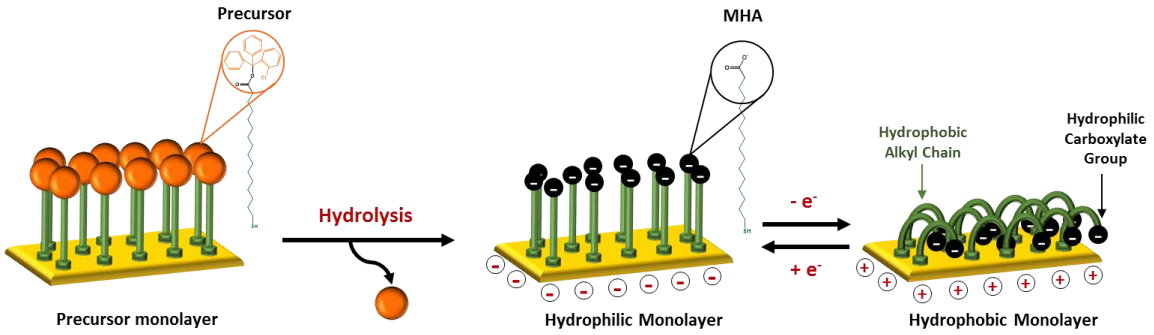

Figure 1.11 – *Illustration of the formation and switching of a LD-SAM by employing a precursor molecule presenting a bulky head-group. Upon the application of an electrical potential the monolayer can reverse its wettability by switching between hydrophilic and hydrophobic states.*

In addition, Liu and co-workers demonstrated that the application of an electrical potential has no effect on protein adsorption for high-density (HD) SAMs, due to the steric hindrance that hampers the bending of the alkanethiolate molecules on the surface. Starting from the pioneering work of Lahann and Liu, several studies have been conducted on the development of smart surfaces[10,173,207–209]. This thesis research work will focus only on the use of electrically switchable surfaces, which will be described in the next section.

1.3.5 Electrically-switchable SAMs

Electrically-switchable surfaces have gained increasing interest during the past decade since it allows control over the interaction between surfaces and peptides[173], proteins[206,208], DNA[210] and cells[173,199]. The rapid response to an electrical stimulus is fundamental for many vital cellular signalling pathways in the body, e.g. the voltage-dependent of sodium and

potassium currents across cell membranes, triggered by an electrical signal coming from the nerves[211,212] and necessary for a correct functioning of the nervous system.

Researchers have been combining the observation of natural processes with advanced biotechnological techniques to fabricate switchable architectures that can control processes at the micro- and nanoscopic scale and mimic complex cellular mechanisms. An interesting label-free method to control and analyse the interactions between proteins and ligands on the surfaces was presented by Knezevic and co-workers in 2012[213]. In this system, negatively charged DNA strands ("levers") tethered to a gold surface, were functionalised at the top end with a cyanine 3 (Cy3) dye. When a positive potential of +0.3V was applied, it caused an attraction of the negatively charged lever toward the substrate, causing a reduction in fluorescence emission from the dye, caused by the quenching effect of the metal surface. On the contrary, when a negative potential of -0.5V was applied, it caused the repulsion of the DNA strands from the surface, exposing the Cy3 dye molecules, therefore increasing the fluorescence emission. By measuring the fluorescence emission, it is possible to calculate the distance between the DNA's top end and the substrate. When the DNA lever is functionalised with a protein at its top end, it is possible to quantify the binding kinetics (K_{on}, K_{off} rate constants), the dissociation constant (K_D in picomolar regime) and the influence of competitive binders (EC_{50} values). In this case, there is a delay behind the dynamics of the bare level, due to the presence of a hydrodynamic drag occurring when a protein is bound to the DNA's distal end (**Figure 1.12**).

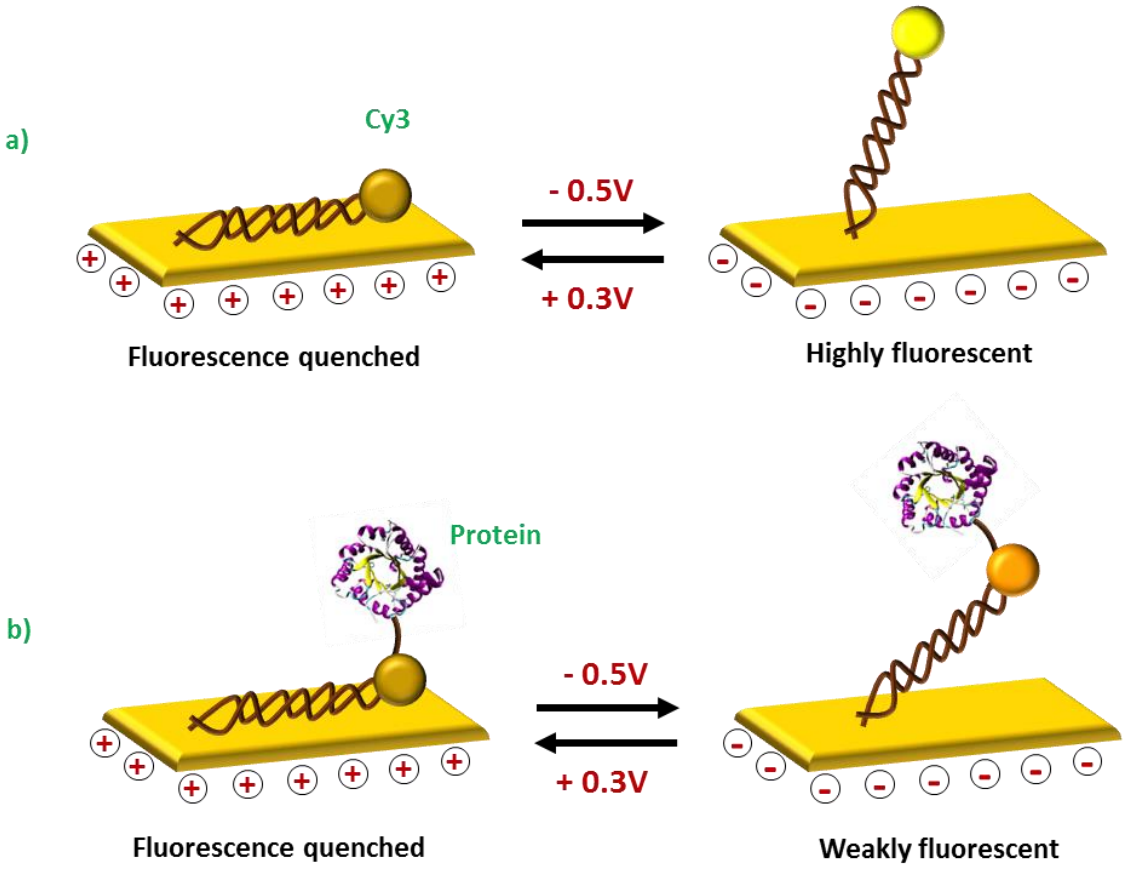

Figure 1.12 – *Schematic representation of the DNA lever; a) lying on the surface when a positive potential is applied and repelled when a negative potential is applied, fully exposing the fluorescent dye. b) When a protein is linked to the DNA's top end, the upward motion is slowed and lags behind the bare lever. The dark yellow circle represents the Cy3 dye when the fluorescence is quenched by the gold surface. The bright yellow circle corresponds to a high fluorescence emission, due to the DNA molecule carrying the fluorophore being fully extended on the surface.*

In addition, this method allowed the calculation of the protein diameter with angstrom resolution, by analysing the time-resolved upward dynamics, but also to collect information about the avidity effect and discriminate between analytes presenting multiple binding sites.

An excellent contribution to the development of electrically-switchable surfaces was given by our group. In the first work[196], switchable surfaces where created by preparing a mixed SAM on gold surfaces, composed by oligopeptide molecules that can undergo reversible molecular changes upon the application of an electrical potential and molecules of triethylene glycol thiol (TEGT) acting as lateral spacers to space out the switchable backbone such that the conformational changes are not hampered by steric limitations. The dynamic oligopeptide is formed by a chain of four positively-charged lysines (4K) linked to a molecule of biotin at the top end and to a cysteine (C) at the bottom end for the tethering to the gold surface. The bioactive molecule (biotin), can be reversibly exposed (ON state) or concealed (OFF state) by applying an electrical potential to the gold surface (**Figure 1.13**).

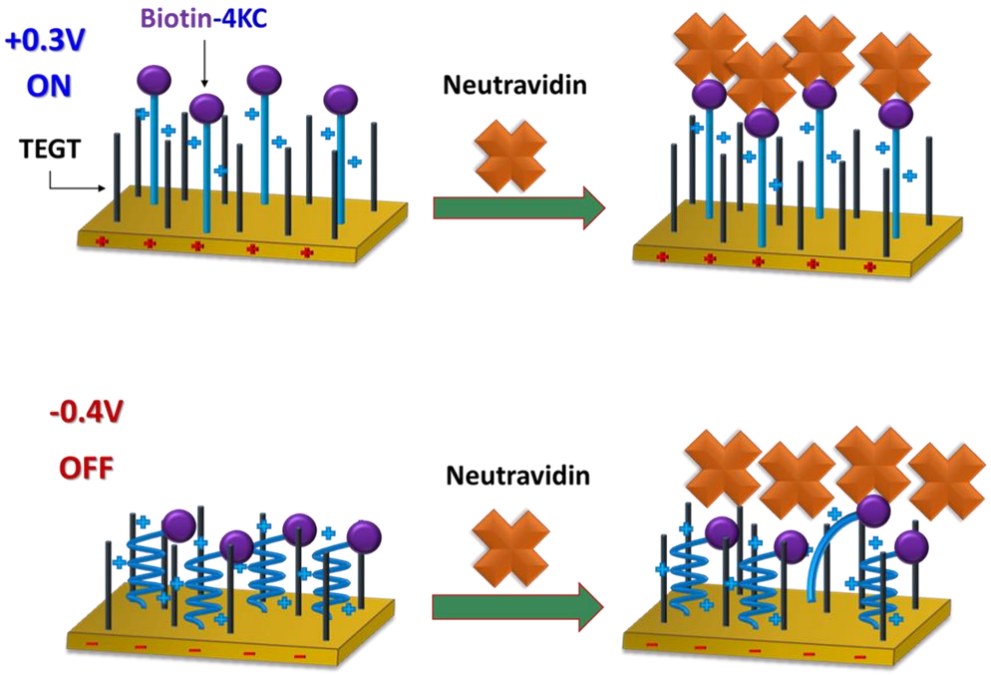

Figure 1.13 – *Schematic representation of the switching of Biotin-4KC:TEGT mixed SAM upon the application of an electrical potential.*

The dynamics of the molecular changes were followed in real-time using surface plasmon resonance (SPR) and fluorescence microscopy, to study the specific binding between biotin and fluorescently labelled Neutravidin[196]. When a potential of +0.3V was applied, high Neutravidin binding was observed both by SPR and by recording an increase in fluorescence, meaning that the biotin moiety is fully exposed on the surface and the interaction with the protein is maximised. On the other hand, when a negative potential of -0.4V is applied, the charged backbone collapses on the surface and the biotin moiety are hindered by the ethylene glycol-terminated thiol molecules and the interaction with Neutravidin is minimal. The bio-inactive state leads to more than 90% reduction in protein binding. The biotin-4KC:TEGT mixed SAM surface was further developed in this research work and experimental studies were also conducted on a shorter (biotin-2K) and longer (biotin-6KC) oligopeptides to study the influence of the length of the charged backbone on switching. The findings will be illustrated in Chapter 3.

In 2013 Pranzetti et al[10,195], tested the use of switchable surfaces to analyse bacterial adhesion by forming a two-component SAM of 11-mercaptoundecanoic acid (MUA) representing the switching unit and the backfiller mercaptoethanol (MET) that can reversibly change its wettability upon the application of an electrical potential. By varying the potential in cycles, between +0.25V, OC (no applied potential) and -0.25V, it was possible to follow the interaction of the mixed SAM with the hydrophobic marine bacterium *Marinobacter hydrocarbonoclasticus* (*Mh*) (**Figure 1.14**).

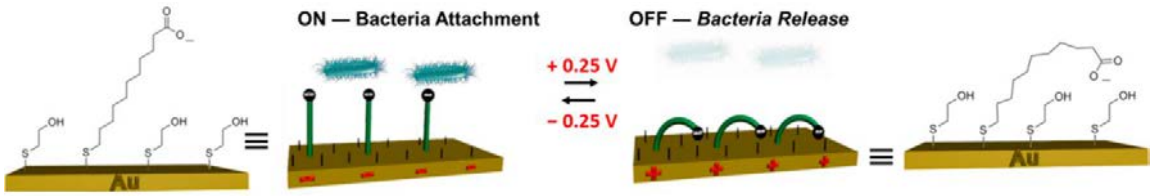

Figure 1.14 – *Cartoon representation of the control of bacteria cells adhesion by switching a MUA:MET mixed SAM.*

When a positive potential was applied, the carboxylate groups on MUA were attracted toward the substrate, exposing the hydrophobic alkyl chains, causing the repulsion of bacteria. It was demonstrated that the attachment of cells can be reversed by moving from a negative potential to a positive one, but the increase of the number of ON/OFF cycles reduce the reversibility of the process. In addition, it was shown that a pure SAM of MUA is not affected by the change of the surface potential.

The studies described above were conducted in limited biological conditions, phosphate buffer saline (PBS) solution was used to analyse the interaction between biotin and Neutravidin, whereas artificial seawater was used in the case of monitoring bacterial adhesion. Starting from the encouraging results obtained in simple media, Lashkor et al.[198] investigated whether more complex biological conditions can affect the efficiency of the induced conformational changes. The switching of biotin-4KC mixed SAMs with various ethylene glycol-terminated thiols was investigated, by electrochemical SPR in real-time, in different media commonly used for cell and tissue culture, namely Dulbecco's modified Eagle's medium (DMEM) containing a mixture of inorganic salts, amino acids, glucose and vitamins, DMEM containing 10% foetal bovine serum (DMEM-FBS) and DMEM-FBS with (4-(2-hydroxylethyl)-1-piperazineethanesulfonic acid) HEPES buffer (DMEM-FBS-HEPES). The results showed that,

when the spacer is a longer ethylene glycol thiol (11-carbon TEG-terminated thiol, C11TEG), the surface is more resistant to non-specific binding coming from the medium, but the switching efficiency is reduced in PBS if compared to the biotin-4KC:TEGT tested before. However, the high protein resistance, make this mixed SAM suitable for the creation of systems that have to operate in complex biological conditions. The dynamic changes were then monitored in the three different media indicated above. From the results, it is possible to infer that both FBS and HEPES both interfere with the switching process, by interacting with the oligopeptide chains on the surface, but the presence of DMEM reduces the antagonistic effect. By diluting the media solutions, the switching efficiency increases, meaning that by carefully controlling the complex biological conditions it is possible to exploit charged oligopeptide chains to achieve maximum conformational changes. After having demonstrated the feasibility of conformational transitions in complex media, the study was developed further to investigate cell adhesion on dynamic SAMs. Putting together the findings of the previous studies, Lashkor et al. developed an arginine-glycine-aspartate (RGD) oligopeptide-based surface[199], able to regulate cell adhesion. RGD is a tripeptide commonly present in the majority of the adhesive proteins on the extracellular matrix and it is specific for integrin-mediated cell adhesion. The switching unit was constituted by a 3-lysine oligopeptide (C3K) functionalised with a glycine-arginine-glycine-aspartate-serine (GRGDS) recognition unit to obtain a C3K-GRGDS:C11TEG mixed SAM on gold substrates. The switching performance was followed by electrochemical SPR using DMEM as medium. When a negative potential was applied (-0.4V), the oligopeptide switching unit was in a collapsed conformation on the surface, hampering cell adhesion. If the conformation/orientation of the RGD peptide is altered upon the application of an electrical potential, it is possible to regulate the exposure and availability of RGD sites for cell surfaces receptors. However, it is not possible to perform switching cycles from adhesive- to

resistant-state, as in the case of bacteria adhesion[195] described before, due to the cell attachment being directed by multiple RGD-integrin bonds in parallel.

Understanding the mechanisms of dynamic changes on the surface is of paramount importance to have a complete insight into the molecular reorganisation that occurs when an electrical stimulus is applied. Two fundamental techniques that can provide numerous information about the switching process are molecular dynamics (MD) simulation and sum-frequency generation (SFG) spectroscopy, the former have been used in this research work in collaboration with Nanjing University (China) and will be described in Chapter 3. SFG was used by Pranzetti et al[194] to study the orientation of biotin moieties on the surface in the biotin-4KC:TEGT mixed SAM. Such technique exploits IR overlapped to visible laser pulse to excite the vibrational states in the molecules of interest and allows the measurement of SFG spectra. By using a special electrochemical cell, it was possible to monitor in real-time the changes occurring on the surface when a positive (+0.3V) and a negative (-0.4V) potential were applied and characterise a molecular vibration associated with the biotin moiety in the mixed SAM. When a positive potential is applied, the switching backbone is fully extended on the surface, exposing biotin in an anisotropic upright orientation resulting in a dip of the biotin vibration within isotropic biotin orientation and a very weak SFG peak is recorded.

1.4 Application of switchable surfaces to the selection of sperm cells for *in-vitro* fertilisation (IVF) techniques

Male infertility is the male's inability to induce pregnancy in a fertile female[214] and it affects the 7% of men[215]. Infertility is commonly due to abnormalities in semen quality[215,216] that can be either caused by age[217], lifestyle[218,219], oxidative stress[220], autoimmune reactions[221]

or genetic problems[222]. One of the genetic factors leading to infertility in males, is the incorrect expression of genes coding for the calcium channels CatSper. These channels are a family of sperm-specific cation channels[223], composed by four pore-forming channel proteins, CatSper 1-4, and three subunits, CatSperβ, CatSperγ and CatSperδ, which control the calcium ion (Ca^{2+}) influx, required for hyperactivation[224–227]. CatSper are permeable channel proteins located on the plasma membrane of spermatozoa[228,229]. Blocking these channels in knockout spermatozoa lead to an impairment of normal sperm function[223,225]. The opening of the calcium channels is regulated by the interaction between sperm cells and progesterone[230]. Therefore, sperm cells that are able to respond to progesterone will then acquire the ability to fertilise the female egg[231,232].

Progesterone, is a steroid hormone, released by cumulus cells surrounding the oocyte in the female oviduct[230,233]. The release of progesterone activates the CatSper channel and therefore the calcium influx into the sperm flagellum[234,235]. When good quality sperm cells interact with progesterone, they undergo a change in their flagellar activity, moving from symmetric to asymmetric[232,236]. If one of the genes coding for one of the CatSper subunits is suppressed, the sperm cells are unable to start the Ca^{2+} influx in response to progesterone and acquire their fertilisation state[226,237]. It has been demonstrated that in both human and mice, all the four subunits composing the CatSper channel are needed for a successful control of spermatozoa hyperactivation, chemotaxis and acrosome reaction[238–240].

When spermatozoa fail to achieve fertilisation naturally, *in-vitro* fertilisation (IVF) methods are necessary to help couples in conceiving[241,242]. Two methods are generally used: the first one is standard IVF, where, after the stimulation of the female ovulation, an egg or eggs (ovum or ova) are removed from the woman's ovaries and incubated with sperm in an

adequate medium, in a laboratory[241,243]. The fertilised eggs (zygotes) are then cultured for 2-6 days in a growth medium and then implanted in the woman uterus[241]. The second method used is intracytoplasmic sperm injection (ICSI), similar to the standard IVF procedure, with the only difference that a single sperm is injected directly into a female egg[241,244]. However, these helpful and advanced procedures are not free from potential risks, such as miscarriage and genetic problems in the foetus[245,246]. The genetic risks are more probable in ICSI than IVF, because sperm cells are selected only by morphological assessment[247]. The UK IVF techniques success rate in 2010 was 32.2% for women aged under 35 and 27.7% for women aged between 35-37 (source NHS). Since the introduction of ICSI methods, no important advancements have been made in the development of diagnostic tools able to select good sperm cells, not carrying genetic dysfunctions. Therefore, the development of a platform able to dynamically reveal or hide progesterone molecules upon the application of an electrical potential, to select responsive sperm cells, would be of paramount importance in both improving the success rates and reducing the risks of IVF techniques.

1.5 Concluding remarks

Several successful studies have been reported in the literature, about the use of switchable surfaces able to respond to the application of a wide range of external stimuli (i.e. thermal, chemical/biological, electrical) and already applied in numerous biological and medical applications. Such surfaces enable the control of specific biomolecular interactions and the modulation of cellular response[193], giving a crucial contribution to biotechnology in the understanding of relevant complex biological processes. To create effective dynamic surfaces, it is of paramount importance to perform a careful study of the desired characteristics in the

smart architectures, such as end groups, molecular spacing, dynamic backbones, and to understand if they are affected under complex biological conditions. This will allow the creation of devices that can closely reproduce natural processes and fully realise their potential.

To date, important progress has already been made in this stimulating research field. Novel platforms with biomimetic features have been created that can offer valuable contributions in the enhancement of clinical methods[1,173,174].

1.6 PhD aim

The aim of this PhD is to design and fabricate novel switchable surfaces, able to selectively control specific binding of biomolecules on the surface and from then recreate the successful switching surface on a micropattern, to achieve the control of calcium signalling in human sperm cells.

The steps needed to achieve this aim are the following:

1) Fabricating mixed SAMs to control biomolecular interactions between biotin and Neutravidin studying the switching efficiency of a biotin-4KC:TEGT at different ratios in Phosphate Saline Buffer medium (PBS), upon the application of an electrical stimulus. Then, investigate the role of the switching unit length on the molecular motion on the surface, by analysing the switching efficiency of a shorter (biotin-2KC) and a longer (biotin-6KC) oligopeptide. The switching systems will be also analysed by Molecular Dynamics (MD) to have a deeper insight into the molecular dynamics. This investigation will provide a better understanding of the relationship between the surfactant backbone and switching efficiency (**Figure 1.15**).

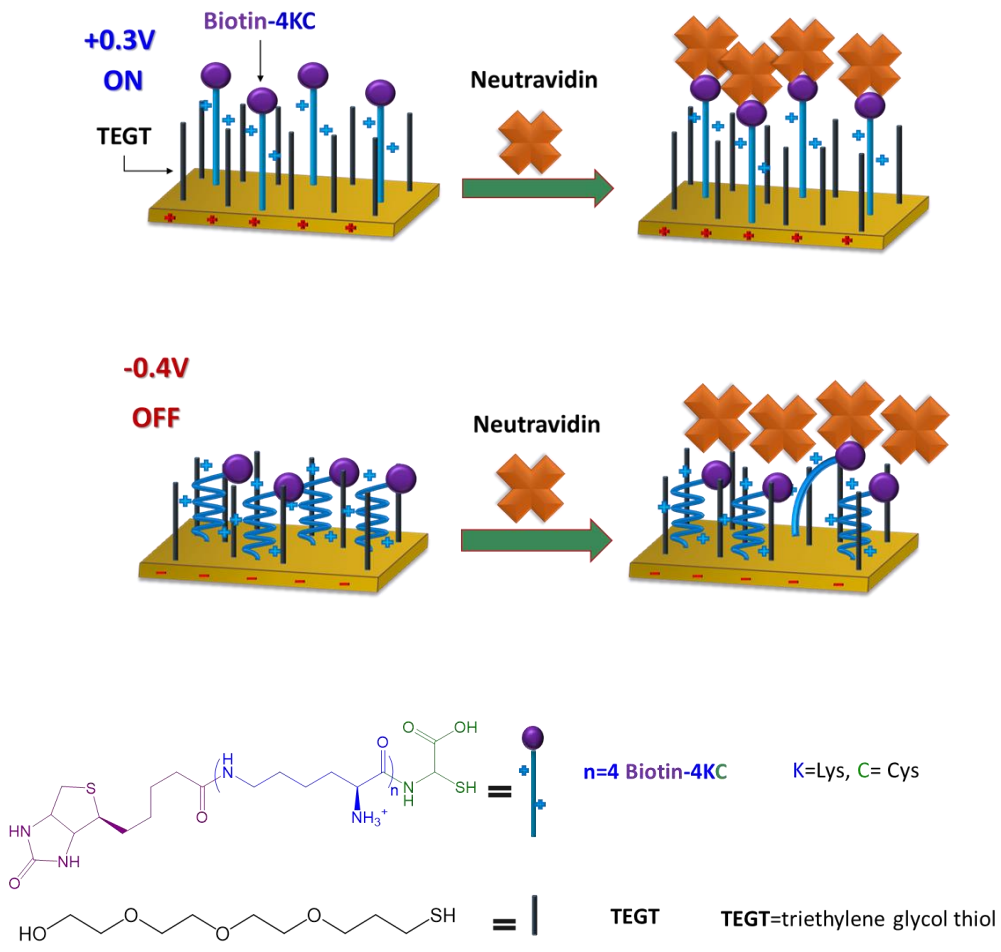

***Figure 1.15** - Molecular structures and related cartoons of the oligopeptide Biotin-4KC and the triethylene glycol-terminated thiol (TEGT) used in the mixed SAMs.*

2) Fabricating mixed SAMs to control biomolecular interactions between progesterone and its murine monoclonal antibody (mAb) by studying the switching efficiency of a Progesterone-C7-4KC:EG6OH mixed SAMs in both Phosphate Saline Buffer medium (PBS) and Earle's Balanced Salt Solution (EBSS), upon the application of an electrical stimulus. This investigation provides a better understanding of the feasibility of the exposure control of Progesterone on the surface, needed to then control the activation of the calcium signalling in human sperm cells (**Figure 1.16**).

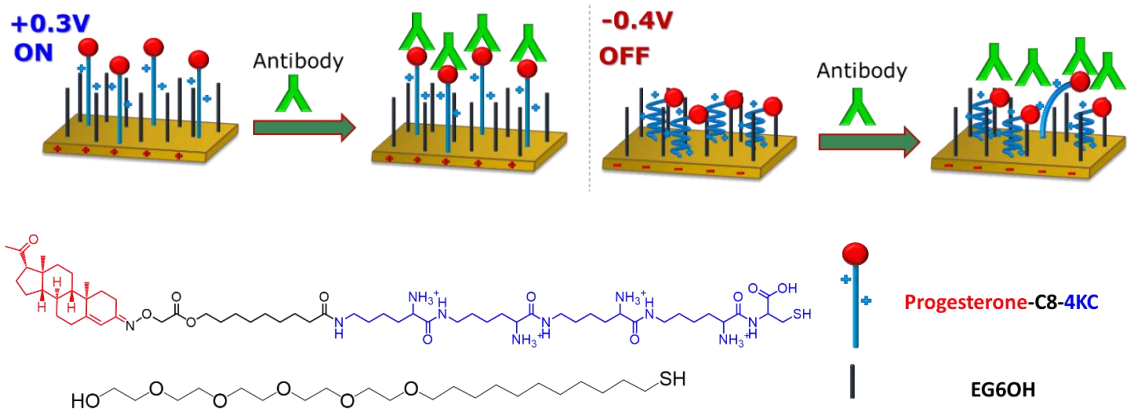

Figure 1.16 – *Cartoon representation of the switchable system (top), molecular structures and related cartoons of the oligopeptide (progesterone-C7-4KC) and the hexaethylene glycol-terminated thiol (EG6OH) used in the mixed SAMs (bottom).*

3) Perform preliminary studies on the feasibility of an orthogonal functionalisation of gold and glass surfaces to create a switchable system, composed by Progesterone-C7-4KC:EG6OH mixed SAMs on gold and silane-poly-D-lysine (silane-PDL) layers. Study sperm cells attachment on silane-PDL layers to set the starting point for the development of an innovative switchable system able to monitor sperm cell response to progesterone in real time.

Chapter 2: Surface Characterisation Techniques

Abstract: *This chapter briefly describes the surface characterisation techniques commonly used in the analysis of surfaces. To design highly-ordered surfaces, it is of predominant importance to understand the chemical and physical properties of a SAM through a detailed and precise characterisation. The overall information about a specific surface is the sum of several data collected using different techniques, each of which is important to achieve a complete and accurate understanding of the different aspects of the surface analysed. Such techniques include contact angle measurements, ellipsometry, fluorescence microscopy, X-ray Photoelectron Spectroscopy (XPS), Surface Plasmon Resonance (SPR) and electrochemical techniques.*

2.1 Contact Angle

Contact angle is a surface characterisation technique, used to evaluate the hydrophilicity/hydrophobicity of a surface by using a droplet of a liquid (usually water) deposited onto the investigated surface. A contact angle goniometer consists of a light source to illuminate the surface, a stage to hold the surface, a syringe filled with a liquid and a camera connected to a computer for measuring contact angle values (**Figure 2.1**).

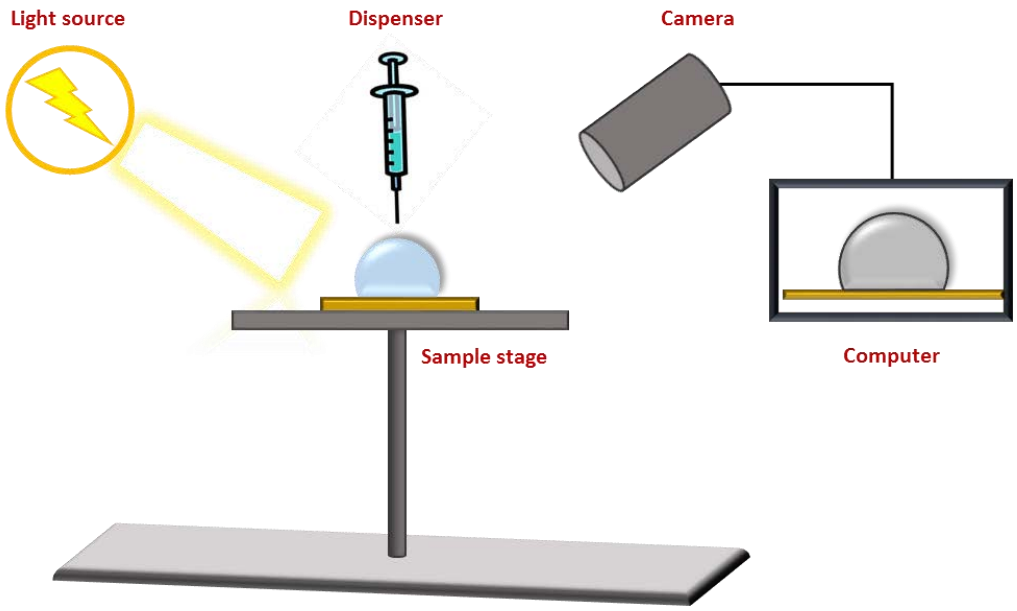

Figure 2.1 – *Schematic representation of a contact angle goniometer*

The contact angle is calculated using Young's equation (**Equation 2.1**)

$$\gamma_{SV} = \gamma_{SL} + \gamma_{LV}\cos\theta$$

Equation 2.1

Where γ is the surface tension (or surface free energy) and γ_{SV}, γ_{SL} and γ_{LV} are the surface tensions for solid-vapour, solid-liquid and liquid-vapour interfaces, respectively[248]. When a droplet of liquid is deposited onto a surface, the three surface tensions are in equilibrium, as showed by **Equation 2.1** and expressed by the calculated contact angle. When a surface possesses a hydrophilic character, the surface energy is high, and the droplet spreads onto the surface to minimise this energy. This results in a low contact angle (<30˚). On the contrary, when a surface possesses a hydrophobic character, the surface energy is lower, and the droplet does not spread onto the surface, resulting in a higher contact angle (>90˚) (**Figure 2.2**).

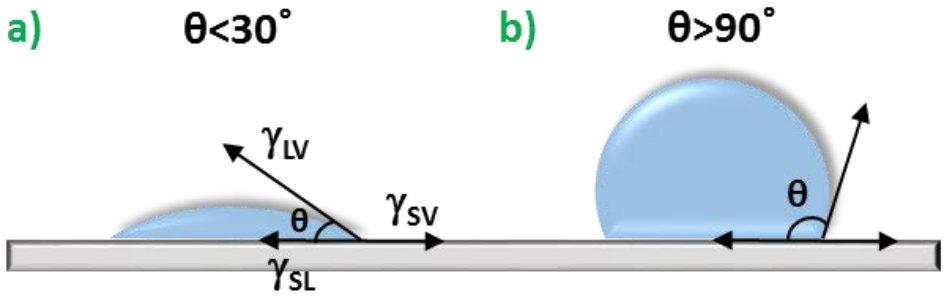

Figure 2.2 – *Representation of contact angles (**θ**) formed by sessile liquid drops on a solid surface. Representation of a) a hydrophilic surface and b) a hydrophobic surface.*

The contact angle can be measured using two different methods: static and dynamic contact angle. In the static method, a droplet of liquid is deposited onto the surface, the contact angle is measured while the droplet volume remains constant. In the dynamic method, many droplets of liquid are deposited onto the surface dropwise, forming one larger drop on top of it, which is then withdrew using a needle. The advancing contact angle (θ_a) is measured during the addition of the liquid, and the receding contact angle (θ_r) is measured during its withdrawal (**Figure 2.3**).

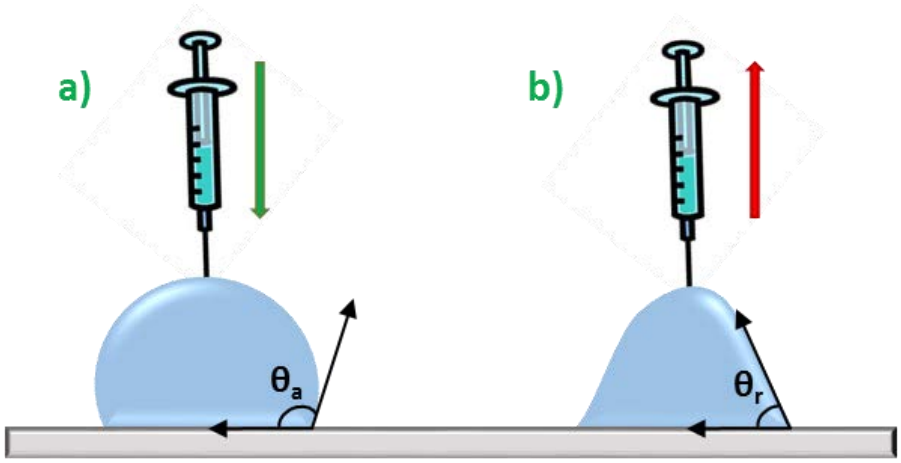

Figure 2.3 – *Schematic representation of a) advancing (θ_a) and b) receding contact angle (θ_r) used in the dynamic contact angle measurements.*

The difference between the advancing and receding angle (θ_a-θ_r) is called contact angle hysteresis (θ_h) and gives indications about the homogeneity of a surface. A small hysteresis (<5˚) indicates that the surface is homogenous and well-ordered, whereas a large hysteresis suggests the surface is contaminated, non-homogenous and/or relatively rough[249].

2.2 X-ray Photoelectron Spectroscopy

XPS is a surface-sensitive quantitative technique, exploited to analyse the elemental composition (for the top 0-10 nm of a surface), the empirical formula, and the chemical and electronic states of elements composing a material[250]. The first high-energy-resolution XPS spectrum was recorded in 1957 by Kai Siegbahn and co-workers at University of Uppsala[251].

This technique uses an electromagnetic source to eject electrons from the analysed sample[252] in an ultra-high vacuum (UHV) environment.

An XPS apparatus comprises an ultra-high vacuum chamber where the sample is placed, an X-ray source, an electron collection lens, an electron energy analyser, an electron detector and a computer where the XPS peaks are visualised (**Figure 2.4**)

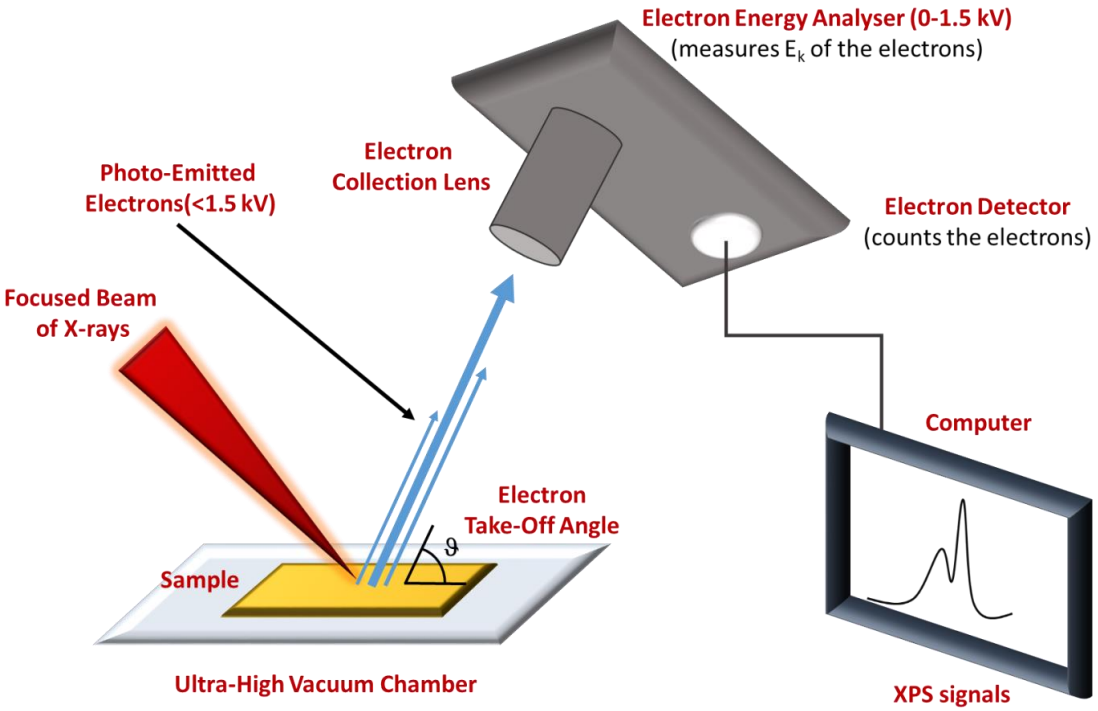

Figure 2.4 *- Cartoon representation of a XPS apparatus*

When an X-ray photon (hν) interacts with an electron in the **K** shell, a 1s photoelectron is emitted from the surface, as a result of atoms being ionised. Subsequently, an electron from a higher energy level (**L**) fills the created vacancy in the inner-shell, leading either to X-ray fluorescence photoemission process (XPS) or radiationless process of Auger electron emission, consisting in the de-excitation and emission of a higher-shell electron (**Figure 2.5**)[250,252,253].

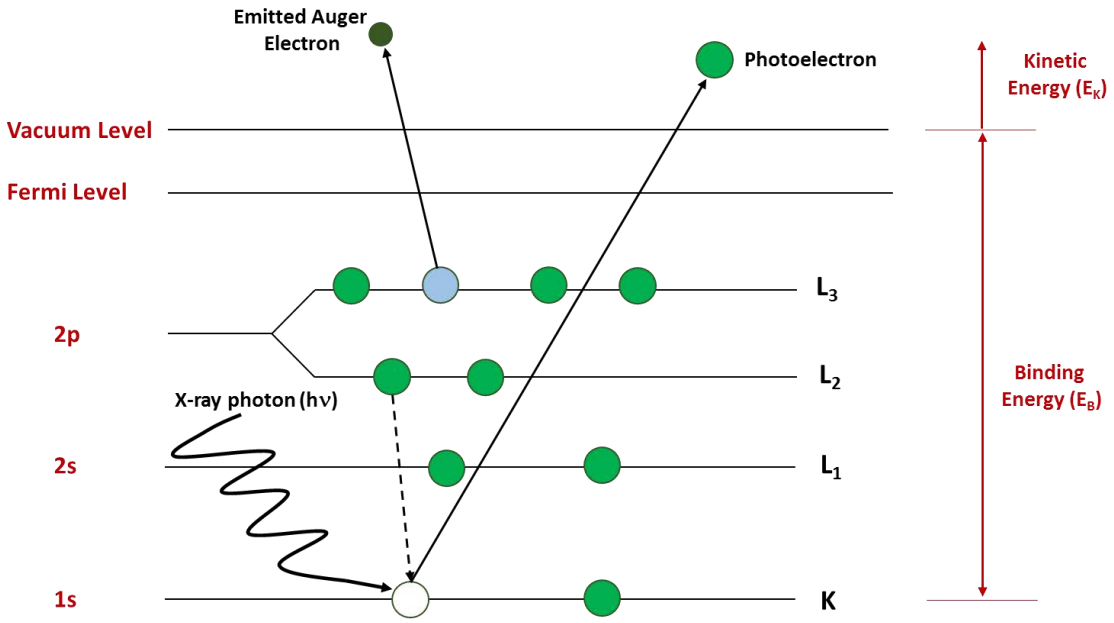

Figure 2.5 – *Schematic diagram of XPS process for a photoelectron emitted from the core energy level. The subsequent relaxation process of an electron from a higher energy level (dashed arrow) fills the created vacancy (white circle), resulting in the emission of an Auger KLL electron (dark green circle).*

When electrons are transferred, for example from the **L** shell to the **K** shell, as in the example above, this results in a decrease of the atom potential energy[253]. Electrons are ejected with discrete kinetic energies **(E_K)**[254] that can be analysed and used to derive the equation to calculate the energy conservation **($E_{h\nu}$)** of the process (**Equation 2.2**),

$$E_{h\nu} = E_K + E_\phi + E_B(i)$$

Equation 2.2

where $E_{h\nu}$ is the X-ray energy, E_K is the photoelectron kinetic energy, E_ϕ is a small correction for solid effects (work function dependent on the spectrometer and the material) and it is a constant, and $E_B(i)$ is the electron binding energy for the i^{th} level.

The conventional photon sources are soft X-rays (MgKα X-rays, hν=1253.6 eV and AlKα X-rays, hν=1486.6 eV) and the detection limit of the technique is 1000 ppm (0.1 atom%)[255,256].

XPS leaves the atomic nuclei being examined unchanged, however some samples can undergo decomposition upon the exposure to an X-ray source, not allowing further analysis of the sample. The power of the X-ray photoelectron method lies in the fact that the measured quantity, the electron binding energy of an atom, is a function of the chemical environment of the atom[254]. Each element on the analysed surface can be therefore easily identified by analysing the XPS peaks produced by each atom.

The elements on the surface can be identified by analysing the binding energy of the core photoelectrons. The intensity (integrated area under the photoelectron peak) is proportional to the atom quantity in the detected volume. The exact position of a photoelectron peak indicates the chemical state of the atom, since the binding energies of the atom core levels are affected by its chemical environment[252].

2.3 Ellipsometry

Ellipsometry is a sensitive, non-destructive, optical technique developed by Drude in 1887[257,258] , to calculate the dielectric function of metals and dielectrics[259]. This technique exploits plane-polarised light interacting with the surface at a certain angle (usually 70˚), to study surfaces and thin films via thickness and morphology measurements at interfaces, up to 1000Å. The measurements are commonly carried out in the UV/VIS region, but they have also

been made in the infrared region[260]. The surface roughness needs to be small (<50Å)[261] and the measurement has to be performed at oblique incidence at an angle that maximises the sensitivity[262]. A high surface roughness would cause light scattering, which dramatically reduces light intensity, and the ellipsometry measurements would therefore become difficult[260,263]. If the light incidence was normal, it would be impossible to distinguish the p- and s- components of the light, making the measurement impossible[263]. **Figure 2.6** shows a schematic representation of an ellipsometer.

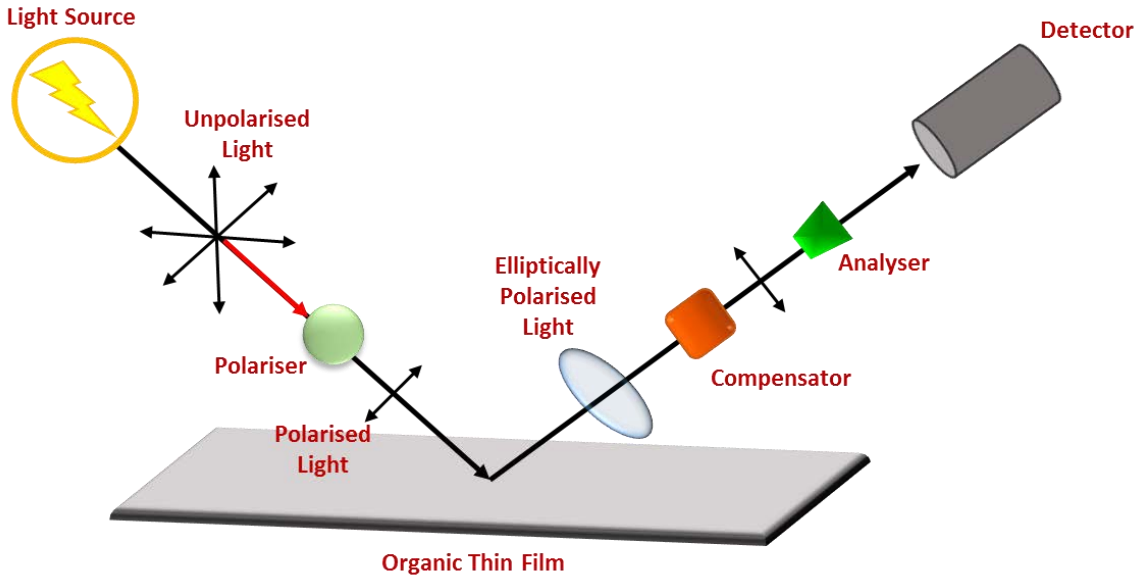

Figure 2.6 – *Schematic representation of an ellipsometer.*

The light beam emitted by the source passes through a polariser, then the linearly polarised beam hits the surface at a selected angle and each component is reflected with a different phase and amplitude, as an elliptically polarised light. The reflected light passes through a compensator that can modify the phase of the beam, to finally reach the analyser that calculates the ratio between the reflection coefficients of the two components of the light (**Equation 2.3**)[264]

$$\rho = \frac{r_p}{r_s} = \tan(\psi)e^{i\Delta}$$

Equation 2.3

where **tan(ψ)** is the amplitude ratio upon reflection and **Δ** is the phase shift (difference). They can both be calculated using Fresnel's equations[260,263]. Since ellipsometry is an indirect method, the values of ψ and Δ cannot be used directly to calculate the optical constants of the sample, but a layer model and an iterative procedure have to be used. The iterative procedure is called "least-squares minimization"[265] and it is used to vary the optical constants and/or thickness parameters. The optical constants are obtained from the values of ψ and Δ that best fit the experimental data and the parameters of the sample. In order to calculate the thickness of a SAM, a three-phase ambient/SAM/substrate model is used, in which the SAM is assumed to be homogeneous with a refractive index ranging between 1.45 and 1.55[266]. This model is based on the Cauchy equation, which considers a SAM as a transparent layer. The thickness of the SAM is then calculated using multi-guess iterations that provide a thickness result with the lowest χ^2 (chi-square distribution) between the measured and the calculated values of ψ and Δ.

2.4 Fluorescence Microscopy

Fluorescence Microscopy is an optical technique, fully developed at the beginning of the 20th century, which, instead of, or in addition to, reflection and adsorption, exploits fluorescence and phosphorescence to analyse biological, organic and inorganic samples[267,268]. This technique uses the sample itself as the light source, inducing it to fluoresce[269]. A fluorescence microscope employs the capability of certain materials to emit energy as visible

light if irradiated with a light beam of a specific wavelength. The studied specimen can be naturally fluorescent (e.g. chlorophyll and some minerals) or it can be labelled with a fluorescing molecule (i.e. fluorescent dye or fluorochrome)[267–270]. This instrument uses a light source at a much higher intensity than a conventional microscope. The fluorescent species present in the sample are excited and emit light at lower energy but longer wavelength that produces the magnified image, instead of the light source. A fluorescence microscope is equipped with special filters designed to isolate and manipulate two distinct sets of excitation and fluorescence emission wavelengths (**Figure 2.7**)[269].

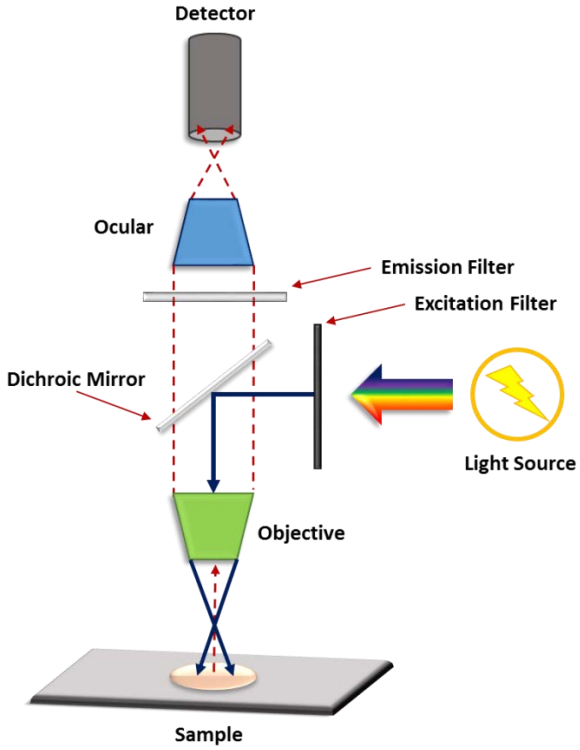

Figure 2.7 – *Schematic illustration of a fluorescence microscope setup.*

The excitation filter selects only the shorter radiation wavelengths coming from the light source which are able to excite the fluorescing material, and send these wavelengths to the sample, while the band of longer wavelengths emitted by the sample itself form an image

of the sample, recorded by the objective[269]. In order to make the microscope work effectively, fluorophores, filters and light source have to be carefully selected for a given application and the quality of the fluorescence signals have to be analysed[271].

Fluorescence microscopy is widely used to study the characteristics, functions and intracellular distribution of numerous metabolites and biomolecules. These applications include the use of fluorescently labelled metabolites, ligands and proteins for the interaction with cell membranes, which in turn become fluorescently labelled[271]. Fluorescent antibodies and proteins (e.g. green fluorescent protein, GFP) can also be used to tag target molecules, and special dyes have also been developed to label organelles and cytoskeletal proteins selectively[272–276]. By using radiometric dyes, it is possible to monitor the concentration of numerous intracellular ionic species, such as Na^+, K^+ and Ca^{2+}.[277]. Advancements in fluorescence microscopes have led to the development of novel fluorescence microscopy techniques, such as FRET, FRAP and TIRF. FRET, or Fluorescence Resonance Energy Transfer, is used to generate fluorescence signals sensitive to molecular conformation, association, and separation in the 1–10 nm range[278]. In this case, two different fluorophores are employed, and when the fluorophore with the shorter wavelength is excited, this causes the excitation of the longer-wavelength fluorophore if the two labelled moieties are separated only by a short molecular distance (in the range 1-10 nm). FRAP, or Fluorescence Recovery After Photobleaching, fluorescence is measured as a function of time and space, and the information about the diffusion coefficients and the binding constants of macromolecules can be recorded[279]. TIRF, or Total Internal Reflection Fluorescence microscopy, is an extremely sensitive technique, employed in the study of molecular events occurring in the close vicinity of the membrane in living cells, due to the short penetration distance (around 100 nm) of this type of microscopy[280–282].

2.5 Surface Plasmon Resonance (SPR)

Surface plasmons were observed for the first time in 1902 by Wood[283–285], who described the phenomenon of anomalous diffraction after illuminating a metallic diffraction grating with polychromatic light[286]. Further work by Fano[287] showed that the narrow dark bands in the diffracted light reported by Wood were associated with the excitation of electromagnetic waves on the surface of the grating[286,288,289].

In 1968 Otto, Kretschmann and Raether demonstrated that the drop in reflectivity in the Attenuated Total Reflection method (ATR) observed by Thurbadar ten years earlier[288–290] was due to the excitation of surface plasmons. When a p-polarised monochromatic light beam interacts with a metal surface evaporated onto a glass prism at a certain angle (surface plasmon resonance angle, $\boldsymbol{\theta_{SP}}$), a surface plasmon wave (SPW) is generated at the interface between the glass prism, characterised by a high refractive index (RI), and the external medium (gas or liquid), characterised by a low RI[286,288–290].

In the Kretschmann geometry of the ATR method, a prism with a high refractive index (n_p) is interfaced with a thin metal film with dielectric constant ε_m, thickness q and a semi-infinitive dielectric with a low refractive index n_d ($n_d<n_p$). When a light wave propagating in the prism hits the metal film, part of the light is reflected back into the prism and part propagates in the metal (Surface Plasmon Wave, SPW) (**Figure 2.8**).

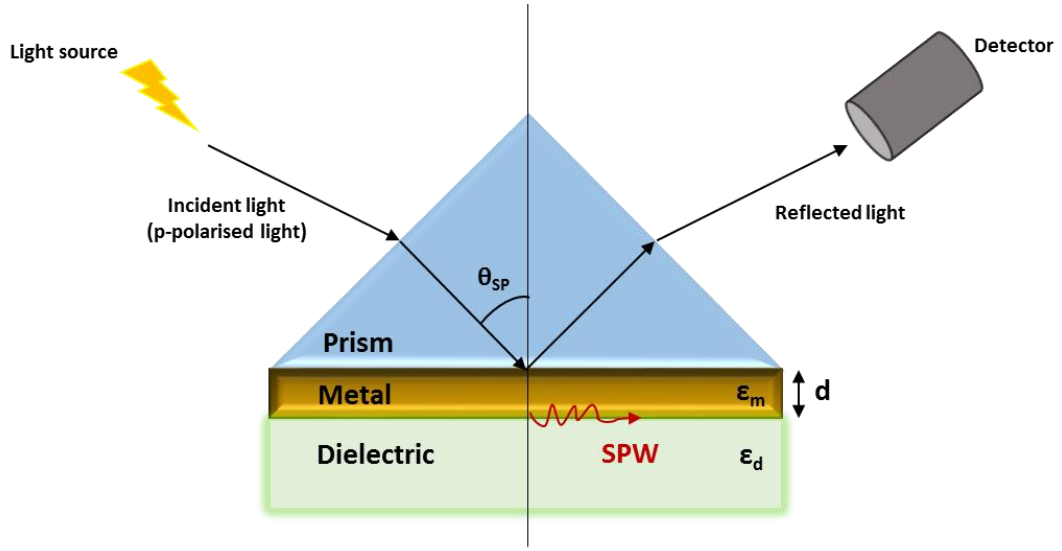

Figure 2.8 *- Kretschmann geometry of the Attenuated Total Reflection (ATR) method.* $\boldsymbol{\theta_{SP}}$ *is the angle at which the incident light is able to excite the surface plasmon wave (SPW) at the metal-dielectric interface, d is the thickness of the metal surface (usually 50 nm) and* ε_m *and* ε_d *are the dielectric constants of the metal and the dielectric, respectively.*

An SPW is characterised by the propagation constant (β) and the electromagnetic field distribution (**Equation 2.4**)

$$\beta = \frac{\omega}{c}\sqrt{\frac{\varepsilon_m\,\varepsilon_d}{\varepsilon_m + \varepsilon_d}}$$

Equation 2.4

where ω is the angular frequency, **c** is the speed of light in vacuum, ε_m is the dielectric constant of the metal ($\varepsilon_m = \varepsilon_{mr} + i\,\varepsilon_{mi}$) and ε_d is the dielectric constant of the dielectric[290–292]. The excitation of surface plasmons can be possible only if the dielectric constant of the metal (ε_m) has a large negative real part at the light wavelength used. This phenomenon can therefore occur only if

at the interface between the two media a so-called “free electron-like” metal is present (generally gold) and its thickness should be a fraction of the wavelength of the incident light (usually 50 nm). Outside the metal, an evanescent electric field that decays exponentially with distance from the metal surface is present, in the direction perpendicular to the prism-metal surface, and interacts with the close vicinity of the metal[287]. The evanescent formed wave penetrates through the metal film and couples with a surface plasmon at the outer boundary of this film. The electromagnetic field of a surface plasmon wave is distributed in an asymmetric manner, and the majority of this field is concentrated in the dielectric. If changes of the optical properties of this region occur, i.e. when an analyte molecule in solution binds to a molecule absorbed on the metal surface, the refractive index at the surface will increase, the SPR angle will be affected and its variations will result in a change of the SPR signal recorded on the computer screen (**Figure 2.9**)[287,293].

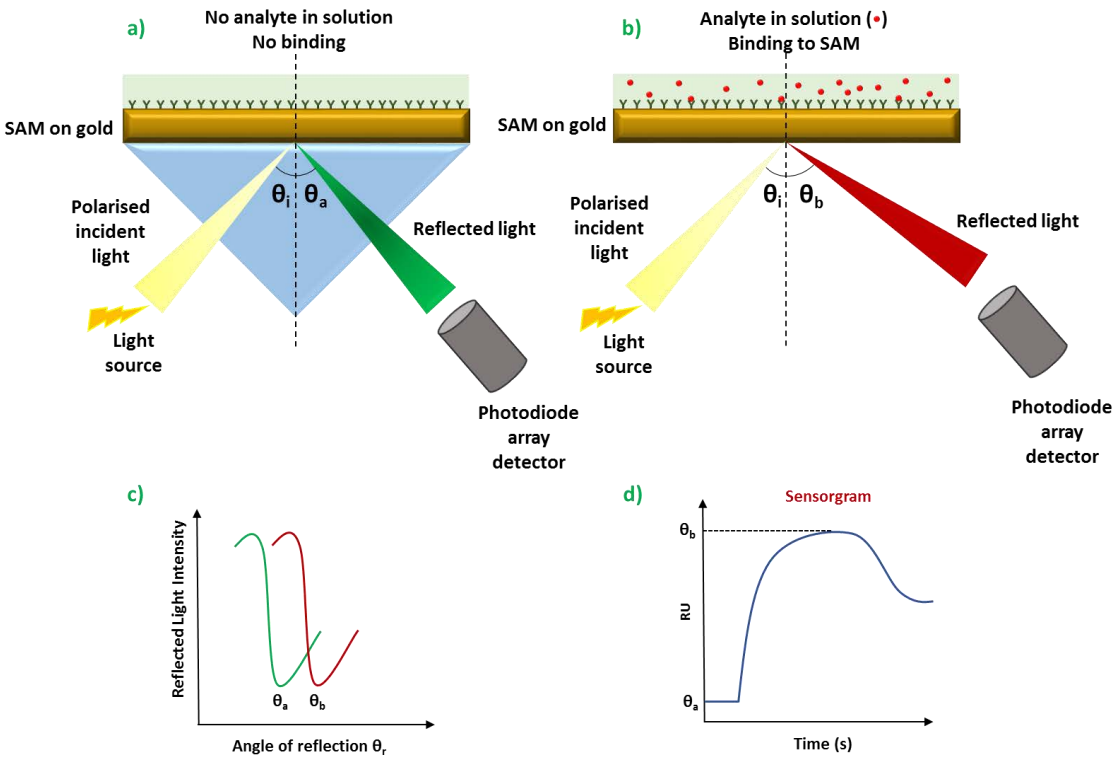

Figure 2.9 – *Illustration of the SPR sensing principle, using the Kretschmann optical configuration. a) The SPR detects the angle of reflection of the light when no analyte is bound to the SAM on the surface; b) when the analyte is present in solution, this comes into contact with the target molecules on the surface. The binding causes a variation in the mass present on the surface, therefore a shift in the angle of reflection (c) occurs, and a change in the intensity of the reflected is recorded by the photodiode array detector. d) A sensorgram is obtained by plotting the resonance angle signal against time, and it is used to monitor the changes occurring on the surface.*

Surface Plasmon Resonance is nowadays fully exploited to follow the interaction between molecules immobilised on the metal surface (molecular recognition elements) and analyte molecules in solution (biorecognition element)[294].

The analyte molecules interact with their relative biorecognition element on the sensor surface, this causes an increase in the refractive index and this change can be measured in real-time. When the buffer solution flows again on the surface, this causes a drop in the refractive index and the occurred variations correspond to a change in the SPR signal recorded. If the nature of the interaction is known, the amount of analyte molecules bound to the biorecognition elements can be calculated from the change of the SPR response units (ΔRU).

SPR was used for the first time for biosensing in 1983 by Liedberg and his collaborators, to investigate the interaction between an immunoglobulin (IgG) absorbed on a silver surface and its relative antibody (anti-IgG). This interaction was demonstrated by recording a shift in the surface plasmon angle and detecting a change in photocurrent when the antibody was injected over the surface[283,295,296].

SPR instrumentation is easy to use, and the sensing chip can usually be regenerated, to which biomolecules could be coupled using known coupling chemistry. The possible applications of SPR for biosensing have been extensively developed since the first demonstration of immunosensing. The application of SPR for biosensing has been extensively developed since the first work of Liedberg et al. SPR biosensors are a label-free real-time analytical technology, and its major application areas include the detection of biological analytes and the analysis of biomolecular interactions[294,297].

In this research work, surface plasmon resonance, coupled to electrochemistry, was exploited to investigate, in real-time, the interaction between neutravidin molecules in solution and biotin moieties on the sensor surface, and between anti-mouse progesterone antibodies in solution and progesterone moieties on the surface.

2.6 Electrochemical techniques

Electrochemical techniques are used to study processes occurring when an electric potential is applied. The most commonly used electrochemical methods are chronoamperometry, linear sweep voltammetry and cyclic voltammetry. They will be briefly described in the following sections.

2.6.1. Chronoamperometry

Chronoamperometry is a sensitive electrochemical technique in which the working electrode potential (V) is changed in one step from V_1 (equilibrium state) to V_2, and then kept to this potential for a defined amount of time. The resulting steady state current, caused by the potential step, is measured as a function of time[298–301]. The potential stepping and the resulting current are shown in **Figure 2.10**.

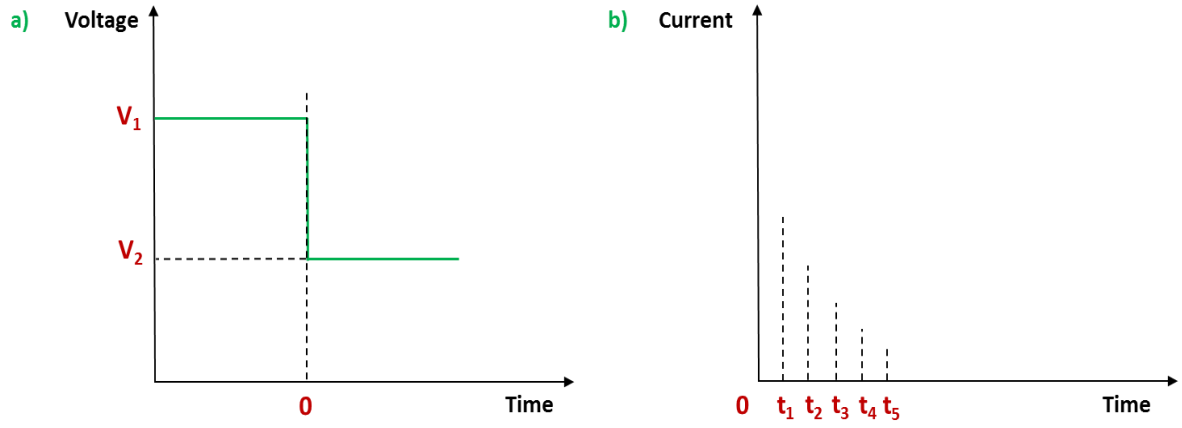

Figure 2.10 – *Illustration of a) chronoamperometry potential stepping and b) current variation with time*

Changes in the current come from the variations in the diffusion layer at the electrode. The concept of "diffusion layer" was introduced by Nernst, and describes the presence of a thin layer of solution in contact with the electrode surface[298,302]. The local analyte concentration at

the electrode surface falls to zero, and the movement of the analyte from the bulk solution of higher concentration is controlled by diffusion. This creates a concentration gradient away from the electrode surface, whereas the convective transfer maintains the concentration of the analyte in the bulk solution constant. Chronoamperometry is often coupled to other techniques such as cyclic voltammetry, for time-dependent system characterisation[302].

2.6.2. Linear Sweep Voltammetry

Linear sweep voltammetry (LSV) is a voltammetric method in which the current at a working electrode is recorded, while the potential between the working and the reference electrode is linearly varied with time (**Figure 2.11**)[303,304].

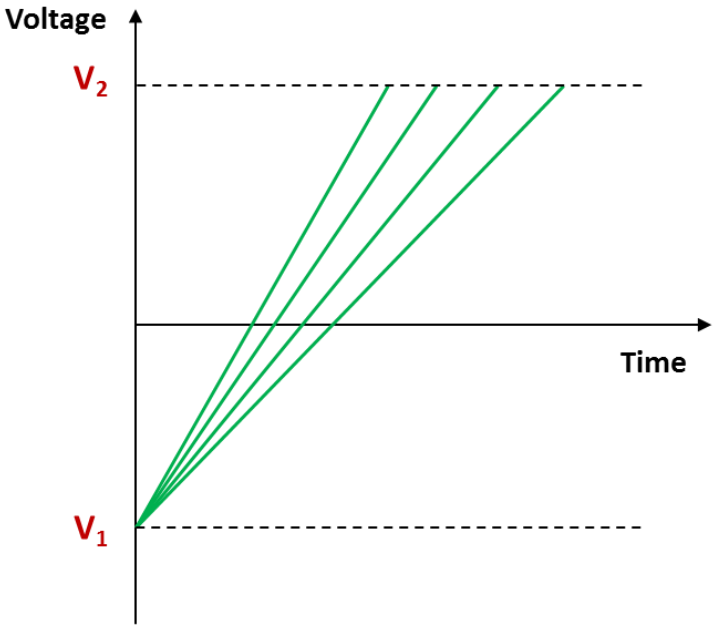

Figure 2.11 – *Series of linear sweep voltammograms recorded at different scan rate*

V_1 is the lower limit of the voltage range applied, at which no reaction occurs, whereas V_2 represents the upper limit. By calculating the slope of the line, it is possible to obtain the

voltage scan rate (**v** = Δy/Δx). When the potential starts to be swept towards $\mathbf{V_2}$, the electrolyte (**A**) present in the electrochemical cell starts to be reduced or oxidised to form the electrochemical product (**Equation 2.5**)[303].

$$A + e^- \rightarrow A^- \text{ (\textbf{Reduction})}$$

$$A \rightarrow A^+ + e^- \text{ (\textbf{Oxidation})}$$

Equation 2.5

The process can be understood by looking at the Nernst equation, which shows the relationship between the concentration of species and the potential difference (**Equation 2.4**)[303]:

$$E = E^0 - \frac{RT}{nF} - \ln\frac{[ox]}{[red]}$$

Equation 2.4

where **E** is the applied potential difference, $\mathbf{E^0}$ represents the standard electrode potential, **R** is the universal gas constant ($R=8.314 JK^{-1}mol^{-1}$), **T** is the absolute temperature (in Kelvin), **F** is the Faraday constant ($F=9.64853x10^4 Cmol^{-1}$) and **n** is the number of electrons being transferred in the half-reactions. The voltage is varied from $\mathbf{V_1}$ to $\mathbf{V_2}$, then the equilibrium at the electrode surface is altered and a current can be recorded[303,304]. At the equilibrium ($\mathbf{V_1}$ applied), there is no electron transfer in the electrochemical cell. The current increases further as the potential is swept towards $\mathbf{V_2}$, due to a greater number of electrons being transferred in the system. The result is a shift of the equilibrium towards the product (conversion of more electrolyte **A**), reaching the full conversion of the analyte at the electrode when the potential applied is equal

to **V_2**. At the redox peak potential (**Vp**), the current reaches its maximum value, due to the diffusion layer having sufficiently grown above the surface of the electrode. This phenomenon makes the movement of reactant to the electrode too slow to satisfy the Nernst equation, causing a fall in the current[303,305] (**Figure 2.12**).

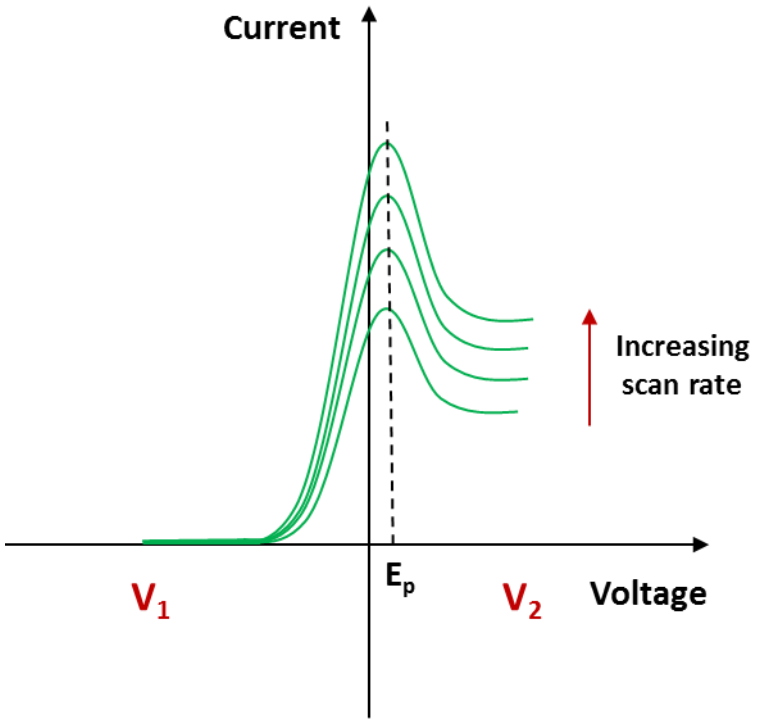

Figure 2.12 – *Changes in current response for voltammograms recorded at different scan rates.*

If the scan rate is varied, this causes a linear change in the current response: if the scan rate is increased, the total current increases. This event can be understood by analysing again the diffusion layer present at the electrode surface, which will change with the voltage scan rate. When the scan rate is slow, the voltammogram will take longer to record and the growth of the diffusion layer will be bigger than in the case of a faster scan rate. This phenomenon will reduce the flux of the analyte (reactant) to the electrode, leading to a smaller current compared to higher scan rates, being this proportional to the flux[303,305].

2.6.3. Cyclic Voltammetry

Cyclic Voltammetry (**CV**) is a potentiodynamic electrochemical measurement, similar to linear sweep voltammetry (**LSV**)[302,304,306]. In this case, the potential of the working electrode is linearly swept versus time between two values at a fixed rate. Contrary to linear sweep voltammetry, when the potential reaches the final value $\mathbf{V_2}$ the scan is reversed, and the voltage is swept back towards the equilibrium position $\mathbf{V_1}$. This results in a triangular potential cycle (**Figure 2.13**).

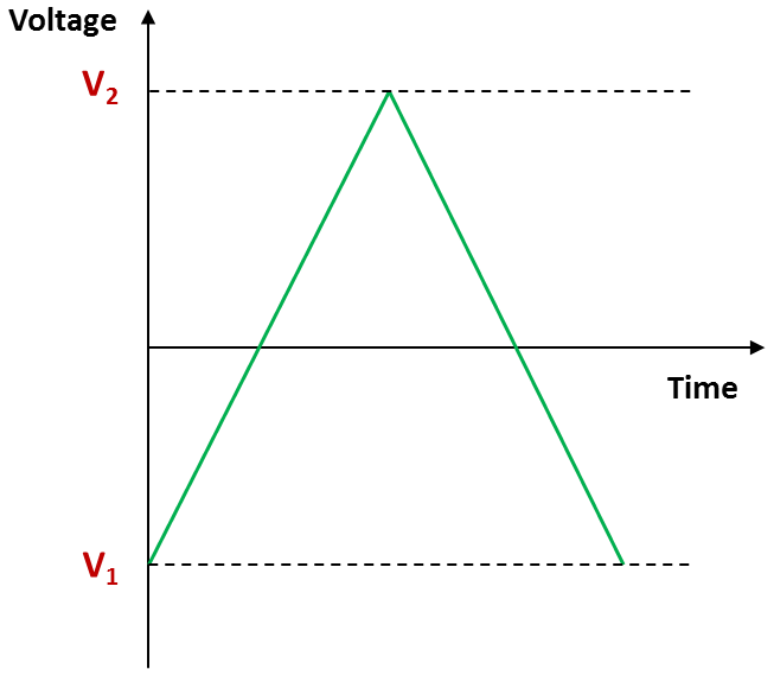

Figure 2.13 – *Schematic representation of the forward and back scans in cyclic voltammetry.*

The forward scan gives an identical response to that given by a LSV scan, but when the scan is reversed, the system moves back towards the equilibrium position, and the product of electrolysis is converted back to reactant. The current is flowing from the solution species back to the electrode, occurring in the opposite direction to the forward scan. The voltage is measured between the reference electrode and the working electrode, whereas the current is

measured between the working electrode and the counter electrode. The current is then plotted versus the voltage, in a graph called cyclic voltammogram (**Figure 2.14**)[303].

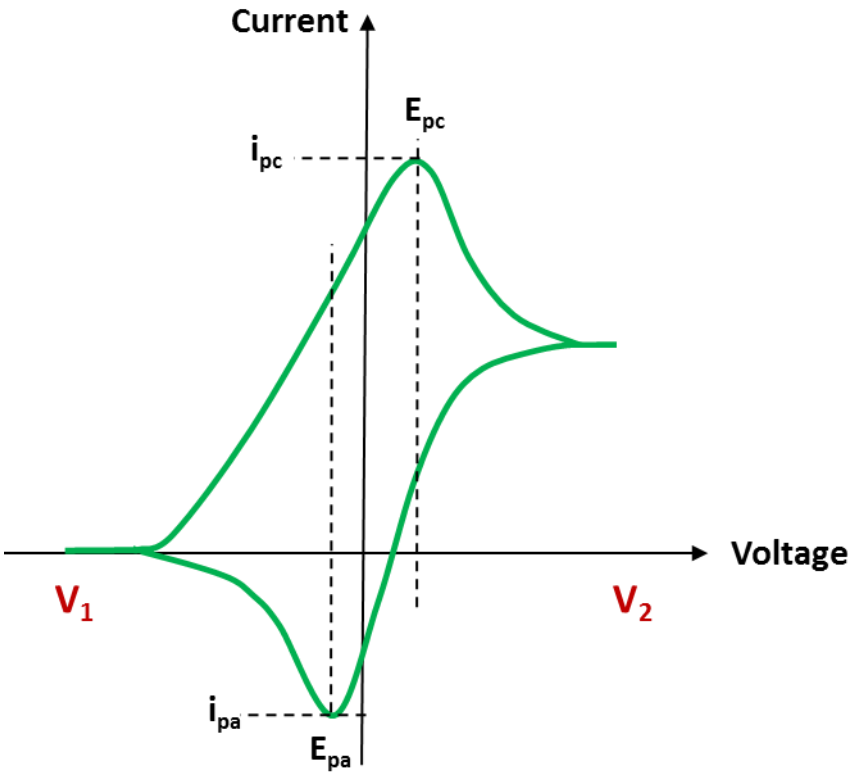

Figure 2.14 – *Schematic representation of a cyclic voltammogram for a reversible single electrode transfer reaction, in the case of a solution containing only a single electrochemical reactant.* E_{pc} *and* i_{pc} *are the peak potential and peak current relative to the cathode, respectively, whereas* E_{pa} *and* i_{pa} *are the peak potential and peak current relative to the anode, respectively*

When the voltage is swept towards the reduction potential of the analyte, an increase in the current occurs. The analyte starts to be reduced at the electrode surface, to form the electrochemical product. Once the potential has passed the reduction potential value, the current decreases, due to the reduction in the concentration of the analyte near the electrode

surface. When the voltage is reversed towards $\mathbf{V_1}$, the formed product starts being reoxidised, to form again the electrochemical reactant, and a current of opposite polarity is produced. This current will first increase, to then decrease after a voltage peak has been formed, as the voltage scan continues toward $\mathbf{V_1}$[302,303].

If a reaction is reversible, the recorded **CV** presents specific characteristics:

1. The difference between the two peak potentials is (**Equation 2.5**)

$$\Delta E = E_{pa} - E_{pc} = \frac{59}{n} mV$$

Equation 2.5

where **a** is relative to the anodic peak, **c** is relative to the cathodic peak and **n** is the number of electrons being transferred in the electrochemical process, **mV** is millivolts.

2. The positions of peak voltage do not vary with the scan rate
3. The peak current ratio is always equal to 1, at each scan rate (**Equation 2.6**):

$$\frac{i_{pa}}{i_{pc}} = 1$$

Equation 2.6

4. The peak currents are proportional to the square root of the scan rate

The scan rate is a critical factor, because each scan has to be high enough to allow the chemical reaction of interest to occur. The diffusion layer thickness can explain the role of the scan rate as with the linear sweep voltammetry[303].

In the case of an irreversible reaction, the electron exchange between the working electrode and the analyte is very slow. This phenomenon causes the peak current for the irreversible reaction to be lower than the reversible one. In this case, the peak current ratio

differs from 1, and the difference between the peak potentials relative to the anode and the cathode is greater than 59/n mV (**Equation 2.7**)[303].

$$\Delta E = E_{pa} - E_{pc} > \frac{59}{n} mV$$

Equation 2.7

This behaviour can be attributed to secondary chemical reactions occurring at the electrode, triggered by the electron transfer[306].

Chapter 3 - Experimental Procedures and Protocols

Abstract: *Materials, methods and experimental techniques used in this work are discussed in this chapter, together with experimental procedures and protocols and data analysis by various types of equipment.*

3.1 Materials and Methods

3.1.1 Gold substrates

Polycrystalline gold substrates were purchased from George Albert PVD, Germany and consisted either of a 50 nm gold layer deposited onto glass covered with a thin layer (5 nm) of chromium as the adhesion layer (for contact angle and XPS analysis) or 100 nm gold layer on 100-4inch-silicon wafer, precoated with titanium as the adhesion layer (for ellipsometry analysis). Polycrystalline gold substrates employed in SPR were purchased from Reichert Technologies, USA, consisted of 49 nm gold with 1 nm chromium.

3.1.2 Glass substrates

Glass substrates approximately 1 cm by 1cm were cut from glass microscope plain slides using a glass cutter. Glass microscope plain slides (26 mm by 76 mm, 0.8-1 mm thick) were purchased from Thermo Fisher Scientific Ltd.

3.1.2 Silicon substrates

Silicon substrates approximately 1 cm by 1cm were cut from silicon wafers using a glass cutter. The silicon wafers were purchased from IDB Technologies Ltd (Whitley, UK), with the following specifications: type: N<100>; size: 76 mm; resistivity: 1-10 ohm-metre (Ω·m); thickness: 381 μm; polish: Single Side Polish (SSP).

3.2 Chemicals

Commercially available chemicals and solvents were purchased from Aldrich Chemicals and Fisher chemicals and used as received. The oligopeptides Biotin-2KC, Biotin-4KC, Biotin-6KC and Progesterone-C7-4KC were synthesised by Peptide Protein Research Ltd. (Wickham, UK) to > 95% purity and verified by HPLC and mass spectrometry. Neutravidin, Calcium Green^{TM}-1, AM and Pluronic Acid F-127 (20% solution in DMSO) were obtained from Invitrogen Life Technologies Ltd. (Paisley, UK). Purified Progesterone-3 Anti-Mouse monoclonal antibody (Affinity Constant: $75x10^{10}$ L/M) was obtained from antibodies-online GmbH (Aachen, Germany) and diluted with Phosphate buffered saline (PBS) solution. Phosphate buffered saline (PBS) solution was prepared from a 10× concentrate PBS solution (1.37 M sodium chloride, 0.027 M potassium chloride and 0.119 M phosphate buffer) from Fisher BioReagents. Modified Earle's Balanced Salt Solution (sEBSS) ($CaCl_2 \cdot 2H_2O$ 1.80 mM, KCl 5.37 mM, $MgSO_4 \cdot 7H_2O$ 0.81 mM, $NaHCO_3$ 26.19 mM, $NaH_2PO_4 \cdot 2H_2O$ 1.01 mM, NaCl 116.36 mM, D-Glucose 5.55 mM, Sodium Pyruvate $C_3H_3O_3Na$ 2.73 mM, Sodium Lactate $C_3H_5O_3Na$ 41.75 mM) was purchased from Biological Industries Ltd. (Beit-Haemek, Israel). Triethylene glycol thiol (TEGT) was synthesised by Dr. Parvez Iqbal, School of Chemical Engineering, University of Birmingham, following a multistep route (**Figure 3.1**). The commercially available triethylene glycol (**1**) was alkylated with alkyl bromide at reflux in basic conditions to obtain **2**, that was then converted to **3** in the presence of thioacetic acid Azobisisobutyronitrile (AIBN) heated at reflux for 1 h. Deprotection of **3** was performed in mild acidic conditions at reflux for 4 h to obtain TEGT (**4**).

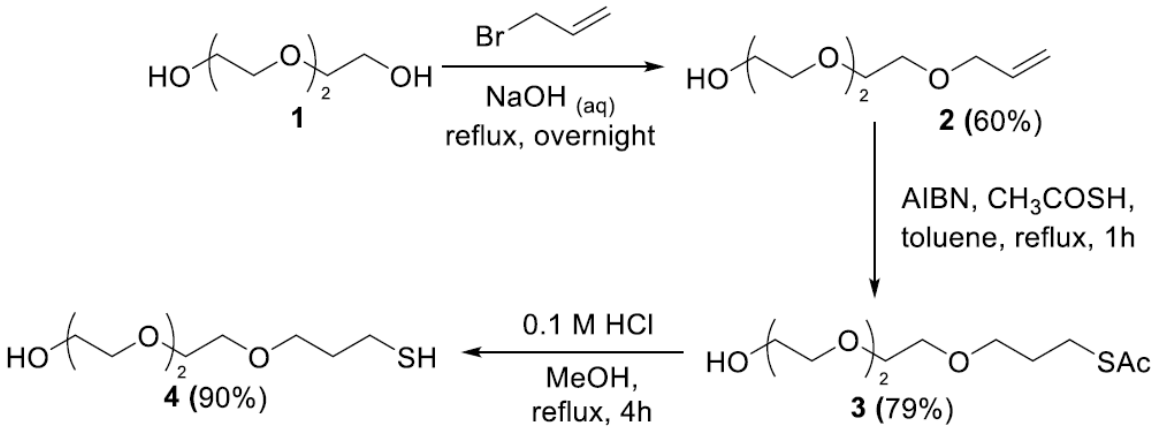

Figure 3.1 – *Multistep route for the synthesis of triethylene glycol thiol (**TEGT**)*

The 11-(Mercaptoundecyl)hexa(ethylene glycol) (EG6OH) was purchased from Sigma Aldrich and used as received.

The carboxyethylsilanetriol di-sodium salt, 25% in water was purchased from Fluorochem Ltd (Hadfield, UK). and used as received. Poly-D-Lysine (PDL) was purchased from Scientific Laboratories Supplies Ltd. (Hessle, UK) and diluted with UHQ water to a concentration of 2 mg/ml and stored in the fridge.

3.3 Experimental Procedures

3.3.1 Surface Preparation

3.3.1.1 Cleaning of gold and glass surfaces

Both gold and glass substrates were cleaned by immersion in piranha solution (70% H_2SO_4, 30% H_2O_2) at room temperature for 8 minutes and then rinsed with Ultra High Quality (UHQ) water and then HPLC grade ethanol thoroughly for 1 min. (*Caution: Piranha solution reacts violently with all organic compounds and should be handled with care*).

3.3.1.2 Preparation of Biotin-2KC:TEGT, Biotin-4KC:TEGT and Biotin-6KC:TEGT mixed Self-Assembled Monolayers (SAMs) on gold substrates

Clean gold substrates were immersed for 24 h in HPLC ethanol 0.1 mM solution of oligopeptide and 0.1 mM TEGT solution containing 3% (v/v) triethylamine $N(CH_2CH_3)_3$ to prevent the formation of hydrogen bonds between the amino groups (NH_2) of the oligopeptide bound to the gold surface and the free oligopeptide in the bulk solution[307]. The different oligopeptides solutions were mixed at the following volume ratios:

- Biotin-2KC:TEGT 1:40 and 1:100
- Biotin-4KC:TEGT 1:0, 1:1, 1:10, 1:40, 1:100 and 1:500
- Biotin-6KC:TEGT 1:40 and 1:2000

The substrates were rinsed with a solution of HPLC ethanol containing 10% (v/v) CH_3COOH to remove triethylamine and then with HPLC ethanol and dried under a stream of Ar.

3.3.1.3 Preparation of silane-PDL on glass substrates and silicon wafer

Either clean glass substrates, microscope plain glass slides or 1 cm^2 chips cut from silicon wafers were coated on one side with a carboxyethylsilanetriol di-sodium salt, 25% in water layer by chemical vapour deposition for 2 h in a vacuum chamber. The coated glass surfaces were cured for 30 minutes at 100˚C under vacuum and then left cooling to room temperature. The substrates (**1**) were then immersed in a 1mM HCl solution in UHQ water for 5 minutes under gentle shaking, to form carboxylic acid groups on the surface to obtain **2**. **2** was rinsed with UHQ water and then immersed in a solution 1:1 of 1-Ethyl-3-(3-dimethylaminopropyl)carbodiimide/*N*-Hydroxysuccinimide (EDC/NHS) for 15 minutes, under gentle shaking, to activate the carboxylic groups on the surface, PDL 2mg/ml

was added to obtain a concentration of 0.5 mg/ml in the solution and left to react overnight, under gentle shaking, to form amide bonds on the surface (**3**) (**Figure 3.2**).

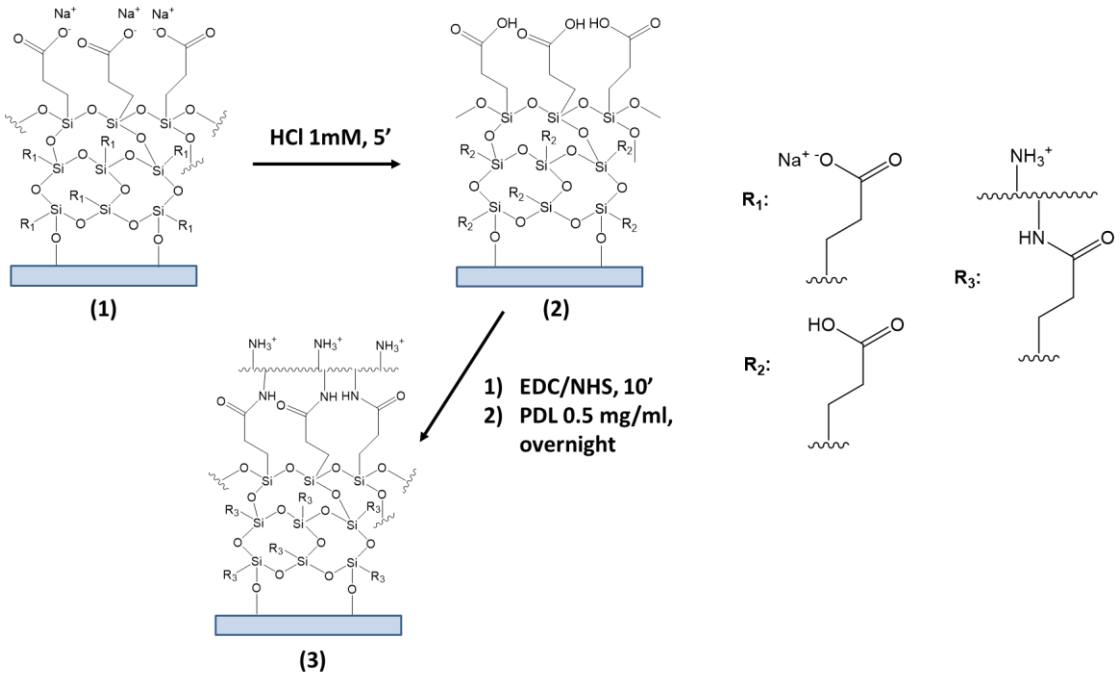

Figure 3.2 – *Multistep route for the functionalisation of glass or silicon substrates with silane-PDL layers*

3.3.2 Surface characterisation

3.3.2.1 Contact angle

Contact angles were determined using a home-built contact angle apparatus, equipped with a charged coupled device (CCD) KP-M1E/K camera (Hitachi) that was attached to a personal computer for video capture. The dynamic contact angles were recorded as micro-syringe was used to quasi-statistically add liquid to or remove liquid from the drop. The drop was shown as a live video image on the PC screen v1.96 (First Ten Angstroms) was used for the

analysis of the contact angle of a droplet of UHQ water at the three-phase intersection. The averages and standard errors of contact angles were determined from five different measurements made for each type of SAM (in triplicate).

3.3.2.2 Ellipsometry

The thickness of the deposited monolayers and layers was determined by spectroscopic ellipsometry, using either (i) a gold on silicon substrate with a gold thickness of 50 nm, or (ii) silicon substrate. A Jobin-Yvon UVISEL ellipsometer with a xenon light source was used for the measurements. The angle of incidence was fixed at 70˚. A wavelength range of 280-820 nm was used. DeltaPsi software was employed to determine the layer thickness and the calculations were based on a three-phase ambient/SAM/substrate model in which the SAM was assumed to be isotropic and assigned a refractive index of 1.50. The thickness reported is the average of five measurements (in triplicate), with the errors reported as standard deviation.

3.3.2.3 Surface Plasmon Resonance

SPR switching experiments were performed with a Reichert SR7000DC Dual Channel Spectrometer (Buffalo, NY, USA) at 25˚C using a three-electrode electrochemical cell and a Gamry PCI4/G300 potentiostat. The SAMs prepared on Reichert gold served as the working electrode, the counter electrode was a Pt wire, and a standard calomel electrode (SCE) was used as the reference electrode (**Figure 3.3**).

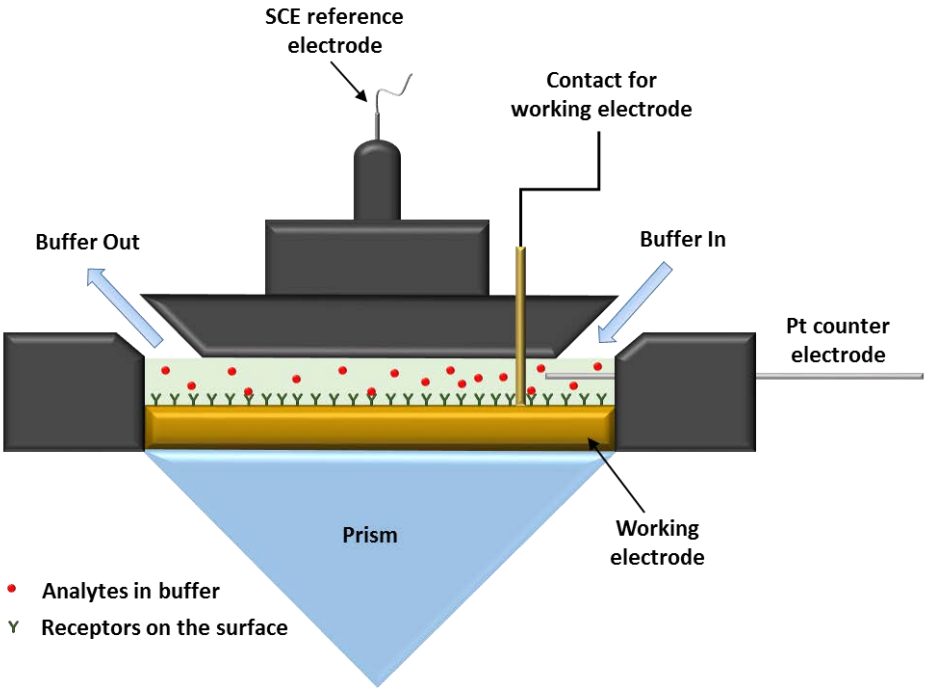

Figure 3.3 – *Cartoon representation of the SPR electrochemical cell*

Prior to the binding studies between Biotin and Neutravidin, the sensors chips were equilibrated by flowing either degassed PBS at 50 μl/min, followed by application of -0.4 V, open circuit or +0.3 V conditions for 10 min while passing degassed PBS through the electrochemical cell at the flow rate of 50 μl/min. While still applying a potential, neutravidin (250 μl, 37 μg/ml) was injected over the sensor chip surface for 10 secs at 1500 μl/min and then 30 min at 8 μl/min (the decrease in flow rate from 1500 to 8 μl/min ensures that sufficient exposure time was provided for binding to occur between the biotin on the surface and Neutravidin in solution). To remove any unbound material, the sensor chips were washed with degassed PBS for 10 secs at a flow rate of 1500 μl/min, followed by 10 min at a flow rate of 50 μl/min while still applying a potential to the chips. The same procedure was used for OC experiments without applying a potential.

Prior to the binding studies between Progesterone and its relative anti-mouse Antibody, the sensors chips were equilibrated by flowing EBBS at 50 μl/min, followed by application of -0.4 V, open circuit or +0.3 V conditions for 10 min while passing either degassed PBS through the electrochemical cell at the flow rate of 50 μl/min. While still applying a potential, the antibody (250 μl, 37 μg/ml) was injected over the sensor chip surface for 30 min at 8 μl/min, followed by 15 min at 50 μl/min while still applying a potential, to allow any dissociation of the antibody from the surface. The same procedure was used for OC experiments without applying a potential.

3.3.2.4 X-ray Photoelectron Spectroscopy

Analysis of biotin-nKC:TEGT (n = 2, 4, 6) mixed SAMs: XPS spectra were obtained on the VG Escalab 250 instrument based at University of Leeds EPSRC Nanoscience and Nanotechnology Facility, UK. XPS experiments were carried out using a monochromatic Al K α X-ray source (1486.7 eV) and a take-off angle of 15°. High-resolution scans of N (1s) and S (2p) were recorded using a pass energy of 150 eV at a step size of 0.05 eV. Fitting of XPS peaks was performed using the Avantage V 2.2 processing software. Sensitivity factors used in this study were: N (1s), 1.73; S (2p), 2.08; Au (4f 7/2), 9.58; Au (4f 5/2), 7.54. The averages and standard errors reported were determined from at least four different XPS measurements.

Analysis of progesterone-C7-4KC:EG6OH mixed SAMs and silane layers: XPS spectra were obtained on the AXIS Nova (Kratos Analytical) instrument based at University of Newcastle (NEXUS), UK. XPS experiments were carried out using a monochromatic Al Kα X-ray source (1486.7 eV) at a take-off angle of 90 degree to the surface plane. High-resolution scans of Au4f, C 1s, O 1s, N 1s, S (2s and 2p) and Si (2s and 2p) were recorded using pass energy of 20

eV at a step size of 0.1 eV. Fitting of XPS peaks was performed using CASA XPS processing software. Sensitivity factors used in this study were: C 1s 1.00; O 1s 2.93; N (1s), 1.80; S (2s), 2.43; S (2p), 2.08; Au (4f), 17.10; Si (2s), 0.95; Si (2p), 0.82.

3.3.2.5 Force Field Test

The Force Field Test was conducted by Dr Xingyong Wang at Nanjing University, China.

Since the conformational switching of biotin-nKC chains mainly results from the rotation of the C-C bonds, the energy scan for biotin-4KC molecule with different C1-C2-C3-C4 dihedrals (θ) was carried out by both force field methods and density functional theory (DFT) calculations with the B3LYP functional and 6-31G(d) basis set. Three kinds of force fields, cvff, compass and pcff were tested. The result is shown in **Figure 3.4**. The cvff force field shows the best performance. Although it overestimates the energies compared to the DFT result, it displays the right shape of the energy curve. In contrast, both compass and pcff force fields result in a significant deviation from the DFT result. So, the cvff force field was adopted throughout our simulations (**Table 3.1**).

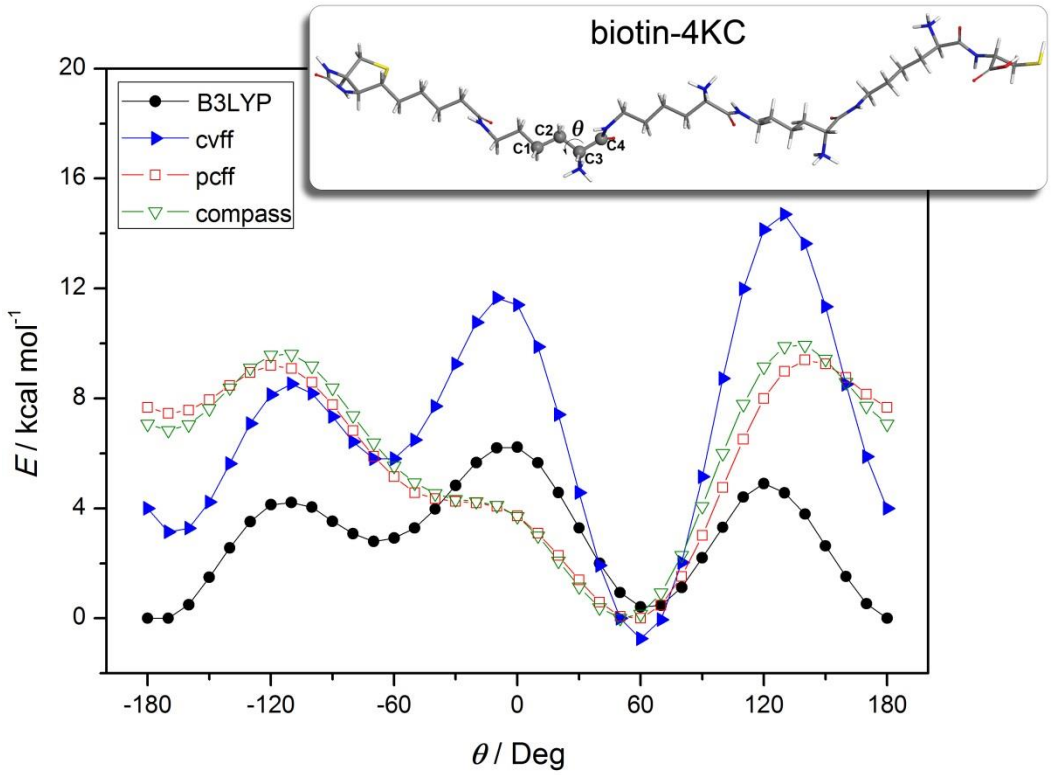

Figure 3.4 - *The energy scanning for biotin-4KC molecule with different C1-C2-C3-C4 dihedrals, θ, obtained by both force field methods and DFT calculations.*

Table 3.1 - *Parameters for the surface models used in the simulations.*

Surface chains	Solvent molecules (H2O)	Ions (Cl-)	Cell parameters (Å3)
Biotin-2KC/8(TEGT)	957	2	25.95 × 25.95 × 65.42
Biotin-4KC/15(TEGT)	2115	4	34.60 × 34.60 × 77.42
Biotin-6KC/15(TEGT)	2728	6	34.60 × 34.60 × 95.42
9(Biotin-4KC)	1982	36	34.60 × 34.60 × 77.42

3.2.2.6 Computational details

Five layers of gold atoms cut from the Au (111) surface were adopted to model the gold substrates used in the experiment and they were fixed during the simulations. All MD simulations were performed in the canonical (NVT) ensemble using the cvff force field. The temperature was set to 298 K by using the Andersen thermostat[308]. The equations of the motion were integrated using the velocity Verlet algorithm[309] with the time step of 1fs. The atomic charges for the biotin-nKC molecules were updated every 100ps by DFT calculations, at the M06-2X/6-31G(d,p) level of theory. The Discover module in the Materials Studio package[310] was employed to run all the MD simulations. All DFT calculations were carried out with the Gaussian 09 program package[311].

3.3 Preparation and Analysis of Sperm Cells

3.3.1 Sperm Cells Incubation and labelling

Sperm cells were prepared at Birmingham Women's Hospital, using the facilities at the Dr Kirkman-Brown's research laboratory. Cells were isolated from seminal plasma using the following procedure: 1 ml of modified Earle's Balanced Salt Solution (sEBSS) containing 0.3% of Bovine Serum Albumin (BSA) were pipetted into a series of 5 ml test tubes. Volumes of 300 μl of fresh semen sample, stored in the incubator at 37°C and 6% CO_2 for no more than 30 min after production, were deposited at the bottom of each test tube. After 1-hour incubation (37°C; 6% CO_2) the top 700 μl of the swim-up suspension is gently removed from each tube and transferred to clean loose-capped test tubes for capacitation. The sperm cells are finally left in the incubator (37°C; 6% CO_2) for at least 3 hours, to allow the capacitation process[312]. After the capacitation was completed, 3 ml of a solution composed by 8 μl of Calcium Green™-1, AM

and 42 μl of Pluronic Acid F-127 (20% solution in DMSO) were added to 300 μl of sperm cells suspension. The sperm cells were then left in the incubator (37°C; 6% CO_2) for 45 min to allow the correct labelling of sperm cells.

3.3.2 Sperm Cells Counting

10 μl of swim-up suspension were deposited in a Neubauer chamber and sperm cells were counted using the Computer Assisted Sperm Analysis (CASA) System[313].

3.3.3 Perfusion Chamber

The polycarbonate perfusion chamber (dimensions 51 mm x 30 mm x 25 mm) was made by Mr Stephen Brookes (School of Physics & Astronomy) and presents openings for the buffer flow in and out of the chamber and the microscope objective to analyse the cell adhesion to the glass surfaces (**Figure 3.5**).

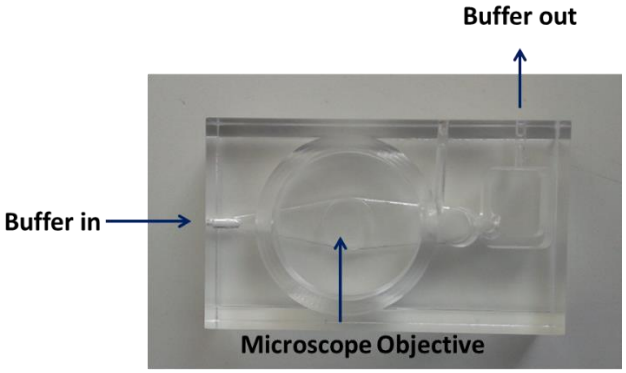

Figure 3.5 – *Picture of the polycarbonate perfusion chamber. The labels correspond, from left to right, to the openings for the buffer perfusion inside the chamber, the microscope objective and the buffer flowing out of the chamber.*

3.3.4 Fluorescence Microscopy

The fluorescence image time-lapses were acquired on an Olympus BX60M upright microscope, using an Olympus LUMPlanFL 40x/0.80 W dipping objective. Samples were illuminated with a Cairn OptoLED LED (470 nm), filtered to 480/40 nm, and emission fluorescence, filtered to 535/50nm, was captured with a Photometrics QuantEm:512SC Camera.

Chapter 4 - Study of the effect of switching unit length on switching ability

This chapter is based on the manuscript "Modulation of Biointeractions by Electrically Switchable Oligopeptide Surfaces: Structural Requirements and Mechanism" by C. L. Yeung, X. Wang, M. Lashkor, E. Cantini, F. J. Rawson, P. Iqbal, J. A. Preece, J. Ma, P. M. Mendes, Advanced Materials Interface, 2014, 1, 1300085. (My personal contribution to this work regarded the formation of mixed Self-Assembled Monolayers on gold substrates, their characterisation by XPS and the study of mixed monolayers switching properties by electrochemical SPR).

Abstract: *This chapter presents a detailed analysis of the development of switchable mixed self-assembled monolayers exploiting charged oligopeptides as switching units. A model system composed by a biotinylated lysine oligopeptide has been used for the purposes of this work. Herein a detailed study is presented, on the influence of the switching unit length on the mixed SAMs performance under an electrical potential. The role of triethylene-glycol (TEGT) molecules, used as second component in the mixed SAMs, has also been investigated. The desired results have been obtained by testing different biotinylated oligopeptides/TEGT ratios on the gold surfaces. TEGT molecules are fundamental to both confer protein-resistant properties to the surface, to prevent any Neutravidin unspecific binding, and ensure enough space for the switchable units to efficiently undergo their molecular rearrangement on the gold surface, upon the application of an electrical potential. Furthermore, molecular dynamics simulations have been conducted on the mixed SAMs employed in this study, to have a detailed understanding of the dynamics regulating the molecular activity on the surface. This work creates the basis for the design of efficient switchable materials, that can be employed in the control of complex biological processes.*

4.1 Introduction

The possibility of modulating the surface properties by applying different stimuli has attracted research interest in the past decades[1,173]. By changing the surface characteristics using temperature[314,315], light[316,317], magnetic field[318] and electrical potential[174,194,196,208,319], is possible to create devices with tailored features, able to mimic biological processes[1,173] and have potential biomedical applications[9,10,320].

The range of applications of stimuli-responsive surfaces is wide and includes drug delivery systems[321,322], biosensors[210,323,324], separation, bioanalysis and microfluidic systems[325–328], but also regenerative medicine[1,173]. Among the different variety of stimuli-responsive surfaces, self-assembled monolayers able to rearrange themselves upon the application of an electrical potential, have gained growing interest as devices able to selectively control biomolecular interactions[174,194,196,198,199]. The noticeable characteristics of these smart surfaces are a fast response time and the easiness of orthogonal functionalisation[1,173,329], allowing the creations of different switchable regions on the same substrates. Another important feature is the possibility of inducing conformational changes on the surface, by using biologically compatible low voltages or electric fields[330]. These monolayers have been shown to be able of regulating the interactions between proteins[196,208,319], DNA[331,332] and both mammalian[199,330] and bacterial[195] cells, and the biomolecules on the surface. Specifically, oligopeptides can be employed as switching units. Charged aminoacid, such as lysine or aspartic acid, present either a positive or a negative charge on their side chains at pH 7. Chains composed by charged oligopeptide can then undergo a molecular rearrangement on the surface, upon the application of an electrical potential and they can be used to expose or conceal target molecules on demand.

Different bioactive moieties can be bound to the switchable units, making charged oligopeptide SAMs an excellent tool to study biological processes in different conditions[1,173,174,208]. In this work, a detailed study was conducted to analyse how both the length of the switching unit and the mixed SAM surface ratio, can control the performance of the smart monolayers under an electrical potential. The first component of the chosen mixed SAM for this work, is a lysine (K) oligopeptide, functionalised at one end with a biotin moiety, able to strongly interact with the Neutravidin protein and at the other end with an aminoacid of cysteine (C) to anchor the oligopeptide to the gold substrates via the thiol group. The second component is represented by a triethylene glycol-terminated thiol (TEGT). The aim of TEGT molecules is both to space out the oligopeptide to allow enough space on the surface for molecular rearrangement and impede any undesired unspecific binding of neutravidin protein on the gold surfaces (**Figure 4.1**).

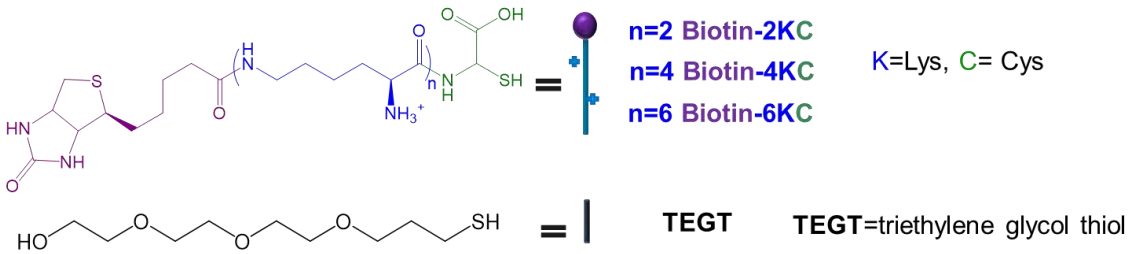

Figure 4.1- *Chemical structures of the oligopeptides (biotin-2KC, biotin-4KC and biotin-6KC) and tri(ethylene glycol)-terminated thiols used to form the mixed SAMs tested in this research project.*

The essential characteristic of oligolysine peptides is the presence positive charge on the side chains at pH 7. This feature gives the possibility of an "ON/OFF" switching of the biotin-

Neutravidin interaction on the surface upon the application of an electrical potential. It has already been demonstrated that these SAMs can control the interaction between biotin on the surface and neutravidin in solution[196], but the nature of the molecular changes has not been clarified yet. To understand the dynamics of the studied process, molecular dynamics simulations have also been conducted on the developed system. The biotin-neutravidin interactions can be followed by electrochemical SPR, that presents an advantage if compared to the standard SPR technique. In fact, in addition to the easiness of use and the quick response time, it offers the possibility of monitoring the changes happening on the surface when an electrical potential is applied, in real-time, as illustrated in section 2.5.

The results of this analysis will permit a better design of switchable mixed SAMs, that can therefore be tailored, according to the biological requirements and applications of the desired device.

4.2 Objectives

1. Characterisation of different biotin-4KC/TEGT ratios on gold surfaces by XPS, to evaluate the differences between solution ratio and surface ratio.
2. Analysis, by electrochemical SPR, of the switching properties of the different mixed SAM ratios, to select the one with the highest switching efficiency.
3. Comparison of biotin-4KC switching efficiency with the one of a shorter (biotin-2KC) and a longer (biotin-6KC) oligopeptide, to analyse how the switching unit length influences the molecular rearrangement on the surface.
4. Testing the switching properties of the different oligopeptides used in this work by molecular dynamics simulations, to have an insight into the mechanism regulating the molecular switching.

4.2 Results and discussion

4.2.1 Formation of mixed biotin-4KC:TEGT SAMs

Piranha-cleaned gold substrates were incubated into different solution ratios of mixed biotin-4KC:TEGT SAMs. The biotin-4KC peptide is composed by a chain of four lysines functionalised at one end with a biotin moiety, that can bind to the Neutravidin molecules in solution and, at the other end, with a cysteine aminoacid for the anchoring to the gold substrate. The flexible lysine backbone presents a positive charge at pH 7, making it employable as the mixed SAM switching unit. Upon the application of a negative potential to the gold substrate, the lysine oligopeptide is expected to be attracted towards the surface. This attraction will drag the biotin moiety, that will then be hindered from the interaction with neutravidin, by the TEGT molecules. When a positive potential is applied, an opposite behaviour is expected: the lysine oligopeptide will be repelled by the charge, being fully extended on the surface, therefore completely exposing the biotin moiety for the interaction with neutravidin. TEGT molecules were employed to prevent non-specific binding of proteins on the surface and to give enough conformational freedom to the biotin-4KC component to undergo the switching (**Figure 4.2**).

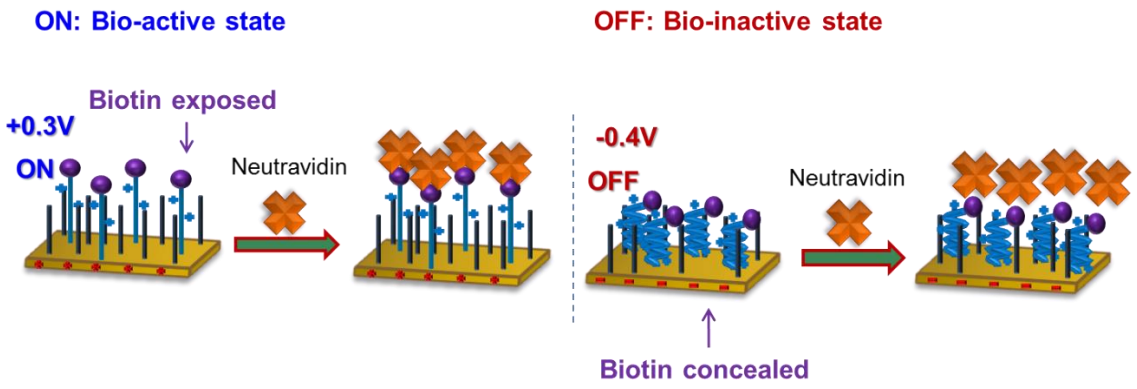

Figure 4.2 – *Schematic representation of the biotin-4KC:TEGT mixed SAMs in the bio-active state (+0.3V), where the biotin moiety is fully exposed on the gold surface, and in the bio-inactive state, where the biotin moiety is concealed and hindered from the binding to neutravidin.*

4.2.2 XPS characterisation of mixed biotin-4KC:TEGT SAMs

One of the objectives of this research work was the selection of the mixed biotin-4KC:TEGT SAM ratio presenting the highest switching performance. The first step was to characterise the different SAMs ratios by XPS, to analyse if the two components were forming the ratio they had in solution, on the surface. In addition, the XPS analysis was important to understand if an increase of one of the two mixed SAM components in solution, was resulting in an increase of the same component on the surface. The different mixed SAMs were prepared from biotin-4KC:TEGT solution ratios 1:0 (pure biotin-4KC SAM), 1:1, 1:10, 1:40, 1:100 and 1:500, by immersing piranha-cleaned gold substrates in each solution ratio for 24 h, as reported in section 3.3.1. The XPS spectra were recorded by Dr C. Yeung and analysed by myself. The XPS spectra of the mixed monolayers revealed the presence of signals from C 1s, O 1s, N 1s and S 2p, confirming the formation of the mixed biotin-4KC:TEGT SAMs. For simplicity, only the

spectra of nitrogen and sulphur atoms are reported, since these are the elements used to calculate the surface ratio.

The mixed SAM surface ratio can be calculated from the integrated peaks areas, using the equation below (**Equation 4.1**):

$$Number\ of\ TEGT = \left(No\ of\ N\ per\ peptide\ x \frac{S\ area}{N\ area} \right) - No\ of\ S\ per\ peptide$$

Equation 4.1

As seen from the molecular structure of biotin-4KC (**Figure 4.1**), 11 nitrogen atoms are present, whereas the number of sulphur atoms is only 1. TEGT molecules do not possess any nitrogen atom, but only a sulphur atom. Using the **Equation 4.1** is possible to estimate the number of sulphur atoms remaining when the sulphur from cysteines are subtracted, corresponding to the number of TEGT molecules. **Table 4.1** shows an example of how the surface ratio was calculated from the solution ratio, using **Equation 4.1**.

Table 4.1 – *XPS data of biotin-4KC:TEGT 1:10 solution ratio and average number of TEGT molecules per biotin oligopeptide on the surface. The calculated average and error are based on three experiments (a, b and c).*

Solution ratio	N area	S area	S/N	No. of TEGT	Rounded No of TEGT	Average	Error
1:10 a	0.00691	0.00538	0.778	6.564	7	5	2
1:10 b	0.00653	0.00365	0.559	4.148	4		
1:10 c	0.00688	0.00402	0.584	4.427	4		

The first tested mixed biotin-4KC:TEGT SAM ratio was 1:0, that corresponds to a SAM by biotin-4KC molecules only. The S 2p spectrum (**Figure 4.3**) can be deconvoluted into two doublet peaks[86,333,334]. The first doublet peak is centred at 163.3 eV (S $2p_{1/2}$) and 162.0 eV (S $2p_{3/2}$), corresponding to the sulphur chemisorbed to the gold substrate. The second doublet peak, attributed to S-C bonds on the biotin moieties, is centred at 164.1 eV and 165.3 eV, respectively[86,333,334]. The N 1s spectrum (**Figure 4.3**), presents a large peak centred at 400.0 eV, corresponding to amino (NH_2) and amide (CONH) groups[333–335]. The second, smaller peak centred at 402.0 eV can be attributed to charged amino groups (NH_3^+), present on lysine side chains[333–335].

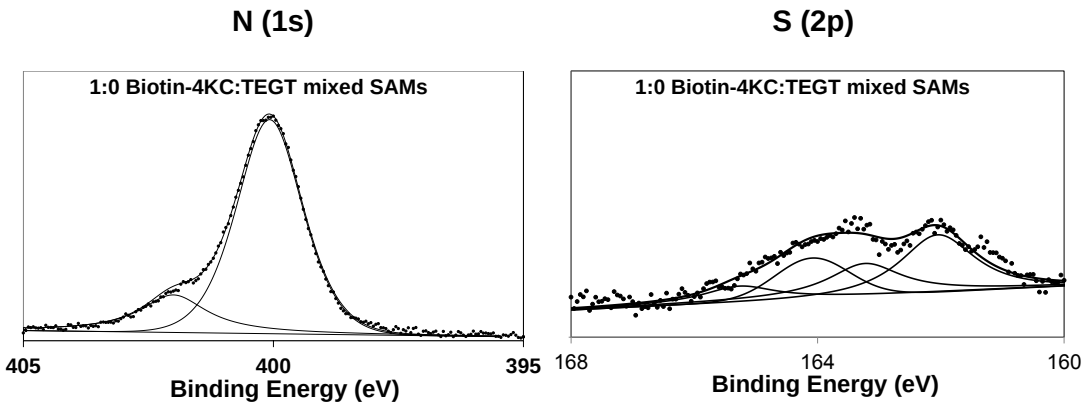

Figure 4.3 – *XPS spectra of N 1s (left) and S 2p (right) for biotin-4KC:TEGT 1:0 solution ratio*

The second ratio of mixed biotin-4KC:TEGT SAM tested was 1:1. The S 2p spectrum (**Figure 4.4**) presents two doublets peaks, the first one centred at 163.2 eV (S $2p_{1/2}$) and 162.0 eV (S $2p_{3/2}$), refers to the sulphur chemisorbed on the gold substrates, whereas the second doublet peaks, centred at 163.8 eV and 165.0 eV, respectively, can be assigned to S-C bonds present on biotin moieties. As expected, the N 1s spectrum (**Figure 4.4**) presents a smaller peak, compared to the 1:0 ratio, due to a smaller number of biotin-4KC molecules on the surface.

The first peak, corresponding to amino (NH_2) and amide (CONH) groups, is centred at 400.3 eV, whereas the smaller peak centred at 402.2 eV is assignable to charged amino groups (NH_3^+), present on lysine side chains[333–335]. By using Equation 3.1, it is possible to calculate the mixed biotin-4KC:TEGT SAM surface ratio. The calculated surface ratio does not directly correspond to the solution ratio, in fact it is equal to 1:3±3 (**Table 4.2**). This discrepancy has been reported before for other mixed monolayers[79,80,336]. This trend has been observed also for the all the solution ratios tested.

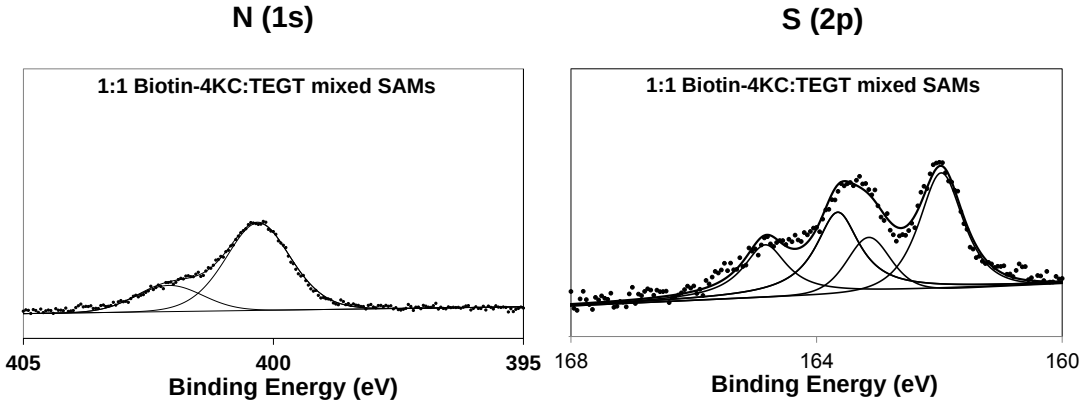

Figure 4.4 – *XPS spectra of N 1s (left) and S 2p (right) for biotin-4KC:TEGT 1:1 solution ratio*

The third biotin-4KC:TEGT solution ratio analysed by XPS was 1:10. The S 2p spectrum (**Figure 4.5**) presents two doublets peaks, the first one centred at 163.4 eV (S $2p_{1/2}$) and 162.0 eV (S $2p_{3/2}$), refers to the sulphur chemisorbed on the gold substrates, whereas the second doublet peaks, centred at 163.7 eV and 165.2 eV, respectively, can be assigned to S-C bonds present on biotin moieties. As expected, the N 1s spectrum (**Figure 4.5**) presents a smaller peak, compared to the 1:1 ratio, due to a smaller number of biotin-4KC molecules on the surface and the charged amino group peak start to be difficult to be identified. The first peak, centred at 400.4 eV, can be assigned to amino (NH_2) and amide (CONH) groups, whereas the smaller peak

centred at 401.8 eV is ascribable to charged amino groups (NH_3^+), present on lysine side chains[333–335]. Again, by using **Equation 4.1**, it is possible to calculate the mixed biotin-4KC:TEGT SAM surface ratio. As expected, the calculated surface ratio does not directly correspond to the solution ratio, in fact it is equal to 1:5±2 (**Table 4.2**).

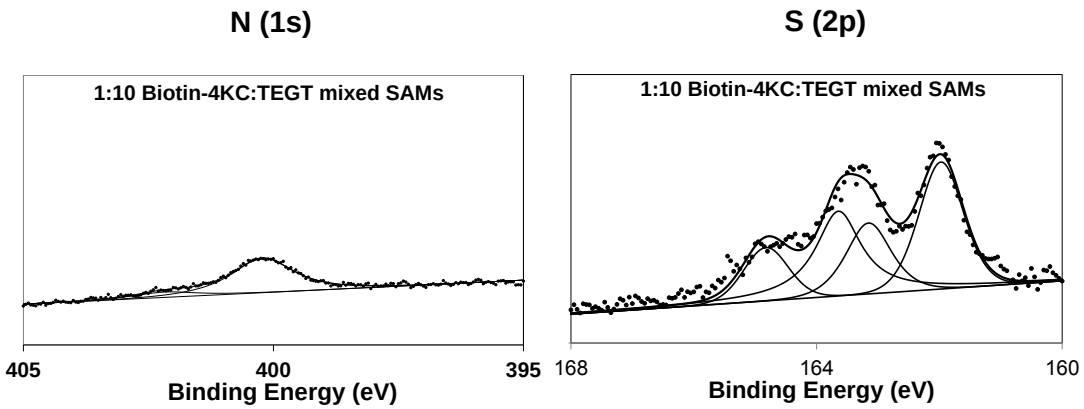

Figure 4.5 – *XPS spectra of N 1s (left) and S 2p (right) for biotin-4KC:TEGT 1:10 solution ratio*

The fourth biotin-4KC:TEGT solution ratio analysed by XPS was 1:40. The S 2p spectrum (**Figure 4.6**) presents two doublets peaks, the first one centred at 163.4 eV (S $2p_{1/2}$) and 162.1 eV (S $2p_{3/2}$), refers to the sulphur chemisorbed on the gold substrates, whereas the second doublet peaks, centred at 163.7 eV and 165.0 eV, respectively, can be assigned to S-C bonds present on biotin moieties. As expected, the N 1s spectrum (**Figure 4.6**) presents a smaller peak, compared to the 1:10 ratio, due to a smaller number of biotin-4KC molecules on the surface and the peak corresponding to charged amino groups is barely identifiable. The first peak, centred at 400.5 eV, can be assigned to amino (NH_2) and amide (CONH) groups, whereas the smaller peak centred at 402.0 eV is ascribable to charged amino groups (NH_3^+), present on lysine side chains[333–335]. Again, by using **Equation 4.1**, it is possible to calculate the mixed biotin-

4KC:TEGT SAM surface ratio. As expected, the calculated surface ratio does not directly correspond to the solution ratio, in fact it is equal to 1:16±4 (**Table 4.2**).

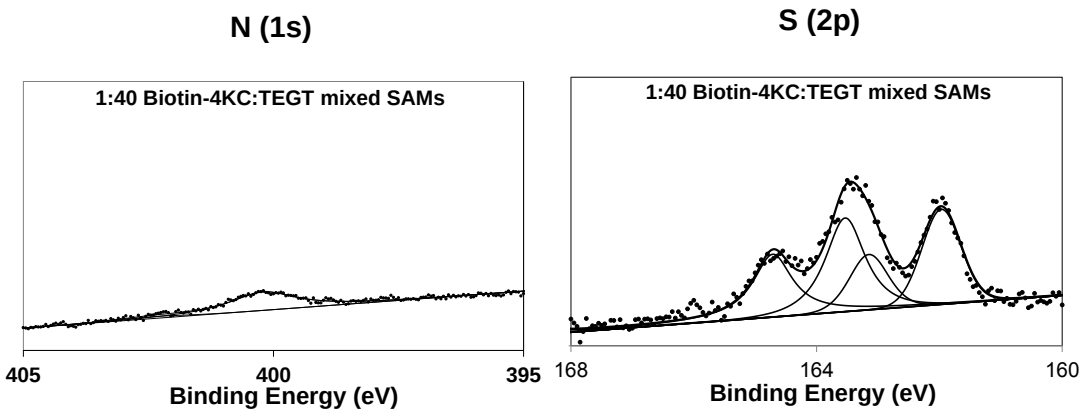

Figure 4.6 – *XPS spectra of N 1s (left) and S 2p (right) for biotin-4KC:TEGT 1:40 solution ratio*

The fifth biotin-4KC:TEGT solution ratio analysed by XPS was 1:100. The S 2p spectrum (**Figure 4.7**) presents two doublets peaks, the first one centred at 163.2 eV (S $2p_{1/2}$) and 162.0 eV (S $2p_{3/2}$), refers to the sulphur chemisorbed on the gold substrates, whereas the second doublet peaks, centred at 163.6 eV and 164.8 eV, respectively, can be assigned to S-C bonds present on biotin moieties. As expected, the N 1s spectrum (**Figure 4.7**) presents a smaller peak, compared to the 1:10 ratio, due to a smaller number of biotin-4KC molecules on the surface and the peak corresponding to charged amino groups cannot be identified. The peak centred at 400.3 eV, can therefore be assigned to amino (NH_2) and amide (CONH) groups only[333–335]. Again, by using Equation 3.1, it is possible to calculate the mixed biotin-4KC:TEGT SAM surface ratio. As expected, the calculated surface ratio does not directly correspond to the solution ratio, in fact it is equal to 1:22±8 (**Table 4.2**).

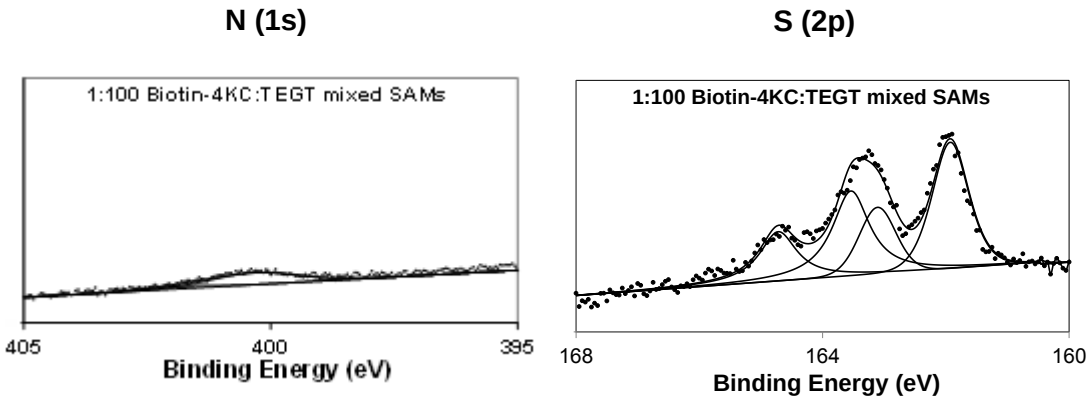

Figure 4.7 – *XPS spectra of N 1s (left) and S 2p (right) for biotin-4KC:TEGT 1:100 solution ratio*

The sixth biotin-4KC:TEGT solution ratio analysed by XPS was 1:500. The S 2p spectrum (**Figure 4.8**) presents two doublets peaks, the first one centred at 163.3 eV (S $2p_{1/2}$) and 162.1 eV (S $2p_{3/2}$), refers to the sulphur chemisorbed on the gold substrates, whereas the second doublet peaks, centred at 163.3 eV and 164.5 eV, respectively, can be assigned to S-C bonds present on biotin moieties. The only N 1s peak recorded (**Figure 3.8**), centred at 400.4 eV, can be ascribed to amino (NH_2) and amide (CONH) groups[333–335].

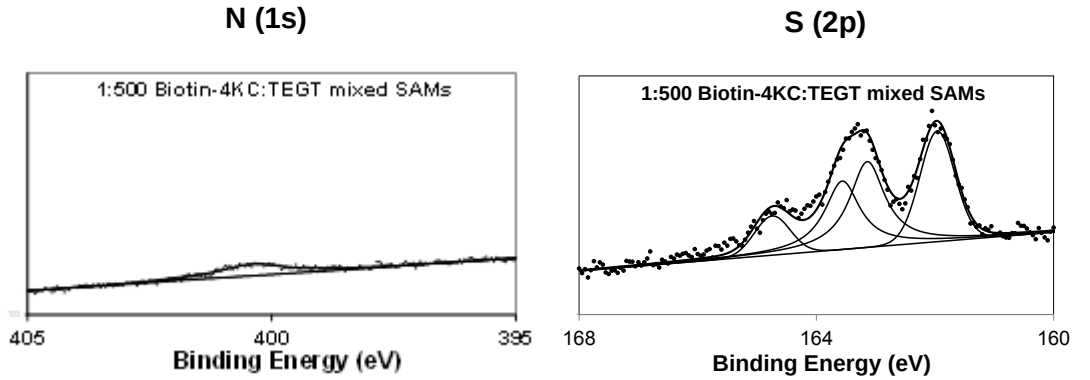

Figure 4.8 – *XPS spectra of N 1s (left) and S 2p (right) for biotin-4KC:TEGT 1:500 solution ratio*

As expected, the calculated surface ratio does not directly correspond to the solution ratio, in fact it is equal to 1:38±6 (**Table 4.2**).

Table 4.2 – *Biotin-4KC:TEGT solution ratios and respective surface ratios calculated after XPS analysis.*

Biotin-4KC:TEGT ratio	
Solution	**Surface**
1:0	1:0
1:1	1:3±3
1:10	1:5±2
1:40	1:16±4
1:100	1:22±8
1:500	1:38±6

The results obtained always showed a difference between the biotin-4KC:TEGT solution ratios and the surface ratio calculated from the XPS nitrogen and sulphur peaks. The averages and standard errors reported in the calculated surface ratios are the result of at least four different XPS measurements. All the samples were reproducible. By using correlation analysis, it is possible to find a logarithm relationship between the solution and the surface ratios of mixed biotin-4KC:TEGT SAMs, with the biotin-4KC surface composition being significantly higher than it solution composition. This result is in agreement with previous studies on mixed SAM composed by different chain lengths thiols, showing a preference in the absorption of the longer chain thiol[79,80,336]. The exact reason for this phenomenon is still unclear[337]. Mixed SAMs can present microscopic phase separation[80,337], where the two components are not randomly

dispersed throughout the monolayer. The longer alkyl-thiol molecules have to adopt complex conformation and tilt at an angle greater than 30˚ to the surface normal to maximise Van der Waals interactions[80]. In this way, the alkyl chains near the gold surface adopt a more disordered conformation than in pure alkanethiolate SAMs. On the contrary, the molecules of the shorter alkanethiolate component, are organised in a highly-oriented form[80], similar to the one they present in a pure SAM. In addition, long alkyl chain tend to organise in a gauche conformation, in which the backbone chains are not orderly-packed over the surface[80]. As stated in section 1.3.3, alkyl-thiols composing mixed SAMs are motile, feature resulting in a dynamic adsorption and desorption of the molecules of excess adsorbate[80]. The preferential absorption of longer thiol molecules it is due to thermodynamically cohesive interactions between the alkyl chains.[337] The rate of this thermodynamic process increases with the molecular length of the component and as the chain length increases, the preferential adsorption of the longer thiol increases as a consequence[337].

4.2.3 Investigation on biotin-4KC:TEGT binding capacity and switching efficiency

To understand if the biotin-4KC:TEGT mixed SAMs could control the biotin bioactivity upon the application of an electrical stimulus, the different solution ratios, ranging from 1:1 to 1:500 and previously analysed by XPS, were tested by electrochemical SPR. The pure biotin-4KC SAM was also tested. Switching studies were conducted by monitoring the Neutravidin binding to the biotin end groups on the oligopeptide. Previously, our research group had already demonstrated that oligopeptide mixed SAM can be employed to modulate bioactivity[196], upon the application of an electrical potential, while not affecting the SAM integrity. Thus, similar potentials were used in this research work. The SPR experiments were

conducted in three different states: bio-active (ON), while a positive potential of +0.3 V was applied, open circuit (OC) while no potential was applied and bio-inactive (OFF), while a negative potential of -0.4 V was applied. The recorded sensorgrams are reported in **Figure 4.9**.

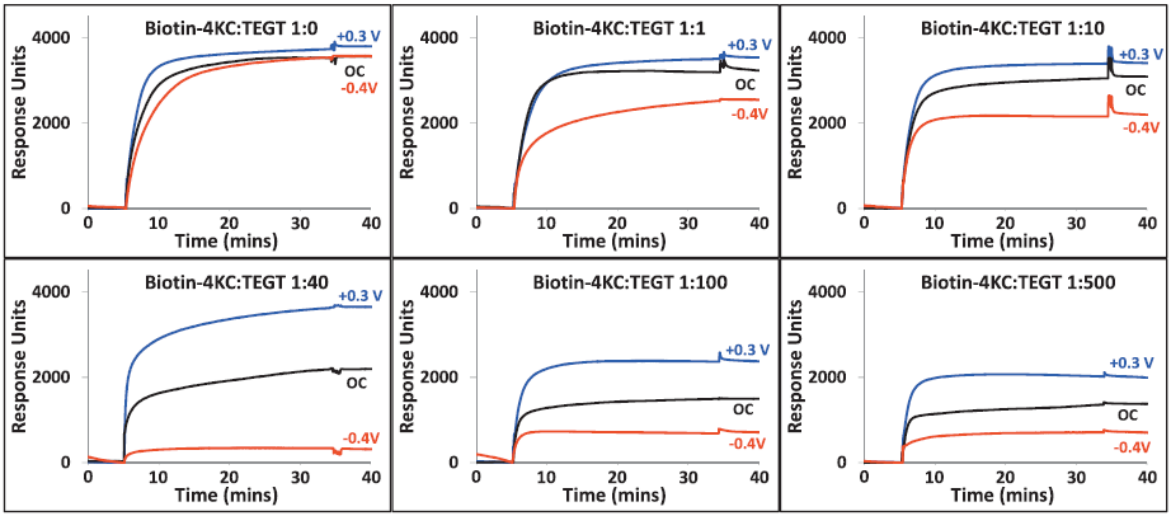

Figure 4.9 – *SPR sensorgram traces showing the binding of neutravidin to the biotin-4KC:TEGT mixed SAMs at solution ratios of 1:0, 1:1,1:10, 1:40, 1:100 and 1:500 under OC (no applied potential), ON (+0.3 V) and OFF (−0.4 V) conditions.*

Phosphate Buffer Saline (PBS) was flushed over the surface for 10 minutes to equilibrate the sensor chip and set the SPR baseline, in either ON (+0.3 V), OC (no potential) or OFF (-0.4 V) states. This step was followed by injection of Neutravidin, diluted in PBS, over the surface for 30 minutes, necessary for neutravidin to bind to the accessible biotin moieties on the surface. After this exposure time, the chip was rinsed with degassed PBS, to remove any unbound protein still present in the sensor cell and the binding capacity was recorded. The binding capacity (BC) is defined as the difference in the SPR response units between the beginning of Neutravidin injection and the end of washing with PBS. The averages and the

standard errors in the reported binding capacity were calculated from at least three different SPR measurements for each ratio (**Table 4.3**).

Table 4.3 – *Biotin-4KC:TEGT Binding Capacity (BC), expressed in Resonance Units (RU) and Switching Efficiency calculated from SPR experiments.*

Biotin-4KC:TEGT ratio		**Binding Capacity (RU)**	**Switching Efficiency (%)**
Solution	**Surface**		
1:0	1:0	3553±258	7±2
1:1	1:3±3	3192±164	27±3
1:10	1:5±2	3053±69	34±5
1:40	1:16±4	2195±161	90±3
1:100	1:22±8	1492±72	62±8
1:500	1:38±6	1375±75	60±4

The switching efficiency (SE) was calculated as the percentage between the binding capacity when a positive potential was applied (BC_{ON}) and the binding capacity when a negative potential was applied (BC_{OFF}), divided by BC_{ON}:

$$SE = \frac{BC_{ON} - BC_{OFF}}{BC_{ON}} \; x \; 100$$

Equation 4.2

From the results obtained, it is possible to infer that a pure biotin-4KC SAM, which presents a neutravidin immobilisation capacity of 3.5 ng/mm^2 (1000 RU = 1 ng/mm^2)[196], is not able to control the biotin bioactivity on the surface, showing only 7±2% of switching efficiency. The binding capacity of the biotinylated mixed SAM decreased significantly with the reduction

of biotin moieties concentration on the gold substrate. A reduced number of biotin oligopeptide molecules on the surface, results in the decrease of neutravidin immobilisation capacity. In fact, the 1:1 solution ratio presents a neutravidin immobilisation capacity of 3.2 ng/mm^2, that is then lowered to 3 ng/mm^2 and 2.2 ng/mm^2 for the 1:10 and 1:40 solution ratios, respectively. However, the diminution in the binding capacity does not show proportionality with the reduction of the amount of biotinylated oligopeptide on the surface. it is therefore possible to assume that both the steric hindrance and the restricted mobility of the densely-packed oligopeptide molecules might limit the neutravidin binding to the biotin ends at low ratio of TEGT to biotin-4KC[338]. The 1:16 surface ratio (1:40 solution ratio) of the biotin-4KC:TEGT mixed SAM presented the highest switching efficiency, resulting to be the optimum ratio for controlling the biotin bioactivity. The data collected demonstrated that a densely-packed switchable oligopeptide SAM cannot undergo a molecular rearrangement on the surface and some free space is needed for the oligopeptide chains to change their conformation when a negative potential is applied (**Figure 4.10**).

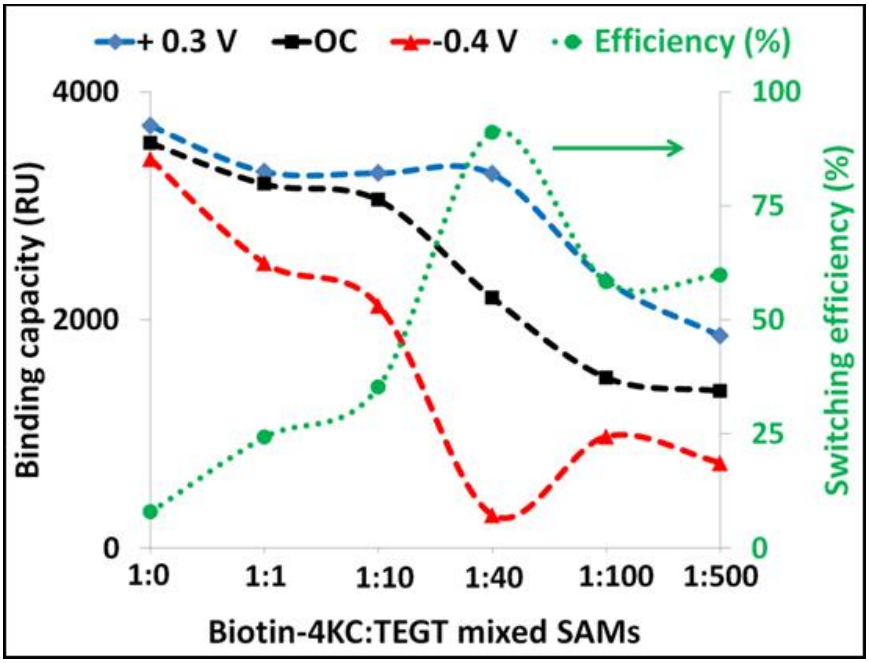

Figure 4.10 – *Binding capacity and switching efficiency in ON (+0.3 V), OC (no potential applied) and OFF (-0.4 V) states of biotin-4KC:TEGT mixed SAMs at the different solution ratios tested in this study (1:0, 1:1, 1:10, 1:40, 1:100 and 1:500).*

By progressively reducing the density of biotinylated oligopeptides on the surface, the mixed SAM showed an increased capability of controlling the bioactivity of biotin moieties on the surface. However, at a surface ratio lower than 1:16, the switching efficiency decreased significantly. This phenomenon is due to the formation of a more packed ethylene glycol thiol matrix that limit the oligopeptide free movement on the surface. Our hypothesis is that the switching mechanism between bio-active and bio-inactive states is controlled by the conformational changes occurring on the surface upon the application of an electrical potential. These changes result into a reorganisation of the biotin end on the surface. In addition, the presence of enough free space on the surface is fundamental to permit the molecular rearrangement of bioactive molecules. From these observations, we can also conclude that the gap distance between the bioactive molecules and the ethylene glycol thiol

matrix is an important factor that has to be considered in the design of mixed switchable monolayers. This distance should enable biotin to correctly be buried into the binding pocket of the neutravidin barrel.

It is possible to conclude that the molecular rearrangement of oligopeptides may induce: a) a change in the gap distance between biotin and the ethylene glycol thiol matrix, and b) a variation in the orientation of the biotin itself that could become more or less available for protein binding.

4.3 Study on the influence of switching unit length on switching efficiency

To investigate the influence of both the gap distance and the length of the oligopeptide chain on the switching efficiency, a shorter (biotin-2KC) and a longer (biotin-6KC) oligopeptide were chosen as model systems. Starting from the results obtained for biotin-4KC:TEGT mixed SAMs at different surface ratios, two surface ratios were selected, namely 1:5 and 1:16. In addition to evaluating the switching ability of biotin-2KC and biotin-6KC, using an underperforming (1:5) and an optimum (1:16) ratio found for biotin-4KC aimed to a) compare the oligopeptides behaviour and b) reveal if there is a correlation between the switchable backbone length and the molecular area required for the molecular rearrangement to occur under an electrical stimulus.

4.3.1 XPS characterisation of biotin-2KC:TEGT and biotin-6KC:TEGT mixed SAMs

The XPS spectra were recorded by Dr C. Yeung and analysed by myself. The XPS spectra of the mixed monolayers revealed the presence of signals from C 1s, O 1s, N 1s and S 2p, confirming the formation of both mixed biotin-2KC:TEGT and biotin-6KC:TEGT SAMs. For simplicity, only the spectra of nitrogen and sulphur atoms are reported, since these are the

elements used to calculate the surface ratio. The mixed SAM surface ratio can be calculated from the integrated peaks areas, using **Equation 4.1**. The solution ratios giving the desired surface ratios were 1:40 and 1:100, for biotin-2KC:TEGT mixed SAMs and 1:40 and 1:2000 for biotin-6KC:TEGT mixed SAMs, respectively.

The XPS spectra for biotin-2KC:TEGT 1:40 solution ratio are reported in **Figure 4.11**. The S 2p spectrum presents two doublets peaks, the first one centred at 163.3 eV (S $2p_{1/2}$) and 162.2 eV (S $2p_{3/2}$), refers to the sulphur chemisorbed on the gold substrates, whereas the second doublet peaks, centred at 163.5 eV and 165.1 eV, respectively, can be assigned to S-C bonds present on biotin moieties. As expected, the N 1s spectrum presents a small peak, centred at 400 eV, can be assigned to amino (NH_2) and amide (CONH) groups.

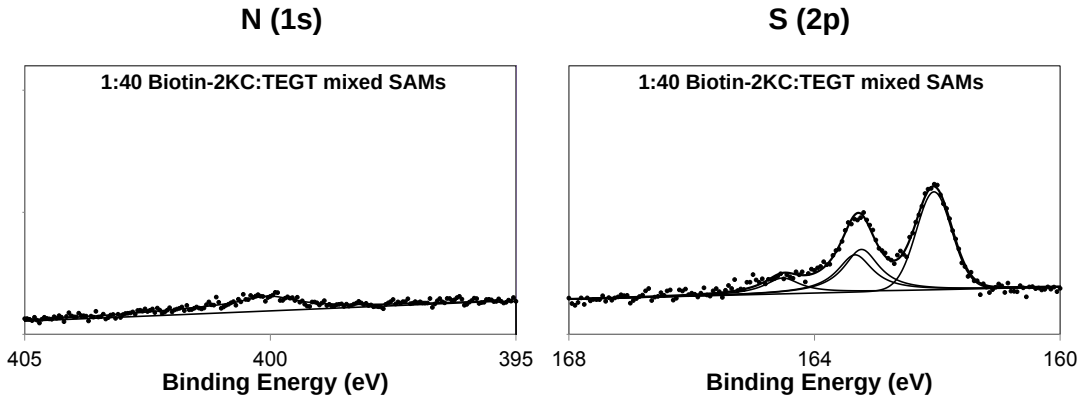

Figure 4.11 – *XPS spectra of N 1s (left) and S 2p (right) for biotin-2KC:TEGT 1:40 solution ratio*

The XPS spectra for biotin-2KC:TEGT 1:100 solution ratio are reported in **Figure 4.12**. The S 2p spectrum presents two doublets peaks, the first one centred at 163.4 eV (S $2p_{1/2}$) and 162.0 eV (S $2p_{3/2}$), can be assigned to the sulphur chemisorbed on the gold substrates, whereas the second doublet peaks, centred at 163.7 eV and 165.4 eV, respectively, refers to S-C bonds

present on biotin moieties. The N 1s spectrum presents a single, small peak, centred at 400.2 eV, can be assigned to amino (NH_2) and amide (CONH) groups.

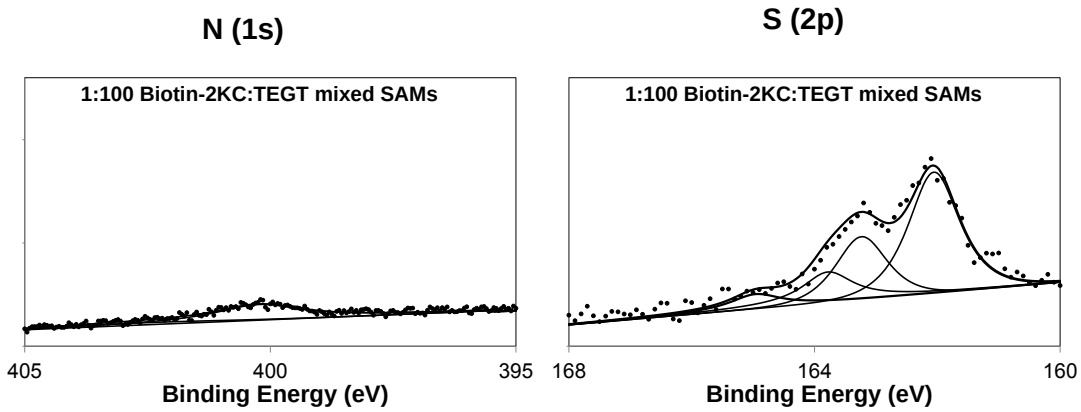

Figure 4.12 – *XPS spectra of N 1s (left) and S 2p (right) for biotin-2KC:TEGT 1:100 solution ratio*

The XPS spectra for biotin-6KC:TEGT 1:40 solution ratio are reported in **Figure 4.13**. The S 2p spectrum presents two doublets peaks, the first one centred at 163.3 eV (S $2p_{1/2}$) and 161.8 eV (S $2p_{3/2}$), is ascribable to the sulphur chemisorbed on the gold substrates, whereas the second doublet peaks, centred at 163.6 eV and 165 eV, respectively, can be assigned to S-C bonds present on biotin moieties. The N 1s spectrum, consisted of only one peak, centred at 400.3 eV, corresponds to amino (NH_2) and amide (CONH) groups.

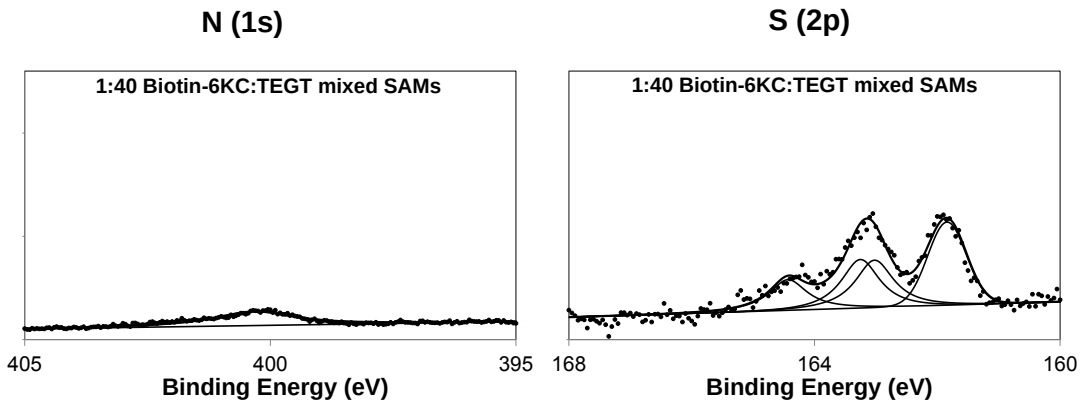

Figure 4.13 – *XPS spectra of N 1s (left) and S 2p (right) for biotin-6KC:TEGT 1:40 solution ratio*

The XPS spectra for biotin-6KC:TEGT 1:2000 solution ratio are reported in **Figure 4.14**. The S 2p spectrum presents two doublets peaks, the first one centred at 163.3 eV (S $2p_{1/2}$) and 161.8 eV (S $2p_{3/2}$), refers to the sulphur chemisorbed on the gold substrates, whereas the second doublet peaks, centred at 163.6 eV and 165.0 eV, respectively, can be assigned to S-C bonds present on biotin moieties. The N 1s spectrum presents an extremely small peak, that was magnified, centred at 400.3 eV, can be assigned to amino (NH_2) and amide (CONH) groups.

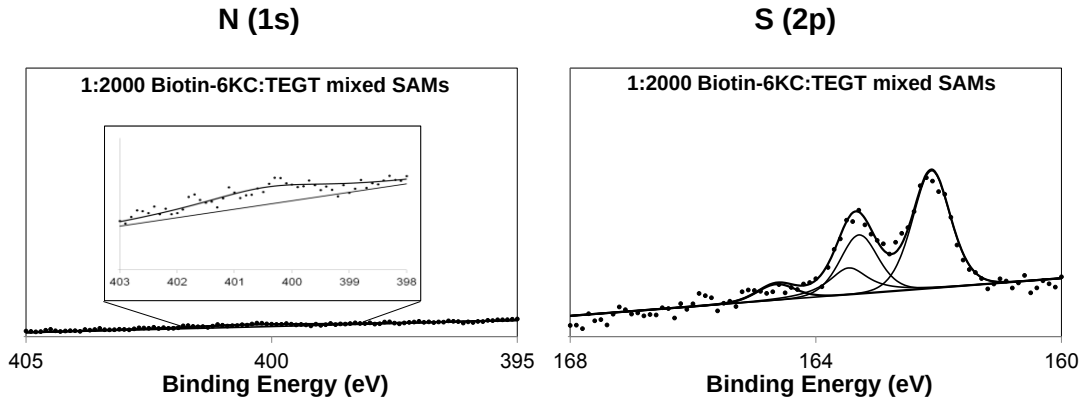

Figure 4.14 – *XPS spectra of N 1s (left) and S 2p (right) for biotin-6KC:TEGT 1:2000 solution ratio*

The calculated surface ratios for both biotin-2KC:TEGT and biotin-6KC:TEGT mixed SAMs analysed are reported on **Table 4.4**.

Table 4.4 – *Solution ratios of biotin-2KC:TEGT and biotin-6KC:TEGT mixed SAMs and relative surface ratios calculated by XPS.*

	Ratio	
	Solution	**Surface**
Biotin-2KC:TEGT	1:40	1:6 ± 1
	1:100	1:16 ± 2
Biotin-6KC:TEGT	1:40	1:7 ± 2
	1:2000	1:17 ± 2

From the results collected, it is possible to infer that the length of the oligopeptide influences the surface ratio. To obtain a surface ratio of ≈1:5, a solution ratio of 1:40 is needed

for both biotin-2KC:TEGT and biotin-6KC:TEGT mixed SAMs, whereas only a solution ratio of 1:10 was sufficient for the biotin-4KC:TEGT mixed SAMs. A different behaviour is observed for the ≈1:16 surface ratio. In this case, the biotin-6KC:TEGT mixed SAMs need a higher content of TEGT molecules in solution than the biotin-2KC:TEGT mixed SAM to obtain the same surface ratio. This is due to a preferential absorption of the longer chain thiol. As stated before as the chain length increases, the preferential adsorption of the longer thiol increases as consequence.[79,80,336,337]

4.3.2 SPR analysis of biotin-2KC:TEGT and biotin-6KC:TEGT mixed SAMs switching properties

The switching properties of biotin-2KC:TEGT and biotin-6KC:TEGT mixed SAMs were tested by electrochemical SPR, in the same ON (+0.3 V), OC and OFF (-0.4 V) conditions used with biotin-4KC:TEGT and described before. The recorded SPR sensorgrams are reported in **Figure 4.15**.

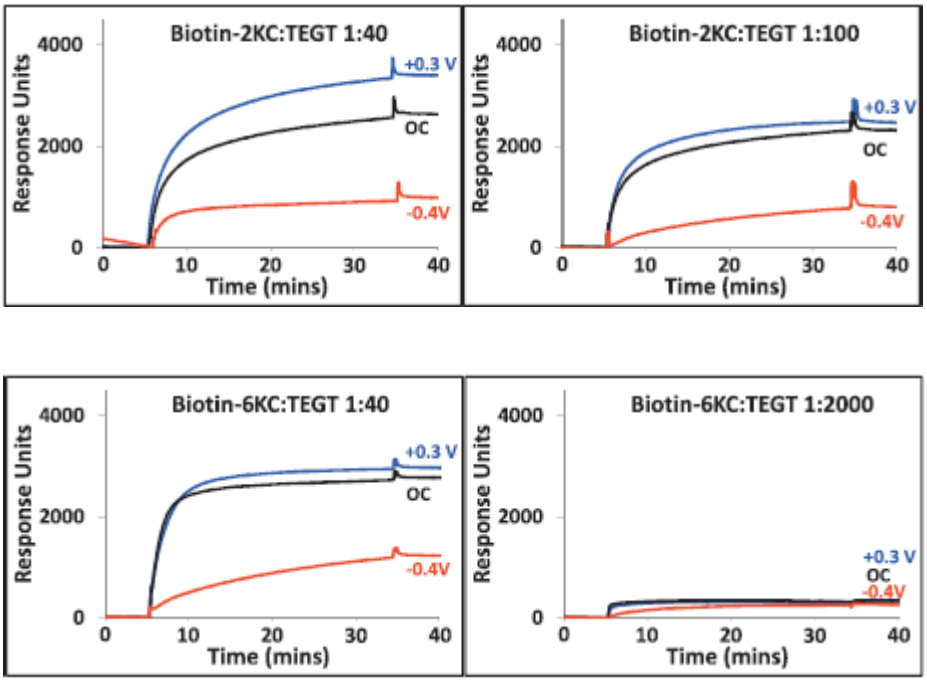

Figure 4.15 – *SPR sensorgram traces showing the binding of neutravidin to the biotin-2KC:TEGT mixed SAMs (solution ratios of 1:40 and 1:100) and biotin-6KC:TEGT mixed SAMs (solution ratios of 1:40 and 1:2000) under open circuit conditions, an applied positive (+0.3 V) and negative(−0.4 V) potential.*

The binding capacity and the switching efficiency of both biotin-2KC:TEGT and biotin-6KC:TEGT mixed SAMs calculated from electrochemical SPR experiments are shown in **Table 4.5**.

Table 4.5 – *Binding capacity expressed in Resonance Units and switching efficiency calculated from electrochemical SPR experiments on biotin-2KC:TEGT and biotin-6KC:TEGT mixed SAMs.*

	Ratio		**Binding Capacity (RU)**	**Switching Efficiency (%)**
	Solution	**Surface**		
Biotin-2KC:TEGT	1:40	1:6 ± 1	2634 ± 183	74 ± 4
	1:100	1:16 ± 2	2295 ± 87	67 ± 8
Biotin-6KC:TEGT	1:40	1:7 ± 2	2822 ± 129	71 ± 7
	1:2000	1:17 ± 2	229 ± 58	7 ± 4

By comparing the experimental data with those collected for biotin-4KC:TEGT mixed SAMs at the same surface ratios, it is possible to see that the binding capacity of biotin-4KC and biotin-2KC are similar, whereas it decreased significantly in the case of 1:16 biotin-6KC:TEGT surface ratio. From the results obtained it is possible to assume that the low binding capacity of biotin-6KC:TEGT mixed SAMs is due to the unfavourable orientation of the biotin molecules on the surface, caused by the long and flexible six-lysine oligopeptide chains.

In the case of the ≈1:5 surface ratio, it is possible to observe a discrepancy between the switching efficiency for the biotin-4KC:TEGT mixed SAM and the one for the biotin-2KC:TEGT mixed SAM. This difference can be understood by looking at the calculated molecular lengths. Biotin-4KC molecules measure 5.2 nm, needing a greater free volume on the surface than biotin-2KC (3.4 nm), to successfully undergo the molecular switching. Notably, the switching

efficiency of biotin-6KC:TEGT at the same surface ratio (≈1:5) is also higher than for the biotin-4KC:TEGT mixed SAMs. This behaviour can be explained by considering the possible intercrossing between biotin-6KC molecules, induced by conformation changes, reducing the availability of biotin moieties for neutravidin binding. This can be due to the greater chain-chain repulsion forces of longer charged oligopeptides, resulting in a highly-disordered arrangement on the gold surface.[339,340] In the case of ≈1:16 surface ratio, the switching of biotin-6KC:TEGT is significantly impaired relative to biotin-2KC:TEGT and biotin-4KC:TEGT mixed monolayers. The differences in switching efficiency demonstrated that the switching unit length plays and important role in regulating the molecular changes triggered by the application of an electrical potential. A longer switching unit can place constraints on the rearrangement of the biotin moiety on the surface, such that it can be available or not for neutravidin binding.

4.2.5 Molecular Dynamics Simulations

The SPR results showed that the 1:40 biotin-4KC:TEGT solution ratio is the best performing one, in terms of switching ability. When the biotin-4KC in the mixed SAM is high (1:0-1:10 solution ratios), the oligopeptide backbone is unable to correctly undergo a molecular rearrangement on the surface, resulting in the exposure of the biotin moiety also when a negative potential is applied. As demonstrated by the SPR studies, a high concentration in oligopeptide molecules in the surface results in a poor switching efficiency. The main hypothesis arising from the observation made so far was that the ON/OFF behaviour of the mixed biotin-4KC:TEGT, biotin-2KC:TEGT and biotin-6KC:TEGT SAMs is due to a spatial modification of the switching backbone on the surface. This modification causes a change in the availability of biotin on the gold substrate for binding with neutravidin in solution.

To have an insight into the mechanism governing the switching performance of the tested mixed SAMs, molecular dynamics (MD) simulations were performed by Dr Xingyong Wang at Nanjing University (China). The MD simulations results are included in this dissertation thesis to explain and support the electrochemical SPR results collected during this research work. The success of MD simulations is strongly related to the force field used for the test. Three different force fields were chosen and tested: cvff (consist-valence force field), compass (condensed-phase optimized molecular potentials for atomistic simulation studies) and pcff (polymer consistent force field). The cvff force field gave the best results and it was chosen for our simulations. The surface models used in the simulations are shown in **Figure 4.16**.

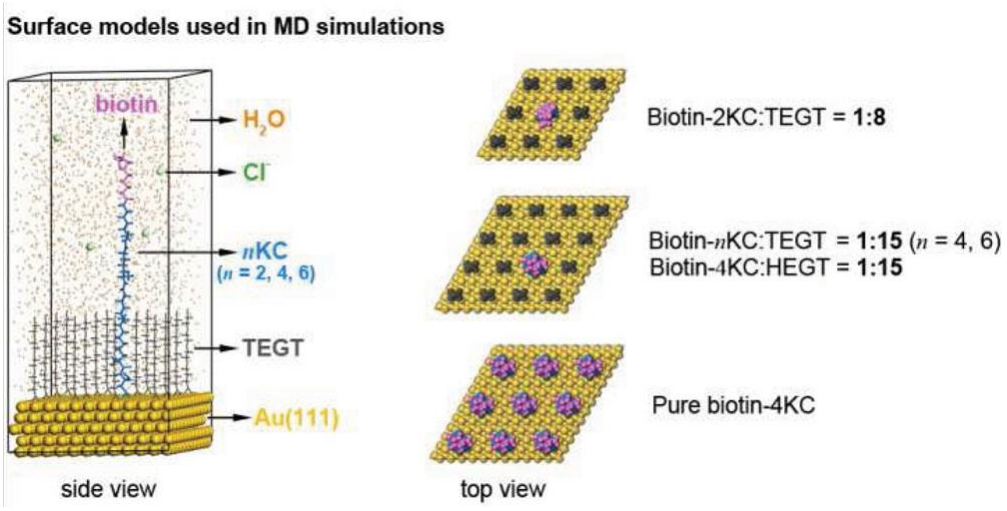

Figure 4.16 – *The surface models used in the MD simulations. The different colours in the biotin-nKC chain represent the biotin moiety (purple), the four lysine (blue) and the cysteine residues (dark green), respectively. Water molecules are represented by the orange dots. The green and yellow balls denote the chloride ions and the gold atoms respectively, and the short grey chains represent TEGT molecules.*

Two-dimensional rhombic periodic boundary condition and slab models were applied during the simulations. The PBS buffer solution was simulated by employing water molecules and chloride ions. The model parameters are summarised in detail in Chapter 3 – Experimental Procedures and Protocols (**Table 3.1**).

The electrical potentials employed in the SPR experiments were modelled by applying external electric fields. These electric fields caused a polarisation that can be considered by employing the density functional theory-derived partial charge, in the simulations. Simulations were carried out on biotin-nKC:TEGT (n= 2,4,6) and pure biotin-4KC SAMs.

An evident switching behaviour can be observed for biotin-2KC:TEGT (surface ratio 1:8) and biotin-4KC:TEGT (surface ratio 1:16), when a positive electric field E_z was applied turning the system to the "ON" state (**Figure 4.17**).

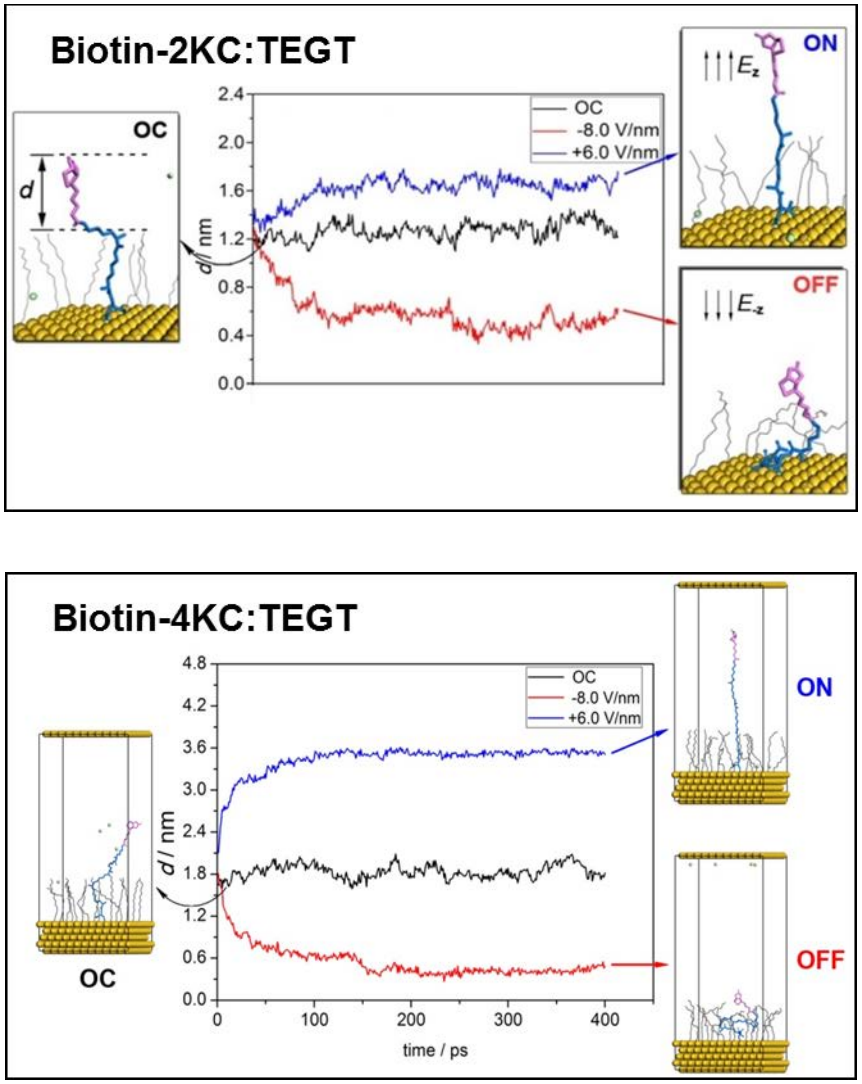

Figure 4.17 – *Conformational changes of biotin-2KC:TEGT (surface ratio of 1:8) and biotin-4KC:TEGT (surface ratio of 1:16) mixed SAMs, under different electric field, along with the MD simulation snapshots. The direction of the applied electric field is indicated by the black arrows. Water molecules and hydrogen atoms are omitted for clarity. The gap distance variation between the biotin moiety and the TEGT matrix is indicated by* ***d****.*

In this state, the oligolysine chain is fully extended on the surface, completely exposing the biotin head. Neutravidin molecules will then bind strongly with the available biotin moiety, resulting in a high binding capacity, as verified by SPR. When a negative electric field E_{-z} was

applied, the system was switched to the “OFF” state. In this case, the oligopeptide backbone rearranged on the surface, adopting a collapsed conformation. The biotin moiety resulted being partially concealed by the TEGT molecules and unable to biointeract with neutravidin, showing no bioactivity. When no electric field was applied, this corresponded to the OC state studied by SPR. In this state, the switchable backbone adopted an intermediate conformation, resulting in a moderate bioactivity. The MD simulation results were in fair agreement with the data collected with the SPR experiments for the best-performing ratio of biotin-4KC:TEGT mixed SAM. SPR analysis of the switching capacity revealed high binding when a positive potential of +0.3V is applied.

The switching mechanism is controlled by the electrostatic interaction between the positively charged oligolysine side chains and the applied electric field. In the case ofbiotin-6KC:TEGT (1:15 surface ratio), the oligopeptide backbone is composed by six lysine, being too long to allow the shielding of biotin moieties by TEGT molecules in the folded conformation (**Figure 4.18**). Another important characteristic of note is that, when a negative electric field is applied to the biotin-6KC:TEGT mixed SAM, the biotin head is still highly available for binding. This can be observed from the gap distance variation between the biotin and the TEGT matrix (**d**), which is more than 1.5 nm.

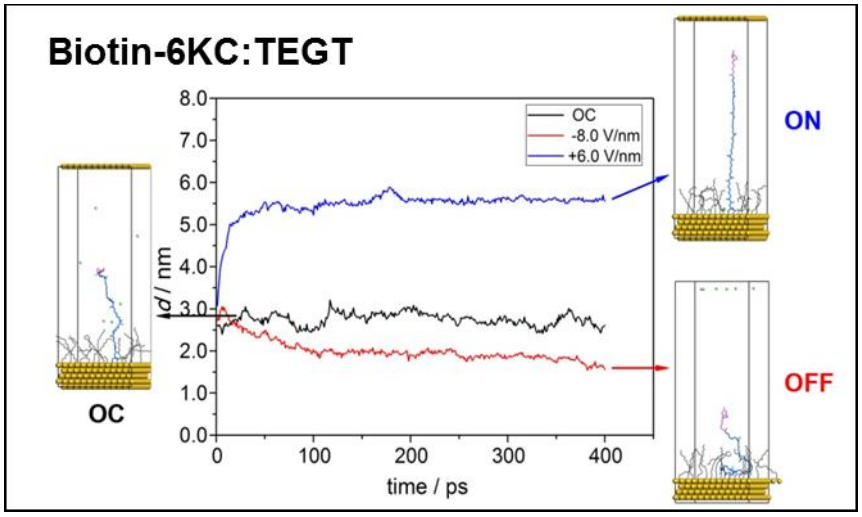

Figure 4.18 – *Conformational changes of biotin-6KC:TEGT (surface ratio of 1:15) mixed SAMs, under different electric field, along with the MD simulation snapshots. The direction of the applied electric field is indicated by the black arrows. Water molecules and hydrogen atoms are omitted for clarity.*

The MD simulations data were in agreement with the experimental data and confirmed that a long switching unit is not suitable for controlling ligand bioactivity under an electrical potential. These results are in line with previous research demonstrating that a longer biotin linker lead to a high protein binding efficiency[341].

X-ray crystallographic analysis showed that the biotin is buried quite deeply inside the Neutravidin barrel, indicating that the biotin moiety needs to be completely inserted into the Neutravidin binding pocket to have an efficient binding[342–345]. From these results, it is possible to infer that a space of more than 1.5 nm is needed between the biotin moiety and the ethylene glycol thiol matrix. These hypotheses are also consistent with the data obtained for biotin-2KC and biotin-4KC under a negative electric field E_z and the poor binding capacity obtained in the SPR experiments.

In the case of OC conditions, the charged oligopeptide chains are not blocked in an upright position by the positive potential, increasing the chances of intercrossing between the oligopeptide chains, this phenomenon causes the biotin to be partially hindered from interaction with biotin, justifying the lower bio-activity observed, compared to the ON state. These findings can then be used to explain how each component of the mixed SAM and each electrical condition govern the switching mechanism of the oligopeptide mixed monolayer.

The last consideration to be done is on the influence of the oligopeptide density on the switching performance. In the case of pure biotin-4KC SAM, the oligopeptide chains are closely packed on the surface, not allowing enough free space for the chains to undergo a molecular rearrangement when a negative potential is applied (**Figure 4.19**).

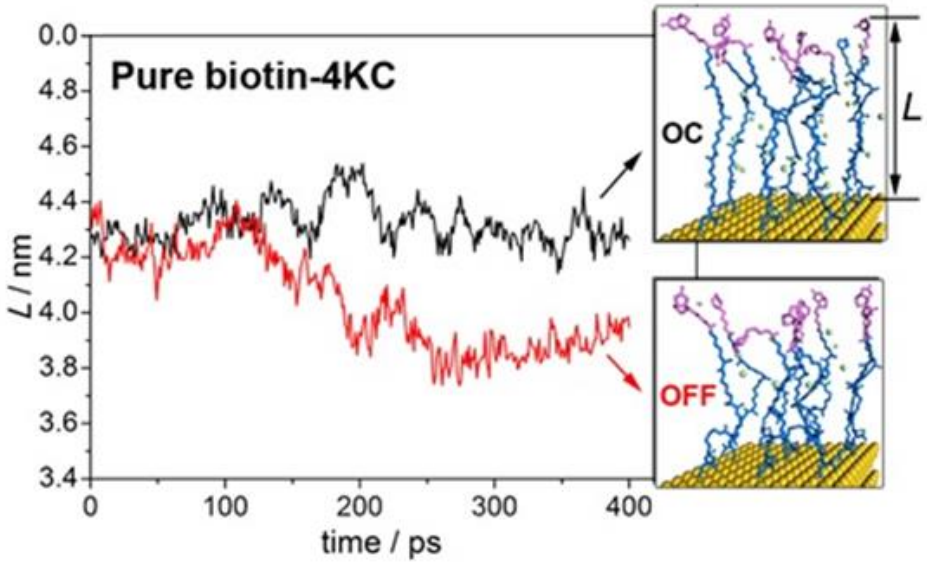

Figure 4.19 – *Conformational changes of the pure biotin-4KC SAM under different electric fields (left) and MD simulation snapshots (right).* ***L*** *represents the variation of the gap distance between the biotin end group and the gold substrate.*

Consequently, the biotin moieties were fully exposed on the surface at all time, leading to a persistent bio-activity. This observation is consistent with the experimental data collected by SPR in ON, OC and OFF conditions. It is therefore important to design mixed SAMs where the switchable component possesses enough free space for conformational transitions.

4.4 Conclusions

Devices able to control the bioactivity of molecules on the surface, upon the application of a stimulus, can have wide biological and medical applications in the study of cellular processes regulation[10,173]. In this work, it was demonstrated that the switching mechanism of charged oligopeptides mixed monolayers is based on a molecular rearrangement on the surface, between a collapsed bio-inactive and a fully extended, bio-active conformation of the oligopeptide chains.

These dynamic changes are controlled by the electrostatic attraction or repulsion between the oligopeptide charged side chains and the substrate, resulting in a variation of the gap distance (d) between the biotin end group and the ethylene glycol thiol matrix. When the biotin moiety moves closer to the matrix, it is partially hindered and prevented from the binding with neutravidin. On the contrary, when the oligopeptide chains are fully elongated on the surface, the increase in the distance of the biotin from the matrix gives the biotin enough free space to correctly be inserted in the Neutravidin binging pocket.

The detailed experimental and computational studies conducted in this research work, imply that steric hindrance due to the neighbouring surface-confined oligopeptide chains, significantly affects the switching efficiency of the mixed SAMs tested. The switching unit length is an important factor to be considered in the design of switchable surfaces. In addition

to this, the ratio of the SAMs component has to be optimised to maximise the switching efficiency of the system.

The findings of our research can help in the development of new dynamic surface materials that can find various applications in cellular studies and drug delivery systems.

Chapter 5 - Study of the switching properties of progesterone-C7-4KC:EG6OH mixed SAMs

Abstract: *This chapter presents a detailed analysis of the development of switchable mixed self-assembled monolayers exploiting the antigen-antibody (Ag-Ab) interaction. A model system composed by a lysine oligopeptide carrying a progesterone moiety has been used for the purposes of this work. Herein a detailed study is presented, on the feasibility of controlling the interaction between the progesterone group and its anti-mouse antibody upon the application of an electrical potential. The effect of different percentages of Bovine Serum Albumin (BSA) on the switching abilities of the studied system has also been investigated. Hexaethylene glycol thiol (EG6OH) molecules have been used as second component in the mixed SAMs. The investigation has been conducted on different progesterone oligopeptide/EG6OH ratios on the gold surfaces to identify the best performing one. The presence of EG6OH molecules on the gold surface prevent any undesired antibody unspecific binding and donate protein-resistant characteristics to the surface itself. In addition, it provides molecular space to the oligopeptide units to efficiently undergo their molecular rearrangement on the gold surface, upon the application of an electrical potential.*

5.1 Introduction

The interaction between an antigen and its relative antibody has been widely exploited in several immunosensors platforms[346]. Such biosensors exploit the biorecognition between a ligand on the surface (usually the antibody) and its binding partner in solution, called analyte (antigen)[347]. These devices find important application in biomedical research, for diagnostic purposes, especially for the identification of cancer markers. In this case, the ability to detect low concentration of biomolecules involved in the early stages of cancer development is of

paramount importance for the success of cancer therapies and still remains one of the major challenges for researchers[348].

A well-known, label-free detection method for immunosensing is provided by surface plasmon resonance[349]. SPR was used for immunosensing in 1983 for the first time[283], since then several SPR platform exploiting the antibody-antigen interaction have been developed. These platforms usually present the antibody immobilised on the metal surface, that is able to discriminate between different isoforms of an antigen in solution. However, due to the small molecular weight of the antigen molecules, if compared to the antibody one, the SPR response could not always be detectable[347]. The immobilisation of an antigen chemically modified with a molecular linker to allow the binding to the metal surface present the advantage of enhancing the surface plasmon resonance response when a high-molecular weight antibody, leading to a large shift in the SPR signal[347].

The current research on immunosensors does not present any work on the control of the antigen exposure on the sensor surface upon the application of an electrical potential. The interaction is always studied in static conditions and it is only used to either discriminate between different antigens able to bind to the same antibody or between different antibodies, able to bind the same epitope on an antigen molecules[350,351]. Designing a smart surface able to expose or conceal an antigen molecule, by simply switching between a positive and a negative potential can easily find an application in the biomedical research field.

In Chapter 4 we described how to selectively control the interaction between a biotin moiety bound to a 4-lysine chain and anchored to the gold surface thanks to a cysteine molecule and molecules of neutravidin in solution. The same system was also used to investigate the concealment and exposure of arginine–glycine–aspartate (RGD) oligopeptides

to control cell adhesion, with successful results[199]. Starting from this background, the antigen molecules can be chemically modified by binding lysine oligopeptide chains that have already been successfully used as switching units[196–199]. The lysine aminoacid presents a positive charge at pH 7, that can be exploited to obtain a molecular rearrangement of defined molecules on the sensor surface.

In this work, we want to develop a novel system able to control the exposure of a chemically modified antigen anchored to the gold surface, by applying an electrical potential. In particular, we want to achieve the possibility, to control the exposure of progesterone moieties on the sensor surface, never analysed before. The results of this work can then be used to investigate the hyperactivation of sperm cells, one of the crucial steps during fertilisation[238,239].

In this work, different mixed SAM were studied, with molecules of progesterone as the antigen end group. The progesterone molecule was bound to an alkyl chain through an oxime group, connected to a switchable oligolysine chain, used in our previous work[197]. The first component of the chosen mixed SAM for this work, is a lysine (K) oligopeptide, functionalised at one end with a progesterone moiety, able to strongly interact with the anti-mouse progesterone antibody, and at the other end with an aminoacid of cysteine (C) to anchor the oligopeptide to the gold substrates via the thiol group. The alkyl chain composed by eight methylene groups has been chosen to space out the progesterone moiety from the hydrophilic chain of four lysine. A hydrophobic spacer will allow the progesterone to be inserted inside the sperm cells hydrophobic membrane, where its receptors are located[352–355]. The second component is represented by a hexaethylene glycol-terminated thiol (EG6OH). The aim of EG6OH molecules is both to space out the oligopeptide to allow enough space on the surface

for molecular rearrangement and impede any undesired unspecific binding of anti-mouse progesterone antibody on the gold surfaces (**Figure 5.1**).

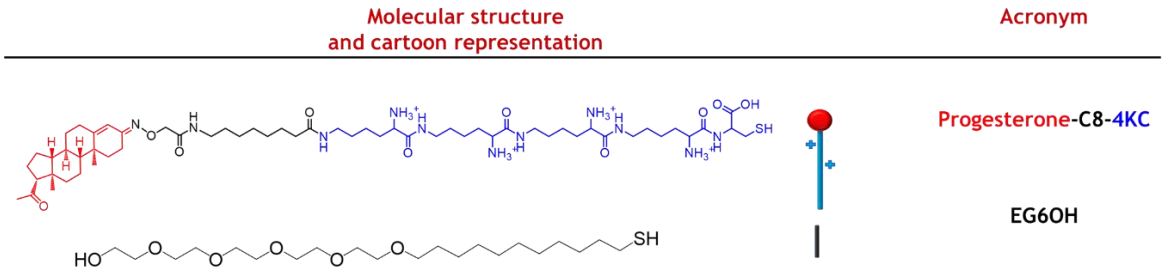

Figure 4.1 *- Molecular structures and related cartoons of the oligopeptide (progesterone-C7-4KC) and the hexaethylene glycol-terminated thiol (EG6OH) used in the mixed SAMs, and their calculated molecular lengths in fully extended conformations.*

The results of this analysis will permit a better design of novel sensing platforms, that can discriminate between damaged and healthy sperm cells, applicable to *in-vitro* Fertilisation (IVF) research purposes.

5.2 Objectives

1. Characterisation of different progesterone-C7-4KC:EG6OH solution ratios (1:10, 1:40 and 1:100) on gold surfaces by XPS, to evaluate the differences between solution ratio and surface ratio.
2. Analysis, by electrochemical SPR of the specificity of the anti-mouse progesterone antibody, in OC conditions, on both a pure biotin-4KC and a pure EG6OH SAMs.
3. Analysis, by electrochemical SPR, of the switching properties in PBS of the different mixed SAM ratios, to select the one with the highest switching efficiency and develop a novel platform for the control over the antigen-antibody interaction, upon the application of an electrical potential. The switching efficiency of the best performing mixed SAM will be then be tested in sEBSS+0.3%BSA, buffer that will be used for the preparation of sperm cells (see Chapter 6).
4. Comparison of the best performing surface ratio of progesterone-C7-4KC switching efficiency in PBS, EBSS and EBSS containing different percentages of BSA (0.1% and 0.3%)

5.3 Results and Discussion

5.3.1 Formation of mixed progesterone-C7-4KC:EG6OH mixed SAMs

The aim of this work is to develop a switchable sensing platform able to control the exposure of progesterone molecules on the gold substrates. Piranha-cleaned gold substrates were incubated into different solution ratios of mixed progesterone-C7-4KC:EG6OH SAMs.

In this research work, we chose to immobilise a molecule of progesterone (antigen) purposely chemically modified to contain a switching unit and a sulphur atom for the binding to the gold surface. This strategy will allow the obtainment of an enhanced SPR response when the antibody in solution will bind to the progesterone moiety anchored to the gold surface[347].

When a negative potential is applied to the to the gold substrate, the lysine oligopeptide is expected to be attracted towards the surface. This attraction will drag the progesterone moiety, that will then be hindered from the interaction with the anti-mouse monoclonal progesterone antibody, by the EG6OH molecules. On the contrary, when a positive potential is applied the lysine oligopeptide will be repelled by the positive charge on the gold surface, being fully extended on the surface, therefore completely exposing the progesterone moiety for the interaction with the monoclonal anti-mouse antibody. EG6OH molecules were employed to prevent non-specific binding of antibody on the surface and to give enough conformational freedom to the progesterone-C7-4KC component to undergo the switching (**Figure 5.2**).

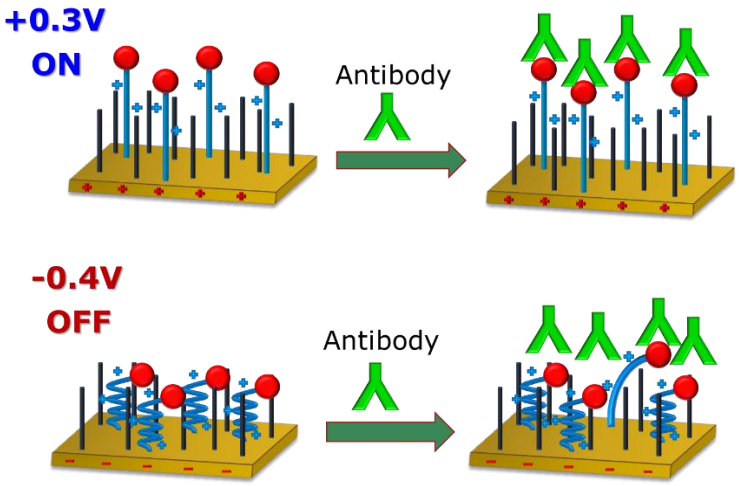

Figure 5.2 *- Cartoon representation of the ON-OFF switching system that controls the biomolecular interaction between progesterone (red) on the surface and antibody (green) in solution.*

5.3.2 XPS characterisation of progesterone-C7-4KC:EG6OH mixed SAMs

One of the aims of this research work is to create a mixed SAM platform that can present a similar switching ability to the one obtained with the biotin-4KC:TEGT system, described in Chapter 3[197]. Three progesterone-C7-4KC:EG6OH solution ratios of 1:10, 1:40 and 1:100 were characterised by XPS. The 1:40 solution ratio was chosen, because, as demonstrated in Chapter 3, it gives to the switching oligopeptide the correct spatial area on the surface to undergo the desired molecular rearrangement[197].

5.3.2.1 Progesterone-C7-4KC:EG6OH 1:10 solution ratio

The XPS analysis carried out for the 1:10 mixed SAM revealed the presence of the elemental species S, N, C and O, confirming the formation of the mixed SAM. The S 2p spectrum (**Figure 5.3 a**), consists of a doublet peak at 163.2 eV (S $2p_{1/2}$) and 162.1 eV (S $2p_{3/2}$) corresponding to the S-Au bond[252,255,334,335]; the second doublet peak centred at 164.7 (S $2p_{1/2}$)

eV and 163.8 eV (S $2p_{3/2}$) can be assigned to the S-H group, due to the presence of an undesired amount of free, unbound thiol molecules on the gold surface[252,255,334,335]. The unattached molecules can be either those of the ethylene glycol thiol or those of the oligopeptide molecules.

In the N 1s spectrum (**Figure 5.3 b**), only one peak can be fit, due to the high background noise. This peak is centred at 400.0 eV, attributable to amino (NH_2) and amide (CONH) groups and one [252,255,334,335].

The C 1s spectrum can be de-convoluted into three peaks (**Figure 4.3 c**), attributable to five different binding environments. The first peak at 284.8 eV corresponds to C-C bonds, the second peak at 286.6 eV can be attributed to the binding environments of C-S, C-N and C-O and the smaller third peak at 288.0 eV corresponds to the carbonyl moiety C=O[252,255,334,335].

The O 1s spectrum (**Figure 4.3 d**) can be de-convoluted into two different peaks, one at 532.7 eV corresponding to C-O bonds and one at 531.3 eV corresponding to C=O bonds[252,255,334,335].

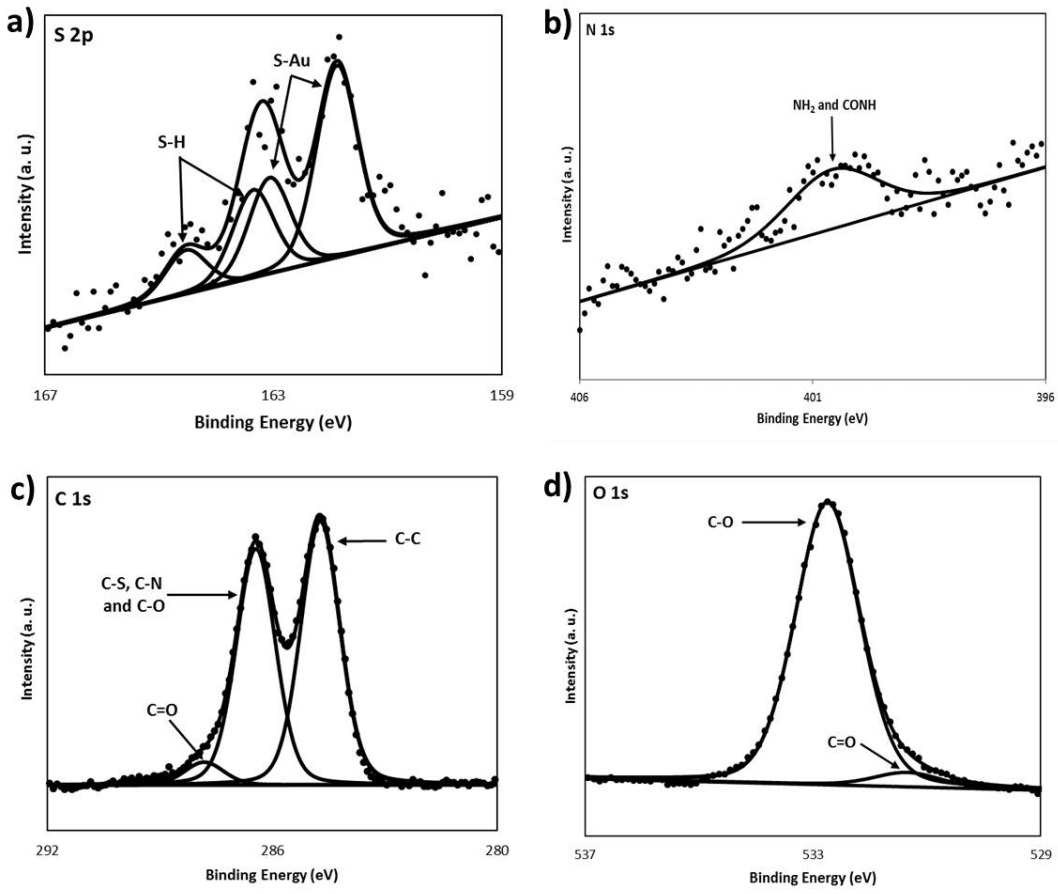

Figure 5.3 – *XPS spectra of the a) S 2p, b) N 1s, c) C 1s and d) O 1s regions for the 1:10 progesterone-C7-4KC:EG6OH mixed SAM solution ratio.*

To calculate the surface ratio of the mixed SAM, the areas of S 2p and N 1s peaks were integrated and it was taken into consideration that the progesterone-C7-4KC oligopeptides (**Figure 5.1**) contain 11 N atoms and 1 S atom and that EG6OH presents no N atoms and only 1 S atom. **Equation 5.1** was used to calculate the number of ethylene glycol thiol molecules per oligopeptide on the gold surface.

$$No.of\ EG6OH = \left(No.of\ N\ per\ peptide\ x\ \frac{S\ area}{N\ area}\right) - No.of\ S\ per\ peptide$$

Equation 5.1

The calculated surface ratio for the progesterone-C7-4KC:EG6OH mixed SAM, corresponded to 1:9±3, different from the solution ratios, as described in previous studies of two-components SAMs[79,80].

The surface ratio obtained for the 1:10 progesterone-C7-4KC:EG6OH mixed SAMs is slightly higher compared to the one obtained for the 1:10 biotin-4KC:TEGT mixed SAMs solution ratio. This discrepancy could be due to the longer chains composing the progesterone-C7-4KC:EG6OH mixed SAMs. In addition, the presence of different chemical groups attached to the oligopeptide chains and the higher number of ethylene glycol thiol groups in the EG6OH molecules, compared to the TEGT molecules can drive to a different chemical rearrangement of thiols on the gold surfaces[35,87,108,356,357]. By observing the behaviour of longer oligopeptide molecules of Biotin-6KC, analysed in Chapter 4, it is possible to hypothesise that the high concentration of progesterone-C7-4KC molecules will lead to a similar molecular intercrossing phenomenon, resulting in a poor switching efficiency of the 1:10 solution ratio. This hypothesis will be verified by electrochemical SPR in section 5.4.2.

5.3.2.2 Progesterone-C7-4KC:EG6OH 1:40 solution ratio

In Chapter 3 was shown that 1:40 solution ratio of Biotin-4KC:TEGT mixed SAM, corresponding to 1:16±4 surface ratio, possess the best switching characteristics amongst the system tested. Thus, the same solution ratio was first tested and characterised, to analyse how the differences between the biotin-4KC:TEGT mixed SAMs and the

progesterone-C7-4KC:EG6OH mixed SAMs, such as the molecular length of the SAMs components, could influence their organisation on the gold surface.

XPS analysis showed the presence of S, N, C and O elements (**Figure 5.4**) confirming the formation of the mixed SAM. The S 2p spectrum (**Figure 5.4 a**) consists of two doublet peaks, the first one at 163.3 eV (S $2p_{1/2}$) and 162.1 eV (S $2p_{3/2}$), assignable to the sulphur chemisorbed to the gold surface[252,255,334,335]. The second one is centred at 163.8 eV (S $2p_{3/2}$) and 165 eV (S $2p_{1/2}$) assignable to unbound sulphur present on the gold surface[252,255,334,335]. The N 1s spectrum (**Figure 5.4 b**) is de-convoluted into one single peak, centred at 399.7 eV corresponding to amino (NH_2) and amide (CONH) groups[252,255,334,335]. As expected, the N 1s spectrum is smaller than the one recorded for the 1:10 progesterone-C7-4KC:EG6OH mixed SAM ratio.

The C 1s spectrum (**Figure 5.4 c**) is de-convoluted into three peaks, which can be attributed to five different binding environments. The peak at 284.7 eV corresponds to C-C bonds, while the peak at 286.6 eV corresponds to the three binding environments of C-S, C-N and C-O. The smaller peak at 287.7 eV can be assigned to the carbonyl moiety C=O[252,255,334,335]. The O 1s spectrum (**Figure 5.4 d**) is de-convoluted into two peaks, the first one at 533.1 eV is attributable to C-O bonds and the second one at 531.8 eV corresponds to C=O bonds[252,255,334,335].

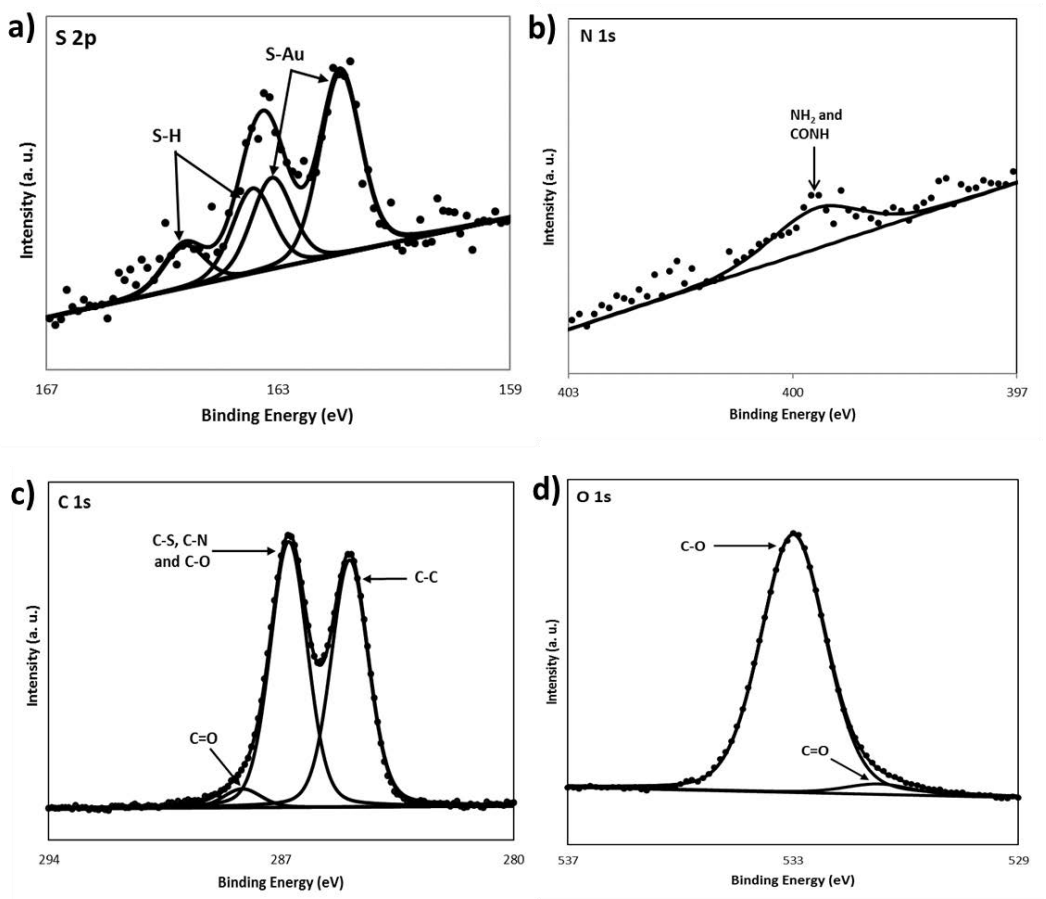

Figure 5.4 – *XPS spectra of the a) S 2p, b) N 1s, c) C 1s and d) O 1s regions for the 1:40 progesterone-C7-4KC:EG6OH mixed SAM solution ratio.*

By using **Equation 5.1** it is possible to calculate the surface ratio for the progesterone-C7-4KC:EG6OH mixed SAM, corresponding to 1:22±5, not matching the solution ratio, as expected[79,80]. The differences with the surface ratio obtained from the 1:40 biotin-4KC solution ratio can be attributed to the different chain lengths of the components of the mixed monolayer, the different end group on the oligopeptide chain and the different type of ethylene glycol thiol. In fact, EG6OH molecules are composed by six ethylene glycol groups and a spacer of 11 carbon atoms, between the ethylene glycol groups and the sulphur head group, offering the conditions to form a highly-packed matrix[35,87,108,356,357].

5.3.2.3 Progesterone-C7-4KC:EG6OH 1:100 solution ratio

The XPS analysis of the Progesterone-C7-4KC:EG6OH mixed SAM at a solution ratio of 1:100 showed the presence of S, C and O elements, but no N signal could be recorded (**Figure 5.5**).

The S 2p spectrum (**Figure 5.5 a**) present two doublet peaks, the first one centred at 163.3 eV (S $2p_{1/2}$) and 162.1 eV (S $2p_{3/2}$), that can be attributed to the sulphur atom of the thiol groups, covalently bound to the gold substrate[252,255,334,335]. The second one is visible at 164.8 eV (S $2p_{1/2}$) and 163.7 eV (S $2p_{3/2}$) and it is ascribable to the unbound sulphur (S-H) present on the gold surface[252,255,334,335]. However, it is possible to infer that a small quantity of unbound sulphur is present on the gold surface. The N 1s spectrum was recorded (**Figure 5.5 b**) but no peak could be identified, due to high noise of the background, not allowing a quantitative interpretation of the surface ratio. The C 1s spectrum (**Figure 5.5 c**) showed the presence of five different binding environments and it can be de-convoluted into three peaks. The first one at 284.8 eV is referred to C-C bonds, the second peak at 286.6 eV can be assigned to C-S, C-N and C-O bonds. The smaller peak at 288.0 eV is assigned to the carbonyl moiety (C=O)[252,255,334,335].

The O 1s spectrum (**Figure 5.5 d**) can be de-convoluted into two peaks, corresponding to the binding environments of C-O (532.8 eV) and C=O (531.3 eV), respectively[252,255,334,335].

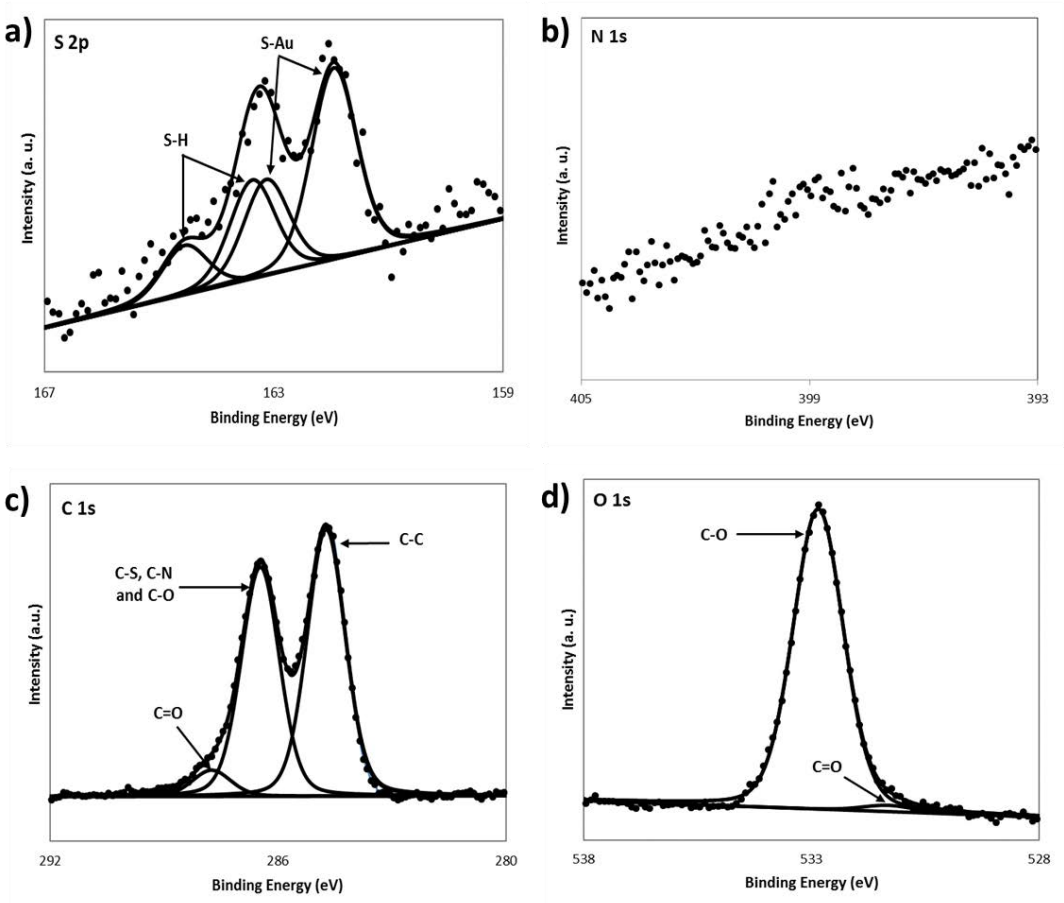

Figure 5.5 – *XPS spectra of the a) S 2p, b) N 1s, c) C 1s and d) O 1s regions for the 1:100 progesterone-C7-4KC:EG6OH mixed SAM solution ratio.*

Due to the impossibility of recording the nitrogen spectrum, it is possible to hypothesise a high percentage of ethylene glycol thiol molecules on the gold surface, forming a well-packed EG6OH matrix. This matrix should confer slightly hydrophilic characteristics to the 1:100 solution ratio surfaces and also constrain the oligopeptide molecules from undergoing a molecular rearrangement over the surface, leading to a low switching ability.

Ellipsometry, contact angle and SPR analysis of the selected surfaces were conducted to verify our hypothesis and are illustrated in the next sections.

5.3.3 Contact angle and ellipsometry characterisation of progesterone-C7-4KC:EG6OH mixed SAMs

The formation of progesterone-C7-4KC:EG6OH mixed monolayers, at 1:10; 1:40 and 1:100 solution ratios, were analysed by contact angle and ellipsometry. Pure progesterone-C7-4KC and pure EG6OH SAMs were characterised as a control (**Table 4.1**). The water advancing (**Adv**) and receding (**Rec**) contact angles for EG6OH revealed hydrophilic characteristics, whereas the pure progesterone-C7-4KC presented more hydrophobic characteristic. This behaviour can be due both to the oligopeptide molecules being collapsed on the chip surface, exposing the hydrophobic 8-carbon alkyl chain, and to the hydrophobic progesterone end group.

Ellipsometry analysis confirmed the formation of pure progesterone-C7-4KC SAMs, pure EG6OH SAM and mixed progesterone-C7-4KC:EG6OH mixed SAMs, but, as expected, the homogeneity of the mixed monolayers on surface was poor, due to difficulties in controlling the organisation of the two components of the mixed SAM on the gold surfaces. Ellipsometry results were fitted using a model based on the Cauchy equation, an empirical relationship between the refractive index and wavelength of light, which considers a SAM as a transparent layer. The thickness of the SAM was then calculated using multi-guess iterations that provide a thickness result with the lowest χ^2 (chi-square distribution) between the measured and the calculated values of ψ and Δ (see **section 2.3**). The formation of pure progesterone-C7-4KC monolayer resulted in an ellipsometric thickness of 4.4 ± 0.2 nm which is significantly lower that the calculated theoretical molecular length of 6 nm. As mentioned above, this difference can be explained with the oligopeptide chains being collapsed on the surface, exposing the hydrophobic alkyl spacers. The exact theoretical molecular length of progesterone-C7-4KC:EG6OH mixed SAM cannot be calculated, because this monolayer is composed by two

molecules presenting different molecular length. However, it is important to notice that the molecular lengths measured for the different ratios of the mixed SAM resulted in between the measured lengths for the pure progesterone-C7-4KC SAM and the EG6OH SAM. Interestingly, as the concentration of ethylene glycol molecules increased in the mixed SAM solution, the measured length became closer to the pure EG6OH SAM measure length, confirming the increment in the number of ethylene glycol thiol molecules on the surface.

Table 5.1 - *Advancing and receding water contact angle and ellipsometric thickness for the different monolayers formed for 24h. The calculated molecular lengths were determined using ChemBio3D Ultra 12.0 in which the molecules were in fully extended conformation. The averages and standard errors were calculated from at least three different measurements.*

Layer	**Contact Angle**		**Thickness (nm)**	
	Adv.	*Rec.*	*Calc.*	*Measured*
Progesterone-C7-4KC 0.1mM	70° ± 3	67° ± 4	6	4.4 ± 0.2
EG6OH 0.1 mM	41° ± 2	39° ± 3	3.3	2.4 ± 0.1
Progesterone-C7-4KC:EG6OH 1:10	52° ± 2	45° ± 3	-	3.8 ± 0.5
Progesterone-C7-4KC:EG6OH 1:40	43° ± 2	38° ± 4	-	3.1 ± 0.4
Progesterone-C7-4KC:EG6OH 1:100	40° ± 5	35° ± 2	-	2.8 ± 0.3

The contact angle results indicate that progesterone-C7-4KC:EG6OH mixed SAMs presented hydrophilic characteristics, comparable to the one obtained for the pure ethylene glycol thiol monolayer, indicating the larger presence of this component on the gold surface, compared to the oligopeptide chains. It has to be highlighted that, as the concentration of the EG6OH component increased on the gold surface, the mixed SAMs acquired more hydrophilic characteristics. The large hysteresis ($\theta_{Adv} - \theta_{Rec}$) presented by the mixed progesterone-C7-4KC:EG6OH monolayers are an indication of the low order of both layers. In addition, the difference in molecular length of the two SAM components lead to an uneven surface, causing such a large difference between the advancing and receding angles.

The measured thickness of both the pure progesterone-C7-4CK and pure EG6OH SAMs are lower than the theoretical thickness calculated using ChemDraw 3D. It is possible to infer that on both the resulting monolayer the molecules are partially collapsed on the gold surface, leading to a smaller thickness than the expected one.

5.4 SPR analysis of the progesterone-C7-4KC:EG6OH mixed SAMs and anti-mouse progesterone antibody

5.4.1 Testing the anti-mouse progesterone antibody specificity by SPR

Before starting the analysis of the switching capability of the chosen system, it was necessary to verify that the anti-mouse progesterone antibody was not recognising the second component of the mixed monolayer, EG6OH, as possible epitope. Pure EG6OH SAMs were tested by electrochemical SPR in OC conditions, in the presence of the antibody. A biotin-4KC:EG6OH mixed SAM of 1:40 solution ratio was also tested as an additional control.

Phosphate buffer saline (PBS) was flushed over the surface for 10 minutes to equilibrate the sensor chip and set the SPR baseline, in OC (no potential) state. This step was followed by injection of monoclonal anti-mouse progesterone antibody, diluted in degassed PBS, over the surface for 30 minutes, necessary to potentially allow the correct interaction between the antibody and both EG6OH and biotin molecules, attached to the gold substrate. After this exposure time, the chip was rinsed with degassed PBS, to remove any unbound protein still present in the sensor cell and the binding capacity was recorded.

As expected, no significant SPR signal shift was recorded with both EG6OH and biotin-4KC:EG6OH SAMs (**Figure 5.6**).

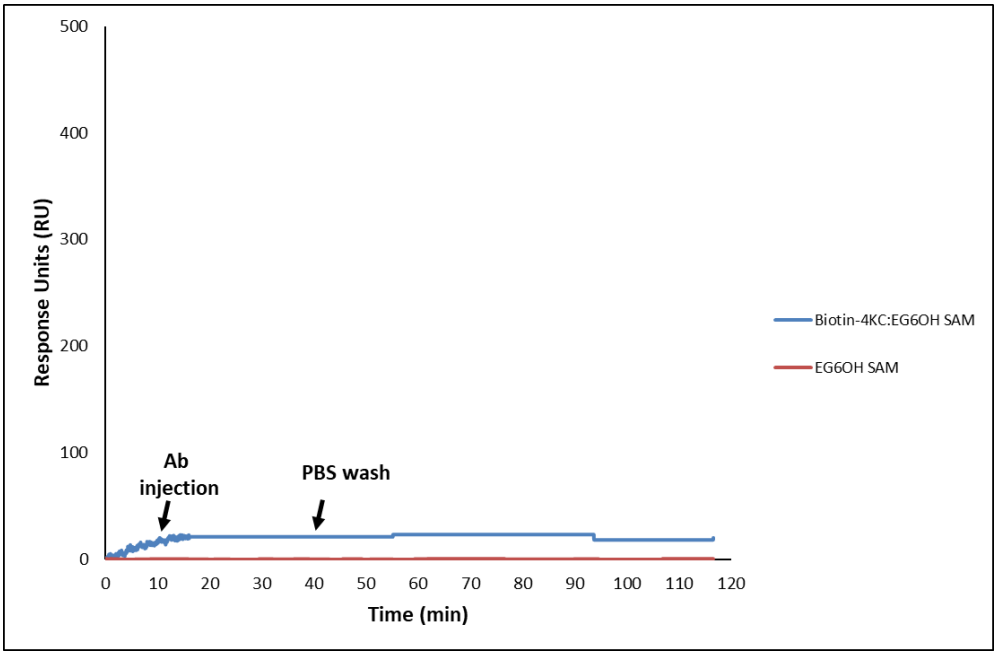

Figure 5.6 - *SPR sensorgram, recorded in OC (no potential applied) conditions, for the injection of anti-mouse progesterone antibody on both biotin-4KC:EG6OH and EG6OH SAMs.*

The results obtained confirmed that the second component of the progesterone-C7-4KC:EG6OH mixed SAM could not affect the binding capacity of the antibody to its relative antigen on the surface (progesterone moieties).

5.4.2 SPR analysis of the switching capabilities of progesterone-C7-4KC:EG6OH mixed SAMs in Phosphate Saline Buffer

To understand if the progesterone-C7-4KC:EG6OH mixed SAMs could control the progesterone exposure upon the application of an electrical stimulus, the three different solution ratios, 1:10, 1:40 and 1:100 and previously analysed by XPS, were tested by electrochemical SPR in Phosphate-Buffered Saline (PBS). These preliminary SPR experiment had the aim of identifying the best performing ratio to be selected to be tested in sEBSS+0.3% BSA. Switching studies were conducted by monitoring the binding of the monoclonal anti-mouse progesterone antibody to the progesterone end groups on the oligopeptide. Our research group had already demonstrated that oligopeptide mixed SAM can be used to control both protein adhesion and cell adhesion[196], upon the application of an electrical potential, without affecting the SAM integrity, as also illustrated in Chapter 4. Thus, the same electrical potentials were used in this research work. The SPR experiments were conducted in three different states: bio-active (ON), while a positive potential of +0.3 V was applied, open circuit (OC) while no potential was applied and bio-inactive (OFF), while a negative potential of -0.4 V was applied. The recorded sensorgrams are reported in **Figure 5.7**.

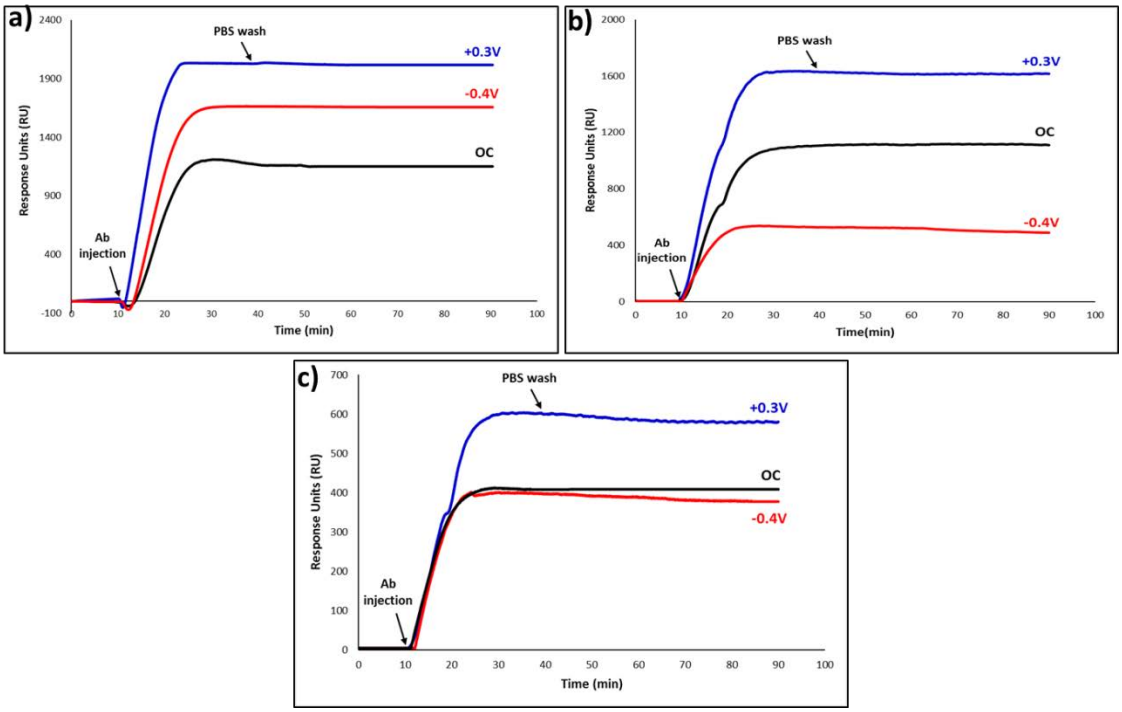

Figure 5.7 - *SPR sensorgrams for the binding of anti-mouse progesterone antibody to the progesterone-C7-4KC:EG6OH at a) 1:10, b) 1:40 and c) 1:100 solution ratio, in PBS, under OC (no applied potential), ON (+0.3 V) and OFF (−0.4 V) conditions.*

PBS was flushed over the surface for 10 minutes to equilibrate the sensor chip and set the SPR baseline, in either ON (+0.3 V), OC (no potential) or OFF (-0.4 V) states. This step was followed by injection of monoclonal anti-mouse progesterone antibody, diluted in degassed PBS, over the surface for 30 minutes, necessary to allow the correct interaction between the antibody and its antigen, represented by the progesterone moieties anchored to the gold substrate. After this exposure time, the chip was rinsed with degassed PBS, to remove any unbound protein still present in the sensor cell and the binding capacity was recorded. The binding capacity (BC) is defined as the difference in the SPR response units between the beginning of the antibody injection and the end of washing with PBS. The averages and the

standard errors in the reported binding capacity were calculated from at least three different SPR measurements for each ratio (**Table 5.2**).

Table 5.2 – *Progesterone-C7-4KC:EG6OH Binding Capacity (BC), expressed in Resonance Units (RU) and Switching Efficiency calculated from SPR experiments.*

Progesterone-C7-4KC:EG6OH Ratio		**Binding Capacity (RU)**	**Switching Efficiency (%)**
Solution	**Surface**		
1:10	1:9±3	1173±35	25±6
1:40	1:22±5	1195±22	73±3
1:100	-	526±149	37±17

The progesterone-C7-4KC:EG6OH mixed SAMs at solution ratio of 1:10 and 1:40 show high antibody binding with immobilization capacities of 1.17 ng/mm^2 and 1.20 ng/mm^2, respectively (1000 RU = 1 ng/mm^2).[196] However, for the solution ratio at 1:100, there is a significant decrease in antibody binding (0.53 ng/mm^2) that reflects a decrease in the amount of progesterone-C7-4KC in the mixed SAM. This behaviour is to a certain extent expected and indicates that there is good accessibility of the antibody to the surface tethered-antigen at progesterone-C7-4KC:EG6OH surface ratios of 1:9 and 1:22. The switching efficiency (SE) was calculated as the percentage between the binding capacity when a positive potential was applied (BC_{ON}) and the binding capacity when a negative potential was applied (BC_{OFF}), divided by BC_{ON}:

$$SE = \frac{BC_{ON} - BC_{OFF}}{BC_{ON}} \; x \; 100$$

Equation 5.2

From the results obtained, it is possible to infer that both 1:10 and 1:100 progesterone-C7-4KC:EG6OH SAMs cannot provide enough control over the anti-mouse progesterone antibody over the gold surface, showing only 25±6% and 37±17% of switching efficiency, respectively (**Figure 5.8**).

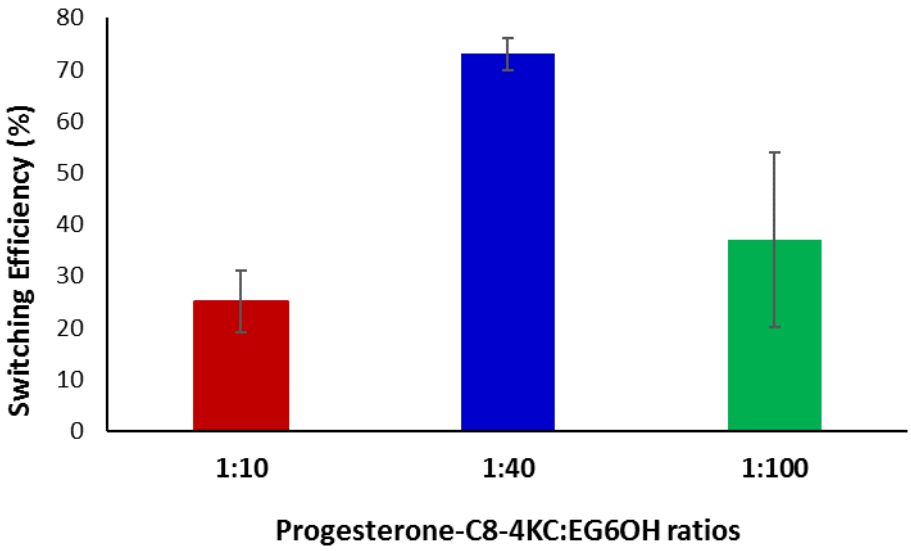

Figure 5.8 – *Bar Chart representing the switching efficiency obtained for 1:10, 1:40 and 1:100 progesterone-C7-4KC:EG6OH mixed SAMs solution ratios*

In the case of the 1:10 solution ratio, the results can be attributed to a high density of progesterone-C7-4KC chains. These long switching chains can cause intercrossing between each other, with a similar phenomenon as the one seen in Chapter 4 for biotin-6KC molecules. This behaviour is confirmed by the low binding capacity recorded in the OC conditions, that resulted lower than the binding capacity when a negative potential was applied (**Figure 5.7 a**).

In this case, the oligopeptide molecules are not forced by the electrical potential to be oriented in a particular direction, therefore they present a higher flexibility that can lead to an increased molecular intercrossing occurrence. It must be highlighted that the 1:10 solution ratio presents a higher binding capacity, but a lower switching efficiency, if compared to the one obtained for the 1:40. The results can be attribute to the high concentration of EG6OH molecules on the gold substrate. The highly-packed matrix of ethylene glycol thiol molecule can force the progesterone-C7-4KC molecules in an upright orientation, not leaving free movement to the alkyl spacer to possibly orient the progesterone moiety in the wrong direction for the binding to the antibody, as it could happen in the case 1:40 solution ratio where the oligopeptide molecules are more spaced out.

In the case of the 1:100 progesterone-C7-4KC:EG6OH solution ratio, the decrease in the binding capacity of the mixed SAM is due to the reduction of progesterone presence on the surface. The phenomena mentioned above resulted in poor switching capabilities of both 1:10 and 1:100 mixed SAMs ratios. In addition, as observed in the case of biotin-4KC:TEGT mixed SAMs, the decrease in the binding capacity is not proportional with the reduction of the concentration of biotinylated oligopeptide on the surface. Again, it is possible to assume that both the steric hindrance and the restricted mobility of the densely-packed oligopeptide molecules might limit the antibody binding to the progesterone moiety at low ratio of EG6OH to progesterone-C7-4KC[197]. The data collected confirmed the phenomenon observed in Chapter 4: a densely-packed switchable oligopeptide SAM cannot undergo a molecular rearrangement on the surface and some free space is needed for the oligopeptide chains to change their conformation when a negative potential is applied.

Noticeably, the switching efficiency obtained for the 1:40 progesterone-C7-4KC:EG6OH solution ratio is much lower than the one for the same solution ratio of biotin-4KC:TEGT. The difference in the switching behaviour can either be explained by the different surface ratio and/or the different chemical composition of the switching molecules. In fact, in the case of the 1:40 progesterone-C7-4KC:EG6OH solution ratio, the resulting surface ratio is higher than the biotin-4KC:TEGT one (1:22±5 vs 1:16±4). In addition, the progesterone molecule is not directly bound to the oligolysine chain and the alkyl spacer is not affected by the application of an electrical potential. This chemical characteristic can lead to lower constraints affecting the exposure of the progesterone molecules upon the application of a negative electrical potential and it can donate more free movement to the progesterone moieties for the binding to the antibody in solution.

The 1:22 surface ratio (1:40 solution ratio) of the progesterone-C7-4KC:EG6OH mixed monolayer presented the highest switching efficiency and was selected to study the switching efficiency of the progesterone oligopeptide in sEBSS containing 0.4% BSA.

5.4.3 SPR analysis of the switching capabilities of 1:40 progesterone-C7-4KC:EG6OH mixed SAMs solution ratio in modified Earle's Buffer Saline Solution containing 0.3% of Bovine Serum Albumin

To understand if the best performing progesterone-C7-4KC:EG6OH mixed SAMs ratio could present a similar switching efficiency in the buffer that will be used for the treatment of sperm cells, the electrochemical SPR experiments illustrated in section 5.4.2, were repeated in sEBSS + 0.3% BSA. The sEBSS buffer mimics the uterus environment, whereas the BSA is necessary for the sperm cells to lose the cholesterol external layer in order to undergo

capacitation and help their motility[223,236,242,358–360]. It is therefore important to verify if the molecular rearrangement over the surface can be induced also in the sEBSS+0.3% BSA buffer. The same procedure illustrated in section 5.4.2 was followed, monitoring the binding of the monoclonal anti-mouse progesterone antibody to the progesterone end groups on the oligopeptide. The SPR experiments were conducted in three different states: bio-active (ON), while a positive potential of +0.3 V was applied, open circuit (OC) while no potential was applied and bio-inactive (OFF), while a negative potential of -0.4 V was applied.

Modified Earle's Buffer Saline Solution (sEBSS) containing 0.3% of BSA was flushed over the surface for 10 minutes to equilibrate the sensor chip and set the SPR baseline, in either ON (+0.3 V), OC (no potential) or OFF (-0.4 V) states. This step was followed by injection of monoclonal anti-mouse progesterone antibody, diluted in sEBSS+0.3%BSA, over the surface for 30 minutes, necessary to allow the correct interaction between the antibody and its antigen, represented by the progesterone moieties anchored to the gold substrate. The buffer was not degassed, due to the presence of BSA that could have caused the formation of bubbles, under the argon flux. In addition, the sperm cells will be prepared using not degassed sEBSS+0.3%BSA[312]. After this exposure time, the chip was rinsed with sEBSS + 0.3% BSA, to remove any unbound antibody still present in the sensor cell and the binding capacity was recorded. The recorded sensorgram is reported in **Figure 5.9**.

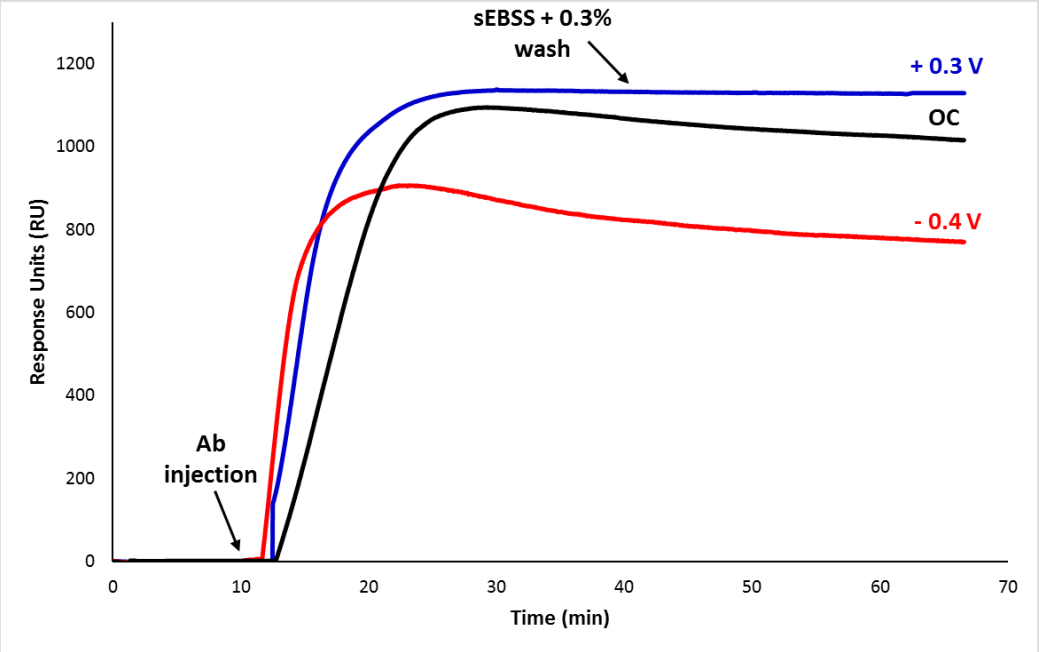

Figure 5.9 *- SPR sensorgrams for the binding of anti-mouse progesterone antibody to the progesterone-C7-4KC:EG6OH at 1:40 solution ratio, in sEBSS + 0.3% BSA, under OC (no applied potential), ON (+0.3 V) and OFF (−0.4 V) conditions.*

The binding capacity (BC) and the switching efficiency (SE %) in sEBSS + 0.3% BSA were calculated using **Equation 5.2**, to obtain values of 1048±286 and 35±10%. The averages and the standard errors in the reported binding capacity were calculated from at least three different SPR measurements. The results showed that the switching efficiency in sEBSS + 0.3% BSA is much lower compared to the one obtained in PBS and it is too poor to permit the achievement of an efficient switching system in the presence of sperm cells. The difference in the switching performances can be attributed to the presence of Bovine Serum Albumin. In fact, BSA is a non-reactive protein used in immunohistochemistry to bind to non-specific binding sites, to increase the chances for the antibodies to bind only to the specific antigens[361,362]. In addition, BSA also present an overall negative charge at pH 7[363]. From the analysis of these two characteristics, we can infer that BSA could be interacting with either the positively-charged

oligolysine peptide chains and/or the negatively-charged gold surface, when the -0.4 V potential is applied[364], leading to a poor switching behaviour and a high standard error.

5.4.4 SPR analysis of the switching capabilities of 1:40 progesterone-C7-4KC:EG6OH mixed SAMs solution ratio in modified Earle's Buffer Saline Solution containing 0.1% and 0% of Bovine Serum Albumin

To understand if the presence of BSA could interfere with the switching as hypothesise in the previous section, electrochemical SPR switching experiments were conducted on the 1:40 progesterone-C7-4KC:EG6OH mixed SAMs solution ratio, in both sEBSS+0.1%BSA and sEBSS+0%BSA as buffer. This detailed analysis will give us an in-depth understanding of the molecular events occurring on the gold surface, that will be also be fundamental to plan our future studies.

Again, the procedure used in section 5.4.2 was followed, monitoring the binding of the monoclonal anti-mouse progesterone antibody to the progesterone end groups on the oligopeptide. The SPR experiments were conducted in three different states: bio-active (ON), while a positive potential of +0.3 V was applied, open circuit (OC) while no potential was applied and bio-inactive (OFF), while a negative potential of -0.4 V was applied.

Firstly, modified Earle's Buffer Saline Solution (sEBSS) containing 0.1% of BSA was flushed over the surface for 10 minutes to equilibrate the sensor chip and set the SPR baseline, in either ON (+0.3 V), OC (no potential) or OFF (-0.4 V) states. This step was followed by injection of monoclonal anti-mouse progesterone antibody, diluted in sEBSS+0.3%BSA, over the surface for 30 minutes, necessary to allow the correct interaction between the antibody and its antigen, represented by the progesterone moieties anchored to the gold substrate. The buffer

was not degassed for the same reasons explained in the previous section[312]. After this exposure time, the chip was rinsed with sEBSS + 0.1% BSA, to remove any unbound antibody still present in the sensor cell and the binding capacity was recorded. The recorded sensorgram is reported in **Figure 5.10**.

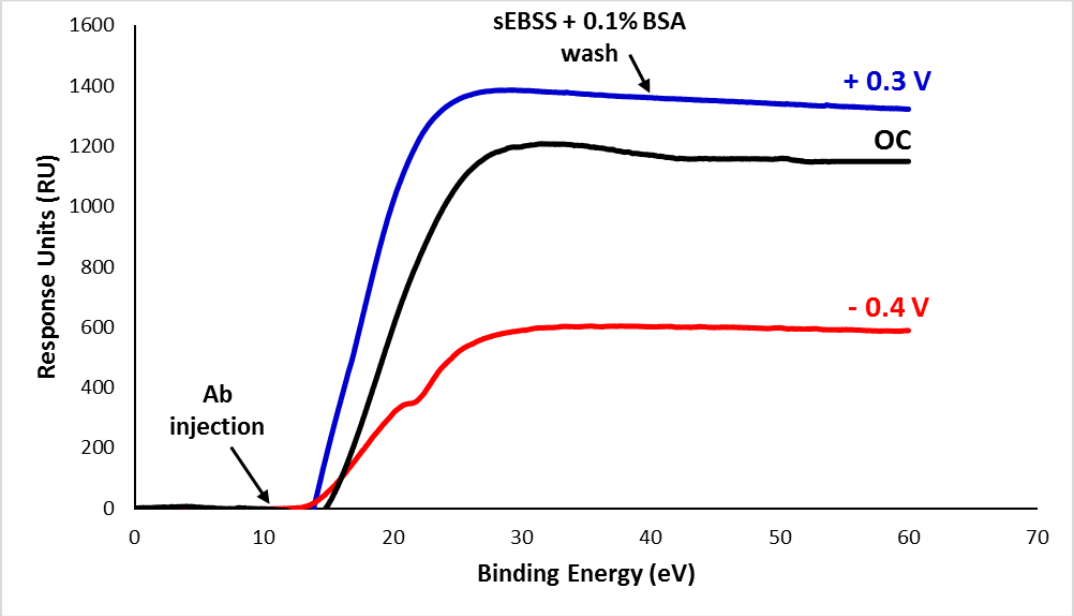

***Figure 5.10** - SPR sensorgrams for the binding of anti-mouse progesterone antibody to the progesterone-C7-4KC:EG6OH at 1:40 solution ratio, in sEBSS + 0.1% BSA, under OC (no applied potential), ON (+0.3 V) and OFF (−0.4 V) conditions.*

The SPR analysis in sEBSS + 0.1% BSA showed that the reduced amount of Bovine Serum Albumin slightly improved the binding efficiency from the value of 1048±286 obtained in sEBSS + 0.3% BSA to 1291±78. The switching efficiency, calculate using **Equation 4.2**, resulted increased to 44±8%. However, the switching efficiency remains too poor to select the buffer sEBSS + 0.1% BSA as ideal to perform the switching experiments in the presence of sperm cells. It is also important to notice that in the presence of BSA the standard error for the calculated

switching efficiency is high, indicating that the protein is critically affecting the possibility of obtaining the desired molecular rearrangement on the gold surfaces, upon the application of an electrical potential.

Finally, we analysed the switching behaviour of the progesterone-C7-4KC:EG6OH mixed SAM in presence of no BSA in the sEBSS buffer. Modified Earle's Buffer Saline Solution (sEBSS) containing 0.1% of BSA was flushed over the surface for 10 minutes to equilibrate the sensor chip and set the SPR baseline, in either ON (+0.3 V), OC (no potential) or OFF (-0.4 V) states. This step was followed by injection of monoclonal anti-mouse progesterone antibody, diluted in sEBSS+0.3%BSA, over the surface for 30 minutes, necessary to allow the correct interaction between the antibody and its antigen, represented by the progesterone moieties anchored to the gold substrate. The buffer was not degassed again, for the same reasons previously examined[312]. After this exposure time, the chip was rinsed with sEBSS + 0% BSA, to remove any unbound antibody still present in the sensor cell and the binding capacity was recorded. The recorded sensorgram is reported in **Figure 4.11**.

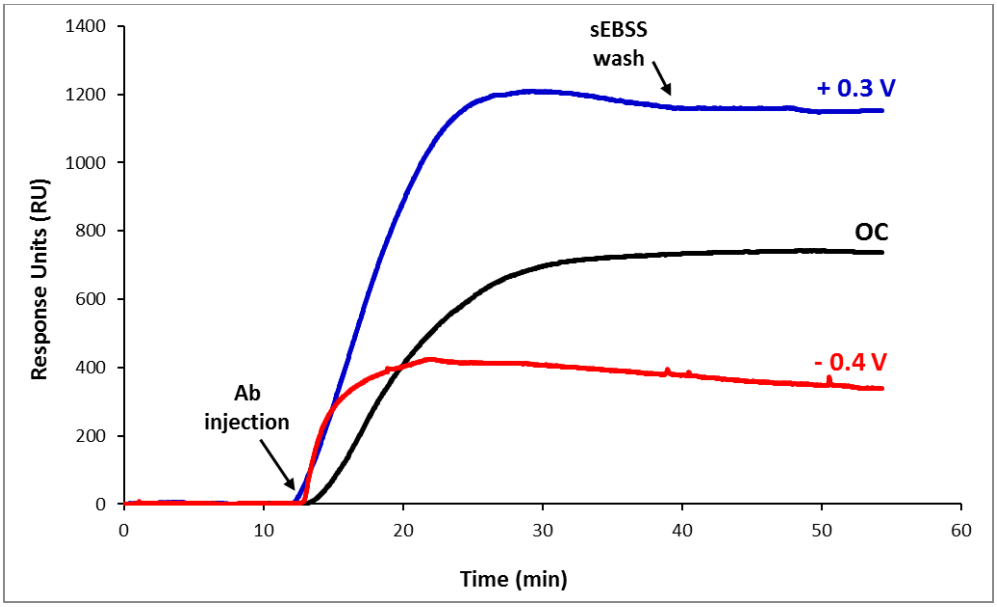

Figure 5.11 *- SPR sensorgrams for the binding of anti-mouse progesterone antibody to the progesterone-C7-4KC:EG6OH at 1:40 solution ratio, in sEBSS + 0% BSA, under OC (no applied potential), ON (+0.3 V) and OFF (−0.4 V) conditions.*

The binding capacity (BC) and the switching efficiency (SE %) in sEBSS + 0% BSA were calculated using **Equation 2**, to obtain values of 1091±94 and 70±4%. The averages and the standard errors in the reported binding capacity were calculated from at least three different SPR measurements. The SPR data collected for the four different buffer conditions are reported in **Table 5.3**, alongside the calculated switching efficiencies.

Table 5.3 – *SPR data and switching efficiency of the progesterone-C7-4KC:EG6OH mixed SAMs in PBS, sEBSS + 0% BSA, sEBSS + 0.1% BSA and sEBSS + 0.3% BSA respectively*

PBS	
Binding Capacity	**Switching Efficiency**
1195±22	73±3%
sEBSS + 0% BSA	
Binding Capacity	**Switching Efficiency**
1091±94	70±4%
sEBSS + 0.1% BSA	
Binding Capacity	**Switching Efficiency**
1291±78	44±8%
sEBSS + 0.3% BSA	
Binding Capacity	**Switching Efficiency**
1048±286	35±10%

A comparison of the switching behaviour presented by the 1:40 progesteron-C7-4KC:EG6OH solution ratio in the different buffers tested is reported in **Figure 5.12**.

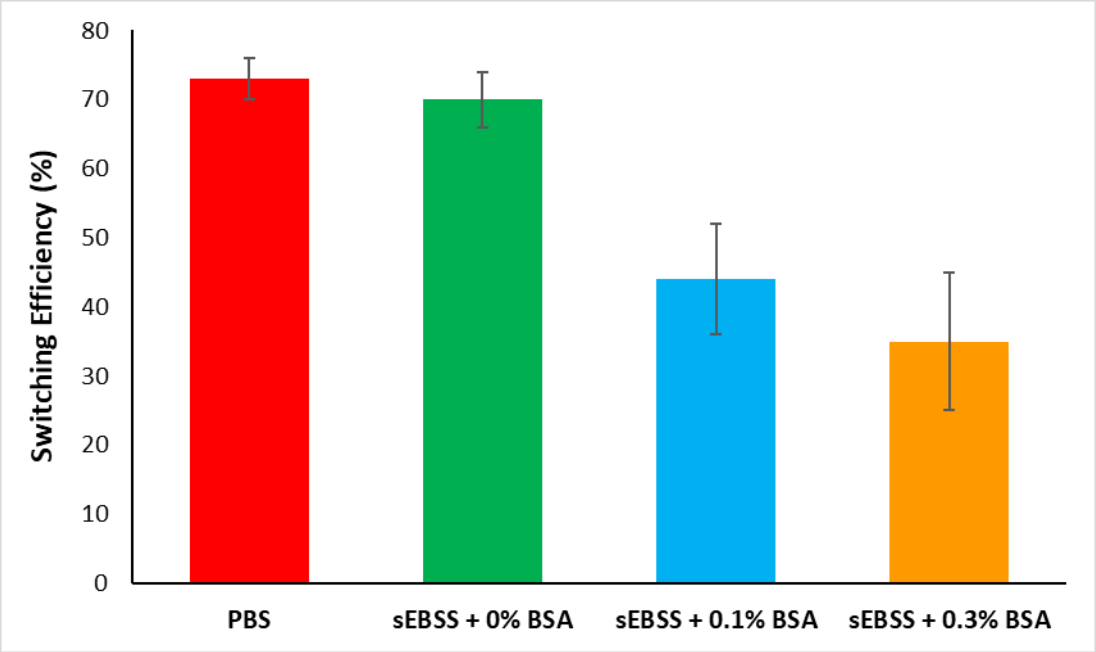

Figure 5.12 – *Bar chart reporting the switching efficiency of the progesterone-C7-4KC:EG6OH mixed SAMs in PBS, sEBSS + 0% BSA, sEBSS + 0.1% BSA and sEBSS + 0.3% BSA respectively.*

The results showed that the switching efficiency in sEBSS + 0% BSA is comparable to the one obtained in PBS and confirmed our hypothesis stating the possible influence of a charged protein such as BSA in the molecular rearrangement over the gold substrate when an electrical potential is applied.

4.5 Conclusions and Future Work

Immunosensors are a well-studied and reliable platform to control the interactions between a protein (Ab) and a small molecule (Ag) and Surface Plasmon Resonance (SPR) is widely used as immunosensing analytical technique[297,349,365,366]. In this work, the findings of our previous research[194,196–199] were applied to the aim of creating a switchable platform able to control the exposure of an antigen molecule (progesterone) on the surface and the binding to its antibody in solution (anti-mouse progesterone antibody), upon the application of an electrical potential. It was successfully demonstrated that the 4-Lys oligopeptide molecule used in our previous studies, is able to expose or conceal on demand the moieties of progesterone, leading to a selective control over the antibody binding, upon the application of an electrical potential, never demonstrated before. However, its switching activity is influenced by both the presence of a spacer between the switching oligopeptide and the end group and the presence of Bovine Serum Albumin (BSA) in the buffer.

Firstly, the spacer of 8-carbon atoms, increases the gap distance between the progesterone end group and the ethylene glycol thiol (EG6OH) matrix. In addition, this alkyl chain is not influenced by the application of an electrical potential to the gold substrate. When no potential is applied (OC conditions), the alkyl spacer can lead to intercrossing on the gold surface, between the progesterone-C7-4KC chains, leading to a lower binding capacity compared to the one recorded for biotin-4KC in the same conditions. When an electrical potential is applied, the alkyl chains of the spacer are neither attracted towards or repelled from the surface, leading to an undesired orientation of the progesterone molecules and resulting into a lower switching efficiency, compared to the one recorded for the same solution ratios of biotin-4KC, in the same conditions (PBS buffer).

Secondly, from our findings we can infer that the presence of BSA in the buffer used for the switching studies, greatly influences the switching performances of the studied progesterone-C7-4KC:EG6OH system. This phenomenon can be attributed to overall negative charge presented by BSA at pH 7[363], that could permit the interaction between this protein and either the positively-charged oligolysine peptide chains and/or the negatively-charged gold surface, when the -0.4 V potential is applied[364]. However, the complete removal of BSA from the sEBSS buffer could influence the motility and the function of spermatozoa[367,368] in the future switching studies aimed to control the calcium ion influx and the hyperactivation in sperm cells.

Starting from the results obtained in this chapter, our future work will be directed to the understanding of: 1) the influence of the alkyl spacer length on the switching efficiency, by testing the binding of anti-mouse progesterone antibody to different progesterone-C_n-4KC:EG6OH mixed SAM (with n either < or > 8) by electrochemical SPR and 2) the ability of different progesterone-C_n-4KC:EG6OH mixed SAM (with n either < or > 8) to trigger the calcium ion influx and hyperactivation in sperm cells.

The results illustrated in this chapter will create the basis for the development of novel immunosensing platforms, applicable to biomedicine, such as the studies of autoimmune diseases and several pathologies involving the interaction between antigens and antibodies.

Chapter 6 – Orthogonal Functionalisation of Surfaces for Controlling Sperm Cell Adhesion and Hyperactivation

Abstract: *This chapter describes the development of an orthogonal functionalisation method of a glass-gold micropattern, for the control of both sperm cells adhesion and hyperactivation. The cells adhesion was studied on two different surfaces, composed by poly-D-lysine (PDL) or silane-PDL layers, to select the most suitable one for functionalisation purposes. Each step of the orthogonal functionalisation was studied in detail and each surface was characterised by XPS. This work shows the importance of an appropriate orthogonal molecule selection, to achieve the desired surface properties. This study represents a starting point for developing effective orthogonal surfaces able to control cellular response and activity.*

6.1 Introduction

The continuous advancements in nanotechnology set new challenges in the development of new surfaces with multiple bioactive molecules, intended for cell biology and nanomedicine applications[369]. To create a bi- or multifunctional platform, different chemistries are needed, especially if the platform is composed by different substrate materials. The use of a multi-material substrate enables a better and efficient control over the localisation of the different biomolecules. This control permits to create surfaces with well-defined and desired density, spacing and molecular orientation[370]. Such surfaces can be tailored to present a large variety of features making them flexible for a vast range of chemical and biological conditions and purposes, ranging from biosensors to microarrays [369,371]. Being some substrates negatively affected by the reiteration of chemical reactions on the surface, it is necessary to reduce the number of reaction steps, the use of protective groups and create simple functionalisation protocols. Different techniques are used to achieve the orthogonal functionalisation of

substrates, such as photolithography[372], soft[373] and electron-beam lithography[374], dip-pen nanolithography[62] and micro-contact printing (μCP)[121,122,370]. Several challenges must be addressed in building such complex molecular architectures: the types of chemistry used could interfere with each other or lead to undesired side-products, the conditions must be mild and often biocompatible, the patterning techniques could damage the molecules present on the surfaces (e.g. UV irradiation in photolithography[370]). Orthogonal self-assembly of molecules was demonstrated for the first time in 1989 by Whitesides[79] and it has now become a major research focus especially in the preparation of devices able to enhance the signal in localised SPR (LSPR). Orthogonal ligation chemistry permits the creation of pre-patterned surfaces with multifunctional characteristics, exploitable to immobilise molecules on discrete areas, in a specific manner, under mild conditions[370].

Several examples of orthogonally functionalised surfaces have been reported in the literature in the last decade[375–377], but a noteworthy work for the aim of this research project, was the one done by Durán and co-workers on polysilicon-gold chips[378]. They created a bi-functional platform displaying two different biomolecules on the same device, with potential employability as biosensor, biomarker or therapeutic agent[378]. By using a five-steps process, the polysilicon area of the device was functionalised with molecules of 11-(triethoxysilyl)undecanal (TESUD) carrying a fluorescein conjugate concanavalin (F-ConA) fluorescent tag, whereas on the gold area of the same device a SAM of mercaptoundecanoate-NHS that was then linked to a Texas Red conjugated WGA (TR-WGA) molecule (**Figure 6.1**).

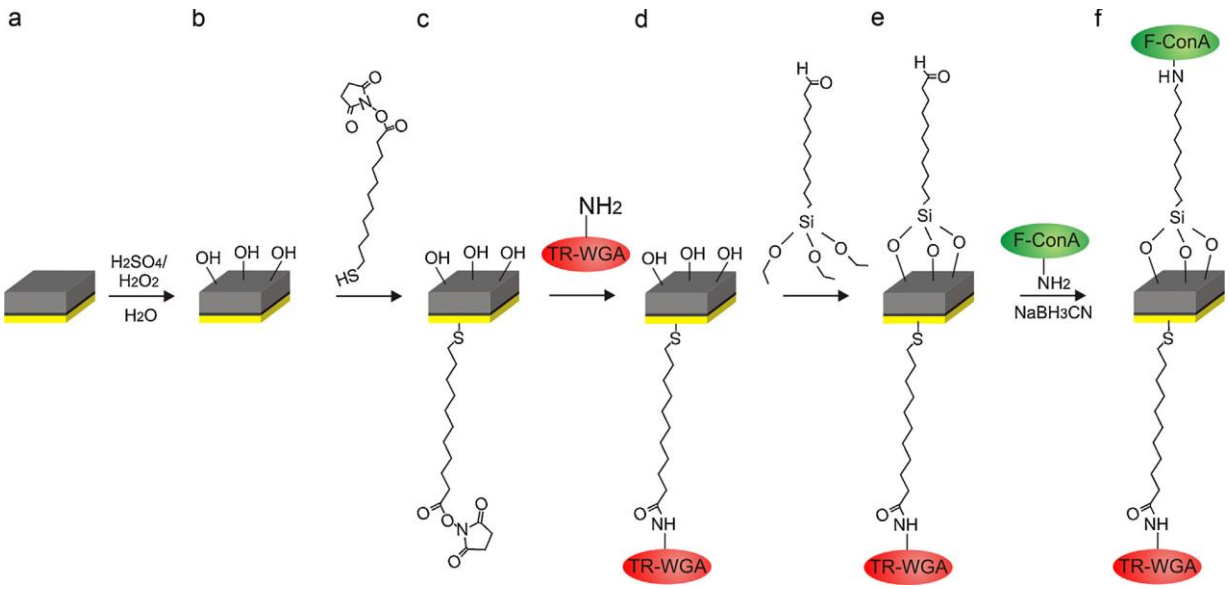

Figure 6.1 – *Steps involved in the preparation of double biofunctionalized chips. (a) Polysilicon–chromium–gold chip, (b) Polysilicon surfaces activation by piranha cleaning, (c) Mercaptoundecanoate-NHS SAM formation on gold, (d) TR-WGA immobilization via amide bond formation, (e) TESUD SAM formation on polysilicon substrates and (f) F-ConA immobilization via amide bond formation.*

The successful completion of the orthogonal bi-functionalisation was then verified by fluorescent microscopy. Herein, it is illustrated the preliminary studies performed to plan an orthogonal functionalisation procedure of gold-glass microelectrodes. Our work is aiming to create a molecular architecture containing both positively molecules of poly-D-lysine (PDL) for sperm cells adhesion and a switchable mixed self-assembled monolayer that can be tuned to control the sperm cells response to progesterone.

6.2 Objectives

1) To study and optimise the adhesion of sperm cells on glass substrates, reproducing the glass areas of a micropatterned surface.
2) To form the oligopeptide mixed SAM progesterone-C7-4KC:EG6OH previously studied on gold substrates, reproducing the gold areas of a micropatterned surface.
3) To fully characterise the surfaces prepared in objectives 1 and 2 via XPS, contact angle and ellipsometry.
4) To analyse the feasibility of the proposed orthogonal functionalisation strategy.

6.3 Results and Discussion

6.3.1 Study of sperm cells attachment on poly-D-lysine and silane/poly-D-lysine layers and surface characterisation

Both poly-D-lysine (PDL) coating and silane-PDL layers were studied as an option for sperm cells immobilisation, to analyse the effect on cell adhesion of the different bonding of PDL to the surface. In the case of PDL coating, a layer of PDL is physisorbed on the glass substrate, whereas in the case of silane-PDL, poly-lysine molecules are linked to the glass surface thanks to strong covalent glass-silane and silane acid groups-lysine amino groups bonds.

One of our future aims will be the use of the results obtained in this chapter to plan the step for the orthogonal functionalisation of a micropatterned electrode. The orthogonal functionalisation of a surface usually involves several steps[329]. Having the desired molecules covalently bonded will avoid the risk of layer removal during the process.

Cleaned glass microscope slides were functionalised with 1) a layer of poly-D-lysine (PDL) coating (**Figure 6.2**), obtained upon evaporation of a PDL solution in UHQ water (0.1 mg/ml) at room temperature, presenting weak electrostatic interaction between charged amine groups and the glass surfaces and 2) a layer of carboxyethylsilanetriol was first deposited by chemical vapour deposition (CVD) to form strong covalent bonds between the hydroxyl groups on glass and silicon atoms in the silane molecules. The carboxylic groups present on the silane molecules were then bound to PDL molecules via carboxylic acid activation with EDC/NHS, to form covalent amide bonds, as described in "Chapter 3 – Experimental Procedures and Protocols".

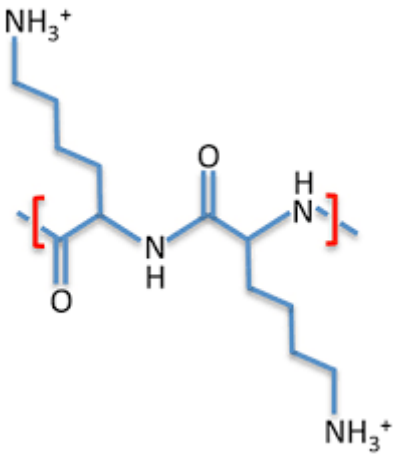

Figure 6.2 – *Chemical structure of monomer units composing poly-D-lysine (PDL)*

Poly-D-lysine is a polymer of molecular weight >300,000 Da, composed by lysine aminoacid monomers. The lysine residues provide a positively charged backbone, due to the presence of protonated amino groups (NH_3^+) at pH 7, below the amino pKa of 9.06, which can interact with the negatively charged sites present on the sperm cells membrane, supporting adhesion. It is widely used in cell research as standard method for facilitating cell attachment[379–381].

6.3.1.1 XPS characterisation of poly-D-lysine and silane/poly-D-lysine layers

The surfaces used in the study of sperm cells attachment were analysed by XPS, that revealed the presence of the elemental species C, N, O and Si on both layers, confirming the formation of both PDL and silane-PDL layers. The C 1s spectrum (**Figure 6.3 a**) can be deconvoluted into three peaks, corresponding to three different binding environments. The peak at 284.8 eV is attributed to C-C bonds[334,335], while the peak at 286.1 eV corresponds to C-N binding environment. The third peak at 288.0 eV can be assigned to the C=O moiety, that could be assigned to sodium carbonate, naturally present in glass substrates [334,335,382]. The N 1s spectrum (**Figure 6.3 b**) consist in a large peak that can be deconvoluted into three peaks. Due to high concentration of amino groups on the surface, the nitrogen peak is intense, and three peaks are observable. The first peak is centred at 401.0 eV, can be assigned to protonated amino groups (NH_3^+), whereas the second peak at 399.7 eV corresponds to amide (CONH) and amino (NH_2) groups[383], the third peak at 397.7 eV is ascribable to silicon nitrates that can be a component of glass[312]. The O 1s spectrum (**Figure 6.3 c**) can be deconvoluted into two peaks, assignable to C-O groups (531.6 eV) and C=O plus SiO_x (533.0 eV), due to silicon oxides being naturally present in glass substrates[334,335]. The peak at 535 eV can be assigned to the sodium Auger peak (Na KLL), that could be assigned to sodium carbonate, one of the components of glass.[334,335,382]. In this case, the Si 2p spectrum (**Figure 6.3 d**) is only attributable to the silicon oxides SiO_x (103.0 eV) and SiOH (103.8 eV) groups naturally present in the glass substrate[116,334,335,383–391]. The small shift of the N, O and Si peaks (less than 0.5 eV) is due to the limited conductivity of glass, causing a charge accumulation on the surface[392].

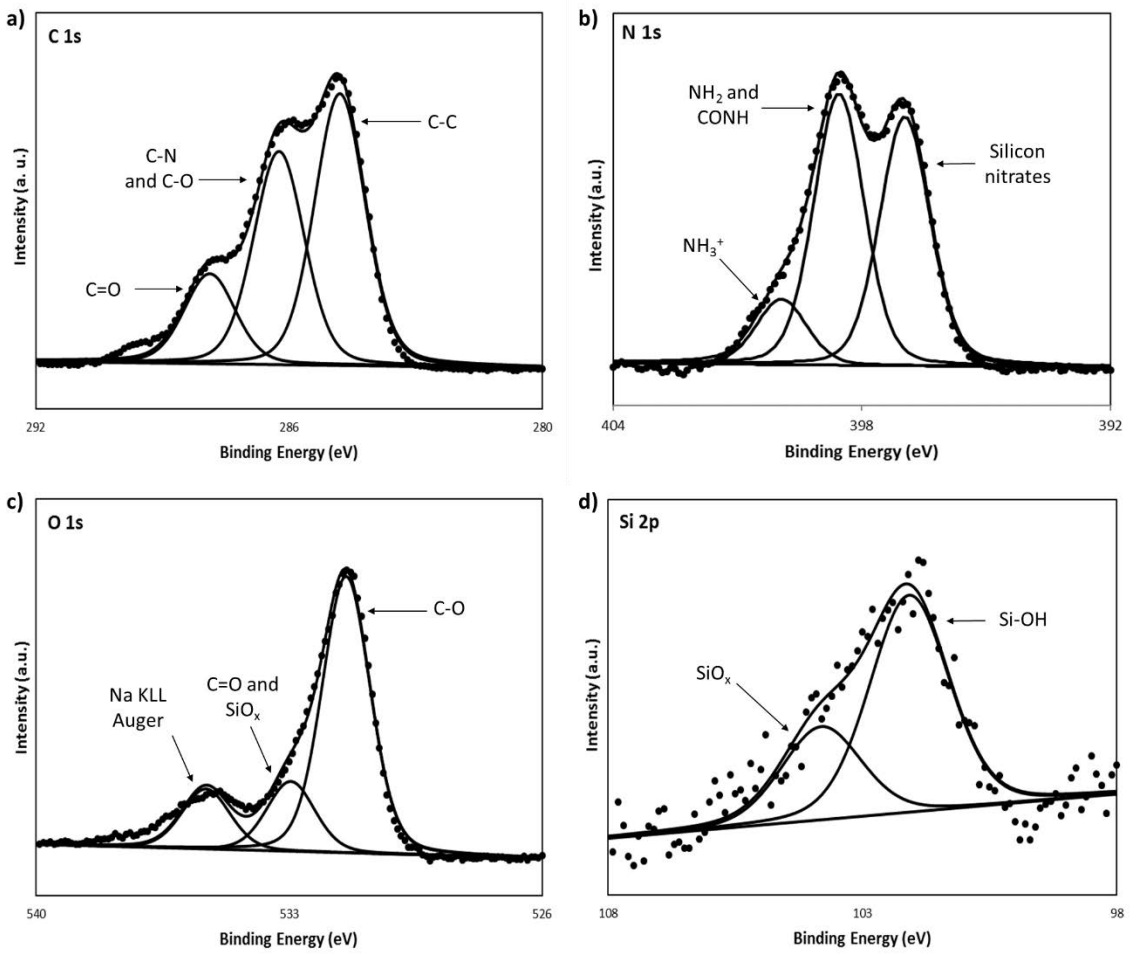

Figure 6.3 – *XPS spectra of the a) C 1s, b) N 1s, c) O 1s and d) Si 2p regions of pure 0.5 mg/ml PDL layers on glass substrates.*

The XPS analysis was also performed on silane-PDL layers (**Figure 6.4**) on glass substrates, revealing the presence of the elemental species C, Si, N and O, confirming the formation of the layer.

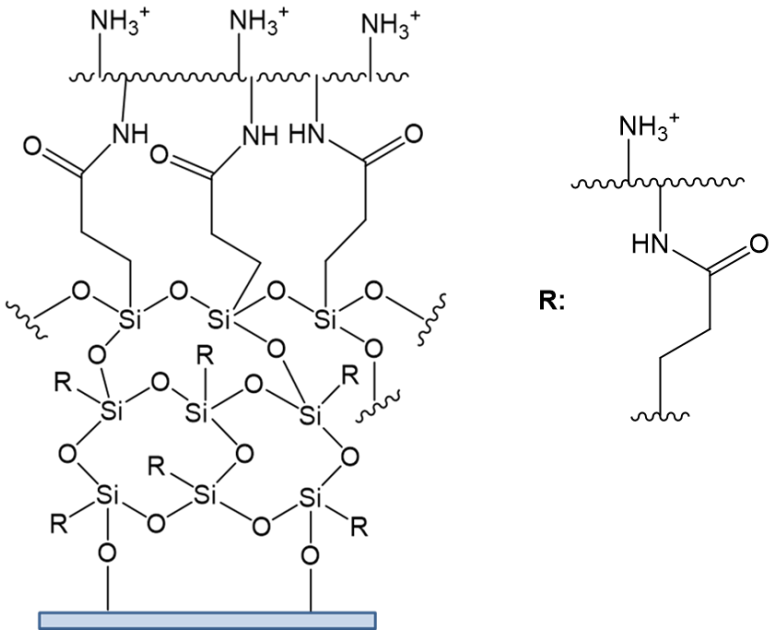

Figure 6.4 – *Schematic representation of silane-PDL layers on glass substrates*

The C 1s spectrum (**Figure 6.5 a**) is formed by three peaks, which are attributable to the following binding environments[334,335]: C-C and C-Si (284.8 eV)[393], C-N (286.4 eV) and C=O (288.3 eV). The Si 2p spectrum (**Figure 6.5 b**) is formed by two peaks, that can be assigned to the binding environments of SiOx and Si-O-Si groups (103.4 eV) and Si-C and Si-OH (102.5 eV)[116,334,335,383–391]. The N 1s spectrum (**Figure 6.5 c**) can be deconvoluted into two peaks, which support the presence of lysine moieties on the surface. The first peak at 399.0 eV can be assigned to amino (NH_2) and amide (CONH) groups. The second peak at 401.6 eV corresponds to protonated amino groups (NH_3^+)[383]. The silicon nitrates peak coming from the glass itself cannot be distinguished from the background noise. This difference can be due to the presence of silane-PDL molecules covering the glass surface. It can in fact be noticed the higher intensity of the protonated amino groups (NH_3^+) peak, indicating a high presence of PDL on the surface. The O 1s spectrum (**Figure 6.5 d**) can be deconvoluted into two different peaks, corresponding

to three binding environments. The first peak centred at 532.7 eV can be assigned to Si-O and C=O bonds and the second peak at 531.5 eV can be assigned to Si-OH moieties[334,335]. The limited conductivity associated with the glass substrate, cause a charge accumulation on the surface that leads to small binding shifts (less than 0.5 eV), if compared to the peak values obtained on gold substrates[392].

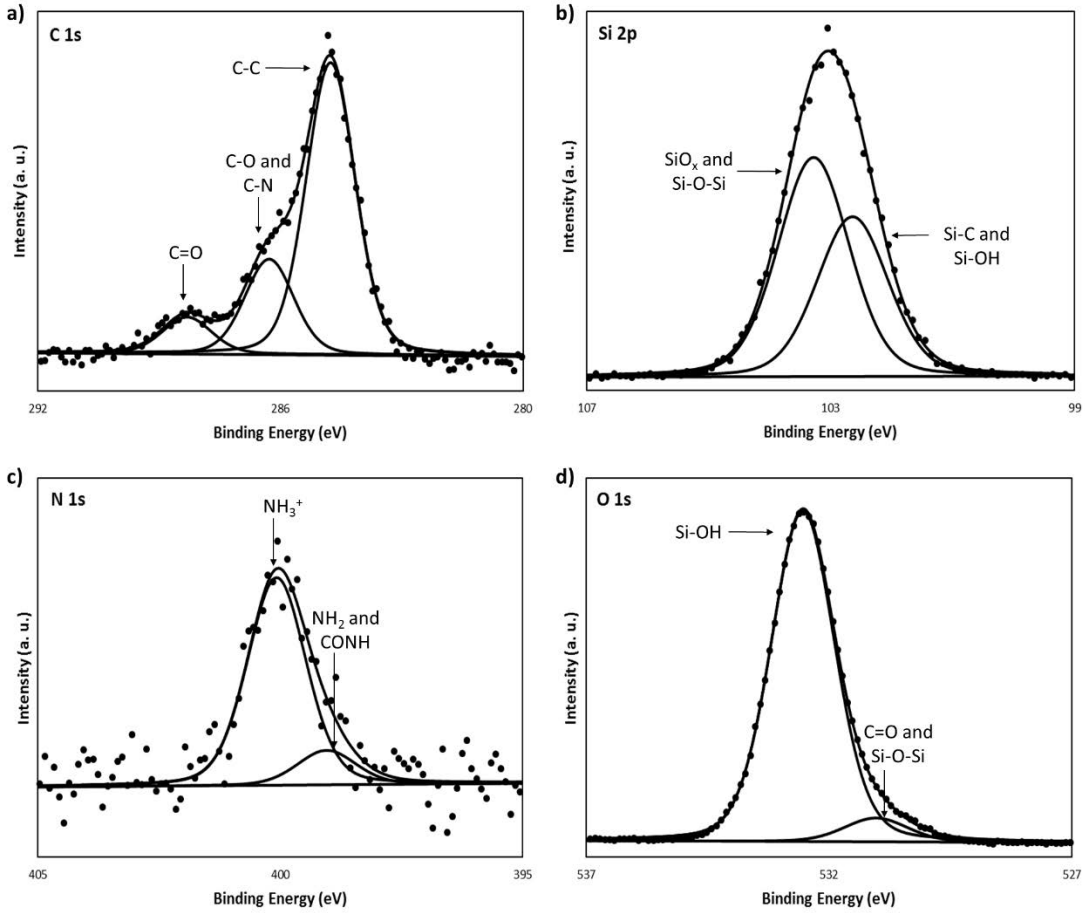

Figure 6.5 – *XPS spectra of the a) C 1s, b) Si 2p, c) N 1s and d) O 1s regions of silane-PDL layers on glass substrates.*

6.3.1.2 Contact angle and ellipsometry analysis of poly-D-lysine and silane/poly-D-lysine layers

The formation of poly-D-lysine (PDL) and silane-PDL layers were analysed by contact angle and ellipsometry. As expected, the water advancing (Adv) and receding (Rec) contact angles for silane-PDL layers revealed hydrophilic characteristics, whereas it was impossible to measure the contact angle for the layer of pure PDL, since the water droplet re-dissolved the PDL itself (**Table 6.1**).

Ellipsometry analysis confirmed the formation of both PDL and silane-PDL layers, but, as expected, the homogeneity of both layers on surface was poor, due to the lack of control over the molecular organisation on surfaces. The formation of pure silane layer resulted in an ellipsometric thickness of 1.7 ± 0.2 nm which is significantly higher that the theoretical molecular length of 0.53 nm. This difference can be explained with the formation of a possible tri-layer of silane, instead of a monolayer. The surfaces were formed on silicon wafer substrates, to allow the ellipsometry measurements. Ellipsometry measurements cannot be performed on glass, due to the transparency of the surface. Silicon wafers are not transparent and form covalent bonds with silane molecules, in the same way glass surfaces do. The exact theoretical molecular length of poly-D-lysine cannot be calculated, because the number of lysine units in the polymer is not exactly known

Table 6.1 - *Advancing and receding water contact angle and ellipsometric thickness for the different layers formed for 24h. The theoretical molecular lengths were calculated using ChemBio3D Ultra 12.0 in which the molecules were in fully extended conformation. The averages and standard errors were calculated from at least three different measurements.*

Layer	**Contact Angle**		**Thickness (nm)**	
	Adv.	*Rec.*	*Theor.*	*Measured*
Silane	61° ± 2	56° ± 3	0.53	1.7 ± 0.2
Silane-PDL	70° ± 5	63° ± 3	-	5.8 ± 2
PDL	-	-	-	16 ± 4

The contact angle results indicate that both silane and silane-PDL layer show slightly hydrophilic properties as expected. The large hysteresis ($\theta_{Adv} - \theta_{Rec}$) of 5˚ for the silane layer and 7˚ for the silane-PDL layer are an indication of the low order of both layers. In addition, when PDL is bond to the surface, the contact angle become more hydrophobic and measured thickness increases, confirming a change in the layer, that can indicate the successful attachment of PDL.

The measured thickness of the silane layer is higher than the theoretical thickness calculated using ChemDraw 3D. It is possible to state that the resulting silane layer is not a monolayer, result that can be attributed to the lack of control over the chemical vapour deposition conditions.

6.3.1.4 Effect of different solvents on poly-D-lysine and silane/poly-D-lysine layers and sperm cells attachment

Sperm cells were prepared following the procedure described in detail in Chapter 6. 300 μl of fresh sperm sample where first added to 700 μl of EBSS buffer containing 0.3% BSA in several falcon tubes and left in the incubator for an hour, to allow sperm cells to lose the cholesterol layer on cell membrane. After this first step, the top layer (swim-up) containing sperm cells, was collected from each falcon tube and left in the incubator to capacitate for two hours. Then 300 μl of cell suspension, containing capacitated sperm cells labelled with Calcium Green 1-AM, were deposited on glass microscope slides functionalised with 1) Poly-D-lysine coating and 2) silane/Poly-D-lysine layers with PDL concentrations of 0.1 mg/ml and 0.5 mg/ml to compare cell adhesion (section **3.3.1**). The microscope slides were attached with vacuum grease to a purpose-built, perfusable, polycarbonate imaging chamber (section **3.3.3**). The imaging chamber is equipped with two openings, one for the buffer entering the chamber and one for the buffer leaving the chamber, sucked away by a vacuum pump. It also contains a well to allocate the reference electrode and an opening to allocate the platinum counter electrode. The imaging chamber containing sperm cells was left in a wet chamber at room temperature for 30 minutes before being mounted on the microscope, connected to the perfusion system. After the incubation time, the surface was rinsed with sEBSS for 10 minutes at a flow rate of approximately 1 ml/min for at least 15 min, to remove loose sperm cells present on the surface. A roller pump push sEBSS solution into the chamber and overflow is removed by a suction pump with trap from the exit port (**Figure 6.6**).

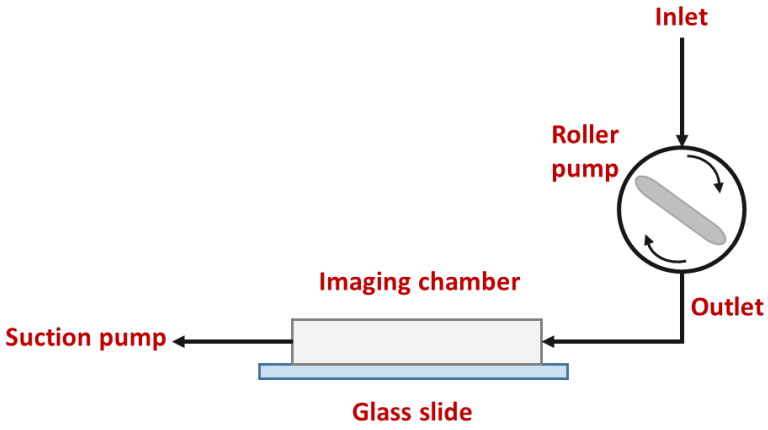

Figure 6.6 – *Schematic representation of the imaging chamber mounted on the microscope slide and connected to the perfusion system.*

The sperm cells attached on the two surfaces tested were then analysed by fluorescence microscopy. Snapshots of different areas of the surface are collected and cell counted on each field. From the images of the two surfaces collected, it is possible to assert that Poly-D-lysine coating is more effective in fostering cell adhesion when compared to silane/PDL layers (**Figure 6.7**).

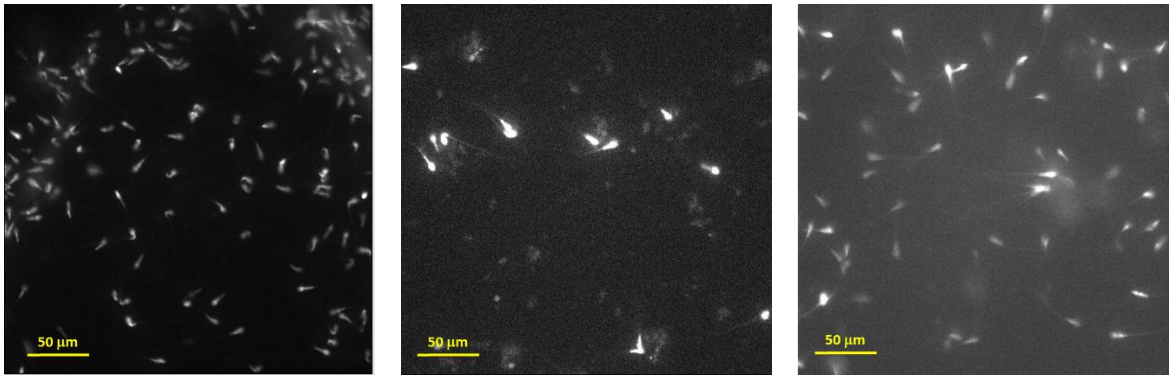

Figure 6.7 – *Fluorescence images of cell adhered on PDL coated-surfaces (left), silane-PDL layers formed using a PDL concentration of 0.1 mg/ml (centre) and silane-PDL layers formed using a PDL concentration of 0.5 mg/ml (right).*

The average number of cells per field in the case of the PDL coating, is 83±7, whereas in the case of silane-PDL (0.1 mg/ml PDL) and silane-PDL (0.5 mg/ml) is 9±4 and 34±5 respectively. The average and the error were calculated based on three different fields of the same sperm sample. The results indicate that the PDL coating is more effective in promoting cell adhesion, whereas on the silane-PDL layer prepared with a PDL concentration of 0.1 mg/ml cell adhesion is scarce. This result is likely due to the presence of a smaller number of charged amino groups free on the surface for interaction with sperm cells membrane.

To understand if the ethanol used as solvent in the formation of Progesterone-C7-4KC:EG6OH mixed SAM, can influence cell adhesion, glass microscope slides treated with both PDL and silane-PDL (0.5 mg/ml of PDL) were immersed in HPLC ethanol overnight. Both surfaces were then tested for cell adhesion, following the procedure described above. By observing the two surfaces, it is possible to notice that ethanol has not an important effect on cell attachment on silane-PDL layers, whereas it seems to affect the quality of the PDL coating. “Stripes” are clearly visible on the surface coated with 0.1 mg/ml of PDL. In addition, the sperm cells look

poorly labelled and less active if compared to the previous experiment, before the ethanol rinsing of the surface. The worse labelling and the poorer activity can also be due to cell starting naturally to die after being kept in the incubator for a long time (**Figure 5.8**).

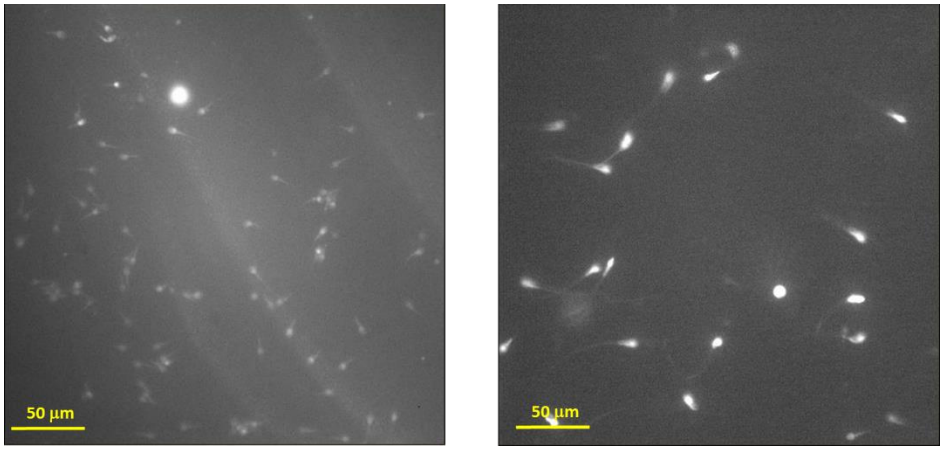

Figure 6.8 – *Fluorescence images of cell adhered on PDL coated-surfaces rinsed with ethanol (left), and silane-PDL layers formed using a PDL concentration of 0.5 mg/ml rinsed with ethanol (right).*

From the picture of the surface, it can be inferred that the presence of ethanol can affect the quality of the PDL coating. The coating appears to be partially re-dissolved by the small percentage of water present in the solvent, or by the ethanol itself, being poly-lysines slightly soluble in ethanol[394]. The silane-PDL surface (0.5 mg/ml of PDL) does not present the same kind of film effect after the ethanol rinsing. In addition, cells appear active and well labelled. The number of cells attached on the surfaces coated with PDL is still greater if compared to that on silane-PDL (0.5 mg/ml) surfaces. However, it is reasonable to hypothesise that the visible change of morphology of the non-covalently formed PDL film on glass, could then affect the switchable moieties on the gold areas of the micropattern. The silane-PDL layer

was therefore chosen to functionalise the glass areas of the micropattern, to promote cell adhesion.

6.3.2 XPS characterisation of clean glass and gold substrates

Glass and gold substrates were chosen as model systems to study the fabrication procedure, due to the impossibility of performing XPS analysis on the micropatterned surfaces. XPS characterisation of glass and gold substrates cleaned in piranha solution was performed to be used as references.

Clean glass

XPS analysis of clean glass substrates showed the presence of elemental species C, N, O, S and Si. The C, N, O and Si peaks are assignable both to substances naturally present in glass, such as carbonates and silanes and to molecules contaminating the laboratory environment[334,335,382]. The C 1s spectrum (**Figure 6.9 a**) can be deconvoluted into three peaks, assignable to C-C and C-Si (284.8 eV), C-O (286.7 eV) and C=O (288.2 eV) groups[334,335]. The N 1s spectrum (**Figure 6.9 b**) consist in a peak centred at 400.5 eV that can be assigned to nitrogen coming from the air (N_2)[383]. The O 1s spectrum (**Figure 6.9 c**) consists in a peak centred at 532.9 eV that can be assigned to silicon oxides (SiO_x) present in the glass and to organic C=O moieties[334,335]. The C, N and O signals can be due to contamination coming either from the air or the laboratory environment. The S 2s spectrum (**Figure 6.9 d**) consists of a peak centred at 233.4 eV[334,335,395], indicating an unexpected presence of sulphur on the surface. The S 2p signal was not recorded, since it is shielded by the Si 2s intense signal. The sulphur can either be due to contamination coming from the laboratory environment or piranha solution residues remained on the glass substrate after the rinsing. The Si 2p spectrum (**Figure 6.9 e**) can be deconvoluted into two peaks, the first one centred at 103.2 eV, can be assigned to silicon

hydroxides (SiOH) and the second one centred at 103.8 eV can be assigned to silicon oxides SiO_x and Si-O-Si groups, both present in the glass substrate[116,334,335,383–391].

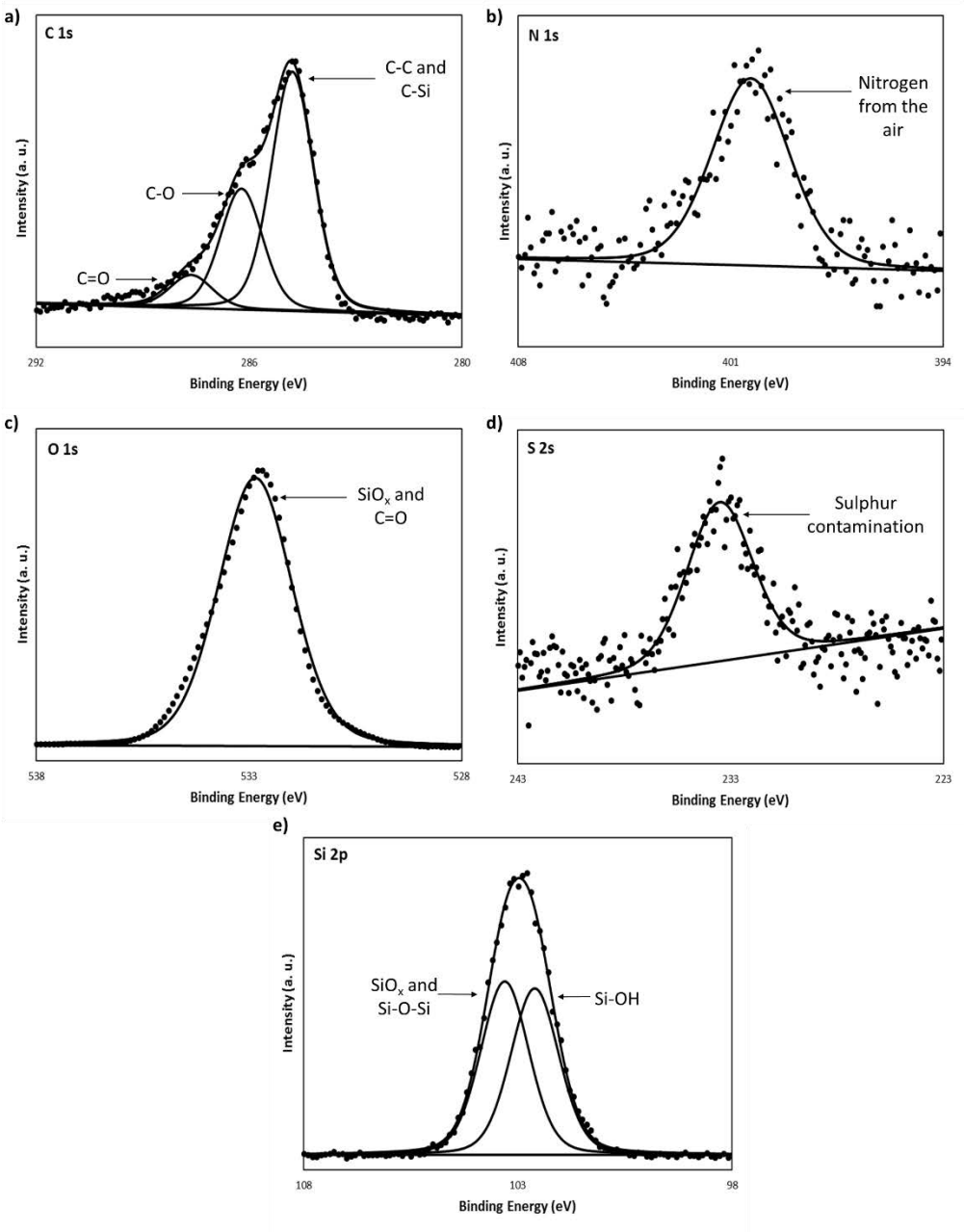

Figure 6.9 - *XPS spectra of the a) C 1s, b) N 1s, c) O, d) S 2s and e) Si 2p regions recorded on clean glass substrates.*

The ratios between the elements analysed (N/C, O/C, S/C and Si/C) were calculated to obtain reference ratios to be used as a comparison in the next steps. The calculated values are 0.13±0.03 for N/C, 33.42±2.23 for O/C, 0.18±0.03 for S/C and 5.76±0.13 for Si/C respectively.

The results show a large presence of oxygen and silicon on clean glass substrates, due to the glass composition, as expected[334,335,382]. There is also a small amount of sulphur, attributable to either contamination from thiols in the laboratory atmosphere or to piranha solution residues. Finally, noticeable is the much larger amount of oxygen than the carbon amount, attributable to both the silicon oxides and carbonates naturally composing glass substrates[334,335,382].

Clean gold

XPS analysis of clean gold substrates showed the presence of elemental species C, N, O and S. The C, O and peaks can be the result of contamination due to handling and/or the presence volatile molecules present in the laboratory environment. The C 1s spectrum (**Figure 6.10 a**) can be deconvoluted into two peaks, assignable to C-C (284.4 eV) and C-O (286.2 eV) groups[334,335]. The N 1s spectrum (**Figure 6.10 b**) consist in a small peak centred at 399.8 eV that can be assigned to both nitrogen gas and nitrogen-containing volatile molecules present in the air of the laboratory[383]. The O 1s spectrum (**Figure 6.10 c**) consists in a small peak centred at 532.0 eV that can be assigned to organic C-O moieties[334,335]. The S 2p spectrum (**Figure 6.10 d**) consists of a doublet peak centred at 162.1 and 163.3 eV, indicating an unexpected presence of unbound sulphur on the surface[395]. The sulphur can either be due to contamination coming from volatile thiols present in the laboratory atmosphere. No presence of silicon was recorded.

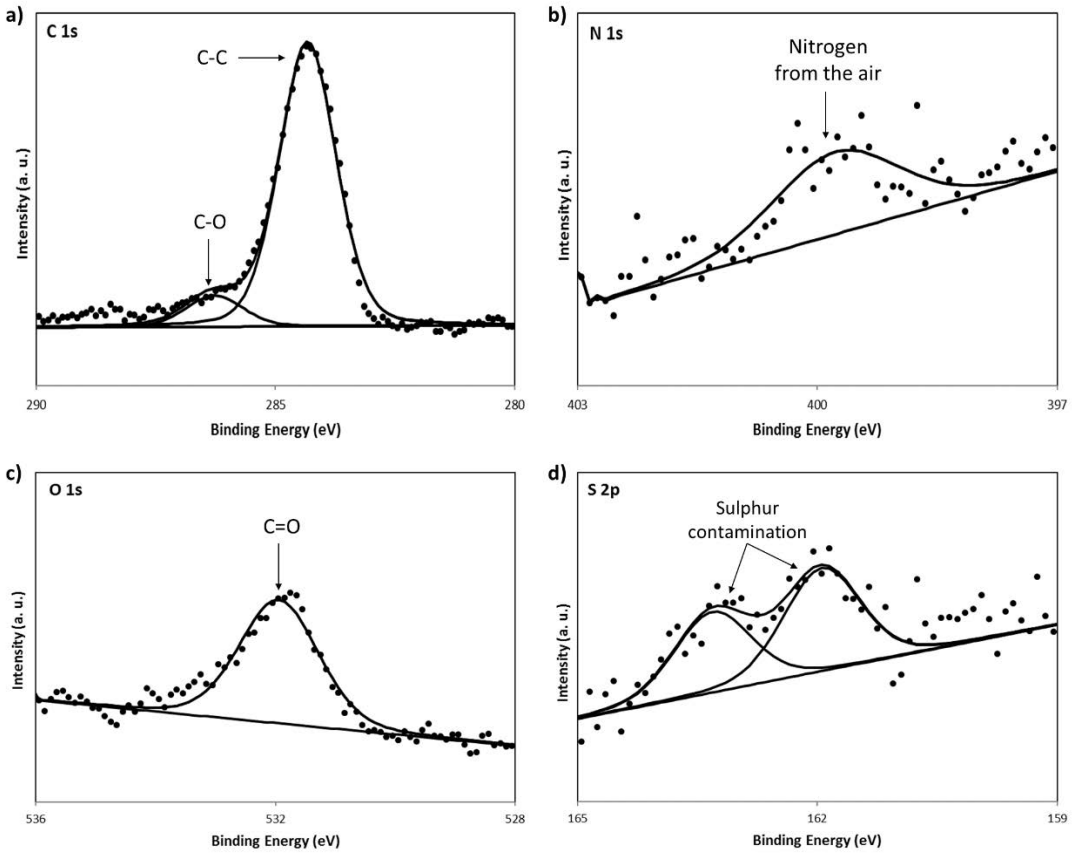

Figure 6.10 - *XPS spectra of the a) C 1s, b) N 1s, c) O and d) S 2p regions recorded on clean gold substrates.*

The ratios between carbon and the other elements (N, O and S) were calculated to obtain reference ratios to be used as a comparison in the next steps.

The calculated N/C and S/C ratios of 0.05±0.02 and 0.08±0.01, respectively, show a small presence of both nitrogen and sulphur if compared to the amount of carbon. In addition, the O/C ratio of 0.20±0.10 confirms a high presence of carbon if compared to the other elements. The recorded carbon can either be due to organic contamination from the laboratory of from handling of the samples. The foil used to wrap the samples for shipment, could have transferred some organic compounds to the surfaces.

6.3.3 XPS characterisation of each step performed on either plain gold or glass surfaces

The formation of the two different surfaces on the glass and gold was done via the following steps:

1) Deposition of a 11-mercapto-1-undecanol protective SAM on gold.
2) Formation of a silane-PDL layer on glass.
3) Removal of the protective SAM by applying a potential of -1.5V for ten minutes to the gold microelectrodes.
4) Formation of progesterone-C7-4KC:EG6OH mixed SAM on gold.

Both gold and glass were exposed to all these steps to simulate what will happen on the micropatterned substrates. To understand if each step can affect either the sperm cells adhesion and the achievement of the final molecular structure on the micropattern, a detailed XPS analysis was made.

6.3.3.1 First step: protective thiol on gold and glass

Gold substrates:

The XPS analysis was performed on 11-mercapto-1-undecanol SAMs on gold, revealing the presence of the elemental species S, C and O, confirming the presence of thiol molecules on the surface. The S 2p spectrum (**Figure 6.11 a**) consists of two doublet peaks, with the first one at 163.2 eV (S $2p_{1/2}$) and 162.0 eV (S $2p_{3/2}$) assignable to sulphur chemisorbed on the gold surface (S-Au)[395,396]. The second doublet peak centred at 164.3 eV (S $2p_{1/2}$) and 163.1 eV (S $2p_{3/2}$) can be ascribed to unbound sulphur on the gold surface (S-H)[395,396]. The C 1s spectrum (**Figure 6.11 b**) is formed by two peaks, which are attributable to the following binding environments: C-C (284.7 eV) and C-S, C-N and C-O (286.4 eV)[334,335]. The O 1s spectrum (**Figure 6.11 c**) is formed by a peak centred at 532.7 eV corresponding to C-O[334,335]. No presence of N

was recorded, as expected (**Figure 6.11 d**). The difference in the nitrogen presence compared to the clean gold case can be explained with the ease for clean gold to absorb volatile molecules from the air. On the contrary, the presence of a well-packed matrix of alkyl thiol prevents this contamination phenomenon. These peaks will be used as reference to analyse the changes on the substrates, as a result of the formation of the different layers on the gold substrates.

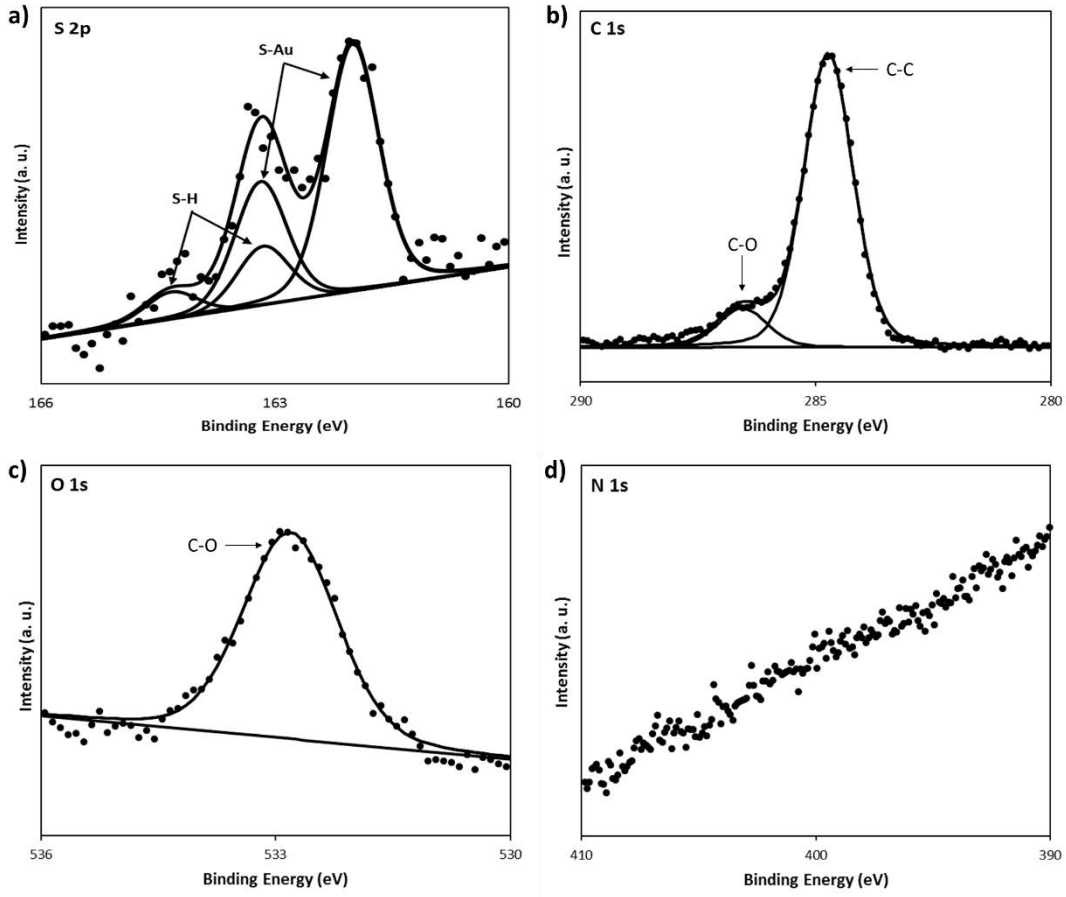

Figure 6.11 – *XPS spectra of the a) S 2p, b) C 1s, c) O 1s and d) N 1s regions of 11-mercapto-1-undecanol SAMs on gold.*

The calculated O/C and S/C ratios were compared with the ones calculated from the analysis of clean gold to verify if the 11-mercapto-1-undecal monolayer was formed correctly.

Every molecule of 11-mercapto-1-undecanol (**Figure 6.12**) contains 11 C atoms, 1 O atom and 1 S atom, from which it is possible to calculate the both the expected C/O and C/S as equal to 11.

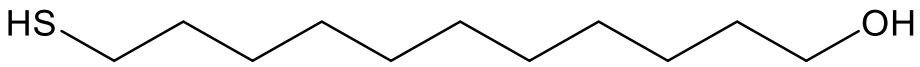

Figure 6.12 – *Molecular structure of 11-mercapto-1-undecanol*

The calculated O/C ratio of 0.28±0.01 shows no significant change if compared to the one calculated for the clean gold (0.20±0.10). In addition, both the calculated C/O and C/S ratios (3.55±0.09 and 9.25±0.90) are smaller than the expected C/O and C/S ratios for 11-mercapto-1-undecanol (both equal to 11), showing that the desired MUD monolayer did not form correctly on the gold substrates. It is reasonable to infer that there was an additional contribution to the carbon content due to contamination.

Glass substrates:

The XPS analysis of 11-mercapto-1-undecanol SAMs on glass, confirmed that no monolayer was formed as S 2s peaks were not present. However, the XPS analysis of clean glass substrate showed the presence of sulphur on the surface. This discrepancy can be due to the different time of preparation and the presence of thiol contaminants in the atmosphere of the laboratory. The C, N, O and Si peaks recorded are ascribable both to substances naturally present in glass, such as carbonates and silanes and to the nitrogen present in the air (**Figure 5.9**)[334,335,382]. The C 1s spectrum (**Figure 6.13 a**) is formed by three peaks, which are attributable to the following binding environments: C-C and C-Si (284.6 eV), C-O (286.5 eV) and C=O (288.1

eV)[334,335]. The Si 2p spectrum (**Figure 6.13 b**) can be deconvoluted into two peaks, attributed to silicon oxides (SiO_x) and Si-O-Si groups (103.3 eV) and Si-OH groups (102.7 eV), present on the glass substrates[116,383,385–387,389–391]. The N 1s spectrum (**Figure 6.13 c**) is characterised by a high background noise and a single peak centred at 400.2 eV can be identified. This peak can be assigned to the nitrogen in the air. The S 2s spectrum (**Figure 6.13 d**) indicates that sulphur is not present on the surface. The O 1s spectrum (**Figure 6.13 e**) is formed by a peak centred at 532.7 eV corresponding to C-O[334,335].The S 2p spectrum could not be recorded since it is shielded by the intense Si 2s peak. However, the absence of the S 2s peak already suggested the absence of sulphur residues on the surface. These peaks will be used as reference to analyse the changes on the substrates, as a result of the formation of the different layers on the glass substrates.

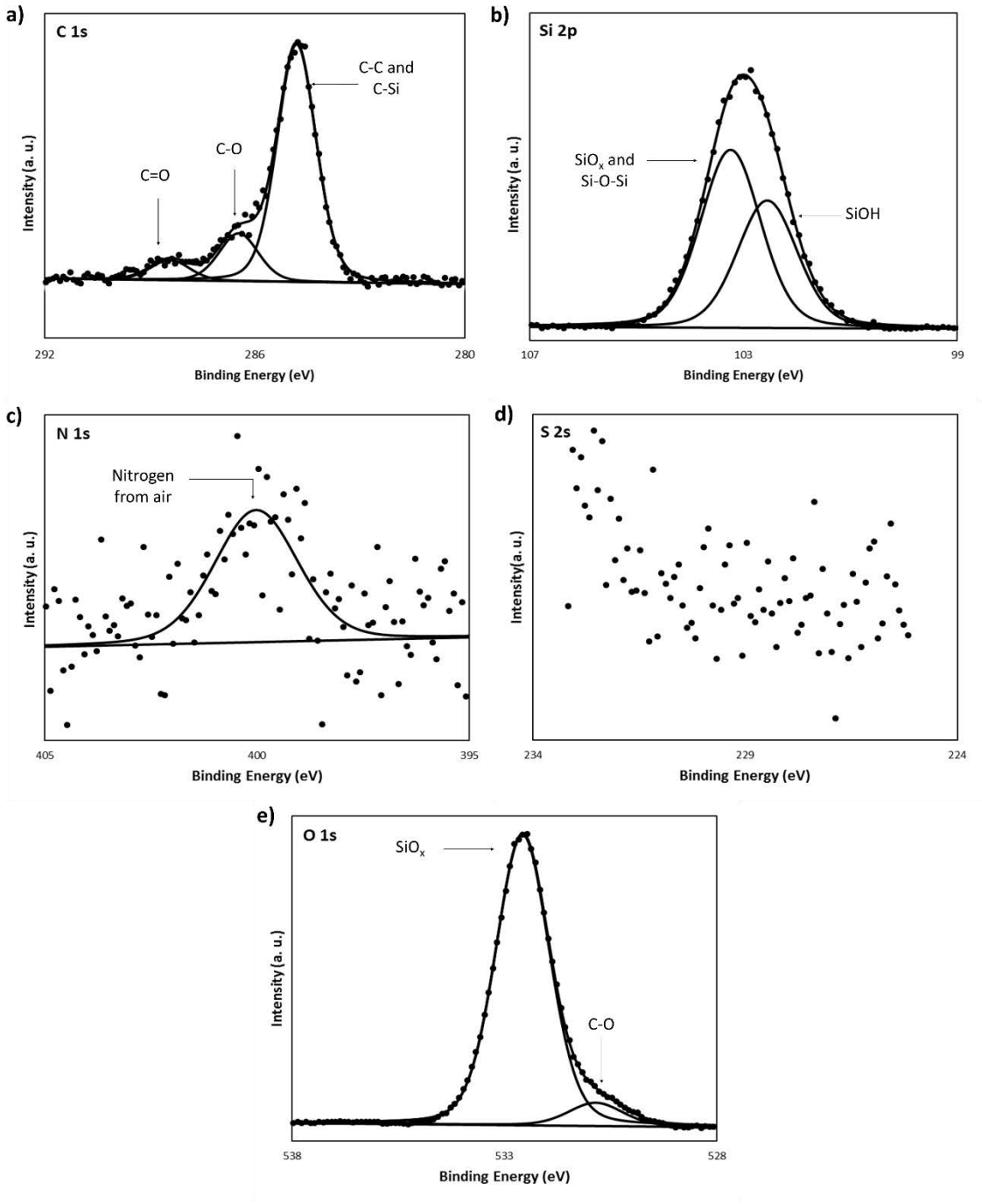

Figure 6.13 – *XPS spectra of the a) C 1s, b) Si 2p, c) N 1s, d) S 2s and e) O 1s regions of 11-mercapto-1-undecanol SAMs on glass.*

The ratios between the elements analysed (C, N, O and Si) were calculated and compared to the ones obtained from the analysis of clean glass substrates.

The results show an increase in the carbon amount on glass surfaces after the protective thiol immobilisation, compared to the carbon present on clean glass surfaces. In fact, the C/N ratios went from 7.8±1.9 to 24.4±3.11. There is also a significant decrease in the oxygen amount, since the O/C ratio decreased from 33.42±2.23 to 0.12±0.01. It is possible that some molecules of 11-mercapto-1-undecanol are physisorbed on the glass substrates and the rinsing with ethanol is not enough to remove them. However, the signal of S 2p cannot be recorded due to the strong Si 2s shielding and the S 2s signal is too noisy to identify the presence of sulphur on the glass surface.

6.3.3.2 Second step: silane-PDL on gold and glass

The silane-PDL layer was formed following the procedure illustrated in Chapter 3 – Experimental Procedures and Protocols. The silane molecules were deposited on the substrates via Chemical Vapour Deposition (CVD) by incubating either the gold or glass substrates in a vacuum chamber in silane atmosphere for an hour. After the deposition step, the silane layer was cured by leaving the functionalised substrates in the vacuum oven at 100˚C for 30 minutes.

The substrates were then immersed in a 1mM HCl solution in UHQ water for 5' under gentle shaking, to form carboxylic acid groups on the surface and then immersed in a solution 1:1 of 1-Ethyl-3-(3-dimethylaminopropyl)carbodiimide/*N*-Hydroxysuccinimide (EDC/NHS) overnight as illustrated in section 6.3.1.3.

Gold substrates:

The XPS analysis was performed on silane-PDL layer formed after the deposition of 11-mercapto-1-undecanol SAMs on gold, revealing the presence of the elemental species C, N, O,

S and Si. The C 1s spectrum is formed by three peaks (**Figure 6.14 a**), which are attributable to the following binding environments[334,335]: C-C and C-Si (284.8 eV) and C-S, C-N and C-O (286.3 eV), the third small peak at 288 eV, corresponds to C=O groups and it can be attributed to the carboxyl group on the silane or the carboxyl groups on the PDL chain[334,335,397]. The N 1s spectrum (**Figure 6.14 b**) consists in one small peak centred at 400.2 eV[383], that can be attributed either to the presence of poly-D-lysine on the gold surface or to the nitrogen present in the air.[383]. The O 1s spectrum (**Figure 6.14 c**) is formed by two peaks[334,335], the peak centred at 532.4 eV can be assigned to both C-O and Si-OH groups and the small peak at 533.0 eV is ascribable to both C=O and Si-O-Si groups, indicating the presence of either silane or silane-PDL on the surface. The S 2p spectrum (**Figure 6.14 d**) consists of a doublet peak at 163.4 eV (S $2p_{1/2}$) and 162.3 eV (S $2p_{3/2}$), indicating that there a small quantity of sulphur chemisorbed on the gold surface, corresponding to the presence of the thiol on the surface[395]. However, the peak at 163.4 eV can also be assigned to unbound sulphur on the gold surface, but the relative doublet peak could not be fitted using CASA XPS, due to the shielding effect of the Si 2s peak. The Si 2s spectrum (**Figure 6.14 e**) is formed by a peak centred at 153.5 eV showing the possible presence of unexpected silane on the gold surface [334,335,384]. The presence of the silicon peak can be due to the unwanted deposition of silane on the whole or part of the gold substrate. The Si 2p could not be recorded, since its regions overlaps with the Au 5d region[116,334,335,383–391]. It must be highlighted that in this case the Si 2s and S 2p signal were recorded together in the same region, leading to a high background noise in the less intense sulphur peak, compared to the silicon one. The recorded results suggest that the second step of the fabrication, that should result in the formation of a silane layer only on the glass substrate, also affect the gold substrate. This could lead to the presence of PDL on the gold surface, resulting in the cell attachment on both glass and gold substrates.

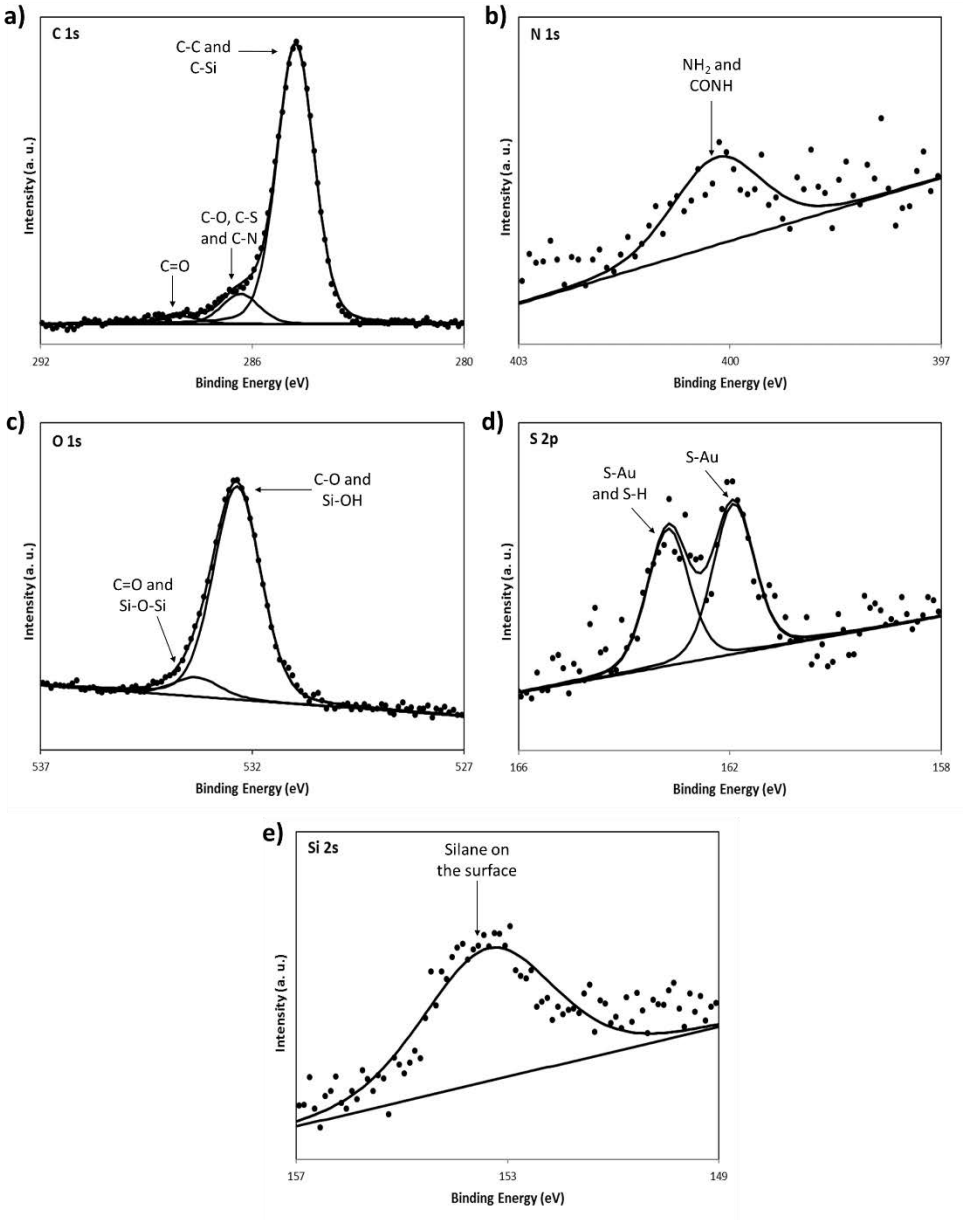

Figure 6.14 – *XPS spectra of the a) C 1s, b) N 1s, c) O 1s, d) S 2p and e) Si 2s regions of silane-PDL SAMs on gold after the first step.*

The calculated ratios determined after this step were compared to the ones calculated after the deposition of the protective thiol, to analyse if the changes on the glass surface could be ascribable to the effective formation of the desired silane-PDL layer.

The O/C ratio shows an increment of the oxygen presence on the gold substrate that went from 0.28±0.01 to 0.62±0.05, together with a small decrease of the sulphur amount, since the S/C ratio moved from 0.11±0.01 to 0.08±0.01. Each molecule of silane contains four oxygen atoms and each amide bond on lysine moieties coming from PDL contains an oxygen atom. The O/C ratio increases from 0.28±0.01 to 0.62±0.05 and nitrogen is present, even if in small quantities, whereas before its peak cannot be recorded. This circumstance could be explained by the physisorption of silane-PDL layer on the gold surface, causing also the shielding of the sulphur peak by the Si 2s signal.

Glass substrates:

The XPS analysis was performed on silane-PDL layer formed after the deposition of 11-mercapto-1-undecanol SAMs on glass, revealing the presence of the elemental species C, N, O and Si, indicating the presence of the silane-PDL structure. The C 1s spectrum is formed by 3 peaks (**Figure 6.15 a**), corresponding to four binding environments[334,335]. The peak centred at 284.8 eV can be assigned to C-C and C-Si bonds[397], the peak at 286.4 eV is ascribable to C-N bonds in C-N groups, whereas the third peak at 288.3 eV is assigned to the C 1s photoelectron of the carbonyl moiety, C=O. The N 1s spectrum (**Figure 6.15 b**) can be deconvoluted into two peaks, the first one corresponding to amino and amide groups (400.0 eV) and the second one ascribable to protonated amino groups (401.6 eV)[383]. The O 1s (**Figure 6.15 c**) composed by two peaks, corresponding to three different binding environments[334,335]. The first peak at 531.2 eV corresponds to Si-OH moieties, whereas the second peak centred at 532.7 eV can be assigned to C=O and Si-O-Si groups. The Si 2p spectrum (**Figure 6.15 d**) can be deconvoluted into two peaks, the first one centred at 102.6 eV can be ascribed to Si-OH groups, whereas the second

peak centred at 103.3 can be assigned to SiO_x present in the glass and Si-O-Si groups present in the silane chains[116,334,335,383–391]. Again, the small binding shift (less than 0.5 eV) is caused by the charge accumulation onto the glass substrate[392].

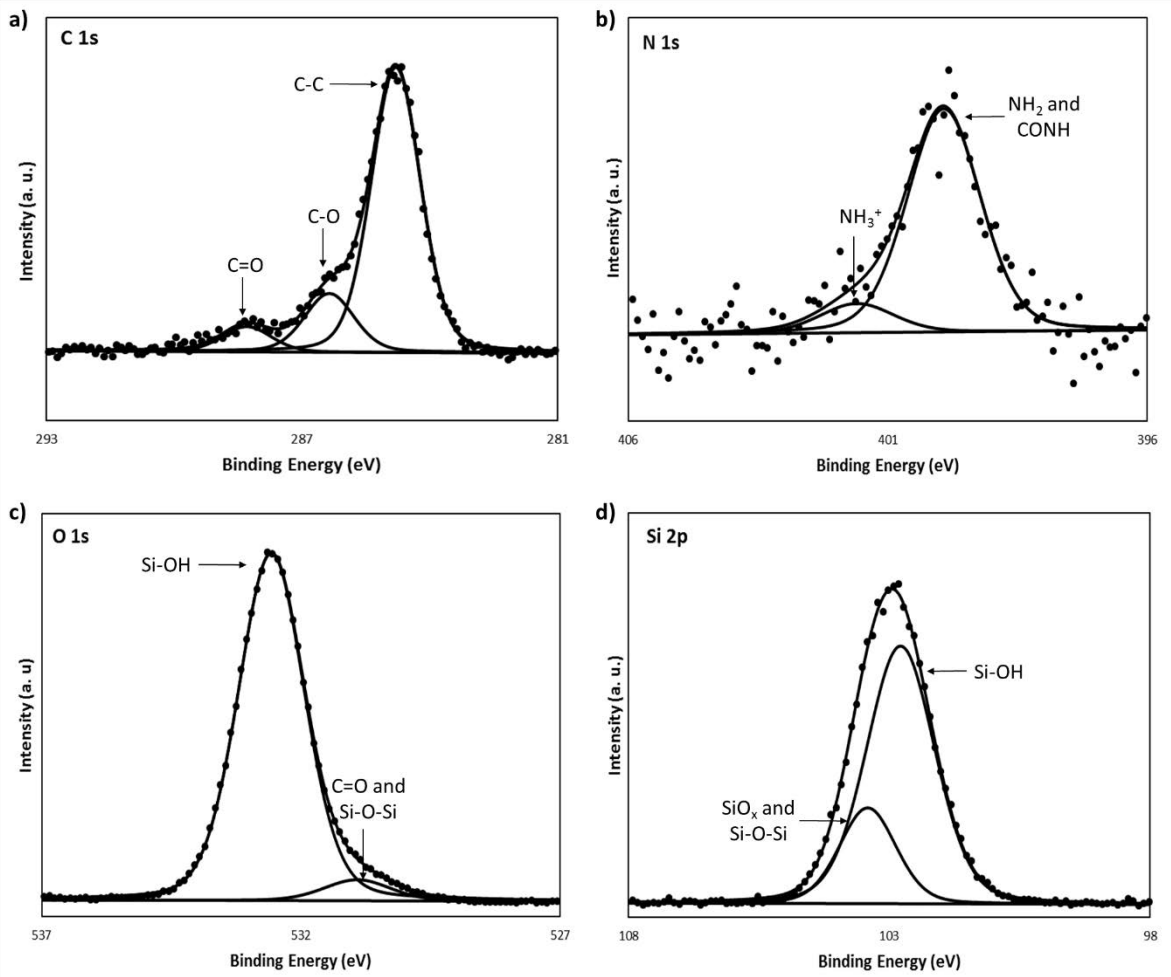

Figure 6.15 – *XPS spectra of the a) C 1s, b) N 1s, c) O 1s and d) Si 2p regions of silane-PDL SAMs on glass after the first step.*

The ratios determined after this step were compared to the ratios calculated after the deposition of the protective thiol, to analyse if the changes on the glass surface are ascribable to the effective formation of the desired silane-PDL layer.

The results show an increment of the amount of both nitrogen and oxygen on the glass surface. In fact, the N/C ratio went from 0.040±0.004 to 0.12±0.02 and the O/C ratio increased from 0.120±0.006 to 8.94±0.60. This is in accordance with the formation of a silane-PDL. In addition, it is important to notice, taking into consideration the standard errors, that the Si/C ratio (1.60±0.20) did not vary from the previous step (1.53±0.32). This phenomenon can be explained by the increment of carbon amount to the same extent as silicon amount. However, it is impossible to determine the quantity of silicon due to silicates present composing the glass substrate itself. The presence of silane-PDL structures was also verified by studying the attachment of sperm cells on glass surfaces (see **section 6.3.4**)

6.3.3.3 Third step: protective thiol removal

After the deposition of the silane-PDL layer, the 11-mercapto-1-undecanol thiol was removed from the gold substrate, to prepare the surface for the functionalisation with progesterone-C7-4KC:EG6OH mixed SAMs. The protective thiol was removed by applying a potential of -1.5V for 10 minutes. Three different times of potential application were tested on different gold substrates functionalised with 11-mercapto-1-undecanol SAM by 5 min, 10 min and 20 min chronoamperometry and a cycle of cyclic voltammetry to verify the success of the removal by the disappearance of the thiol desorption peak. The CV recorded on gold substrates after the overnight incubation of the protective thiol, shows a clear reductive desorption peak at -1.05 (black line on **Figure 6.16**). When the CV is recorded again, after the application of -1.5V for 5, 10 and 20 min, the desorption peak has disappeared, indicating that the thiol has been successfully removed from the gold surface. The 10-min time was chosen to both ensure the complete removal of the thiol and avoid the damage of the gold substrate itself. However,

cyclic voltammetry only shows the curve for thiol reduction and it is impossible to know if the silane-PDL layer is still present on gold. The analysis of this step by XPS is therefore important to study the effectiveness of the protective thiol removal step.

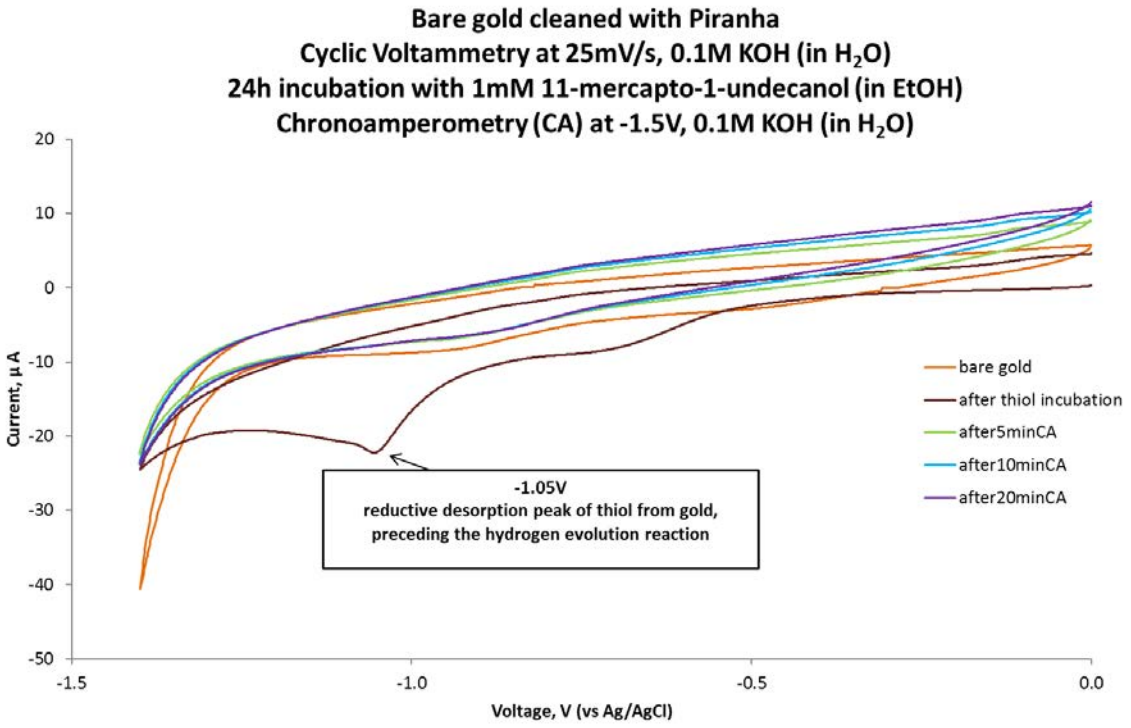

Figure 6.16 - *Cyclic voltammetry of bare gold after piranha cleaning (orange line), after MUD incubation (black line) and after 5, 10 and 20 minutes of -1.5 V chronoamperometry (green, light blue and purple lines)*

Due to the non-conductivity of glass substrates, after the second step the surfaces were immersed for ten minutes in KOH 0.1M in water, to analyse if the basic solution could have any effect on the silane-PDL layer. Both gold and glass surfaces were analysed by XPS.

Gold substrates:

The XPS analysis was performed on the gold substrates after the removal of the protective thiol performed by applying a negative potential of -1.5 V for ten minutes in KOH

0.1M in water. The results of the analysis revealed the presence of the elemental species S, C, N, O and Si, indicating that the removal of the protective thiol and possibly some silane residues, was not 100% successful as expected from CV results. The C 1s spectrum (**Figure 6.17 a**) can be deconvoluted into three peaks, corresponding to the following binding environments[334,335]: the first peak centred at 284.7 eV can be ascribed to C-C and C-Si moieties[397], the second peak centred at 286.2 eV corresponds to C-N groups, whereas the small peak at 288 eV can be assigned to the carbonyl moiety C=O, meaning that the electrochemical treatment of the gold substrate did not completely remove the silane molecules. The N 1s spectrum (**Figure 6.17 b**) consist in a small single peak centred at 400 eV, corresponding to amino and amide groups[383], indicating the presence of nitrogen on the surface, possibly to the undesired presence of lysine molecules on the gold surface. The O 1s signal (**Figure 6.17 c**) is represented by a small and large single peak centred at 532.3 eV that could be assigned to C=O and Si-O-Si groups[334,335]. The Si 2s signal (**Figure 6.17 d**) consists of a single peak centred at 153.2 eV, indicating the undesired presence of silane on the surface. The Si 2p signal cannot be recorded because is shielded by the Au 5d peak. The S 2p spectrum (**Figure 6.17 e**) has not a high resolution, due to the shielding effect of Si 2s peak, but it can be deconvoluted into two small peaks centred at 163.4 eV and 162.2 eV respectively. The first peak at 162.2 eV can be assigned to a small amount of sulphur chemisorbed to the gold surface, whereas the second one at 163.4 eV can be assigned to both bound sulphur and unbound sulphur. The doublet peak of unbound sulphur could not be fitted using CASA XPS due to the shielding effect of Si 2s, but it is reasonable to hypothesise the presence of free thiol groups on the gold substrate. However, the signals of the elements C, N, O and S are recorded also on clean gold surface. This make impossible to confirm the presence of protective thiol on the gold surface with certainty.

On the contrary, silane is still present after the thiol removal, since no silicon signals were recorded on pristine gold.

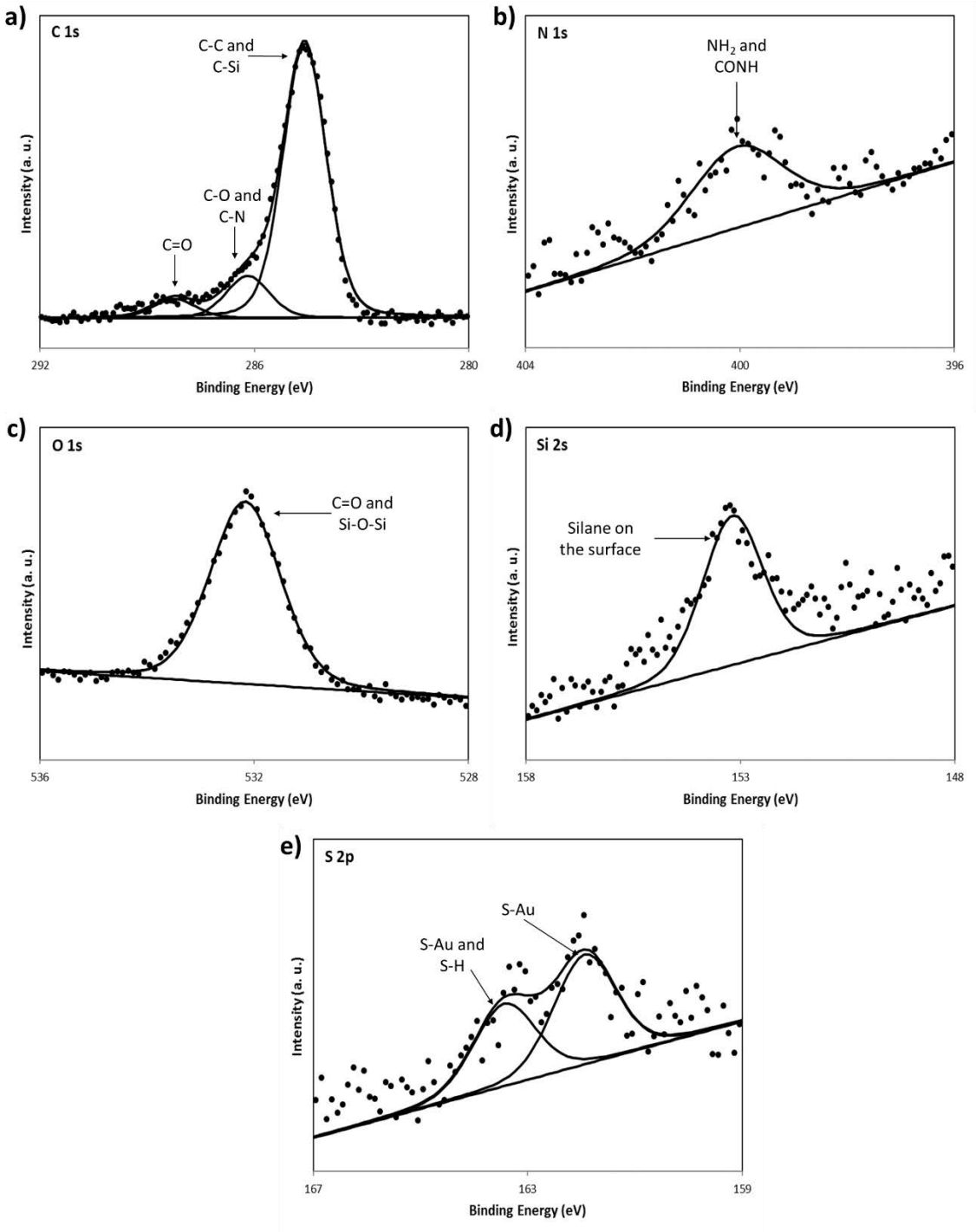

Figure 6.17 – *XPS spectra of the a) C 1s, b) N 1s, c) O 1s, d) Si 2s and e) S 2p regions after thiol removal on gold substrates.*

The ratios between the elements analysed were calculated and compared to the ones obtained from the previous step.

Both the calculated S/C and Si/C ratios, if the standard errors are taken into consideration, indicate that no changes happened on the surface compared to the previous step, in fact the S/C value is still 0.08±0.01 and the Si/C moved from 0.15±0.02 to 0.16±0.03. It is possible to state that the removal of the protective thiol was unsuccessful and silane is still present on the gold surface. This phenomenon could be due to the silane-PDL layer physisorbed on the gold surface, preventing the correct removal of 11-mercapto-1-undecanol protective thiol by cyclic voltammetry.

Glass substrates:

The XPS analysis was performed on the glass substrates after incubation, of the surfaces obtained after the second step, in KOH 0.1M in water for ten minutes. The results of the analysis revealed the presence of the elemental species C, N, O and Si. The C 1s spectrum (**Figure 6.18 a**) can be deconvoluted into three peaks, assignable to different binding environments[334,335]. The first peak centred at 284.8 eV corresponds to C-C and C-Si bonds, the second peak centred at 286.4 eV is ascribable to C-N groups, whereas the third peak at 288.3 eV is assigned to the C 1s photoelectron of the carbonyl moiety, C=O. The N 1s spectrum (**Figure 6.18 b**) can be deconvoluted into two peaks, the first one corresponding to amino and amide groups (400.0 eV) and the second one ascribable to protonated amino groups (401.2 eV)[383]. The O 1s spectrum (**Figure 6.18 c**) is composed by two peaks, corresponding to three different binding environments[334,335]. The first peak at 531.4 eV corresponds to Si-OH moieties, whereas the second peak centred at 532.6 eV can be assigned to C=O and Si-O-Si groups. The Si 2p spectrum (**Figure 6.18 d**) can be deconvoluted into two peaks, the first one centred at 102.6 eV

can be ascribed to Si-OH groups, whereas the second peak centred at 103.4 eV can be assigned to SiO_x present in the glass and Si-O-Si groups present in the silane chains[116,334,335,383–391].

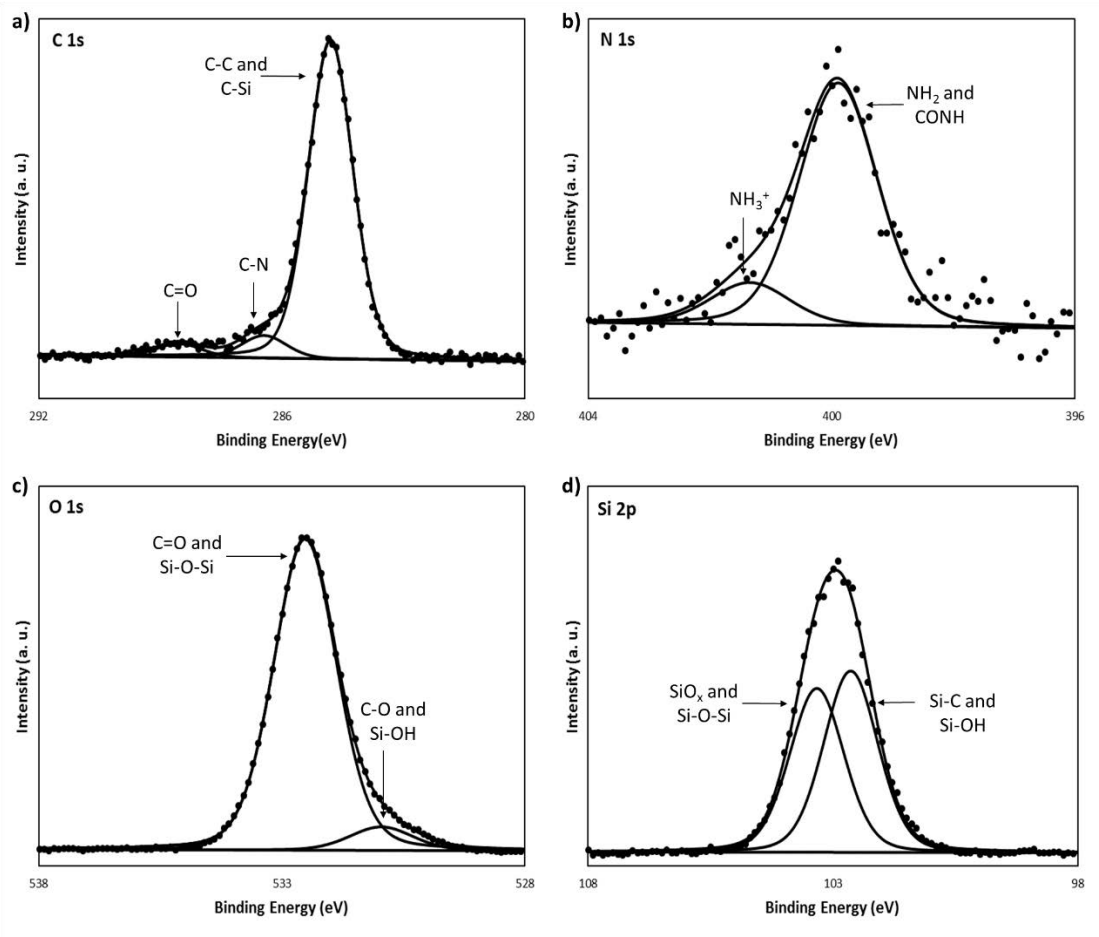

Figure 6.18 – *XPS spectra of the a) C 1s, b) N 1s, c) O 1s and d) Si 2p regions incubation of glass substrates in KOH for ten minutes, demonstrating that removal step will not affect the integrity of the silane-PDL layer on the glass substrate.*

The ratios between the elements analysed (C, N, O and Si) were calculated and compared to the ones obtained from the analysis of the previous step on glass.

The results for the silicon element, demonstrate that the KOH solution does not affect the silane-PDL layer on the glass substrate. The small change recorded in the Si/C ratio (from

1.53±0.32 to 1.0±0.2) could be ascribable to a different surface coverage than the previous step or a slightly different glass substrate composition. The calculated Si/C ratio of 1.0±0.2 shows that there is as much carbon as silicon on the surface. However, it is again impossible to deduct the quantity of both atoms arising from pure glass composition.

6.3.3.4 Fourth step: Progesterone-C7-4KC mixed SAM

Gold substrates

The XPS analysis was performed on the gold substrates incubated in Progesterone-C7-4KC:EG6OH mixed SAMs (1:40 solution ratio), after the removal of the 11-mercapto-1-undecanol SAM. The results of the analysis revealed the presence of the elemental species C, N, O and S. The C 1s spectrum (**Figure 6.19 a**) can be deconvoluted into three peaks, assignable to different binding environments[334,335]. The first peak centred at 284.6 eV corresponds to C-C bonds, the second peak centred at 286.4 eV is ascribable to C-S, C-N and C-O groups, whereas the third peak at 288.4 eV is assigned to the C 1s photoelectron of the carbonyl moiety, C=O. The N 1s spectrum (**Figure 6.19 b**) consists in one small corresponding to amino (NH_2) and amide (CONH) groups (400.3 eV)[383]. The O 1s spectrum (**Figure 6.19 c**) is deconvoluted two peaks, corresponding to two different binding environments[334,335]. The first peak at 532.8 eV corresponds to C-O moieties, whereas the second peak centred at 531.8 eV can be assigned to C=O groups. The Si 2p spectrum (**Figure 6.19 d**) can be deconvoluted into two peaks, the first one centred at 102.6 eV can be ascribed to Si-OH groups, whereas the second peak centred at 103.4 eV can be assigned to SiO_x present in the glass and Si-O-Si groups present in the silane chains[116,334,335,383–391]. The presence of the silane peaks indicate that the silane-PDL layer was not displaced by the presence of progesterone-C7-4KC and EG6OH thiol molecules. Finally, the S 2s spectrum (**Figure 6.19 e**) was recorded instead of the S 2p spectrum, shielded by the

intense Si 2s peak. The S 2s peak centred at 223.2 eV indicate the presence of sulphur on the surface, but it does not discriminate between the sulphur covalently attached to the gold substrate and the unbound sulphur.

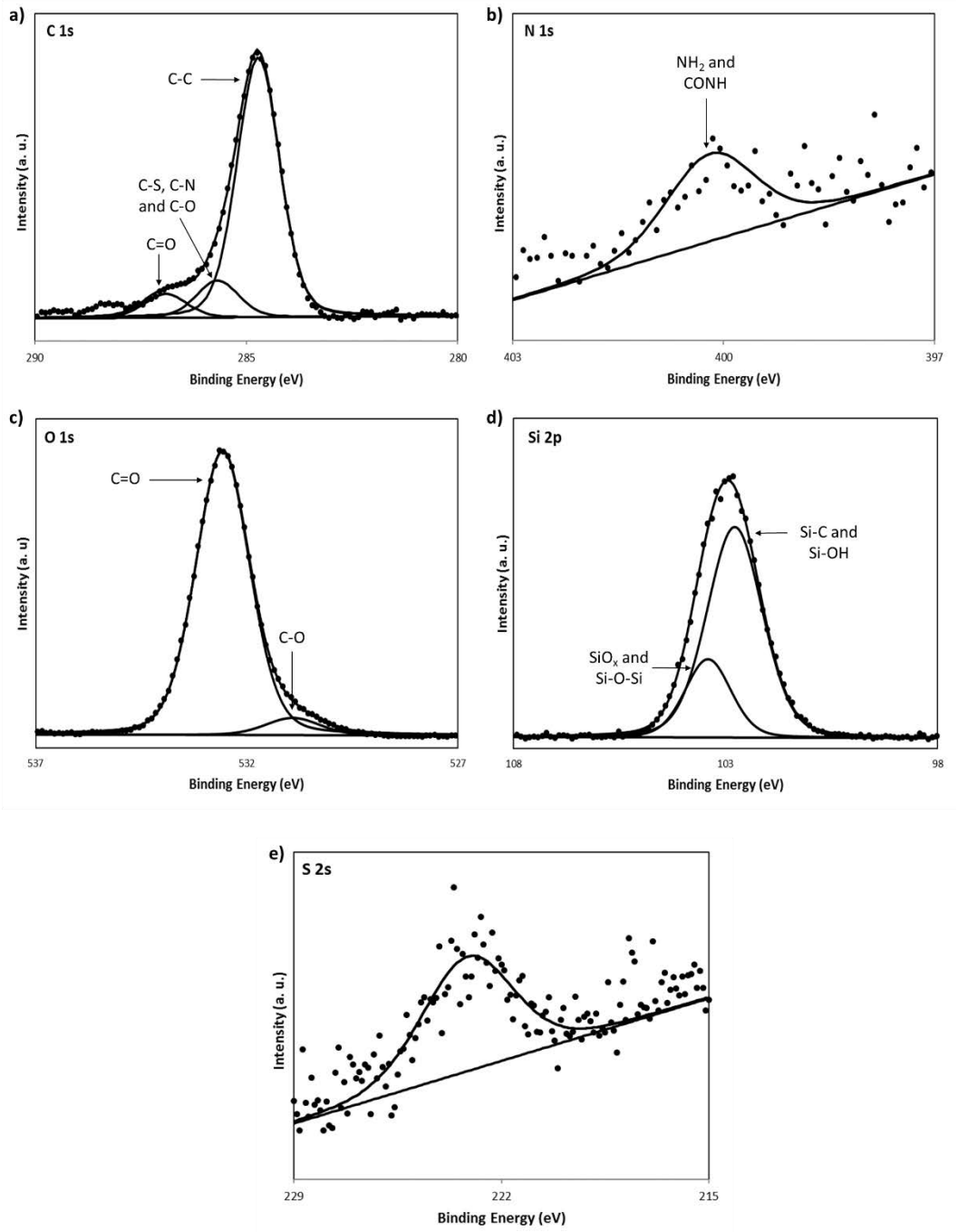

Figure 6.19 – *XPS spectra of the a) C 1s, b) N 1s, c) O 1s, d) Si 2p and e) S 2s regions after the formation of Progesterone-C7-4KC:EG6OH mixed SAMs on gold substrates.*

The calculated ratios after performing the last step on gold showed that there is not a significant change in both C/N and C/Si ratios after this step. In fact, the C/N went from

11.20±0.92 to 11.10±0.30 and the C/Si ratio went from 6.30±1.10 to 6.90±0.40. This can be due to the presence of silane-PDL molecules on the gold substrate, that cannot be displaced by the thiols present in the mixed SAM solution. The only element that increased is oxygen, in fact the O/C ratio increased from 0.55±0.09 to 0.93±0.10. The theoretical O/C ratio for 1:40 progesterone-C7-4KC:EG6OH solution ratio is 0.21, that is lower than the one calculated from the XPS experiments. The theoretical S/C ratio for the same mixed SAM solution ratio is 0.03, that is in line with the calculated one of 0.04±0.03. However, the calculated standard error is too high to assume that the desired mixed SAM has formed correctly on the gold substrates. In fact, it is possible that the progesterone-C7-4KC are not covalently bond to the gold surface, but they are only forming weak hydrogen bonds with the amino groups of the undesired PDL on the surface. Unfortunately, the S 2p peak cannot be recorded due to the presence of the shielding Si 2s peak, therefore the mixed SAM surface ratio cannot be calculated.

Glass substrates

The XPS analysis was performed on the glass substrates incubated in progesterone-C7-4KC:EG6OH mixed SAMs, after the third step described before. The results of the analysis revealed the presence of the elemental species C, N, O and Si. The C 1s spectrum (**Figure 6.20 a**) can be deconvoluted into three peaks, assignable to different binding environments[334,335]. The first peak centred at 284.8 eV corresponds to C-C and C-Si bonds, the second peak centred at 286.2 eV is ascribable to CONH groups, whereas the third peak at 288.0 eV is assigned to the C 1s photoelectron of the carbonyl moiety, C=O. The N 1s spectrum (**Figure 6.20 b**) can be deconvoluted into two peaks, the first one corresponding to amino (NH_2) and amide groups (CONH) at 399.5 eV and the second one ascribable to protonated amino groups (NH_3^+) at 400.4 eV[383]. The O 1s spectrum (**Figure 6.20 c**) is composed by two peaks, corresponding to three

different binding environments[334,335]. The first peak at 531 eV corresponds to Si-OH moieties, whereas the second peak centred at 532.5 eV can be assigned to C=O and Si-O-Si groups. The Si 2p spectrum (**Figure 6.20 d**) can be deconvoluted into two peaks, the first one centred at 102.5 eV can be ascribed to Si-OH groups, whereas the second peak centred at 103.2 eV can be assigned to SiO_x present in the glass and Si-O-Si groups present in the silane chains[116,334,335,383–391]. The silicon peaks recorded on glass were similar to those observed for gold substrates after this last step, confirming that the formation of silane-PDL permanently affects the surface, compromising the success of the orthogonal functionalisation strategy.

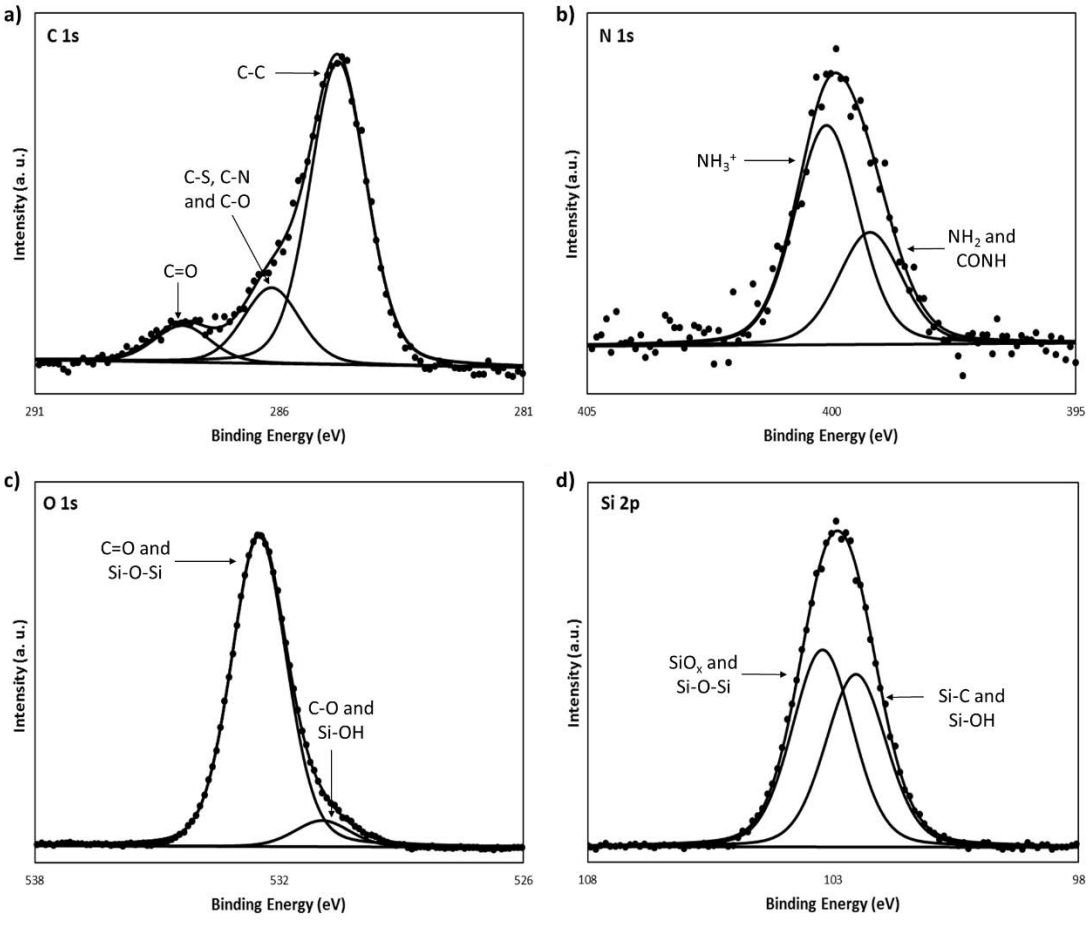

Figure 6.20 – *XPS spectra of the a) C 1s, b) N 1s, c) O 1s and d) Si 2p regions after the formation of Progesterone-C7-4KC:EG6OH mixed SAMs on glass substrates.*

However, in the region between 160.0 eV and 165.0 eV in the Si 2s spectrum, a small peak is visible (**Figure 6.21**).

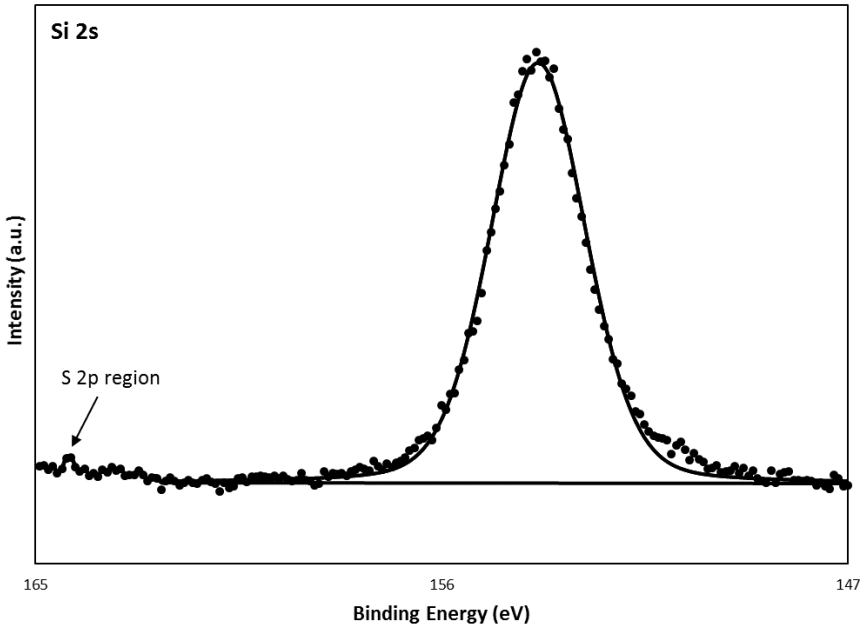

Figure 6.21 – *XPS spectrum of Si 2s. A small peak is visible in the region of S 2p.*

This peak could demonstrate the presence of the mixed SAMs on the glass substrates, and we could hypothesise that it will compromise the sperm cell attachment on the glass substrates. However, if we consider the background noise the peak could be questionable and additional analysis needs to be done in the future. The progesterone present on glass substrates could interact with sperm cells and trigger their hyperactivation[236,240,381]. This phenomenon would make sperm cell to "swim away", due to the hyper-motility acquired. To verify this hypothesis, cell adhesion was tested on microscope glass slides after all four steps.

A deeper insight into the molecular coverage of the glass substrates can be obtained by calculating the ratios between the elements analysed by XPS.

The results evidence only a small increment of the nitrogen amount on the surface, showing a variation in the N/C ratio from 0.132±0.001 to 0.19±0.01. This small change can be due to the presence of some Progesterone-C7-4KC molecules on the surface. This, together with the possible presence of a small S 2p in the silicon spectrum, does not exclude the possibility of molecules of Progesterone-C7-4KC sitting on top of the silane-PDL layer, interacting with poly-D-lysine side chains via hydrogen bonds between amino groups. The interaction can be due to an insufficient percentage of triethylamine (TEA) in the mixed monolayer, unable to prevent the formation of the undesired hydrogen bonds. The orthogonal functionalisation investigated herein, as demonstrated by XPS, was not effective at promoting the solely attachment of PDL on the glass surfaces and the Progesterone-C7-4KC:EG6OH mixed SAMs on gold. Further evidence that further studies are needed in the future to optimise such functionalization was acquired by conducting cell adhesion experiments.

6.3.4 Study of the effect of surface preparation steps on cell adhesion

After the completion of the fourth step of the surface preparation, the treated glass slide was attached to the imaging chamber with vacuum grease and sperm cells were injected into the chamber and left incubating following the procedure described in section 5.2.1.4. The starting hypothesis is that the possible presence of Progesterone-C7-4KC on the glass surface could restrain sperm cells from adhering. This adhesion hindrance could be due to the interaction between the sperm cells and the progesterone. This interaction would trigger the hyperactivation of the sperm cells that will therefore “swim-away” due to the hyper-motility acquired and will be removed from the flow cell by vacuum suction. As expected from XPS analysis results, the fluorescence microscopy analysis of the surface revealed no presence of cells on the surface (**Figure 6.22**).

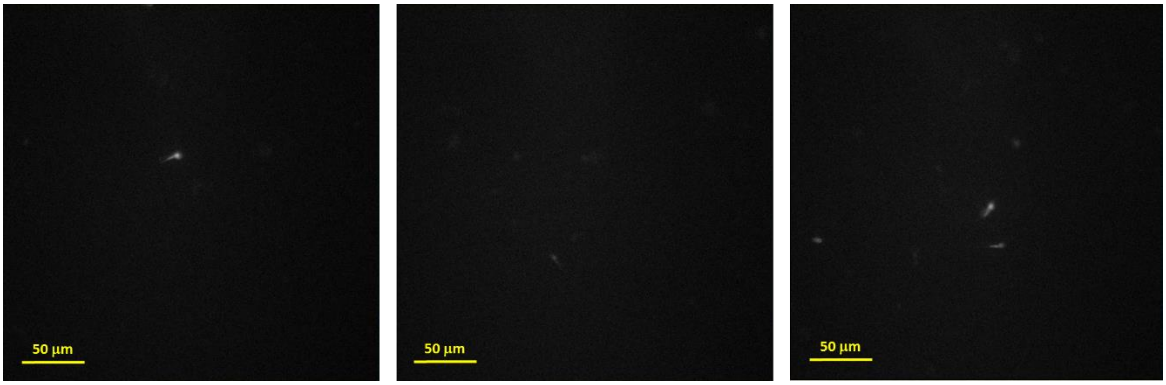

Figure 6.22 – *Fluorescence images of cell adhered on glass slides after the completion of the Progesterone-C7-4KC:EG6OH mixed SAM deposition step.*

The failure in sperm cells attachment can be related to the sulphur peak recorded on the glass substrate, indicating the presence of progesterone-C7-4KC molecules, as seen in the previous section.

6.4 Conclusions and Future Work

In conclusion, we have firstly studied sperm cells adhesion in different conditions. PDL coating is the standard method used to promote cell adhesion[312], but it resulted to be incompatible with the conditions needed for the orthogonal functionalisation of the micropattern that we aim to use in our future research work. We have successfully circumvented this issue, by creating silane-PDL layers on glass. Amide bonds were formed, between the carboxyl groups on silane molecules and amino groups on PDL, using different concentrations of PDL (0.1 mg/ml and 0.5 mg/ml), via EDC/NHS coupling strategy. Labelled sperm cells were then incubated on the different surfaces and the success of cell adhesion was analysed by fluorescence microscopy. The silane-PDL layer formed using 0.5 mg/ml of PDL was selected as the best one at promoting cell adhesion after overnight incubation in HPLC ethanol.

An orthogonal self-assembly strategy was then designed, to create a device able to promote sperm cells adhesion and control their hyperactivation in real-time. The detailed analysis of the surfaces by XPS, after each functionalisation step, allowed us to investigate how each step influences the performance of the next one. The information collected through the XPS investigation was enormous and it will be useful to plan future work. The XPS analysis of both clean glass and clean gold showed that working in a controlled environment (e.g. glove box), is fundamental to avoid undesired contamination from organic compound present in the laboratory environment. The functionalisation of glass surfaces with silane-PDL layers was successful and it is not affected by the use of KOH aqueous solution for the removal of the protective thiol. However, the silane and PDL molecules can contaminate the gold surfaces, contributing to the failure of the removal of the 11-mercapto-1-undecanol monolayer. It will also be important to investigate this step further, splitting it into two different analysis. Firstly, the removal of 11-mercapto-1-undecanol monolayer should be investigated by XPS. Secondly, the removal of the same monolayer should be attempted after the step involving the deposition of silane-PDL molecules. The cyclic voltammogram should be then recorded to verify that the curve corresponding to the thiol desorption is present. The investigation of the last functionalisation step, involving the formation of progesterone-C7-4KC:EG6OH mixed SAM, revealed the possible presence of progesterone-C7-4KC on the glass surface. As stated before, this can lead to the impossibility of achieving a correct cell adhesion on glass surfaces. It will be therefore worth testing different percentages of triethylamine (TEA) in the mixed SAM solution, to find the optimum one that can prevent the formation of hydrogen bonds between the amino groups of lysine groups on both PDL and progesterone-C7-4KC molecules. In addition, each step can be tested again by XPS after sonicating the substrates, to investigate if sonication could be beneficial to the functionalisation process. Finally, after the incubation of

both glass and gold substrates in progesterone-C7-4KC:EG6OH solution, the XPS analysis showed the incorrect formation of the mixed monolayer on gold substrates and the presence of progesterone-C7-4KC molecules on top of silane-PDL layers on glass substrates. To gain a better understanding of what is happening on the gold surfaces after the last step, SPR experiments can be performed on these surfaces. The interaction between progesterone-Ab and progesterone moieties can be tested in OC conditions to verify the presence of the desired progesterone-C7-4KC:EG6OH mixed SAMs on the gold substrates. If the OC experiments are successful, the feasibility of the switching can also be tested to model what we want to obtain once the glass-gold micropattern has been correctly functionalised. Despite the difficulties encountered in achieving the desired molecular system on the chosen substrates, orthogonal functionalisation of surfaces remains an important tool in the development of miniaturised devices possessing a wide range of applications. Such strategy allows the reduction in the use of protective groups and number of reaction step, but also the use of mild conditions. This study will certainly be useful in the development of new orthogonal chemistry strategies and new tools applicable in both cell biology and the improvement of IVF techniques.

Chapter 7 – Conclusions and Future Work

7.1 Conclusions

The research work described in this dissertation was aimed at the development of novel biomolecular platforms able to control biointeractions upon the application of an electrical potential.

Firstly, a switchable oligopeptide mixed SAM was investigated to analyse the possibility of controlling the interaction between biotin end groups and neutravidin protein in solution. The chosen mixed SAM was composed by biotin-4KC and triethylene glycol thiol molecules. The 4-Lys units gave the molecule a flexible and switchable backbone. In fact, lysine amino acids present a positive charge a pH 7 that can be exploited to induce a molecular rearrangement on the gold surface, upon the application of an electrical potential. The interaction between neutravidin and biotin in different biotin-4KC:TEGT mixed SAM were monitored by electrochemical SPR experiments to identify the mixed SAM ratio presenting the highest switching ability.

The successful results obtained where then used to create a switchable platform to control, for the first time, the interaction between an antigen on the surface and its antibody in solution. Specifically, we studied the control of the interaction between progesterone and anti-mouse progesterone antibodies. Different buffers were studied to identify the best conditions for the switching.

Finally, preliminary studies were performed on glass and gold substrates to investigate the feasibility of an orthogonal functionalisation of a micropatterned surface, with the aim of

developing a novel smart molecular system able to expose and conceal progesterone moieties on demand for the control of calcium signalling in sperm cells.

The attachment of sperm cells on different functionalised glass substrates were also investigated.

Briefly:

Chapter 3 described the characterisation experiments and switching studies performed on different biotin-4KC:TEGT ratios to identify the best surface organisation conditions needed to have the best control over the interaction between biotin on the gold surface and neutravidin in solution. Furthermore, the role of the oligopeptide chain was also investigated to elucidate how the gap distance between the biotin end group and the ethylene glycol thiol matrix can influence the dynamics of the switching process. The switching behaviour of two different ratios of biotin-2KC:TEGT and biotin-6KC:TEGT mixed SAM were studied and compare to the biotin-4KC:TEGT performance. An insight into the dynamics governing the molecular rearrangement over the surface, when an electrical potential is applied, was obtained thanks to molecular dynamics simulations performed by Nanjing University. The results showed that the length of the oligopeptide chain has a fundamental role in the switching process and long switchable chains can lead to intercrossing, reducing the switching ability of the mixed SAMs. The matrix of ethylene glycol thiol has a fundamental role in preventing unspecific neutravidin binding over the surface and in spacing out the oligopeptide chains to give them enough free space to undergo the switching. In addition, it allows the embedding of the biotin active group that becomes unavailable for binding to neutravidin. On the other hand, a well-packed ethylene glycol thiol matrix can constrain the lysine chains from undergoing a molecular rearrangement upon the application of an electrical potential.

Chapter 4 illustrated the development of a switchable system for controlling antigen-antibody interactions. Such a system was fabricated starting from the results obtained in Chapter 3. Therefore, similar lysine oligopeptide chains were used to expose or conceal molecules of progesterone on the gold surface, under potential control. After preliminary studies in PBS, electrochemical SPR studies were performed on progesterone-C7-4KC:EG6OH mixed SAMs, in different sEBSS+BSA buffer conditions, to investigate the effect of Bovine Serum Albumin (BSA) on the mixed SAMs switching performance. The results showed that the presence of a negatively charged protein such as BSA can hinder the correct switching of the oligolysine chains. By removing BSA from the buffer, we were able to successfully exploit the mixed monolayer to control, for the first time, the interaction between progesterone and anti-mouse progesterone antibody.

Chapter 5 analysed, firstly, sperm cells adhesion in different conditions. A new adhesion strategy, based on silane-PDL layers was investigated for the first time and compared to the standard PDL coating method. The latter, resulted to be unsuitable for the orthogonal functionalisation of glass-gold micropatterned surfaces that will be the one of the next steps of this research work. An orthogonal surface functionalisation strategy was planned, characterised and analysed, step by step, to find the possible inhibiting factors of the process. The results showed that several factors need to be considered to achieve the desired and correct molecular structure on both glass and gold surfaces. The number of possible and necessary improvements of the strategy were described in detail in Chapter 5 conclusions section. The most important factor to be taken into consideration is the possible cross contamination of the two substrates, as a result of the functionalisation chemistry used.

7.2 Future Work

The work performed in this thesis is the first effort in both controlling the interaction between progesterone and the anti-mouse progesterone antibody and developing an orthogonal functionalisation strategy to create a novel platform to control calcium signalling activation in human sperm cells.

In this thesis, the factors that can influence the switching capability of different mixed SAMs, such as SAM components surface ratio, switching units length and buffer conditions were investigated. In addition, the analysis of the limitations affecting the feasibility of the orthogonal functionalisation process, allowed the understanding of how the functionalisation steps can influence each others and the data collected will be fundamental to plan out future work.

Firstly, it will be important to study the switching ability of different progesterone-C_n-4KC:EG6OH systems, to investigate the role of the alkyl spacer in the switching process. It would also be interesting to investigate how the alkyl spacer length could influence the response of sperm cells from different donors to the progesterone end group. In addition, different antibody/antigen systems could be studied. For example, a different host could be used instead of mouse (e.g. rabbit, goat) to produce monoclonal antibodies with different affinities to progesterone. New SPR experiments in different electrical potential conditions can be performed to compare the SPR response and the switching ability of the progesterone-oligopeptide in the presence of different interacting partners in solution.

Moreover, the concept of using switchable peptide to conceal and expose larger biomolecules on demand can be expanded, by investigating the application of nanobodies.[398] Nanobodies are natural single-domain antibodies, which result to be particularly attractive as

capturing molecules for use in biosensing. They recognise their antigens with high specificity and affinities similar to standard antibodies (i.e. nano- to picomolar affinities), but thanks to their small molecular size, they are able to recognise novel epitopes that regular-size antibodies cannot.[398,399] In fact, nanobodies exhibit a length down to 2-3 nm and molecular weight of 12-15 kDa, which are much smaller than those of antibodies (150-160 kDa).[399]

Additionally, different types of switching can be investigated. For example, future research work can be aimed at the development of a double-armed molecule, exploiting aspartic acid moieties as switching "arms". Aspartic acid aminoacid present negatively-charged side chains at pH 7. In this way, an OFF-ON switching can be studied, which will stop the need to have an electrical potential to control the concealment of the bioactive molecule (**Figure 7.1**).

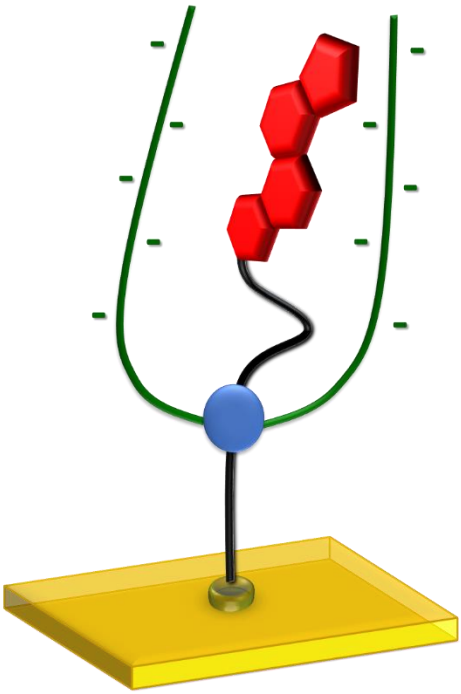

Figure 7.1 – *Cartoon representation of double-armed switching molecule. The aspartic acid oligopeptide arms (green) are connected to the alkyl chain (black) carrying the progesterone moiety (red) through a core central molecule (blue) in a dendron-like structure.*

Additional research interest can also be directed to the study of more rigid charged backbones, such as phosphate backbones, instead of lysine-oligopeptides ones.

Furthermore, it will be fundamental to analyse some of the orthogonal functionalisation steps in more detail, such as studying if sonicating the substrates could have any effect and if changing the percentage of triethylamine (TEA) in the last step, could reduce the formation of hydrogen bonds between lysine side chains.

The switchable mixed SAMs can also be modified and functionalised with different antigens and find an important application in biomedicine, in the study of pathologies involving antibodies.

Reversibility is still an issue and future research focus can be directed to the design of new molecular structures that will allow the formation of a fully reversible system. Also, the long-term stability of switching oligopeptides in complex biological conditions still need to be investigated.

Once all the issues encountered in this research work will have been addressed and solved, it will be possible to develop and analyse an innovative platform, able to control the hyperactivation of human sperm cells, upon the application of an electrical potential. The results of these future studies will be then applied to the selection of “healthy” sperm cells for *in-vitro* fertilisation (IVF) techniques, increasing their success rates and reducing their costs.

References

(1) Mendes, P. M. *Chem. Soc. Rev.* **2013**, *42* (24), 9207–9218.

(2) Kasemo, B. *Surf. Sci.* **2002**, *500* (1–3), 656–677.

(3) Chen, A.; Chatterjee, S. *Chem. Soc. Rev.* **2013**, *42* (12), 5425.

(4) Mendes, P. M.; Yeung, C. L.; Preece, J. A. *Nanoscale Res. Lett.* **2007**, *2* (8), 373–384.

(5) Wang, X.; Liu, L.-H.; Ramstrom, O.; Yan, M. *Exp. Biol. Med.* **2009**, *234* (10), 1128–1139.

(6) Brolo, A. *Nat. Photonics* **2012**, *6* (November), 709–713.

(7) Duke, C. B.; Plummer, E. W. **2002**, *i*, 0–1.

(8) Wang, X.; Hu, Y.; Wei, H. *Inorg. Chem. Front.* **2016**, *3* (1), 41–60.

(9) Nandivada, H.; Ross, A. M.; Lahann, J. *Prog. Polym. Sci.* **2010**, *35* (1–2), 141–154.

(10) Pranzetti, A.; Preece, J. A.; Mendes, P. M. In *Intelligent Stimuli-Responsive Materials*; John Wiley & Sons, Inc.: Hoboken, NJ, USA, 2013; pp 377–422.

(11) Sin, M. L.; Mach, K. E.; Wong, P. K.; Liao, J. C. *Expert Rev. Mol. Diagn.* **2014**, *14* (2), 225–244.

(12) Tothill, I. E. *Semin. Cell Dev. Biol.* **2009**, *20* (1), 55–62.

(13) Soper, S. A.; Brown, K.; Ellington, A.; Frazier, B.; Garcia-Manero, G.; Gau, V.; Gutman, S. I.; Hayes, D. F.; Korte, B.; Landers, J. L.; Larson, D.; Ligler, F.; Majumdar, A.; Mascini, M.; Nolte, D.; Rosenzweig, Z.; Wang, J.; Wilson, D. *Biosens. Bioelectron.* **2006**, *21* (10), 1932–1942.

(14) Rasooly, A.; Jacobson, J. *Biosens. Bioelectron.* **2006**, *21* (10), 1851–1858.

(15) Søndergaard, R. V.; Christensen, N. M.; Henriksen, J. R.; Kumar, E. K. P.; Almdal, K.; Andresen, T. L. *Chem. Rev.* **2015**, *115* (16), 8344–8378.

(16) Holzinger, M.; Le Goff, A.; Cosnier, S. *Front. Chem.* **2014**, *2*.

(17) Zhao, W.-W.; Xu, J.-J.; Chen, H.-Y. *Chem. Rev.* **2014**, *114* (15), 7421–7441.

(18) Razavi, H.; Janfaza, S. *Nanomed J* **2015**, *2* (2), 74–87.

(19) Taleat, Z.; Khoshroo, A.; Mazloum-Ardakani, M. *Microchim. Acta* **2014**, *181* (9–10), 865–891.

(20) Bauch, M.; Toma, K.; Toma, M.; Zhang, Q.; Dostalek, J. *Plasmonics* **2014**, *9* (4), 781–799.

(21) Liu, X.; Li, H.; Jin, Q.; Ji, J. *Small* **2014**, n/a-n/a.

(22) Ravindran, A.; Chandran, P.; Khan, S. S. *Colloids Surfaces B Biointerfaces* **2013**, *105*, 342–352.

(23) Omidfar, K.; Khorsand, F.; Darziani Azizi, M. *Biosens. Bioelectron.* **2013**, *43*, 336–347.

(24) Zhang, X. *Cell Biochem. Biophys.* **2015**, *72* (3), 771–775.

(25) Yang, N.; Chen, X.; Ren, T.; Zhang, P.; Yang, D. *Sensors Actuators B Chem.* **2015**, *207*, 690–715.

(26) Kumar, S.; Ahlawat, W.; Kumar, R.; Dilbaghi, N. *Biosens. Bioelectron.* **2015**, *70*, 498–503.

(27) Gaharwar, A. K.; Peppas, N. A.; Khademhosseini, A. *Biotechnol. Bioeng.* **2014**, *111* (3), 441–453.

(28) Cirillo, G.; Hampel, S.; Spizzirri, U. G.; Parisi, O. I.; Picci, N.; Iemma, F. *Biomed Res. Int.* **2014**, *2014*, 1–17.

(29) Wong, B. S.; Yoong, S. L.; Jagusiak, A.; Panczyk, T.; Ho, H. K.; Ang, W. H.; Pastorin, G. *Adv. Drug Deliv. Rev.* **2013**, *65* (15), 1964–2015.

(30) Mehra, N. K.; Jain, K.; Jain, N. K. *Drug Discov. Today* **2015**, *20* (6), 750–759.

(31) Sajid, M. I.; Jamshaid, U.; Jamshaid, T.; Zafar, N.; Fessi, H.; Elaissari, A. *Int. J. Pharm.* **2016**, *501* (1–2), 278–299.

(32) Ferreira, P.; Alves, P.; Coimbra, P.; Gil, M. H. *J. Coatings Technol. Res.* **2015**, *12* (3), 463–

475.

(33) Crespilho, F. N.; Zucolotto, V.; Oliveira Jr., O. N.; Nart, F. C. *Int. J. Electrochem. Sci.* **2006**, *1* (September), 194–214.

(34) Yost, A. L.; Shahsavari, S.; Bradwell, G. M.; Polak, R.; Fachin, F.; Cohen, R. E.; McKinley, G. H.; Toner, M.; Rubner, M. F.; Wardle, B. L. *Microsystems Nanoeng.* **2015**, *1* (0), 15037.

(35) Schreiber, F. *Prog. Surf. Sci.* **2000**, *65* (5–8), 151–256.

(36) Ferretti, S.; Paynter, S.; Russell, D. A.; Sapsford, K. E.; Richardson, D. J. *TrAC Trends Anal. Chem.* **2000**, *19* (9), 530–540.

(37) Senaratne, W.; Andruzzi, L.; Ober, C. K.; Monolayers, S.-A.; Perspectives, F. *Biomacromolecules* **2005**, *6* (5), 2427–2448.

(38) Schreiber, F. *J. Phys. Condens. Matter* **2004**, *16* (4), 881–900.

(39) Sung, W. C.; Chang, C. C.; Makamba, H.; Chen, S. H. *Anal. Chem.* **2008**, *80* (5), 1529–1535.

(40) Yang, M.; Choi, D.; Choi, M.; Hong, J. *J. Ind. Eng. Chem.* **2016**, *33*, 221–225.

(41) Dai, Z.; Ju, H. *TrAC - Trends Anal. Chem.* **2012**, *39*, 149–162.

(42) Santos, A.; Kumeria, T.; Losic, D. *TrAC - Trends Anal. Chem.* **2013**, *44*, 25–38.

(43) Wei, H.; Wang, E. *Chem. Soc. Rev.* **2013**, *42* (14), 6060–6093.

(44) Wang, X.; Hu, Y.; Wei, H. *Inorg. Chem. Front.* **2016**, *3* (1), 41–60.

(45) Peppas, N. A.; Van Blarcom, D. S. *J. Control. Release* **2015**.

(46) Chik, H.; Xu, J. M. *Mater. Sci. Eng. R Reports* **2004**, *43* (4), 103–138.

(47) Ghicov, A.; Schmuki, P. *Chem. Commun. (Camb).* **2009**, No. 20, 2791–2808.

(48) Wang, Z.; Liu, H.; Yang, S. H.; Wang, T.; Liu, C.; Cao, Y. C. *Proc. Natl. Acad. Sci.* **2012**, *109* (31), 12387–12392.

(49) Dugan, L. L.; Lovett, E. G.; Quick, K. L.; Lotharius, J.; Lin, T. T.; O'Malley, K. L. *Parkinsonism Relat. Disord.* **2001**, *7* (3), 243–246.

(50) Yao, W.-T.; Zhu, H.-Z.; Li, W.-G.; Yao, H.-B.; Wu, Y.-C.; Yu, S.-H. *Chempluschem* **2013**, *78* (7), 723–727.

(51) Qu, K.; Shi, P.; Ren, J.; Qu, X. *Chem. - A Eur. J.* **2014**, *20* (24), 7501–7506.

(52) Li, N.; Yan, Y.; Xia, B.-Y.; Wang, J.-Y.; Wang, X. *Biosens. Bioelectron.* **2014**, *54*, 521–527.

(53) Asati, A.; Santra, S.; Kaittanis, C.; Nath, S.; Perez, J. M. *Angew. Chemie Int. Ed.* **2009**, *48* (13), 2308–2312.

(54) Pirmohamed, T.; Dowding, J. M.; Singh, S.; Wasserman, B.; Heckert, E.; Karakoti, A. S.; King, J. E. S.; Seal, S.; Self, W. T. *Chem. Commun.* **2010**, *46* (16), 2736.

(55) He, W.; Liu, Y.; Yuan, J.; Yin, J. J.; Wu, X.; Hu, X.; Zhang, K.; Liu, J.; Chen, C.; Ji, Y.; Guo, Y. *Biomaterials* **2011**, *32* (4), 1139–1147.

(56) Wei, H.; Wang, E. *Anal. Chem.* **2008**, *80* (6), 2250–2254.

(57) Hoffman, A. S. *Adv. Drug Deliv. Rev.* **2012**, *64*, 18–23.

(58) Kuwana, E.; Liang, F.; Sevick-Muraca, E. M. *Biotechnol. Prog.* **2004**, *20* (5), 1561–1566.

(59) Mader, H. S.; Wolfbeis, O. S. *Microchim. Acta* **2008**, *162* (1–2), 1–34.

(60) Biswas, A.; Bayer, I. S.; Biris, A. S.; Wang, T.; Dervishi, E.; Faupel, F. *Adv. Colloid Interface Sci.* **2012**, *170* (1–2), 2–27.

(61) Pen, P. E. N. .

(62) Wu, C. C.; Reinhoudt, D. N.; Otto, C.; Subramaniam, V.; Velders, A. H. *Small* **2011**, *7* (8), 989–1002.

(63) Koegler, P.; Clayton, A.; Thissen, H.; Santos, G. N. C.; Kingshott, P. *Adv. Drug Deliv. Rev.* **2012**, *64* (15), 1820–1839.

(64) Jung, G. Y.; Li, Z.; Wu, W.; Chen, Y.; Olynick, D. L.; Wang, S. Y.; Tong, W. M.; Williams, R.

S. *Langmuir* **2005**, *21* (4), 1158–1161.

(65) Yu, Y.; Zhang, G. *Updat. Adv. Lithogr.* **2013**, 3–34.

(66) Whitesides, G. M.; Ostuni, E.; Takayama, S.; Jiang, X.; Ingber, D. E. *Annu. Rev. Biomed. Eng.* **2001**, *3* (1), 335–373.

(67) Zhang, J.; Yang, B. *Adv. Funct. Mater.* **2010**, *20* (20), 3411–3424.

(68) Vieu, C.; Carcenac, F.; Pepin, A.; Chen, Y.; Mejias, M.; Lebib, A.; Manin-Ferlazzo, L.; Couraud, L.; Launois, H. *Appl. Surf. Sci.* **2000**, *164*, 111–117.

(69) Manfrinato, V. R.; Zhang, L.; Su, D.; Duan, H.; Hobbs, R. G.; Stach, E. A.; Berggren, K. K. *Nano Lett.* **2013**, *13* (4), 1555–1558.

(70) Xia, Y.; Whitesides, G. M. *Annu. Rev. Mater. Sci.* **1998**, *28*, 153–184.

(71) Xia, Y.; Rogers, J. A.; Paul, K. E.; Whitesides, G. M. *Chem. Rev.* **1999**, *99* (7), 1823–1848.

(72) Yang, S. M.; Jang, S. G.; Choi, D. G.; Kim, S.; Yu, H. K. *Small* **2006**, *2* (4), 458–475.

(73) Wood, M. a. *J. R. Soc. Interface* **2007**, *4* (12), 1–17.

(74) Shimomura, M.; Sawadaishi, T. *Curr. Opin. Colloid Interface Sci.* **2001**, *6* (1), 11–16.

(75) Borges, J.; Mano, J. F. *Chem. Rev.* **2014**, *114* (18), 8883–8942.

(76) Langmuir, I.; Schaefer, V. J. *J. Am. Chem. Soc.* **1937**, *59* (10), 2075–2076.

(77) Blodgett, K. B. *J. Am. Chem. Soc.* **1935**, *57* (6), 1007–1022.

(78) Ulman, a. *Chem. Rev.* **1996**, *96* (4), 1533–1554.

(79) Bain, C. D.; Whitesides, G. M. *J. Am. Chem. Soc.* **1989**, *111* (18), 7155–7164.

(80) Laibinis, P. E.; Nuzzo, R. G.; Whitesides, G. M. *J. Phys. Chem.* **1992**, *96* (12), 5097–5105.

(81) Bain, C. D.; Evall, J.; Whitesides, G. M. *J. Am. Chem. Soc.* **1989**, *111* (18), 7155–7164.

(82) Ulman, A. *An Introduction to Ultrathin Organic Films: From Langmuir-Blodgett to Self-Assembly*; Academic Press, 2013.

(83) Bishop, A. R.; Nuzzo, R. G. *Curr. Opin. Colloid Interface Sci.* **1996**, *1* (1), 127.

(84) Bigelow, W. C.; Pickett, D. L.; Zisman, W. A. *J. Colloid Sci.* **1946**, *1* (6), 513–538.

(85) Nuzzo, R. G.; Allara, D. L. *J. Am. Chem. Soc.* **1983**, *105* (13), 4481–4483.

(86) Love, J. C.; Estroff, L. A.; Kriebel, J. K.; Nuzzo, R. G.; Whitesides, G. M. *Self-assembled monolayers of thiolates on metals as a form of nanotechnology*; 2005; Vol. 105.

(87) Vericat, C.; Vela, M. E.; Benitez, G.; Carro, P.; Salvarezza, R. C. *Chem. Soc. Rev.* **2010**, *39* (5), 1805.

(88) Lee, S.; Puck, A.; Graupe, M.; Colorado, R.; Shon, Y. S.; Lee, T. R.; Perry, S. S. *Langmuir* **2001**, *17* (23), 7364–7370.

(89) Yan, C.; Zharnikov, M.; Gölzhäuser, A.; Grunze, M. *Langmuir* **2000**, *16* (15), 6208–6215.

(90) Crego-Calama, M.; Reinhoudt, D. N. *Adv. Mater.* **2001**, *13* (15), 1171–1174.

(91) Flink, S.; van Veggel, F. C. J. M.; Reinhoudt, D. N. *J. Phys. Org. Chem.* **2001**, *14* (7), 407–415.

(92) Herzer, N.; Hoeppener, S.; Schubert, U. S. *Chem. Commun. (Camb).* **2010**, *46* (31), 5634–5652.

(93) Onclin, S.; Ravoo, B. J.; Reinhoudt, D. N. *Angew. Chemie Int. Ed.* **2005**, *44* (39), 6282–6304.

(94) Badia, A.; Singh, S.; Demers, L.; Cuccia, L.; Brown, G. R.; Lennox, R. B. *Chem. - A Eur. J.* **1996**, *2* (3), 359–363.

(95) Lenahan, K. M.; Wang, Y.-X.; Liu, Y.; Claus, R. O.; Heflin, J. R.; Marciu, D.; Figura, C. *Adv. Mater.* **1998**, *10* (11), 853–855.

(96) Chandross, M.; Lorenz, C. D.; Grest, G. S.; Stevens, M. J.; Webb, E. B. *JOM* **2005**, *57* (9), 55–61.

(97) Petrenko, V. F.; Peng, S. *Can. J. Phys.* **2003**, *81* (1–2), 387–393.

(98) Chaki, N. K.; Vijayamohanan, K. *Biosens. Bioelectron.* **2002**, *17* (1–2), 1–12.

(99) Guo, Y.; Li, M.; Mylonakis, A.; Han, J.; MacDiarmid, A. G.; Chen, X.; Lelkes, P. I.; Wei, Y. *Biomacromolecules* **2007**, *8* (10), 3025–3034.

(100) Inaba, R.; Khademhosseini, A.; Suzuki, H.; Fukuda, J. *Biomaterials* **2009**, *30* (21), 3573–3579.

(101) Sharma, H.; Nguyen, D.; Chen, A.; Lew, V.; Khine, M. *Ann. Biomed. Eng.* **2011**, *39* (4), 1313–1327.

(102) Kumar, S.; Kumar, S.; Ali, M. A.; Anand, P.; Agrawal, V. V.; John, R.; Maji, S.; Malhotra, B. D. *Biotechnol. J.* **2013**, *8* (11), 1267–1279.

(103) Laibinis, P. E.; Fox, M. A.; Folkers, J. P.; Whitesides, G. M. *Langmuir* **1991**, *7* (12), 3167.

(104) Lessel, M.; Bäumchen, O.; Klos, M.; Hähl, H.; Fetzer, R.; Paulus, M.; Seemann, R.; Jacobs, K. *Surf. Interface Anal.* **2015**, *47* (5), 557–564.

(105) MCGOVERN, M. E.; THOMPSON, M. *Anal. Commun.* **1998**, *35* (12), 391–393.

(106) Smith, R. K.; Lewis, P. A.; Weiss, P. S. *Prog. Surf. Sci.* **2004**, *75* (1–2), 1–68.

(107) Garg, N.; Carrasquillo-Molina, E.; Lee, T. R. *Langmuir* **2002**, *18* (7), 2717–2726.

(108) Guo, L.-Y.; Zhao, Y.-P. *J. Adhes. Sci. Technol.* **2006**, *20* (12), 1281–1293.

(109) Sagiv, J. *J. Am. Chem. Soc.* **1980**, *399* (1976), 92–98.

(110) Parikh, A. N.; Allara, D. L.; Azouz, I. Ben; Rondelez, F. *J. Phys. Chem.* **1994**, *98* (31), 7577–7590.

(111) Haensch, C.; Hoeppener, S.; Schubert, U. S. *Chem. Soc. Rev.* **2010**, *39* (6), 2323.

(112) Schwartz, D. K. *Annu. Rev. Phys. Chem.* **2001**, *52* (1), 107–137.

(113) Wouters, D.; Hoeppener, S.; Sturms, J. P. E.; Schubert, U. S. *J. Scanning Probe Microsc.* **2006**, *1* (1), 45–50.

(114) Sun, L. *J. Electrochem. Soc.* **1991**, *138* (8), L23.

(115) Menzel, H.; Stamm, M.; Heise, A.; Duschner, H.; Rauscher, M. *Thin Solid Films* **1998**,

327–329, 199–203.

(116) Chandekar, A.; Sengupta, S. K.; Whitten, J. E. *Appl. Surf. Sci.* **2010**, *256* (9), 2742–2749.

(117) Wang, M.; Liechti, K. M.; Wang, Q.; White, J. M. *Langmuir* **2005**, *21* (5), 1848–1857.

(118) Henderson, A. P.; Seetohul, L. N.; Dean, A. K.; Russell, P.; Pruneanu, S.; Ali, Z. *Langmuir* **2009**, *25* (2), 931–938.

(119) Bürgi, T. *Nanoscale* **2015**, *7* (38), 15553–15567.

(120) Alves, C. A.; Smith, E. L.; Porter, M. D. *J. Am. Chem. Soc.* **1992**, *114* (4), 1222–1227.

(121) Tolstyka, Z. P.; Richardson, W.; Bat, E.; Stevens, C. J.; Parra, D. P.; Dozier, J. K.; Distefano, M. D.; Dunn, B.; Maynard, H. D. *ChemBioChem* **2013**, *14* (18), 2464–2471.

(122) Wilbur James, L.; Kumar, A.; Biebuyck, H. A. **1996**, *452*.

(123) Kang, J. F.; Liao, S.; Jordan, R.; Ulman, A. *J. Am. Chem. Soc.* **1998**, *120* (37), 9662–9667.

(124) Ballav, N.; Terfort, A.; Zharnikov, M. *Langmuir* **2009**, *25* (16), 9189–9196.

(125) Jeuken, L. J. C.; Daskalakis, N. N.; Han, X.; Sheikh, K.; Erbe, A.; Bushby, R. J.; Evans, S. D. *Sensors Actuators, B Chem.* **2007**, *124* (2), 501–509.

(126) Stranick, S. J.; Parikh, A. N.; Tao, Y.-T.; Allara, D. L.; Weiss, P. S. *J. Phys. Chem.* **1994**, *98* (31), 7636–7646.

(127) Choi, I.; Kim, Y.; Kang, S. K.; Lee, J.; Yi, J. *Langmuir* **2006**, *22* (11), 4885–4889.

(128) Jeuken, L. J. C.; Daskalakis, N. N.; Han, X.; Sheikh, K.; Erbe, A.; Bushby, R. J.; Evans, S. D. *Sensors Actuators B Chem.* **2007**, *124* (2), 501–509.

(129) Yaliraki, S. N.; Longo, G.; Gale, E.; Szleifer, I.; Ratner, M. A. *J. Chem. Phys.* **2006**, *125* (7), 74708.

(130) Cossaro, A.; Mazzarello, R.; Rousseau, R.; Casalis, L.; Verdini, A.; Kohlmeyer, A.; Floreano, L.; Scandolo, S.; Morgante, A.; Klein, M. L.; Scoles, G. *Science (80-.).* **2008**, *321* (5891), 943–946.

(131) Smith, R. K.; Reed, S. M.; Lewis, P. A.; Monnell, J. D.; Clegg, R. S.; Kelly, K. F.; Bumm, L. A.; Hutchison, J. E.; Weiss, P. S. *J. Phys. Chem. B* **2001**, *105* (6), 1119–1122.

(132) McCarley, R. L.; Dunaway, D. J.; Willicut, R. J. *Langmuir* **1993**, *9* (11), 2775–2777.

(133) Wirth, M. J. *Science (80-.).* **1997**, *275* (5296), 44–47.

(134) Senaratne, W.; Andruzzi, L.; Ober, C. K. *Biomacromolecules* **2005**, *6* (5), 2427–2448.

(135) Hays, H. C. W.; Millner, P. A.; Prodromidis, M. I. *Sensors Actuators B Chem.* **2006**, *114* (2), 1064–1070.

(136) Chapman, R. G.; Ostuni, E.; Takayama, S.; Holmlin, R. E.; Yan, L.; Whitesides, G. M. *J. Am. Chem. Soc.* **2000**, *122* (34), 8303–8304.

(137) Prime, K. L.; Whitesides, G. M. *J. Am. Chem. Soc.* **1993**, *115* (23), 10714–10721.

(138) Arima, Y.; Iwata, H. *Biomaterials* **2007**, *28* (20), 3074–3082.

(139) Heuberger, R.; Sukhorukov, G.; Vörös, J.; Textor, M.; Möhwald, H. *Adv. Funct. Mater.* **2005**, *15* (3), 357–366.

(140) Zhu, B.; Eurell, T.; Gunawan, R.; Leckband, D. *J. Biomed. Mater. Res.* **2001**, *56* (3), 406–416.

(141) Zheng, J.; Li, L.; Tsao, H.-K.; Sheng, Y.-J.; Chen, S.; Jiang, S. *Biophys. J.* **2005**, *89* (1), 158–166.

(142) Harder, P.; Grunze, M.; Dahint, R.; Whitesides, G. M.; Laibinis, P. E. *J. Phys. Chem. B* **1998**, *102* (2), 426–436.

(143) Diamandis, E. P.; Christopoulos, T. K. *Clin. Chem.* **1991**, *37* (5), 625–636.

(144) Bu, D.; Zhuang, H.; Zhou, X.; Yang, G. *Talanta* **2014**, *120*, 40–46.

(145) Lei, K. F.; Yang, S.-I.; Tsai, S.-W.; Hsu, H.-T. *Talanta* **2015**, *134*, 264–270.

(146) Kendall, C.; Ionescu-Matiu, I.; Dreesman, G. R. *J. Immunol. Methods* **1983**, *56* (3), 329–339.

(147) Chen, Y. P.; Zou, M. qiang; Qi, C.; Xie, M.-X.; Wang, D.-N.; Wang, Y.-F.; Xue, Q.; Li, J.-F.; Chen, Y. *Biosens. Bioelectron.* **2013**, *39* (1), 112–117.

(148) Focsan, M.; Campu, A.; Craciun, A.-M.; Potara, M.; Leordean, C.; Maniu, D.; Astilean, S. *Biosens. Bioelectron.* **2016**, *86*, 728–735.

(149) Kim, M.-C.; Hong, M.-H.; Lee, B.-H.; Choi, H.-J.; Ko, Y.-M.; Lee, Y.-K. *Ann. Biomed. Eng.* **2015**, *43* (12), 3004–3014.

(150) Tallawi, M.; Rosellini, E.; Barbani, N.; Cascone, M. G.; Rai, R.; Saint-Pierre, G.; Boccaccini, A. R. *J. R. Soc. Interface* **2015**, *12* (108), 20150254.

(151) Biju, V. *Chem. Soc. Rev.* **2014**, *43* (3), 744–764.

(152) Patra, D.; Sengupta, S.; Duan, W.; Zhang, H.; Pavlick, R.; Sen, A. *Nanoscale* **2013**, *5* (4), 1273–1283.

(153) Green, N. M. In *Advances in Protein Chemistry*; Elsevier Inc., 1975; pp 85–133.

(154) Piran, U.; Riordan, W. J. *J. Immunol. Methods* **1990**, *133* (1), 141–143.

(155) Morgan, H.; Taylor, D. M. *Biosens. Bioelectron.* **1992**, *7* (6), 405–410.

(156) Zimbron, J. M.; Heinisch, T.; Schmid, M.; Hamels, D.; Nogueira, E. S.; Schirmer, T.; Ward, T. R. *J. Am. Chem. Soc.* **2013**, *135* (14), 5384–5388.

(157) Yue, M.; Stachowiak, J. C.; Lin, H.; Datar, R.; Cote, R.; Majumdar, A. *Nano Lett.* **2008**, *8* (2), 520–524.

(158) Holford, T. R. J.; Davis, F.; Higson, S. P. J. *Biosens. Bioelectron.* **2012**, *34* (1), 12–24.

(159) Wolny, P. M.; Spatz, J. P.; Richter, R. P. *Langmuir* **2010**, *26* (2), 1029–1034.

(160) DeLange, R. J.; Huang, T.-S. *J. Biol. Chem.* **1971**, *246* (3), 698–709.

(161) Holford, T. R. J.; Davis, F.; Higson, S. P. J. *Biosens. Bioelectron.* **2012**, *34* (1), 12–24.

(162) Malmqvist, M. *Curr. Opin. Immunol.* **1993**, *5* (2), 282–286.

(163) Byrne, B.; Stack, E.; Gilmartin, N.; O'Kennedy, R. *Sensors* **2009**, *9* (6), 4407–4445.

(164) Blake, D. A.; Jones, R. M.; Blake, R. C.; Pavlov, A. R.; Darwish, I. A.; Yu, H. *Biosens. Bioelectron.* **2001**, *16* (9–12), 799–809.

(165) Xiao, Y.; Lubin, A. A.; Heeger, A. J.; Plaxco, K. W. *Angew. Chemie* **2005**, *117* (34), 5592–5595.

(166) Kirby, R.; Cho, E. J.; Gehrke, B.; Bayer, T.; Park, Y. S.; Neikirk, D. P.; McDevitt, J. T.; Ellington, A. D. *Anal. Chem.* **2004**, *76* (14), 4066–4075.

(167) Karlsson, R.; Michaelsson, A.; Mattsson, L. *J. Immunol. Methods* **1991**, *145* (1–2), 229–240.

(168) Ashley, J.; Piekarska, M.; Segers, C.; Trinh, L.; Rodgers, T.; Willey, R.; Tothill, I. E. *Biosens. Bioelectron.* **2017**, *88*, 109–113.

(169) Buchatip, S.; Ananthanawat, C.; Sithigorngul, P.; Sangvanich, P.; Rengpipat, S.; Hoven, V. P. *Sensors Actuators B Chem.* **2010**, *145* (1), 259–264.

(170) Wang, W.; Singh, S.; Zeng, D. L.; King, K.; Nema, S. *J. Pharm. Sci.* **2007**, *96* (1), 1–26.

(171) Leenaars, M.; Hendriksen, C. F. M. *ILAR J.* **2005**, *46* (3), 269–279.

(172) Li, J.; Sun, Q.; Han, S.; Wang, J.; Wang, Z.; Jin, C. *Prog. Org. Coatings* **2015**, *87*, 155–160.

(173) Mendes, P. M. *Chem. Soc. Rev.* **2008**, *37* (11), 2512.

(174) Cantini, E.; Wang, X.; Koelsch, P.; Preece, J. A.; Ma, J.; Mendes, P. M. *Acc. Chem. Res.* **2016**, *49* (6), 1223–1231.

(175) Ebara, M. .; Kotsuchibashi, Y. .; Narain, R. .; Idota, N. .; Kim, Y. .; Hoffman, J. M. .; Uto, K. *Smart Biomaterials*; Springer, 2014.

(176) Yamato, M.; Utsumi, M.; Kushida, A.; Konno, C.; Kikuchi, A.; Okano, T. *Tissue Eng.* **2001**, *7* (4), 473–480.

(177) Cammas, S.; Suzuki, K.; Sone, C.; Sakurai, Y.; Kataoka, K.; Okano, T. *J. Control. Release* **1997**, *48* (2–3), 157–164.

(178) Takezawa, T.; Mori, Y.; Yoshizato, K. *Bio/Technology* **1990**, *8* (9), 854–856.

(179) Schmaljohann, D. *Adv. Drug Deliv. Rev.* **2006**, *58* (15), 1655–1670.

(180) Jonas, A. M.; Glinel, K.; Oren, R.; Nysten, B.; Huck, W. T. S. *Macromolecules* **2007**, *40* (13), 4403–4405.

(181) Zhang, X.-Z.; Zhuo, R.-X.; Cui, J.-Z.; Zhang, J.-T. *Int. J. Pharm.* **2002**, *235* (1–2), 43–50.

(182) Schmaljohann, D.; Oswald, J.; Jørgensen, B.; Nitschke, M.; Beyerlein, D.; Werner, C. *Biomacromolecules* **2003**, *4* (6), 1733–1739.

(183) Liu, F.; Urban, M. W. *Prog. Polym. Sci.* **2010**, *35* (1–2), 3–23.

(184) Xia, F.; Zhu, Y.; Feng, L.; Jiang, L. *Soft Matter* **2009**, *5* (2), 275–281.

(185) Jiang, W.; Wang, G.; He, Y.; Wang, X.; An, Y.; Song, Y.; Jiang, L. *Chem. Commun.* **2005**, No. 28, 3550.

(186) Yu, X.; Wang, Z.; Jiang, Y.; Shi, F.; Zhang, X. *Adv. Mater.* **2005**, *17* (10), 1289–1293.

(187) Xia, F.; Feng, L.; Wang, S.; Sun, T.; Song, W.; Jiang, W.; Jiang, L. *Adv. Mater.* **2006**, *18* (4), 432–436.

(188) Park, C.; Oh, K.; Lee, S. C.; Kim, C. *Angew. Chemie Int. Ed.* **2007**, *46* (9), 1455–1457.

(189) Chen, Y.-C.; Xie, R.; Chu, L.-Y. *J. Memb. Sci.* **2013**, *442*, 206–215.

(190) Gawel, K.; Barriet, D.; Sletmoen, M.; Stokke, B. T. *Sensors* **2010**, *10* (5), 4381–4409.

(191) Li, P.-F.; Xie, R.; Fan, H.; Ju, X.-J.; Chen, Y.-C.; Meng, T.; Chu, L.-Y. *Ind. Eng. Chem. Res.* **2012**, *51* (28), 9554–9563.

(192) Czaun, M.; Hevesi, L.; Takafuji, M.; Ihara, H. *Chem. Commun.* **2008**, No. 18, 2124.

(193) Woodward, R. T.; Olariu, C. I.; Hasan, E. A.; Yiu, H. H. P.; Rosseinsky, M. J.; Weaver, J. V. M. *Soft Matter* **2011**, *7* (9), 4335.

(194) Pranzetti, A.; Davis, M.; Yeung, C. L.; Preece, J. A.; Koelsch, P.; Mendes, P. M. *Adv. Mater. Interfaces* **2014**, *1* (5), 1400026.

(195) Pranzetti, A.; Mieszkin, S.; Iqbal, P.; Rawson, F. J.; Callow, M. E.; Callow, J. A.; Koelsch, P.; Preece, J. A.; Mendes, P. M. *Adv. Mater.* **2013**, *25* (15), 2181–2185.

(196) Yeung, C. L.; Iqbal, P.; Allan, M.; Lashkor, M.; Preece, J. A.; Mendes, P. M. *Adv. Funct. Mater.* **2010**, *20* (16), 2657–2663.

(197) Yeung, C. L.; Wang, X.; Lashkor, M.; Cantini, E.; Rawson, F. J.; Iqbal, P.; Preece, J. A.; Ma, J.; Mendes, P. M. *Adv. Mater. Interfaces* **2014**, *1* (2).

(198) Lashkor, M.; Rawson, F. J.; Preece, J. A.; Mendes, P. M. *Analyst* **2014**, *139* (21), 5400–5408.

(199) Lashkor, M.; Rawson, F. J.; Stephenson-Brown, A.; Preece, J. A.; Mendes, P. M. *Chem. Commun.* **2014**, *50* (98), 15589–15592.

(200) Krishnamoorthy, M.; Hakobyan, S.; Ramstedt, M.; Gautrot, J. E. *Chem. Rev.* **2014**, *114* (21), 10976–11026.

(201) Schmidt, S.; Zeiser, M.; Hellweg, T.; Duschl, C.; Fery, A.; Möhwald, H. *Adv. Funct. Mater.* **2010**, *20* (19), 3235–3243.

(202) Wischerhoff, E.; Uhlig, K.; Lankenau, A.; Börner, H. G.; Laschewsky, A.; Duschl, C.; Lutz, J. *Angew. Chemie Int. Ed.* **2008**, *47* (30), 5666–5668.

(203) Synytska, A.; Svetushkina, E.; Puretskiy, N.; Stoychev, G.; Berger, S.; Ionov, L.; Bellmann, C.; Eichhorn, K.-J.; Stamm, M. *Soft Matter* **2010**, *6* (23), 5907.

(204) Flink, S.; Veggel, F. C. J. M. van; Reinhoudt, D. N. *Adv. Mater.* **2000**, *12* (18), 1315–1328.

(205) Lahann, J. *Science (80-.).* **2003**, *299* (5605), 371–374.

(206) Liu, Y.; Mu, L.; Liu, B.; Zhang, S.; Yang, P.; Kong, J. *Chem. Commun.* **2004**, No. 10, 1194.

(207) Liu, F.; Urban, M. W. *Prog. Polym. Sci.* **2010**, *35* (1–2), 3–23.

(208) Mendes, P. M.; Christman, K. L.; Parthasarathy, P.; Schopf, E.; Ouyang, J.; Yang, Y.; Preece, J. A.; Maynard, H. D.; Chen, Y.; Stoddart, J. F. *Bioconjug. Chem.* **2007**, *18* (6),

1919–1923.

(209) Liu, Y.; Mu, L.; Liu, B.; Kong, J. *Chem. - A Eur. J.* **2005**, *11* (9), 2622–2631.

(210) Rant, U.; Arinaga, K.; Scherer, S.; Pringsheim, E.; Fujita, S.; Yokoyama, N.; Tornow, M.; Abstreiter, G. *Proc. Natl. Acad. Sci.* **2007**, *104* (44), 17364–17369.

(211) Doyle, D. A. *Science (80-.).* **1998**, *280* (5360), 69–77.

(212) Catterall, W. A. *Exp. Physiol.* **2014**, *99* (1), 35–51.

(213) Knezevic, J.; Langer, A.; Hampel, P. A.; Kaiser, W.; Strasser, R.; Rant, U. *J. Am. Chem. Soc.* **2012**, *134* (37), 15225–15228.

(214) de Kretser DM1. *Lancet* **1997**, *349* ((9054)), 787–790.

(215) Brugh, V. M.; Lipshultz, L. I. *Med. Clin. North Am.* **2004**, *88* (2), 367–385.

(216) Cooper, T. G.; Noonan, E.; von Eckardstein, S.; Auger, J.; Baker, H. W. G.; Behre, H. M.; Haugen, T. B.; Kruger, T.; Wang, C.; Mbizvo, M. T.; Vogelsong, K. M. *Hum. Reprod. Update* **2010**, *16* (3), 231–245.

(217) Moskovtsev, S. I.; Willis, J.; Mullen, J. B. M. *Fertil. Steril.* **2006**, *85* (2), 496–499.

(218) Sharpe, R. M. *Best Pract. Res. Clin. Endocrinol. Metab.* **2000**, *14* (3), 489–503.

(219) Oliva, A. *Hum. Reprod.* **2001**, *16* (8), 1768–1776.

(220) Tremellen, K. *Hum. Reprod. Update* **2008**, *14* (3), 243–258.

(221) Bozhedomov, V. A.; Nikolaeva, M. A.; Ushakova, I. V.; Lipatova, N. A.; Bozhedomova, G. E.; Sukhikh, G. T. *J. Reprod. Immunol.* **2015**, *112*, 95–101.

(222) Huynh, T. *Hum. Reprod. Update* **2002**, *8* (2), 183–198.

(223) Fraser, L. R. *Hum. Reprod.* **1998**, *13 Suppl 1*, 9–19.

(224) Breitbart, H. *Mol. Cell. Endocrinol.* **2002**, *187* (1–2), 139–144.

(225) Smith, J. F.; Syritsyna, O.; Fellous, M.; Serres, C.; Mannowetz, N.; Kirichok, Y.; Lishko, P. V. *Proc. Natl. Acad. Sci. U. S. A.* **2013**, *110* (17), 6823–6828.

(226) Cai, X.; Wang, X.; Clapham, D. E. *Mol. Biol. Evol.* **2014**, *31* (10), 2735–2740.

(227) Alasmari, W.; Costello, S.; Correia, J.; Oxenham, S. K.; Morris, J.; Fernandes, L.; Ramalho-Santos, J.; Kirkman-Brown, J.; Michelangeli, F.; Publicover, S.; Barratt, C. L. R. *J. Biol. Chem.* **2013**, *288* (9), 6248–6258.

(228) Darszon, A.; Acevedo, J. J.; Galindo, B. E.; Hernández-González, E. O.; Nishigaki, T.; Treviño, C. L.; Wood, C.; Beltrán, C. *Reproduction* **2006**, *131* (6), 977–988.

(229) Darszon, A.; Nishigaki, T.; Beltran, C.; Treviño, C. L. *Physiol. Rev.* **2011**, *91* (4), 1305–1355.

(230) Lishko, P. V; Botchkina, I. L.; Kirichok, Y. *Nature* **2011**, *471* (7338), 387–391.

(231) Munire, M.; Shimizu, Y.; Sakata, Y.; Minaguchi, R.; Aso, T. *J. Med. Dent. Sci.* **2004**, *51* (1), 99–104.

(232) Suarez, S. S.; Dai, X. *Biol. Reprod.* **1992**, *46* (4), 686–691.

(233) Garcia, M. a; Meizel, S. *Biol. Reprod.* **1999**, *60* (1), 102–109.

(234) Sánchez-Cárdenas, C.; Servin-Vences, M. R.; José, O.; Treviño, C. L.; Hernández-Cruz, A.; Darszon, A. *Biol. Reprod.* **2014**, *91* (August), 1–21.

(235) Clapham, D. E. *Cell* **2007**, *131* (6), 1047–1058.

(236) Suarez, S. S.; Ho, H. C. *Reprod. Domest. Anim.* **2003**, *38* (2), 119–124.

(237) Sumigama, S.; Mansell, S.; Miller, M.; Lishko, P. V.; Cherr, G. N.; Meyers, S. A.; Tollner, T. *Biol. Reprod.* **2015**, *93* (6), 130.

(238) Suarez, S. S. *Hum. Reprod. Update* **2008**, *14* (6), 647–657.

(239) Suarez, S. S.; Ho, H. *Reprod Dom Anim* **2003**, *124*, 119–124.

(240) Suarez, S. S.; Katz, D. F.; Owen, D. H.; Andrew, J. B.; Powell, R. L. *Biol. Reprod.* **1991**, *44* (2), 375–381.

(241) England, T. N. *English J.* **2002**, *346* (10), 725–730.

(242) Ortega, N. M.; Bosch, P. **2009**.

(243) Bowdin, S.; Allen, C.; Kirby, G.; Brueton, L.; Afnan, M.; Barratt, C.; Kirkman-Brown, J.; Harrison, R.; Maher, E. R.; Reardon, W. *Hum. Reprod.* **2007**, *22* (12), 3237–3240.

(244) Neri, Q. V.; Tanaka, N.; Wang, A.; Katagiri, Y.; Takeuchi, T.; Rosenwaks, Z.; Palermo, G. D. *Minerva Ginecol.* **2004**, *56* (3), 189–196.

(245) Cox, G. F.; Bürger, J.; Lip, V.; Mau, U. A.; Sperling, K.; Wu, B.-L.; Horsthemke, B. *Am. J. Hum. Genet.* **2002**, *71* (1), 162–164.

(246) Hansen, M.; Kurinczuk, J. J.; Bower, C.; Webb, S. *N. Engl. J. Med.* **2002**, *346* (10), 725–730.

(247) Johnson, M. D. *Fertil. Steril.* **1998**, *70* (3), 397–411.

(248) Good, R. J. *J. Adhes. Sci. Technol.* **1992**, *6* (12), 1269–1302.

(249) Chen, W.; Fadeev, A. Y.; Hsieh, M. C.; Öner, D.; Youngblood, J.; McCarthy, T. J. *Langmuir* **1999**, *15* (10), 3395–3399.

(250) Wang, X.; Liu, L.-H.; Ramstrom, O.; Yan, M. *Exp. Biol. Med.* **2009**, *234* (10), 1128–1139.

(251) Siegbahn, K.; Edvarson, K. *Nucl. Phys.* **1956**, *1* (3), 137–159.

(252) Nascente, P. a. P. *J. Mol. Catal. A Chem.* **2005**, *228*, 145–150.

(253) Verma, H. R. *At. Nucl. Anal. Methods* **2007**, 1–90.

(254) Hollander, J. M.; Jolly, W. L. *Acc. Chem. Res.* **1970**, *3* (193).

(255) Wang, X.; Liu, L.-H.; Ramstrom, O.; Yan, M. *Exp. Biol. Med.* **2009**, *234* (10), 1128–1139.

(256) Fadley, C. S. *J. Electron Spectros. Relat. Phenomena* **2010**, *178–179* (C), 2–32.

(257) Drude, P. *Ann. der Phys. und Chemie* **1888**, *270* (7), 489–531.

(258) Vedam, K. *Thin Solid Films* **1998**, *313–314*, 1–9.

(259) Habraken, F. H. P. M.; Gijzeman, O. L. J.; Bootsma, G. A. *Surf. Sci.* **1980**, *96* (1–3), 482–507.

(260) Fujiwara, H. *Spectroscopic Ellipsometry: Principles and Applications*; John Wiley & Sons, Ltd.: Tokyo, Japan, 2007.

(261) Fenstermaker, C. A.; McCrackin, F. L. *Surf. Sci.* **1969**, *16*, 85–96.

(262) De Feijter, J. A.; Benjamins, J.; Veer, F. A. *Biopolymers* **1978**, *17* (7), 1759–1772.

(263) Tompkins, H. G. *A User's Guide to Ellipsometry*; Elsevier Inc., 1993.

(264) Schubert, M. *Ann. der Phys.* **2006**, *15* (7–8), 480–497.

(265) Loescher, D. H.; Detry, R. J.; Clauser, M. J. *J. Opt. Soc. Am.* **1971**, *61* (9), 1230.

(266) Gonçalves, D.; Irene, E. A. *Quim. Nova* **2002**, *25* (5), 794–800.

(267) Chiarini-Garcia, H.; Parreira, G. G.; Almeida, F. R. C. L. In *Light Microscophy: Methods and Protocols*; 2011; pp 3–18.

(268) *Light Microscopy*; Chiarini-Garcia, H., Melo, R. C. N., Eds.; Methods in Molecular Biology; Humana Press: Totowa, NJ, 2011; Vol. 689.

(269) Spring, K. R.; Davidson, M. W. *Nikon Microsc.* **2008**.

(270) Lichtman, J. W.; Conchello, J.-A. *Nat. Methods* **2005**, *2* (12), 910–919.

(271) In *Fundamentals of Light Microscopy and Electronic Imaging*; John Wiley & Sons, Inc.: Hoboken, NJ, USA, 2012; pp 1–19.

(272) Buckman, J. F.; Hernandez, H.; Kress, G. J.; Votyakova, T. V.; Pal, S.; Reynolds, I. J. *J. Neurosci. Methods* **2001**, *104* (2), 165–176.

(273) Pendergrass, W.; Wolf, N.; Poot, M. *Cytometry* **2004**, *61A* (2), 162–169.

(274) Chikte, S.; Panchal, N.; Warnes, G. *Cytom. Part A* **2014**, *85* (2), 169–178.

(275) Franke, W. W.; Appelhans, B.; Schmid, E.; Freudenstein, C.; Osborn, M.; Weber, K. *Differentiation* **1979**, *15* (1–3), 7–25.

(276) Willig, K. I.; Kellner, R. R.; Medda, R.; Hein, B.; Jakobs, S.; Hell, S. W. *Nat. Methods* **2006**, *3* (9), 721–723.

(277) Grant, E. R.; Dubin, A. E.; Zhang, S.-P.; Zivin, R. a; Zhong, Z. *J. Pharmacol. Exp. Ther.* **2002**, *300* (1), 9–17.

(278) Jares-Erijman, E. A.; Jovin, T. M. *Nat. Biotechnol.* **2003**, *21* (11), 1387–1395.

(279) Seiffert, S.; Oppermann, W. *J. Microsc.* **2005**, *220* (1), 20–30.

(280) Reichert, W. M.; Truskey, G. A. *J. Cell Sci.* **1990**, *96*, 219–230.

(281) Axelrod, D. 2008; pp 169–221.

(282) Axelrod, D. 1989; pp 245–270.

(283) Liedberg, B.; Nylander, C.; Lundström, I. *Biosens. Bioelectron.* **1995**, *10* (8), i–ix.

(284) Wood, R. W. *Philos. Mag. Ser. 6* **1912**, *23* (134), 310–317.

(285) Wood, R. W. *Philos. Mag. Ser. 6* **1902**, *4* (21), 396–402.

(286) Tudos, A. J.; Schasfoort, R. B. M. *Handbook of Surface Plasmon Resonance*; RSC Publishing, 2008.

(287) Homola, J. *Surface Plasmon Resonance Based Sensors*; Homola, J., Ed.; Springer Series on Chemical Sensors and Biosensors; Springer Berlin Heidelberg: Berlin, Heidelberg, 2006; Vol. 4.

(288) Piliarik, M.; Vaisocherová, H.; Homola, J. In *Biosensors and Biodetection*; Rasooly, A., Herold, K. E., Eds.; Humana Press: Totowa, NJ, 2009; pp 65–88.

(289) Piliarik, M.; Homola, J. *Opt. Express* **2009**, *17* (19), 16505.

(290) Homola, J.; Yee, S. S.; Gauglitz, G. *Sensors Actuators B Chem.* **1999**, *54* (1–2), 3–15.

(291) Boardman, A. D. *Electromagnetic surfaces modes*; John Wiley & Sons, 1982.

(292) Homola, J. *Anal. Bioanal. Chem.* **2003**, *377* (3), 528–539.

(293) Ordal, M. A.; Long, L. L.; Bell, R. J.; Bell, S. E.; Bell, R. R.; Alexander, R. W.; Ward, C. A. *Appl. Opt.* **1983**, *22* (7), 1099.

(294) Homola, J. *Chem. Rev.* **2008**, *108* (2), 462–493.

(295) Liedberg, B.; Lundström, I.; Stenberg, E. *Sensors Actuators B Chem.* **1993**, *11* (1–3), 63–72.

(296) Liedberg, B.; Nylander, C.; Lunström, I. *Sensors and Actuators* **1983**, *4*, 299–304.

(297) Homola, J. *Anal. Bioanal. Chem.* **2003**, *377* (3), 528–539.

(298) Zoski, C. *Handbook of Electrochemistry*; Elsevier Science, 2007.

(299) Gueshi, T.; Tokuda, K.; Matsuda, H. *J. Electroanal. Chem. Interfacial Electrochem.* **1978**, *89* (2), 247–260.

(300) Slevin, C. J.; Macpherson, J. V.; Unwin, P. R. *J. Phys. Chem. B* **1997**, *101* (50), 10851–10859.

(301) Coles, B. A.; Compton, R. G.; Brett, C. M. A.; Brett, A. M. C. F. O. *J. Electroanal. Chem.* **1995**, *381* (1–2), 99–104.

(302) Grieshaber, D.; MacKenzie, R.; Vörös, J.; Reimhult, E. *Sensors* **2008**, *8* (3), 1400–1458.

(303) Kounaves, S. P. In *Handbook of Instrumental Techniques for Analytical Chemistry*; Settle, F. A., Ed.; Prentice Hall PTR, 1997; pp 709–725.

(304) Nadjo, L.; Savéant, J. M. *J. Electroanal. Chem. Interfacial Electrochem.* **1973**, *48* (1), 113–145.

(305) Settle, F. A. *Handbook of instrumental techniques for analytical chemistry*; Settle, F. A., Ed.; Prentice Hall PTR, 1997.

(306) Davies, T. J.; Compton, R. G. *J. Electroanal. Chem.* **2005**, *585* (1), 63–82.

(307) Wang, H.; Chen, S.; Li, L.; Jiang, S. *Langmuir* **2005**, *21* (7), 2633–2636.

(308) Andersen, H. C. *J. Chem. Phys.* **1980**, *72* (4), 2384–2393.

(309) Allen, M. P.; Tidesley, D. J. *Computer simulation of liquids*; Oxford University Press, 1989.

(310) *Materials Studio, version 4.0, Accelrys Inc., San Diego, 2006.*; Accelerys Inc.: San Diego,

2006.

(311) Frisch, M. J. et al. *Gaussian 09 (Revision B.01), Gaussian, Inc., Wallingford CT.*; Gaussian, Inc., Wallingford CT., 2009.

(312) Nash, K.; Lefievre, L.; Peralta-Arias, R.; Morris, J.; Morales-Garcia, A.; Connolly, T.; Costello, S.; Kirkman-Brown, J. C.; Publicover, S. J. *J. Vis. Exp.* **2010**, No. 40.

(313) Amman, R. P.; Waberski, D. *Theriogenology* **2014**, *81* (1), 5–17.

(314) Zareie, H. M.; Boyer, C.; Bulmus, V.; Nateghi, E.; Davis, T. P. *ACS Nano* **2008**, *2* (4), 757–765.

(315) Balamurugan, S.; Ista, L. K.; Yan, J.; López, G. P.; Fick, J.; Himmelhaus, M.; Grunze, M. *J. Am. Chem. Soc.* **2005**, *127* (42), 14548–14549.

(316) Young, D. D.; Deiters, A. *ChemBioChem* **2008**, *9* (8), 1225–1228.

(317) Demirel, G. B.; Dilsiz, N.; Ergün, M. A.; Çakmak, M.; Çaykara, T. *J. Mater. Chem.* **2011**, *21* (28), 10415.

(318) Mannix, R. J.; Kumar, S.; Cassiola, F.; Montoya-Zavala, M.; Feinstein, E.; Prentiss, M.; Ingber, D. E. *Nat. Nanotechnol.* **2008**, *3* (1), 36–40.

(319) Mu, L.; Liu, Y.; Zhang, S.; Liu, B.; Kong, J. *New J. Chem.* **2005**, *29* (6), 847.

(320) Castner, D. G.; Ratner, B. D. *Biomedical surface science: Foundations to frontiers*; 2002; Vol. 500.

(321) Soliman, M.; Nasanit, R.; Abulateefeh, S. R.; Allen, S.; Davies, M. C.; Briggs, S. S.; Seymour, L. W.; Preece, J. A.; Grabowska, A. M.; Watson, S. A.; Alexander, C. *Mol. Pharm.* **2012**, *9* (1), 1–13.

(322) Stevenson, M.; Ramos-Perez, V.; Singh, S.; Soliman, M.; Preece, J. A.; Briggs, S. S.; Read, M. L.; Seymour, L. W. *J. Control. Release* **2008**, *130* (1), 46–56.

(323) Immoos, C. E.; Lee, S. J.; Grinstaff, M. W. *J. Am. Chem. Soc.* **2004**, *126* (35), 10814–

10815.

(324) Fan, C.; Plaxco, K. W.; Heeger, A. J. *Proc. Natl. Acad. Sci.* **2003**, *100* (16), 9134–9137.

(325) Huber, D. L. *Science (80-.).* **2003**, *301* (5631), 352–354.

(326) Yamanaka, H.; Yoshizako, K.; Akiyama, Y.; Sota, H.; Hasegawa, Y.; Shinohara, Y.; Kikuchi, A.; Okano, T. *Anal. Chem.* **2003**, *75* (7), 1658–1663.

(327) Yoshizako, K.; Akiyama, Y.; Yamanaka, H.; Shinohara, Y.; Hasegawa, Y.; Carredano, E.; Kikuchi, A.; Okano, T. *Anal. Chem.* **2002**, *74* (16), 4160–4166.

(328) Nagase, K.; Kobayashi, J.; Kikuchi, A.; Akiyama, Y.; Kanazawa, H.; Okano, T. *Langmuir* **2007**, *23* (18), 9409–9415.

(329) Palazon, F.; L??onard, D.; Mogne, T. Le; Zuttion, F.; Chevalier, C.; Phaner-Goutorbe, M.; Souteyrand, ??liane; Chevolot, Y.; Cloarec, J. P. *Beilstein J. Nanotechnol.* **2015**, *6* (1), 2272–2277.

(330) Ng, C. C. A.; Magenau, A.; Ngalim, S. H.; Ciampi, S.; Chockalingham, M.; Harper, J. B.; Gaus, K.; Gooding, J. J. *Angew. Chemie Int. Ed.* **2012**, *51* (31), 7706–7710.

(331) Curreli, M.; Li, C.; Sun, Y.; Lei, B.; Gundersen, M. A.; Thompson, M. E.; Zhou, C. *J. Am. Chem. Soc.* **2005**, *127* (19), 6922–6923.

(332) Yang, W.; Baker, S. E.; Butler, J. E.; Lee, C.; Russell, J. N.; Shang, L.; Sun, B.; Hamers, R. J. *Chem. Mater.* **2005**, *17* (5), 938–940.

(333) Crist, B. V.; Crist, B. V. *Elements* **1999**, *1*.

(334) Wang, X.; Liu, L.-H.; Ramstrom, O.; Yan, M. *Exp. Biol. Med.* **2009**, *234* (10), 1128–1139.

(335) Moulder, J. F.; Stickle, W. F.; Sobol, P. E.; Bomben, K. D. *Handbook of X-ray Photoelectron Spectroscopy*; 1992.

(336) Tong, Y.; Tyrode, E.; Osawa, M.; Yoshida, N.; Watanabe, T.; Nakajima, A.; Ye, S. *Langmuir* **2011**, *27* (9), 5420–5426.

(337) Bain, C. D.; Whitesides, G. M. *J. Am. Chem. Soc.* **1989**, *111* (18), 7164–7175.

(338) Häussling, L.; Michel, B.; Ringsdorf, H.; Rohrer, H. *Angew. Chemie Int. Ed. English* **1991**, *30* (5), 569–572.

(339) Fernandez-Torrente, I.; Monturet, S.; Franke, K. J.; Fraxedas, J.; Lorente, N.; Pascual, J. I. *Phys. Rev. Lett.* **2007**, *99* (17), 176103.

(340) Neff, J. L.; Söngen, H.; Bechstein, R.; Maass, P.; Kühnle, A. *J. Phys. Chem. C* **2015**, *119* (44), 24927–24931.

(341) Spinke, J.; Liley, M.; Schmitt, F. -J.; Guder, H. -J.; Angermaier, L.; Knoll, W. *J. Chem. Phys.* **1993**, *99* (9), 7012–7019.

(342) Barinaga-Rementeria Ramírez, I.; Mebrahtu, S.; Jergil, B. *J. Chromatogr. A* **2002**, *971* (1–2), 117–127.

(343) Hiller, Y.; Gershoni, J. M.; Bayer, E. A.; Wilchek, M. *Biochem. J.* **1987**, *248* (1), 167–171.

(344) Holmberg, A.; Blomstergren, A.; Nord, O.; Lukacs, M.; Lundeberg, J.; Uhlén, M. *Electrophoresis* **2005**, *26* (3), 501–510.

(345) Dundas, C. M.; Demonte, D.; Park, S. *Appl. Microbiol. Biotechnol.* **2013**, *97* (21), 9343–9353.

(346) Casalini, S.; Dumitru, A. C.; Leonardi, F.; Bortolotti, C. A.; Herruzo, E. T.; Campana, A.; de Oliveira, R. F.; Cramer, T.; Garcia, R.; Biscarini, F. *ACS Nano* **2015**, *9* (5), 5051–5062.

(347) Adamczyk, M.; Moore, J. A.; Yu, Z. *Methods* **2000**, *20* (3), 319–328.

(348) Ju, H. *J. Anal. Test.* **2017**, *1* (1), 7.

(349) Mitchell, J. *Sensors* **2010**, *10* (8), 7323–7346.

(350) Byrne, B.; Stack, E.; Gilmartin, N.; O'Kennedy, R. *Sensors (Switzerland)* **2009**, *9* (6), 4407–4445.

(351) Carralero, V.; González-Cortés, A.; Yáñez-Sedeño, P.; Pingarrón, J. M. *Anal. Chim. Acta*

2007, *596* (1), 86–91.

(352) Guiochon-Mantel, A.; Loosfelt, H.; Lescop, P.; Sar, S.; Atger, M.; Perrot-Applanat, M.; Milgrom, E. *Cell* **1989**, *57* (7), 1147–1154.

(353) Blackmore, P. F.; Im, W. Bin; Bleasdale, J. E. *Mol. Cell. Endocrinol.* **1994**, *104* (2), 237–243.

(354) Calogero, A. E.; Burrello, N.; Barone, N.; Palermo, I.; Grasso, U.; D'Agata, R. *Hum. Reprod.* **2000**, *15* (suppl 1), 28–45.

(355) Aurell, C.; Meizel, W. S. *Dev. Biol.* **1993**, *159* (2), 679–690.

(356) Chidsey, C. E. D.; Loiacono, D. N. *Langmuir* **1990**, *6* (3), 682–691.

(357) Dubois, L.; Nuzzo, R. G. *Annu. Rev. Phys. Chem.* **1992**, *43*, 437–463.

(358) Rahman, M. S.; Kwon, W. S.; Pang, M. G. *Biomed Res. Int.* **2014**, *2014*.

(359) De Jonge, C. *Hum. Reprod. Update* **2005**, *11* (3), 205–214.

(360) Xia, J.; Ren, D. *Reprod. Biol. Endocrinol.* **2009**, *7* (1), 119.

(361) Lesaicherre, M.-L.; Uttamchandani, M.; Chen, G. Y. .; Yao, S. Q. *Bioorg. Med. Chem. Lett.* **2002**, *12* (16), 2079–2083.

(362) Spinola, S. M.; Cannon, J. G. *J. Immunol. Methods* **1985**, *81* (1), 161–165.

(363) Böhme, U.; Scheler, U. *Chem. Phys. Lett.* **2007**, *435* (4–6), 342–345.

(364) Jachimska, B.; Pajor, A. *Bioelectrochemistry* **2012**, *87*, 138–146.

(365) Mitchell, J. S.; Wu, Y. *Biosensors* **2010**, No. February, 151–168.

(366) Omidfar, K.; Khorsand, F.; Darziani Azizi, M. *Biosens. Bioelectron.* **2013**, *43* (1), 336–347.

(367) Breitbart, H. *Cell. Mol. Biol.* **2003**, *49* (July), 321–327.

(368) Darszon, A.; Hernández-Cruz, A. *Pflugers Arch.* **2014**, *466* (4), 819–831.

(369) Durán, S.; Duch, M.; Patiño, T.; Torres, A.; Penon, O.; Gómez-Martínez, R.; Barrios, L.; Esteve, J.; Nogués, C.; Pérez-García, L.; Plaza, J. A. *Sensors Actuators B Chem.* **2015**, *209*,

212–224.

(370) Wendeln, C.; Rinnen, S.; Schulz, C.; Kaufmann, T.; Arlinghaus, H. F.; Ravoo, B. J. *Chem. - A Eur. J.* **2012**, *18* (19), 5880–5888.

(371) Wendeln, C.; Rinnen, S.; Schulz, C.; Kaufmann, T.; Arlinghaus, H. F.; Ravoo, B. J. *Chem. - A Eur. J.* **2012**, *18* (19), 5880–5888.

(372) Vong, T.; ter Maat, J.; van Beek, T. A.; van Lagen, B.; Giesbers, M.; van Hest, J. C. M.; Zuilhof, H. *Langmuir* **2009**, *25* (24), 13952–13958.

(373) Rozkiewicz, D. I.; Brugman, W.; Kerkhoven, R. M.; Ravoo, B. J.; Reinhoudt, D. N. *J. Am. Chem. Soc.* **2007**, *129* (37), 11593–11599.

(374) Zhang, G.-J.; Tanii, T.; Zako, T.; Funatsu, T.; Ohdomari, I. *Sensors Actuators B Chem.* **2004**, *97* (2–3), 243–248.

(375) Del Campo, A.; Boos, D.; Spiess, H. W.; Jonas, U. *Angew. Chemie - Int. Ed.* **2005**, *44* (30), 4707–4712.

(376) Slocik, J. M.; Beckel, E. R.; Jiang, H.; Enlow, J. O.; Zabinski, J. S.; Bunning, T. J.; Naik, R. R. *Adv. Mater.* **2006**, *18* (16), 2095–2100.

(377) Li, Y.; Niehaus, J. C.; Chen, Y.; Fuchs, H.; Studer, A.; Galla, H.-J.; Chi, L. *Soft Matter* **2011**, *7* (3), 861–863.

(378) Durán, S.; Duch, M.; Patiño, T.; Torres, A.; Penon, O.; Gómez-Martínez, R.; Barrios, L.; Esteve, J.; Nogués, C.; Pérez-García, L.; Plaza, J. A. *Sensors Actuators, B Chem.* **2015**, *209*, 212–224.

(379) Mazia, D.; Schatten, G.; Sale, W. *J. Cell Biol.* **1975**, *66* (1), 198–200.

(380) Kim, Y. H.; Baek, N. S.; Han, Y. H.; Chung, M.-A.; Jung, S.-D. *J. Neurosci. Methods* **2011**, *202* (1), 38–44.

(381) Ooi, E. H.; Smith, D. J.; Gadêlha, H.; Gaffney, E. A.; Kirkman-Brown, J. *R. Soc. Open Sci.*

2014, *1*.

(382) Pantano, C. G. In *Experimental Techniques of Glass Science*; American Ceramic Society, 1993; pp 129–160.

(383) Hooper, A. E.; Werho, D.; Hopson, T.; Palmer, O. *Surf. Interface Anal.* **2001**, *31* (9), 809–814.

(384) Bozso, F.; Yates, J. T.; Choyke, W. J.; Muehlhoff, L. *J. Appl. Phys.* **1985**, *57* (8), 2771.

(385) Brückner, R.; Chun, H.-U.; Goretzki, H.; Sammet, M. *J. Non. Cryst. Solids* **1980**, *42* (1–3), 49–60.

(386) Serra, J.; González, P.; Liste, S.; Serra, C.; Chiussi, S.; León, B.; Pérez-Amor, M.; Ylänen, H. O.; Hupa, M. *J. Non. Cryst. Solids* **2003**, *332* (1–3), 20–27.

(387) WARD, C.; FRENCH, D. *Fuel* **2006**, *85* (16), 2268–2277.

(388) Gross, T.; Ramm, M.; Sonntag, H.; Unger, W.; Weijers, H. M.; Adem, E. H. *Surf. Interface Anal.* **1992**, *18* (1), 59–64.

(389) Cerofolini, G. F.; Galati, C.; Renna, L. *Surf. Interface Anal.* **2003**, *35* (12), 968–973.

(390) Wang, J.; Yang, X.; Hu, W.; Li, B.; Yan, J.; Hu, J. *Chem. Commun.* **2007**, No. 46, 4931.

(391) Shircliff, R. A.; Stradins, P.; Moutinho, H.; Fennell, J.; Ghirardi, M. L.; Cowley, S. W.; Branz, H. M.; Martin, I. T. *Langmuir* **2013**, *29* (12), 4057–4067.

(392) Wang, Y.; Lieberman, M.; Hang, Q.; Bernstein, G. *Int. J. Mol. Sci.* **2009**, *10* (2), 533–558.

(393) Yan, H.; Li, S.; Jia, Y.; Ma, X. Y. *RSC Adv.* **2015**, *5* (17), 12578–12582.

(394) Hayashi, K.; Matsuda, T.; Takeyama, T.; Hino, T. *Agric. Biol. Chem.* **1966**, *30* (4), 378–384.

(395) Battocchio, C.; Porcaro, F.; Mukherjee, S.; Magnano, E.; Nappini, S.; Fratoddi, I.; Quintiliani, M.; Russo, M. V.; Polzonetti, G. *J. Phys. Chem. C* **2014**, *118* (15), 8159–8168.

(396) Weidner, T.; Bretthauer, F.; Ballav, N.; Motschmann, H.; Orendi, H.; Bruhn, C.;

Siemeling, U.; Zharnikov, M. *Langmuir* **2008**, *24* (20), 11691–11700.

(397) Martín-García, B.; Polovitsyn, A.; Prato, M.; Moreels, I. *J. Mater. Chem. C* **2015**, *3* (27), 7088–7095.

(398) Muyldermans, S. *Annu. Rev. Biochem.* **2013**, *82* (1), 775–797.

(399) Chakravarty, R.; Goel, S.; Cai, W. *Theranostics* **2014**, *4* (4), 386–398.